

ASTROPHYSICS OF INTERACTING BINARY STARS

Vitaly Neustroev

Contact details

2

- **Location:** MA 302
 - **Email:** vitaly@neustroev.net; vitaly.neustroev@oulu.fi
 - **Web:**
<https://vitaly.neustroev.net/teach/autumn-2020-2-aoibs/>
-
- ▣ You are encouraged to ask questions during the lectures.
 - ▣ You can send me your questions by e-mail or phone me.

Aim of the course

3

- The course will provide the necessary understanding of the physics of binary stars with white dwarfs, neutron stars, and black holes, mass-transfer, and the importance of binary stars and populations of binaries to modern astrophysics.
- Theoretical and practical considerations will be supplemented with the home exercises which constitute the important part of the course.

Text Books

4

- *Interacting Binary Stars* (1985) – Edited by J.E. Pringle and R.A. Wade: Cambridge University Press / ISBN 0 521 26608 4.
- *Cataclysmic Variable Stars* (2003) – Brian Warner: Cambridge University Press / ISBN 0 521 54209 X.
- *Accretion Power in Astrophysics* (3rd edition, 2003) – J. Frank, A. King and D. Raine: Cambridge University Press / ISBN 0 521 62957 8.
- *Cataclysmic Variable Stars – How and Why They Vary* (2001) – Coel Hellier / Springer Science & Business Media. ISBN 1852332115.

- I will also give references to original papers where useful.

Home exercises

5

- Compulsory homework sets will be assigned (return by the deadline). You are urged not to start these the night before they are due. For late exercises only **one half points** will be given.
- The most important thing you can learn from homework is how to solve problems yourself. This is what you need to do to succeed in the real world. Therefore, please try each problem for at least 1 hour before discussing it with anyone else.
- Please, write your homework solutions in an extremely clear manner. It will not be possible to give credits for work that is not clearly explained. Please, show your work since this will allow partial credit to be given if you cannot solve the whole problem.
- When it is relevant, use general formulae as long as possible and only plug in numbers at the end of a problem.

Presentation

6

- Presentation (15 min) on one of the suggested topics.
- Practical (or possibly an observational) project.

[?]

Exam

7

- The exam will consist of two large questions requiring a detailed answer, a few questions requiring a few sentence answers, plus two problems similar to (or just from) the home exercises. No help from the books, lecture notes, or any other material is allowed during the exam. A standard non-programmable calculator could be used.

Assessment

8

Your grade will be based on:

- 50% Exam on lecture course
- 30% Homeworks (problems)
- 20% Practical work / presentation

Course Plan

9

- Introduction
 - ▣ Binary Stars and Fundamental Stellar Parameters
- Interaction of stars
 - ▣ The shapes of stars in close binaries
 - ▣ Transfer of mass
 - ▣ Accretion disks
- Nomenclature – the stellar zoo
 - ▣ Cataclysmic Variables
 - ▣ AM CVn binaries
 - ▣ X-ray binaries
 - ▣ Contact binaries
 - ▣ etc
- Close binary evolution

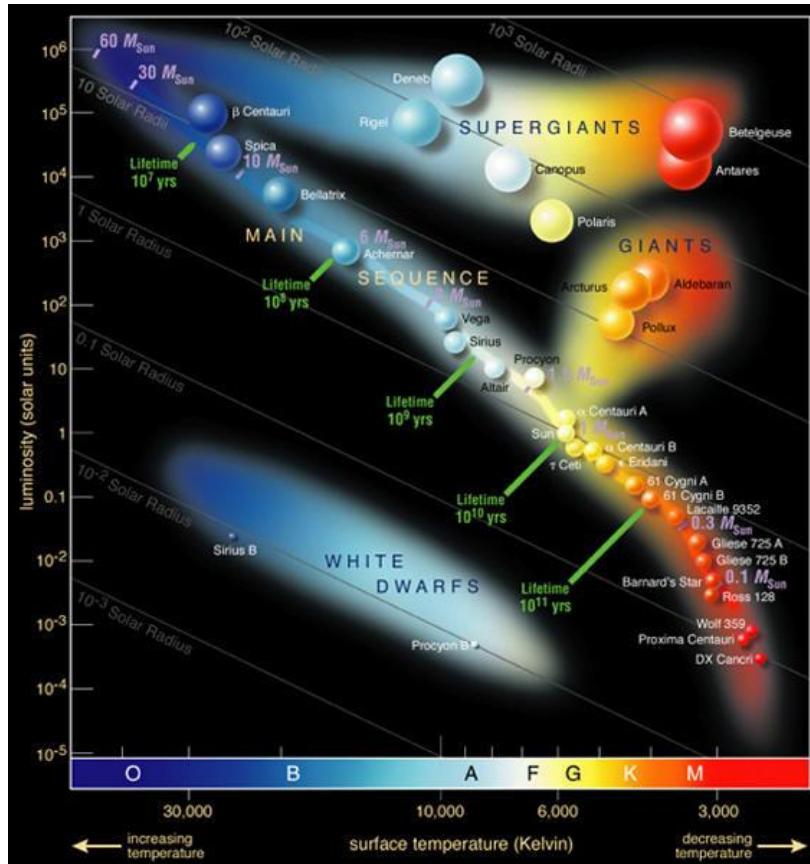
10

Introduction

Binary Stars and
Fundamental Stellar Parameters

How to find the masses of stars ?

11



- Mass: most fundamental of stellar parameters
- Impossible to measure for isolated stars
- Well, then we have to weigh them, i.e to measure gravitational interaction with something else.

Binary Stars

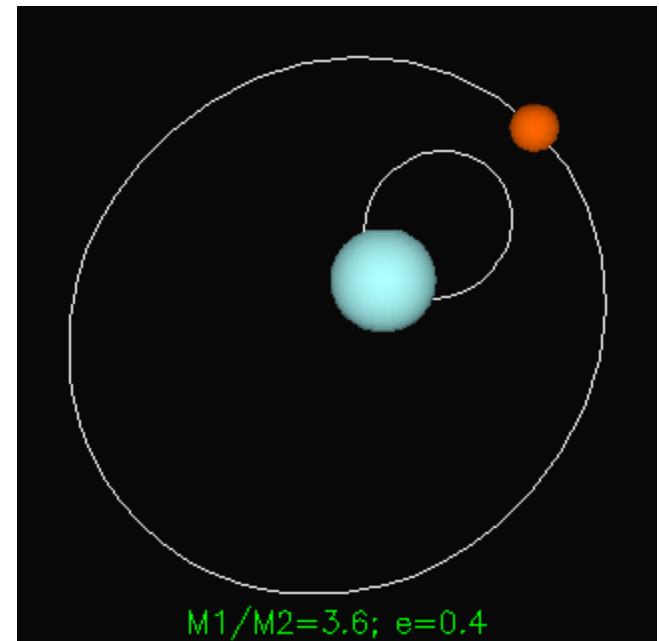
12

- Most stars are not isolated in space.
- About one half of all stars which we see are in a double or multiple star system.
- In a multiple star system, the stars all orbit about the common centre-of-mass of the system.
- This is not accidental! The process of star formation tends to cause many stars to be formed close to each other.

Types of Binary Stars

13

- A double star system where you can see both stars and they appear to move around each other is a **visual binary** (Herschel 1802)
 - >0.2 arcsec
 - both stars seen, orbital motion

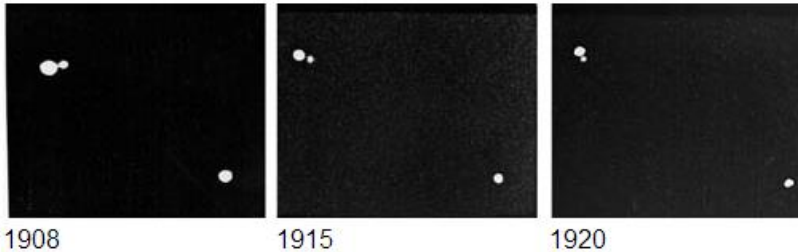


Interacting Binary Stars

Visual Binaries

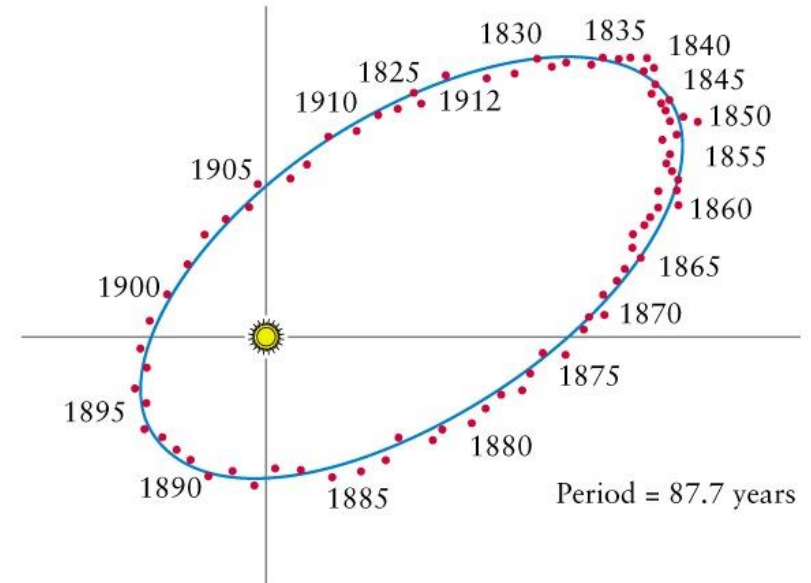
14

Kruegar 60



From 1908 to 1920 the visual binary completed about 1/4 of a revolution.

70 Ophiuchi

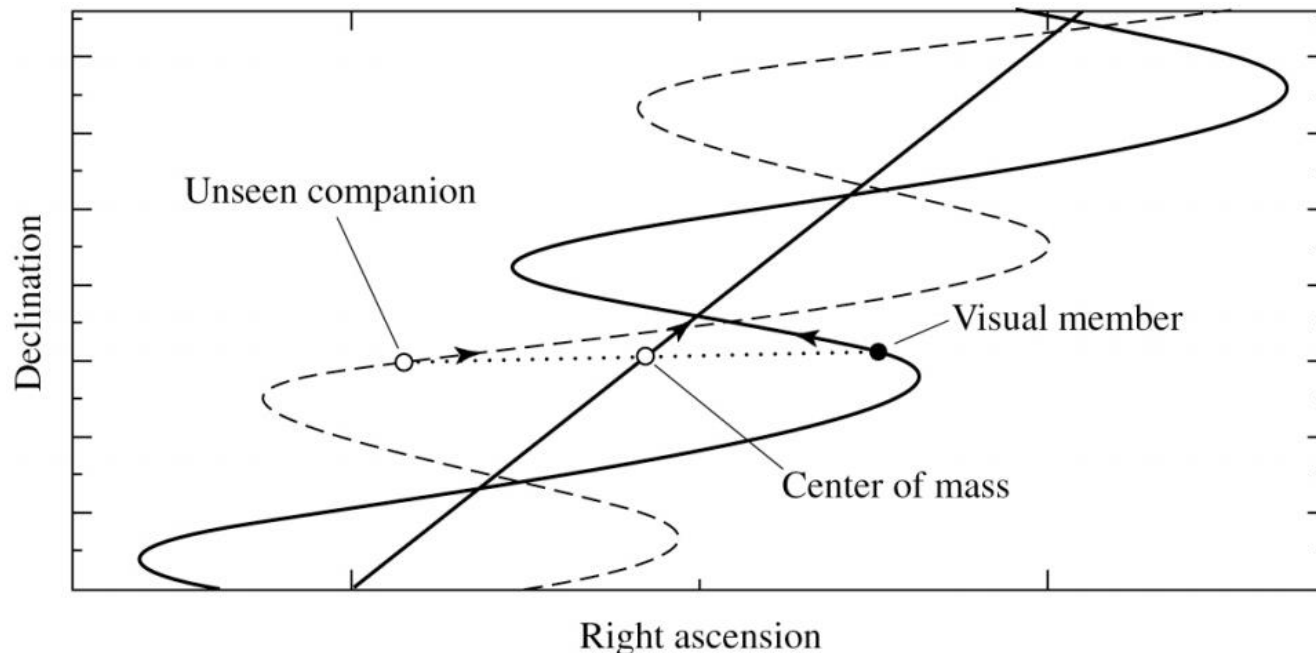


Over the course of 87.7 years, the star makes one full orbit.

Astrometric Binaries (1)

15

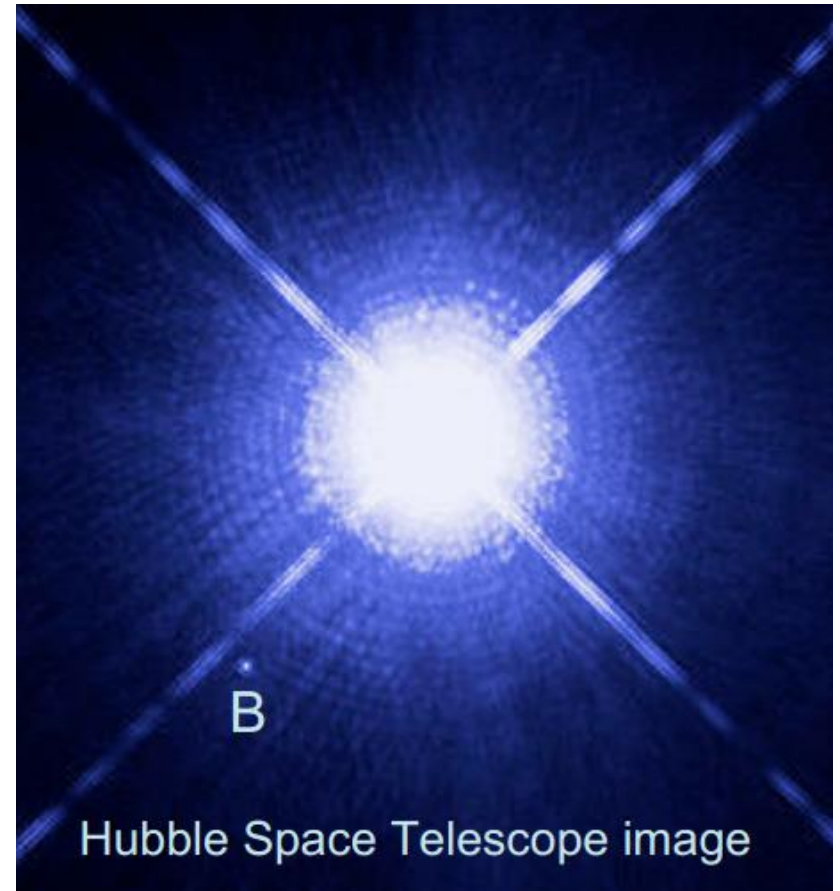
- If only one star is visible, but we can detect that it wobbles about an unseen centre-of-mass, then we have an **astrometric binary**.



Astrometric Binaries (2)

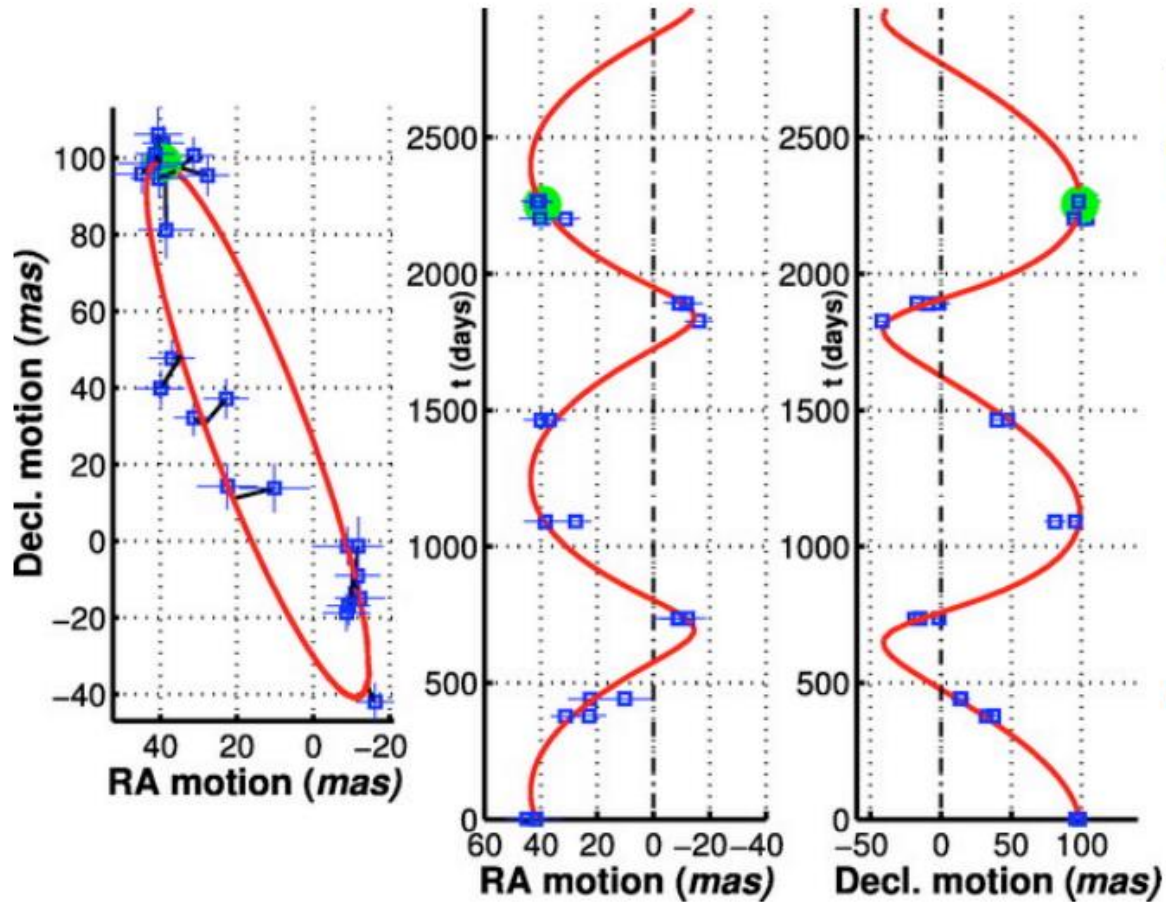
16

- The star Sirius is actually a binary system, but Sirius A is so much brighter than Sirius B that we only see Sirius A.
- Sirius B was first detected by observing the motion of the brighter Sirius A.
- Now also a visual binary.



Astrometric Binary: GJ 802AB

17



unseen
brown dwarf
companion

$a > 0.5-2\text{AU}$

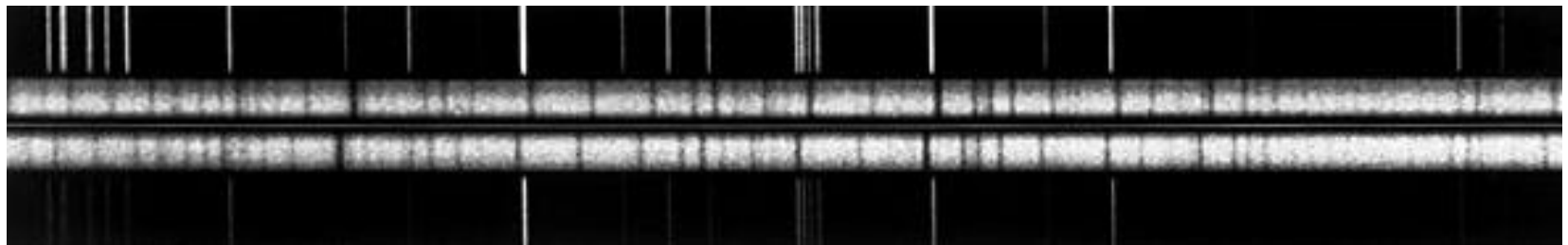
(Pravdo et al. 2005)

Interacting Binary Stars

Spectroscopic Binaries (1)

18

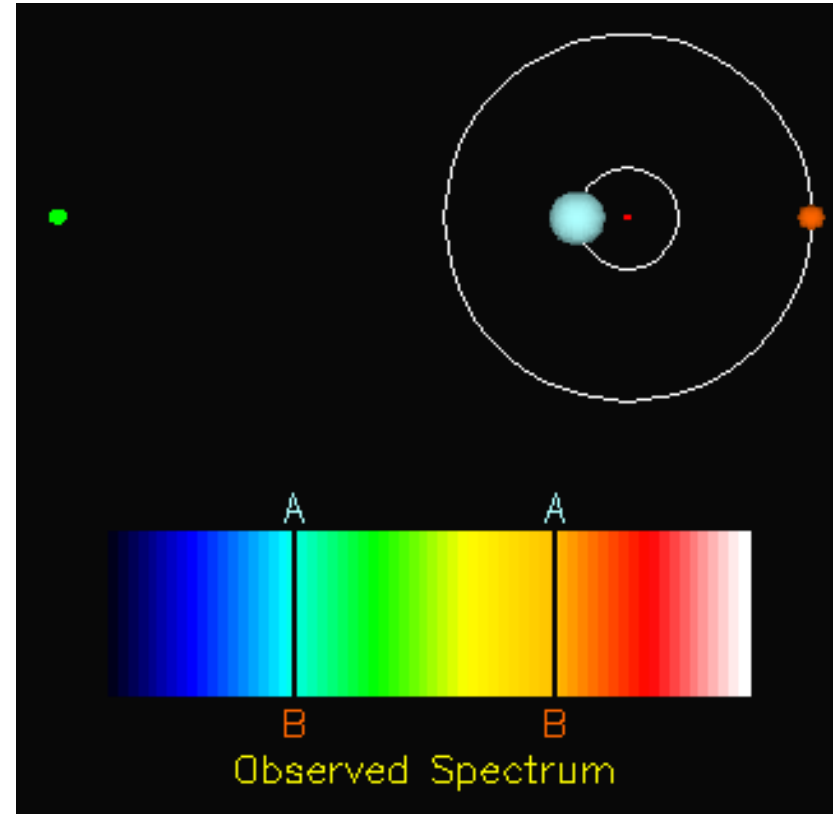
- Sometimes, the only evidence of a binary star comes from the Doppler effect on its emitted light. The spectrum of the star shows Doppler shifts which change from redshift to blueshift periodically.
- **Spectroscopic Binaries**
 - ▣ composite spectra, doppler-shifted lines
 - ▣ SB1, SB2 = spectra from 1 or both stars



Spectroscopic Binaries (2)

19

- The spectral lines in the light emitted from each star shifts first toward the blue, then toward the red, as each moves first toward us, and then away from us, during its motion about their common center of mass, with the period of their common orbit.

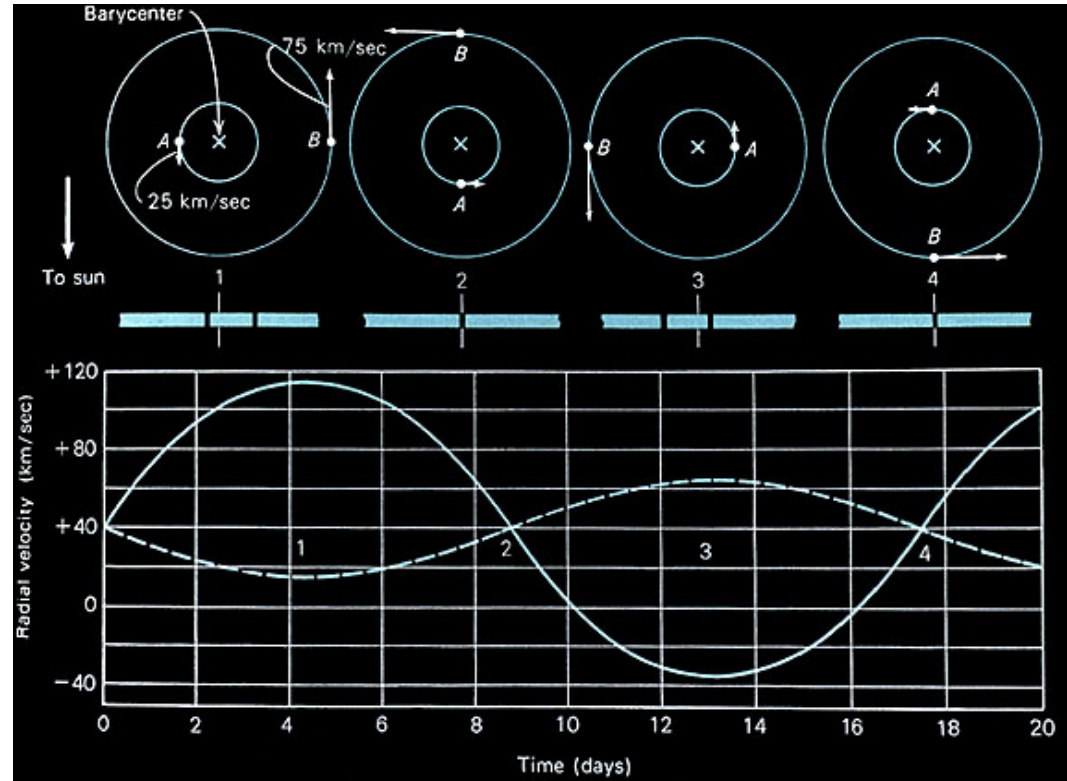


© Richard Pogge (OSU)

Spectroscopic Binaries (3)

20

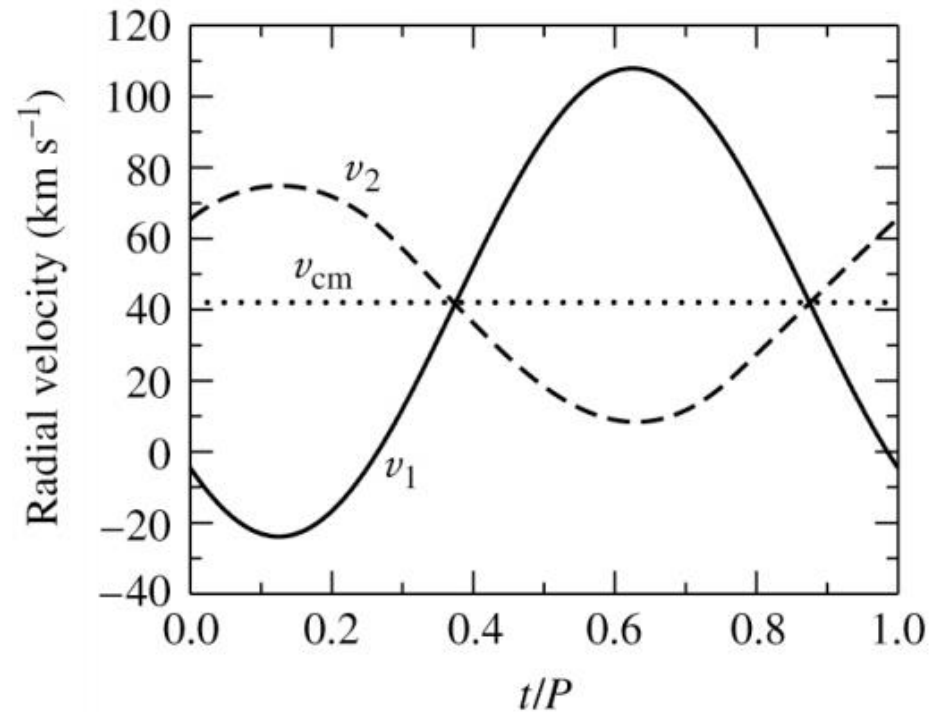
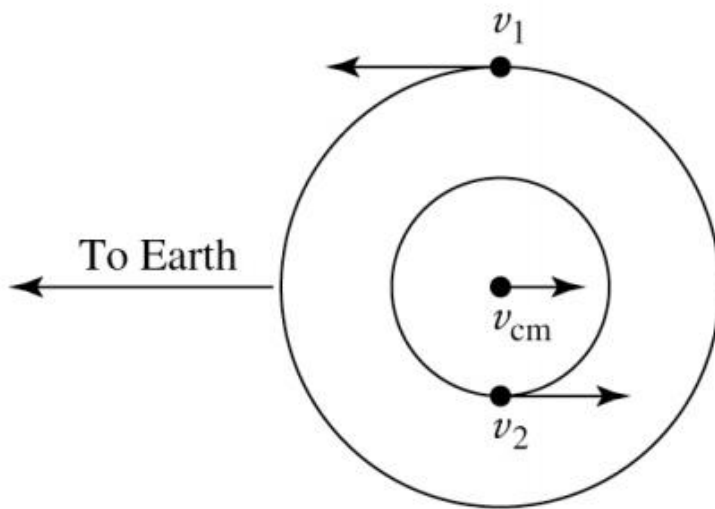
- From the Doppler shift data, we can reconstruct the component of the stars' velocities in our line of sight.
- In *double-lined spectroscopic binaries* it is possible to measure the radial velocity curves of both components, whereas in *single-lined spectroscopic binaries* only one of the radial velocity curves is measurable.
- The true velocities are only known if the binary's inclination angle with our line of sight is known.



Spectroscopic Binaries (4)

21

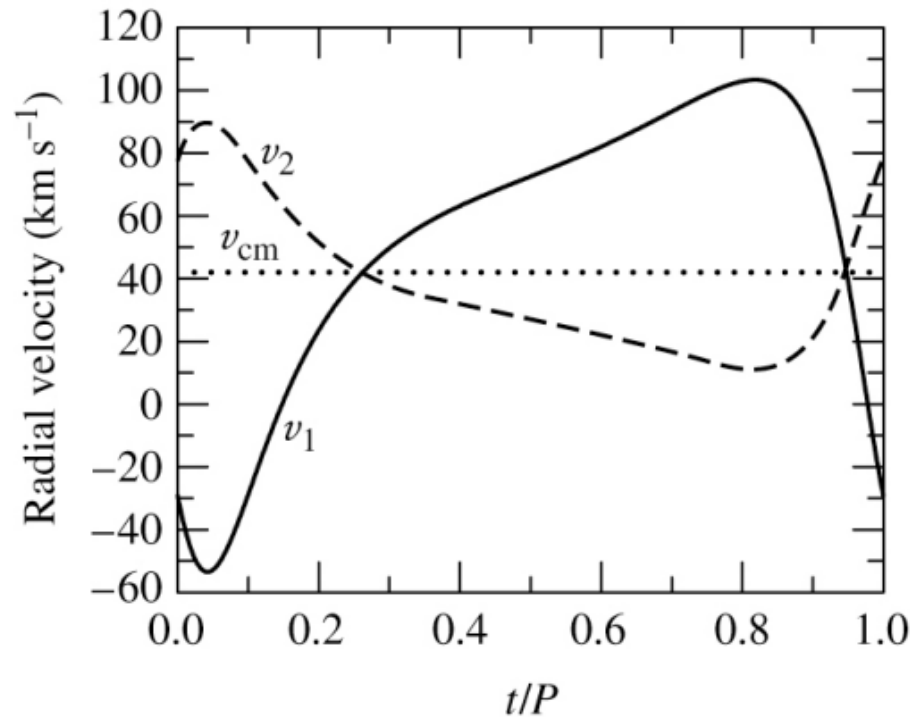
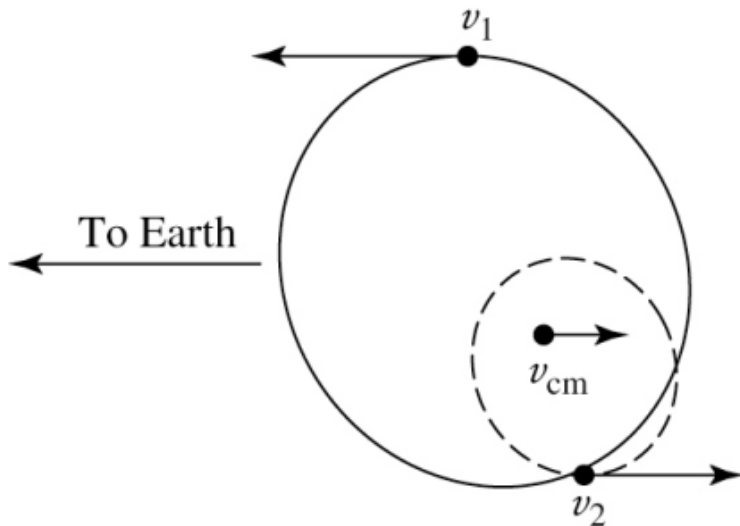
- Radial Velocity curve for Double-lined SB in a Circular Orbit:



Spectroscopic Binaries (5)

22

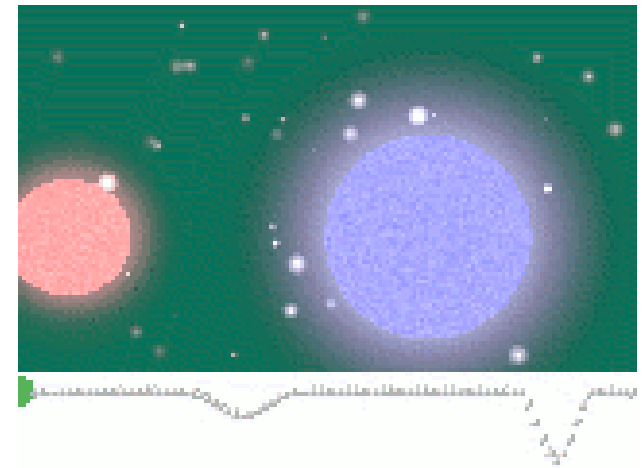
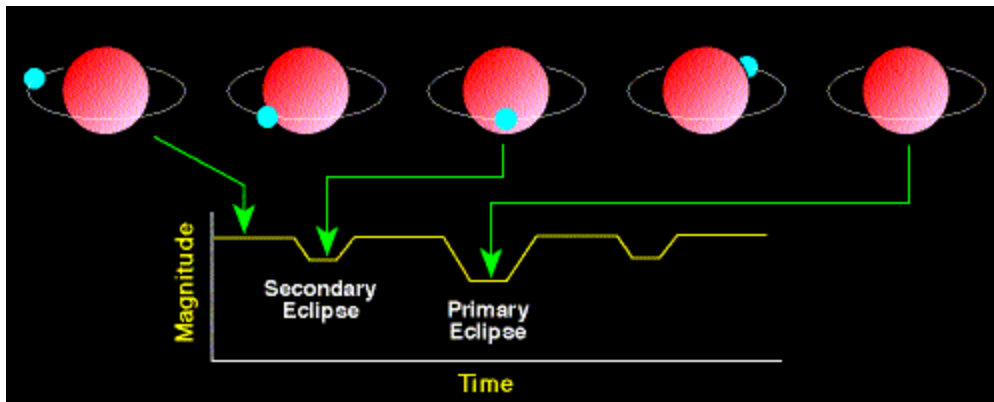
- Radial Velocity curve for Double-lined SB in an Elliptical Orbit ($e=0.4$):



Eclipsing Binaries

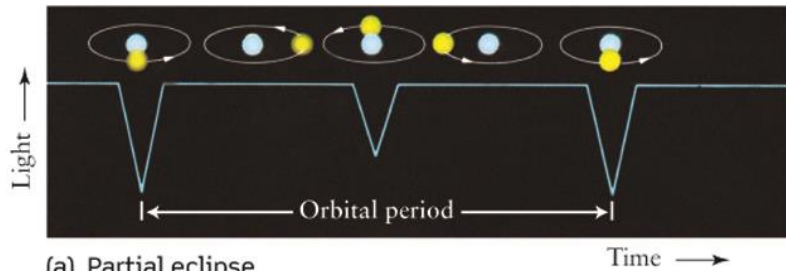
23

- **An eclipsing binary** is a binary which shows regular light variations due to one of the stars passing directly in front of its companion, as viewed from the Earth.

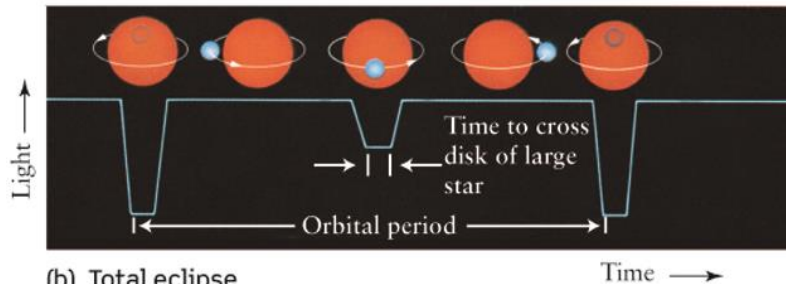


Eclipsing (Photometric) Binaries

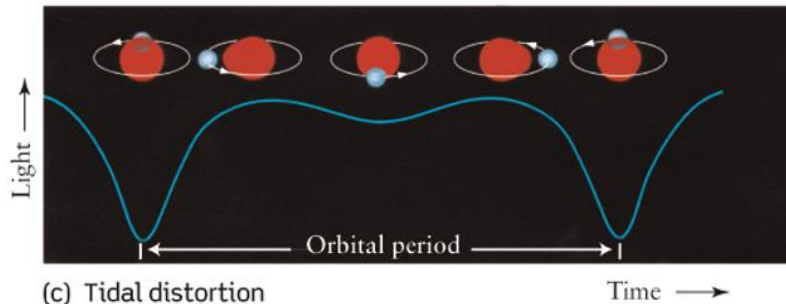
24



(a) Partial eclipse



(b) Total eclipse

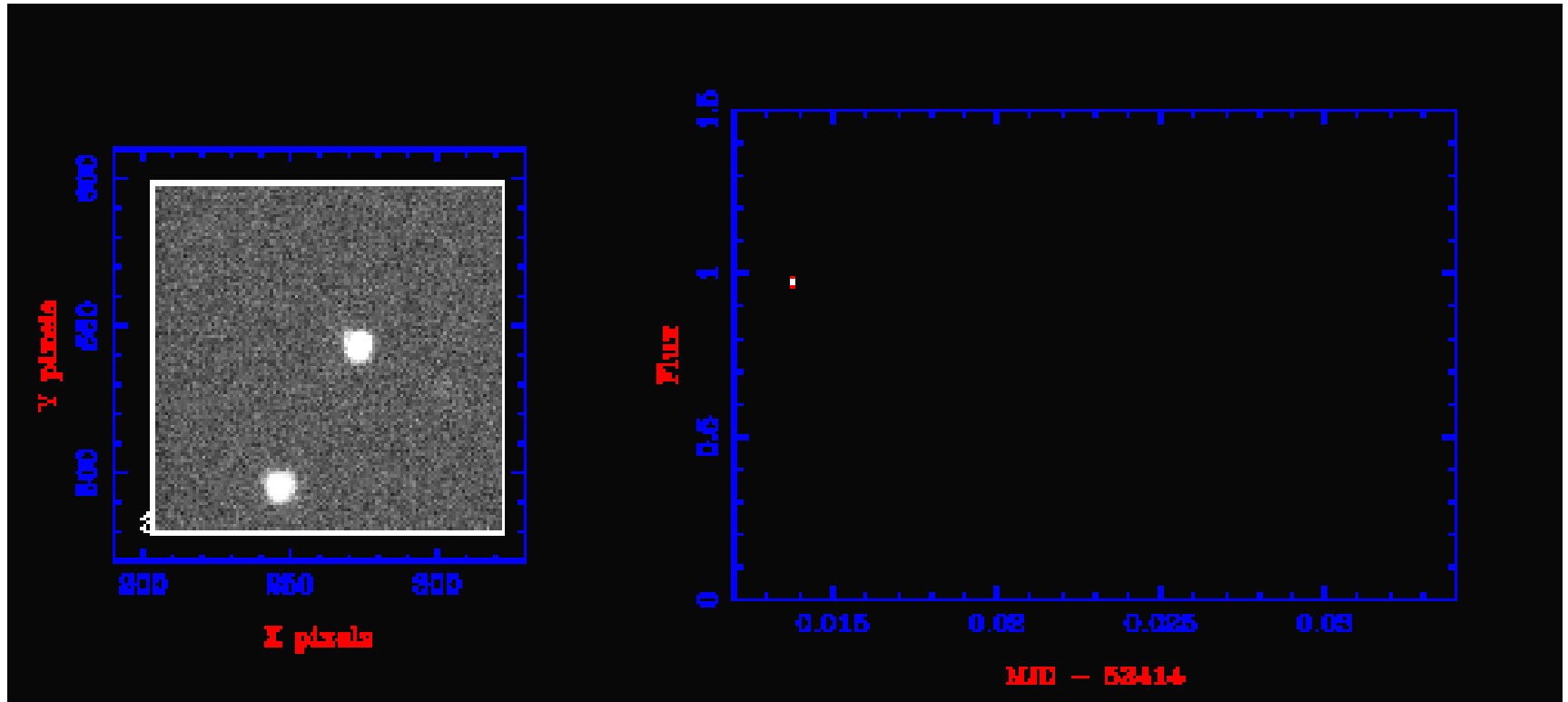


(c) Tidal distortion

- By studying the shape of the eclipses, in conjunction with a knowledge of their radial velocity curves, it is possible to determine the masses and radii of the stars in the binary.
- Eclipsing binaries are hence extremely useful systems.

Totally Eclipsing Binaries (1)

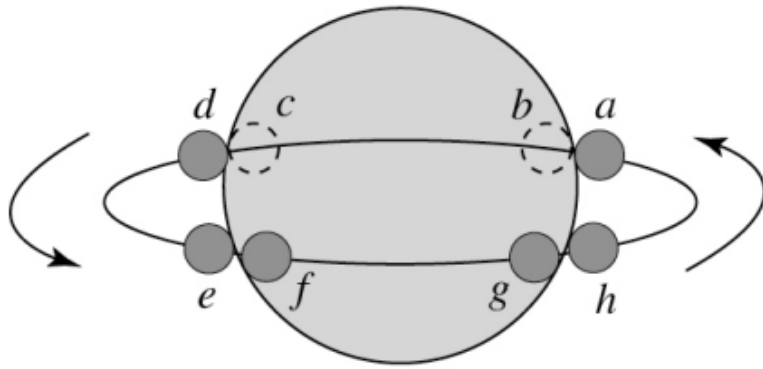
25



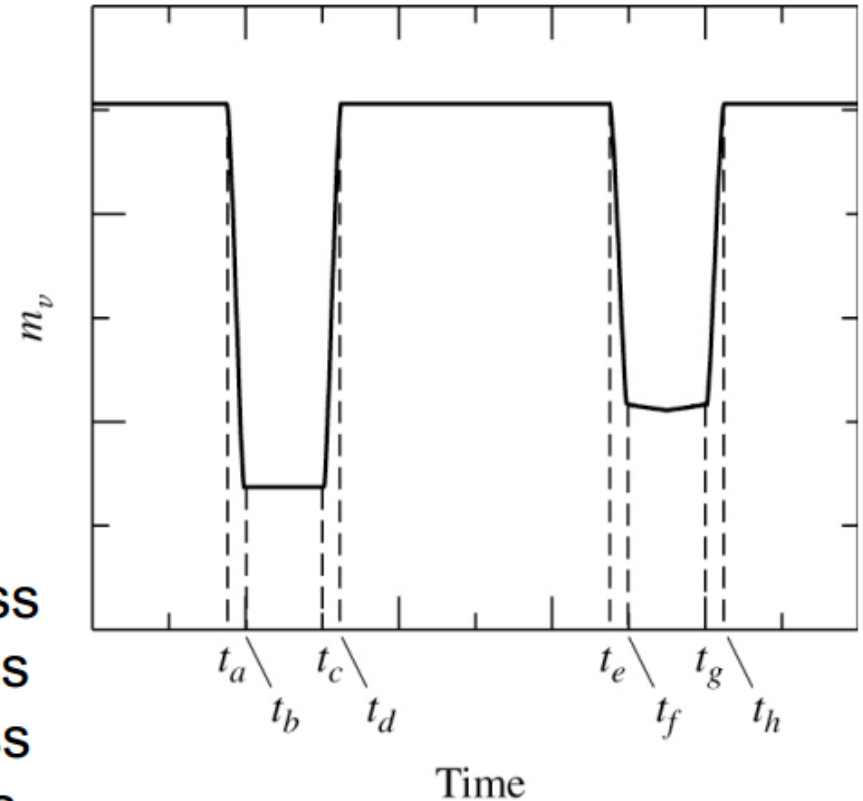
© Vik Dhillon (University of Sheffield)

Totally Eclipsing Binaries (2)

26

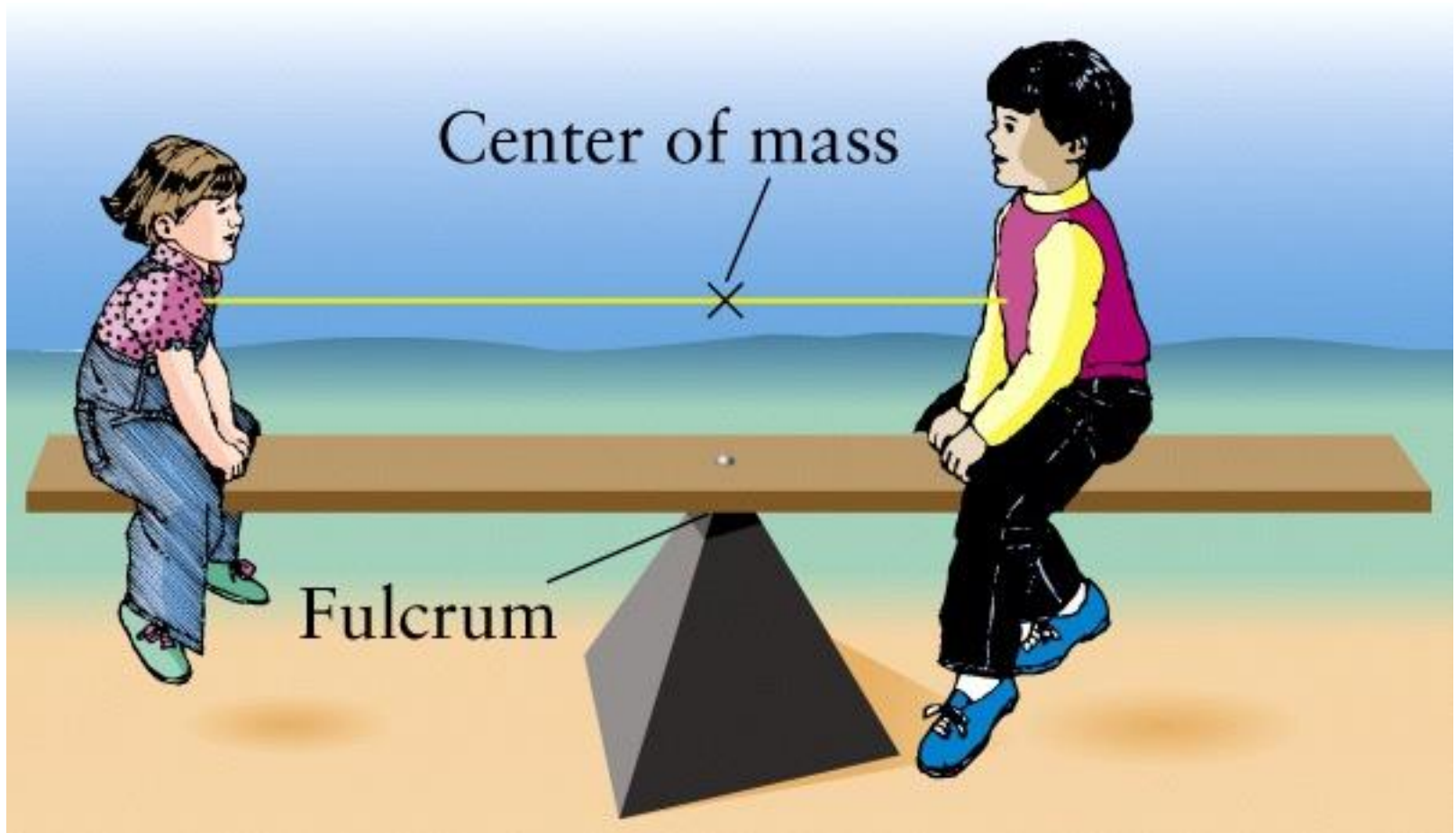


t_a – start of secondary ingress
 t_b – end of secondary ingress
 t_c – start of secondary egress
 t_d – end of secondary egress



Using Binaries to Weigh Stars

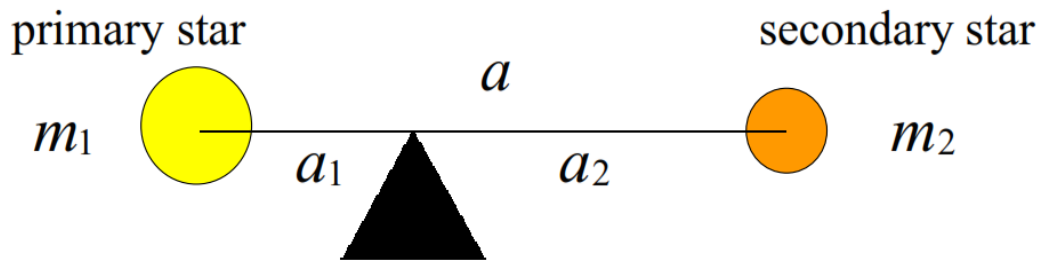
27



Dynamical Mass Determination (1)

28

Centre of Mass



The Centre-Of-Mass Formula is

$$a_1 m_1 = a_2 m_2$$

If orbital major axes (relative to centre of mass) or radial velocity amplitudes are known, then we know the ratio of masses:

$$\frac{m_1}{m_2} = \frac{a_2}{a_1} = \frac{v_{2r}}{v_{1r}}$$

Dynamical Mass Determination (2)

29

- If the period, P , and the sum of semi-major axis lengths, $a = a_1 + a_2$, are known, Kepler's third law can give masses separately:

$$P = \left(\frac{4\pi^2}{G(m_1 + m_2)} a^3 \right)^{1/2}$$

- If only the two radial velocities are known (SB2), the sum of masses (from Kepler's third law) is:

$$m_1 + m_2 = \frac{P}{2\pi G} \left(\frac{v_1 + v_2}{\sin i} \right)^3$$

Dynamical Mass Determination (3)

30

- If only one radial velocity is known (SB1), a useful quantity is the mass function:

$$f(m_1, m_2) = \frac{v_1^3 P}{2\pi G} = \frac{(m_2 \sin i)^3}{(m_1 + m_2)^2}$$

Why ?

- If the orbital inclination, i , is known, this allows determination of m_2/m_1

The mass function

31

- Why the mass function is useful?

$$f(m_1, m_2) = \frac{v_1^3 P}{2\pi G} = \frac{(m_2 \sin i)^3}{(m_1 + m_2)^2}$$

- If **Star 1** is the visible, low-mass companion of the unseen high-mass **Object 2**, so $m_1 \ll m_2$, then

$$f \approx m_2 \sin^3 i$$

- Thus, the mass function f determined from the orbital period P and the radial velocity semi-amplitude v of star 1 gives a lower limit on the mass of the object 2.
- If f appears to be (much) larger than the maximum possible mass for a neutron star ($\sim 2.5 M_\odot$), then star 2 is possibly a black hole.

Determination of Radii and T_{eff} 's

32

- Duration of eclipses and shape of light curve can be used to determine radii of stars:

$$\text{(radius of secondary)} \quad R_s = \frac{v_1 + v_2}{2} (t_2 - t_1)$$

$$\text{(radius of primary)} \quad R_\ell = \frac{v_1 + v_2}{2} (t_3 - t_1)$$

t_1 – start of secondary ingress

t_2 – end of secondary ingress

t_3 – start of secondary egress

- Relative depth of primary (deepest) and secondary brightness minima of eclipses can be used to determine the ratio of effective temperatures of the stars:

$$\frac{F_0 - F_{\text{primary}}}{F_0 - F_{\text{secondary}}} = \left(\frac{T_{e,s}}{T_{e,\ell}} \right)^4$$

Binary Stars (1)

33

- Binary star systems are important because:
 - ▣ they allow us to find the masses and radii of stars
- Test:
 - ▣ stellar evolution
 - ▣ stellar atmospheres
 - ▣ general relativity - pulsars timing
- micro-arcsec tomography
(eclipse / doppler / zeeman)
 - ▣ stellar surfaces
 - ▣ accretion disks

Binary Stars (2)

34

- Properties of some binary stars are inexplicable in terms of the ordinary evolution of isolated stars:
 - ▣ **Algol paradox:** the less massive star ($M_2 = 0.8M_{\text{sun}}$) is already a subgiant, and the star with much greater mass ($M_1 = 3.7M_{\text{sun}}$) is still on the main-sequence.
 - ▣ **Compact binaries:** many binaries containing white dwarfs or other compact stellar remnants have periods $P < 2$ hours, which implies separations $a < R_{\text{sun}}$. Must have been interactions between the progenitors when they were on the main sequence.

Interacting Binary Stars

35

- Resolution of these paradoxical situations is often mass transfer between the components of a close binary.
- By definition, **close (or interacting) binaries** are binary systems in which some significant interaction other than simple inverse square law gravitational attraction between point masses takes place. The interaction may be radiative, as in the heating of the face of one component by a hot companion, or it may be tidal, distorting both components through the combination of gravitational and centrifugal effects.

36

How does mass transfer occur?

Roche lobe and Roche-Lobe overflow

How does mass transfer occur?

37

- Two possible mechanisms for mass transfer between stars in a binary system:
 - Stellar wind accretion:
 - If one component ejects mass in a stellar wind and a part of that material is gravitationally captured by the nearby companion.
 - Roche-lobe overflow:
 - If the binary orbit is sufficiently close, matter from the outer layers of one star can flow directly to the companion.
- Stellar winds from low mass and/or late type stars are not usually strong and mass transfer occurs mainly through **Roche-lobe overflow**.

Roche Model (1)

38

- How large one of the stars can become before it starts to transfer matter to its companion?
- For stars in close binary systems we need to consider the effects of rotational and tidal distortion.
- The stellar surface is determined by the shape of the potential surface $\Phi = \text{constant}$. Thus, determining the shape of a star in a binary is equivalent to determining the shapes of the potential surfaces $\Phi = \text{constant}$.
- A basic tool is the "Roche model": the total potential (gravitational and centrifugal forces) is approximated by the Roche potential Φ_R

Roche Model (2)

39

- Assumptions:
 - ▣ The orbit is **circular**.
 - ▣ Stars **corotate** with the binary system.
 - ▣ The gravitational field generated by the two stars is approximated by that of two **point** masses.

Roche Model (3)

40

- Cartesian coordinates (x,y,z) rotate with the binary, with origin at the primary;
- The x-axis lies along the line of centres;
- The y-axis is in the direction of orbital motion of the primary;
- The z-axis is perpendicular to the orbital plane;
- The total potential:

$$\Phi_{\text{R}} = \underbrace{-\frac{GM(1)}{(x^2 + y^2 + z^2)^{1/2}} - \frac{GM(2)}{[(x - a)^2 + y^2 + z^2]^{1/2}}}_{\text{The gravitational potential due to the two stars}} \underbrace{- \frac{1}{2} \Omega_{\text{orb}}^2 [(x - \mu a)^2 + y^2]}_{\text{The centrifugal potential}}$$

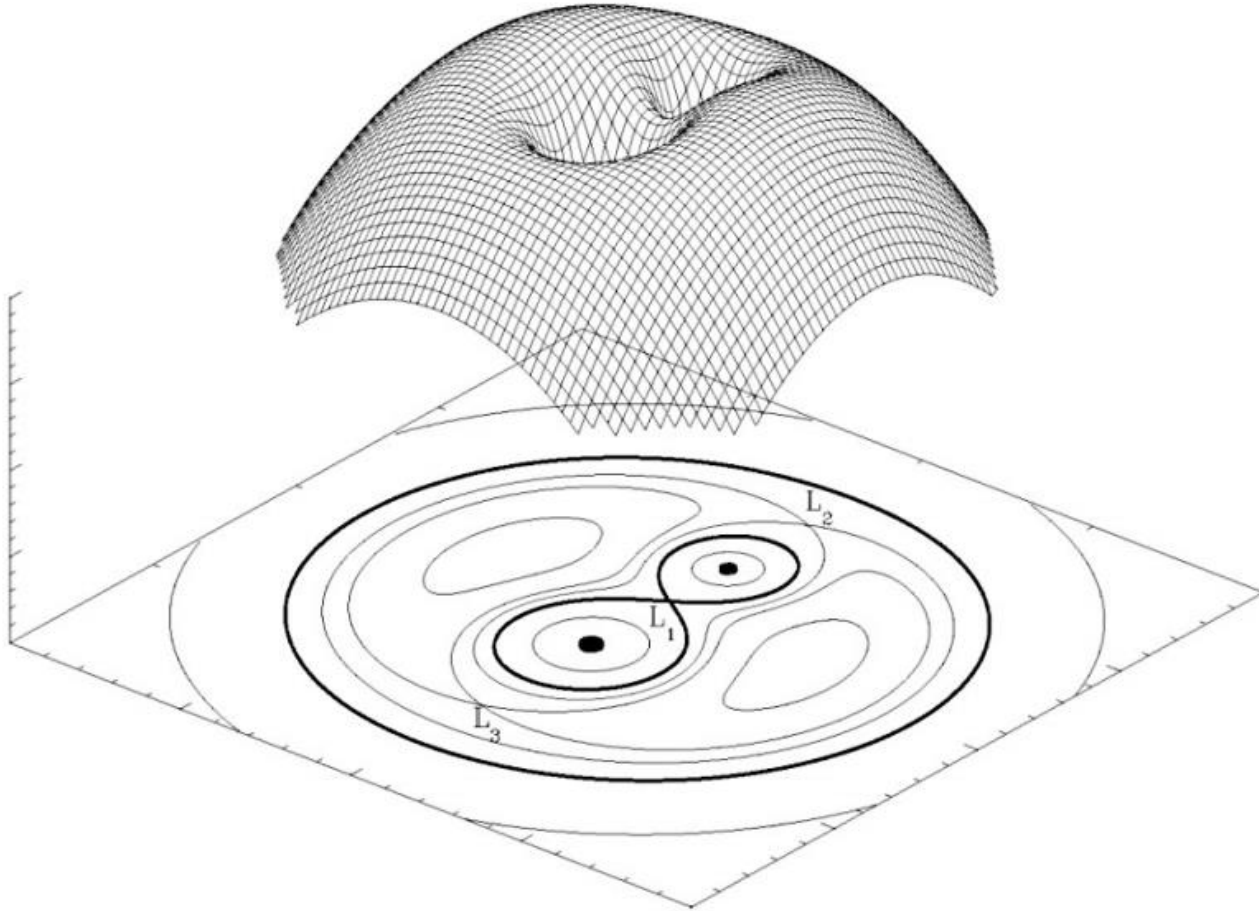
The gravitational potential due to the two stars

The centrifugal potential

where $\mu = M(2)/[M(1) + M(2)]$ and $\Omega_{\text{orb}} = 2\pi/P_{\text{orb}}$.

Roche Model (4)

41



Roche Model (5)

42

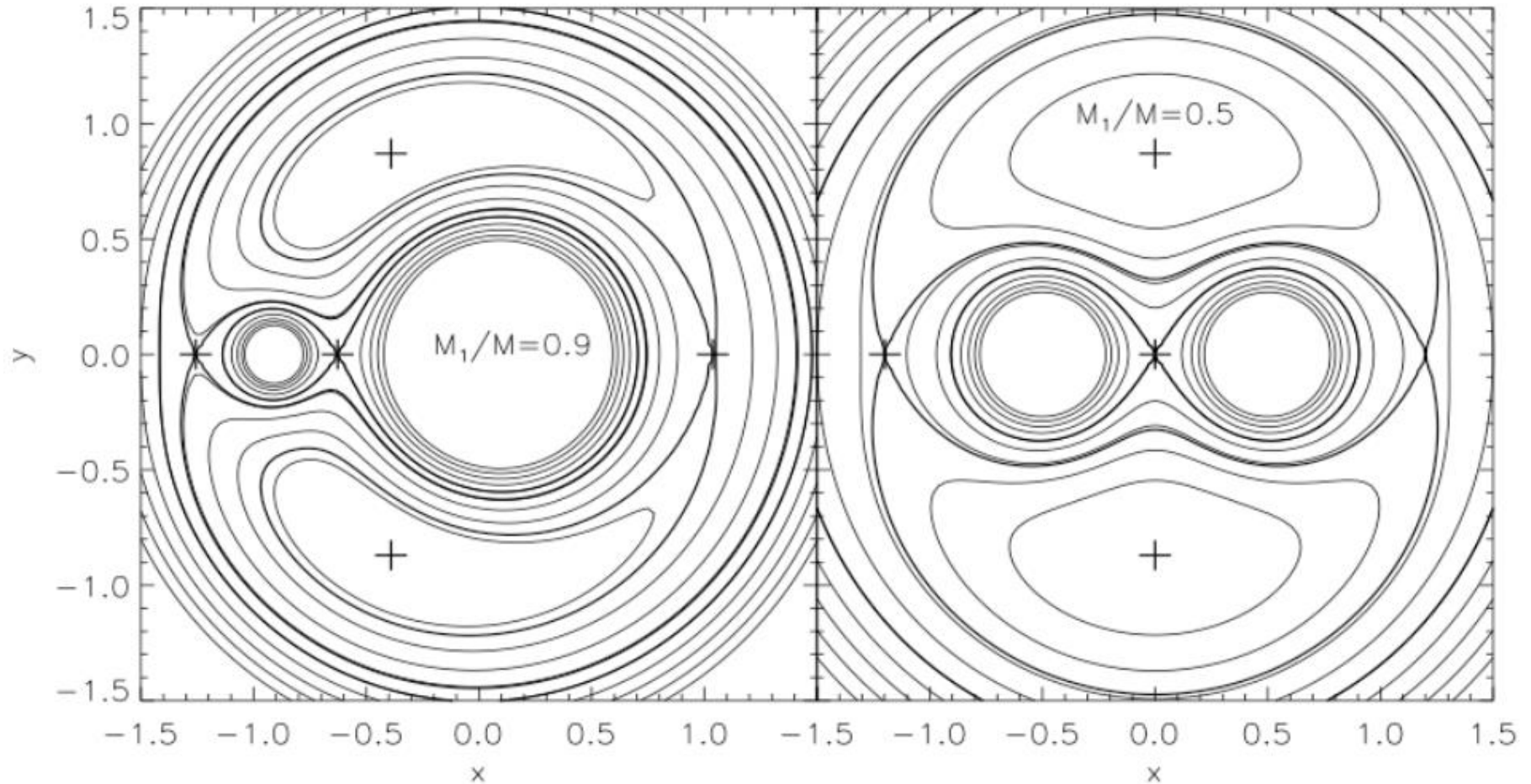
- Combining with Kepler's third law we can see that

$$\Phi_R = \frac{GM(1)}{a} F\left(\frac{x}{a}, \frac{y}{a}, \frac{z}{a}, q\right)$$

- Therefore *the shapes* of the Roche equipotentials, $\Phi_R = \text{const}$, are functions only of q and their scale is determined by a .

Roche Model (6)

43



Interacting Binary Stars

Roche Model (7)

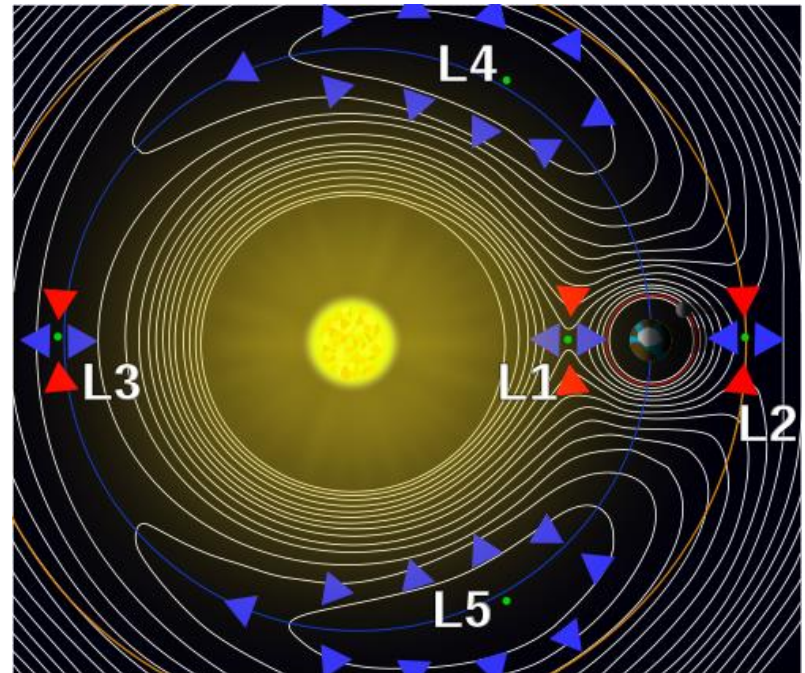
44

- Close to each object, the potential is dominated by the gravitational potential of the star, thus the surfaces are almost spherical.
- As one moves farther from a stellar centre, two effects start to become important:
 - ▣ the tidal effect, which causes an elongation in the direction of the companion
 - ▣ and flattening due to the centrifugal force.
- Consequently the surfaces are distorted in a way that their largest dimension is along the line of centres.
- The innermost equipotential surface which encloses both stars defines the critical “Roche lobe” of each star.

Roche-Lobe overflow

45

- The Roche lobe is the region of space around a star in a binary system within which orbiting material is gravitationally bound to that star.
- Inner Lagrangian point L_1 is the location where a particle, corotating with the binary, feels no net force - gravity from the two stars plus centrifugal force cancel.
- If one star fills its Roche lobe, gas can freely escape from the surface through L_1 and will be captured by the other star.

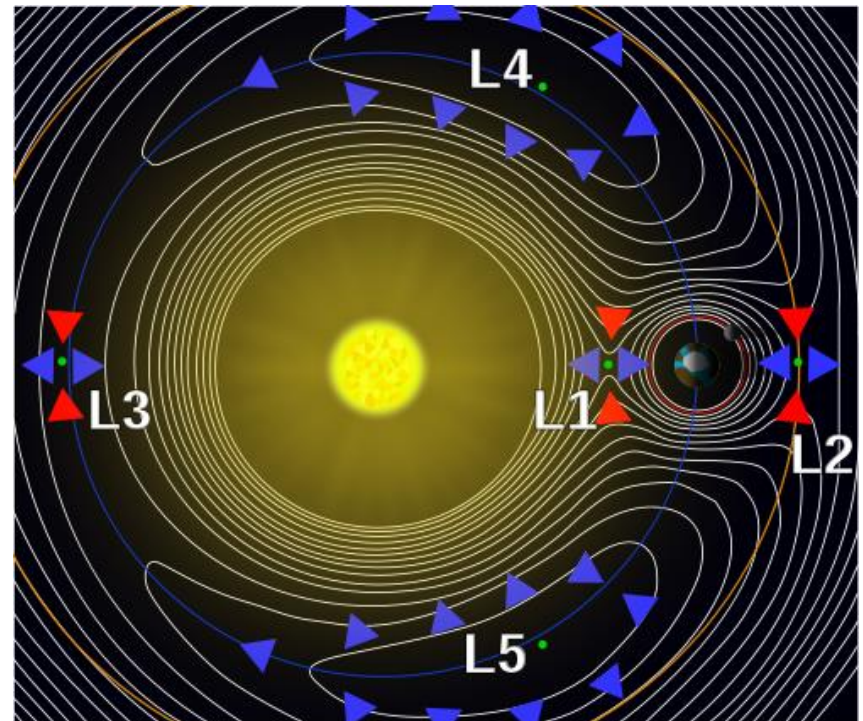


Interacting Binary Stars

Mass transfer and loss (1)

46

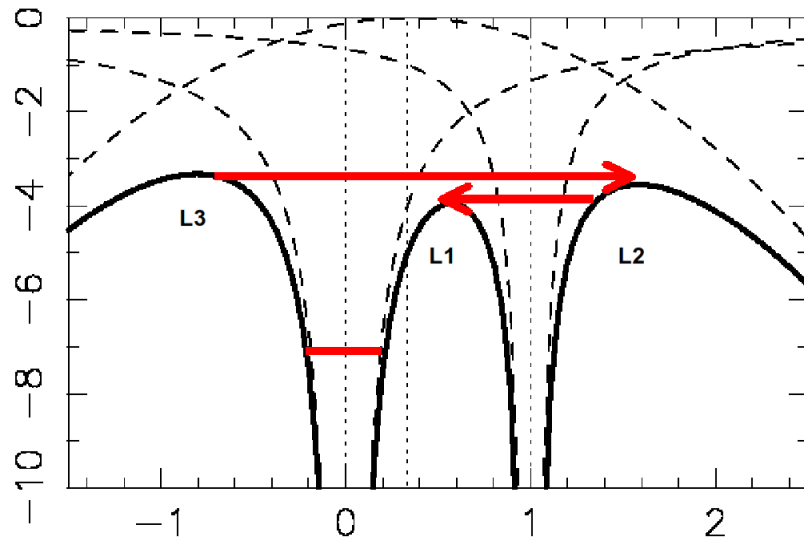
- L_1 – Inner Lagrange Point
 - ▣ matter can flow freely from one star to other
- L_2 – on opposite side of secondary
 - ▣ matter can most easily leave system
- L_3 - on opposite side of primary
- L_4, L_5 – in lobes perpendicular to line joining binary
 - ▣ form equilateral triangles with centres of two stars



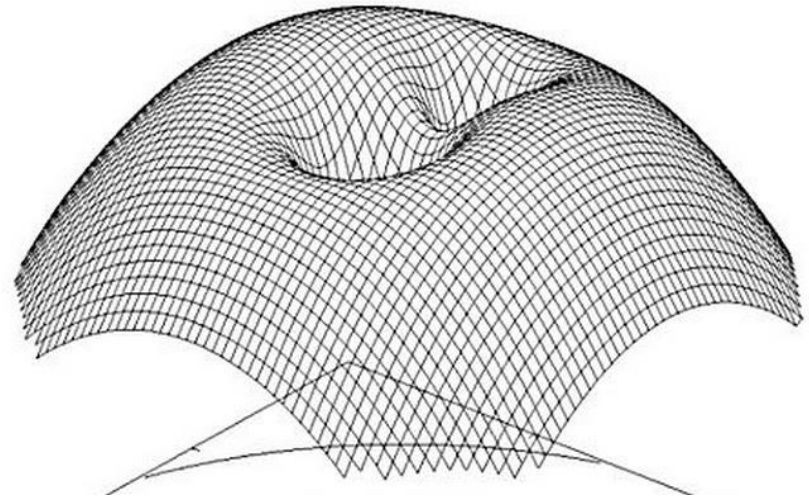
Mass transfer and loss (2)

47

Slice along X axis



X-Y plane, 3D representation



Geometry of the Roche lobe (1)

48

- The precise shape of the Roche lobe must be evaluated numerically. However, for many purposes it is useful to approximate the Roche lobe as a sphere of the same volume. An approximate formula for the radius of this sphere is

$$\frac{R_2}{a} = \frac{0.49 q^{2/3}}{0.6 q^{2/3} + \ln(1 + q^{1/3})}$$

Eggleton (This formula gives results up to 1% accuracy over the entire range of q)

$$q = M_2/M_1$$

Geometry of the Roche lobe (2)

49

- Distance R_{L_1} from centre of primary to inner Lagrangian point:

$$\frac{R_{L_1}}{a} = 1 - w + \frac{1}{3}w^2 + \frac{1}{9}w^3$$

where

$$w^3 = \frac{q}{3(1+q)}$$

$$q \leq 0.1$$

Kopal (1959)

$$\frac{R_{L_1}}{a} = 0.500 - 0.227 \log q$$

$$0.1 \leq q \leq 10$$

Plavec & Kratochvil (1964)

$$= (1.0015 + q^{0.4056})^{-1}$$

$$0.04 \leq q \leq 1$$

error < 1%

Silber (1992)

Geometry of the Roche lobe (3)

50

- Volume radius R_{L2} of the Roche lobe of the secondary:

$$\frac{R_L(2)}{a} = 0.38 + 0.20 \log q \quad 0.3 < q < 20 \quad \text{Paczynski (1971)}$$

accurate to 2%

$$\frac{R_L(2)}{a} = 0.462 \left(\frac{q}{1+q} \right)^{1/3} \quad 0 < q < 0.3 \quad \text{Paczynski (1971)}$$

accurate to 2%

$$\frac{R_L(2)}{a} = \frac{0.49q^{2/3}}{0.6q^{2/3} + \ln(1 + q^{1/3})} \quad 0 < q < \infty \quad \text{Eggleton (1983)}$$

accurate to better than 1%

- Equatorial Roche lobe radius (y direction) of the secondary

$$\frac{R_L(\text{eq})}{a} = 0.378q^{-0.2084} \quad 0.1 < q < 1 \quad \text{Plavec \& Kratochvil (1964)}$$

accurate to 1% over $0.2 \leq q \leq 1$

Reaction to mass loss

51

- Star reacts to mass loss:
 - expands / contracts
 - Roche-lobe also expands or contracts
- $q > 5/6$ - unstable mass transfer
 - Roche lobe shrinks down around the star, stripping it down
 - Rapid (dynamical)
 - violent
 - rare because very fast
 - must occur (more massive stars evolve first)
- $q < 5/6$ - stable mass transfer
 - conservative mass transfer makes Roche lobe expand.
 - – cuts off mass transfer

Mass transfer in binary systems (1)

52

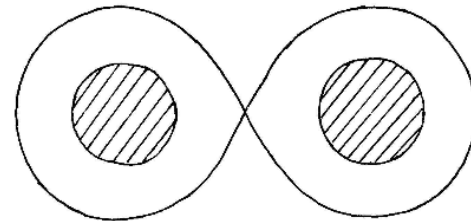
- A star can fill its Roche lobe either:
 - ▣ Due to expansion - e.g. the star swells to become a giant on leaving the main sequence.
 - ▣ Because the Roche lobe shrinks: binary loses angular momentum, stars spiral together, Roche lobe closes in on one or both stars.
- Four cases:
 - ▣ Case A: mass transfer while donor is on main sequence
 - ▣ Case B: donor star is in (or evolving to) Red Giant phase
 - ▣ Case C: donor star is in Super-Giant phase
 - ▣ Case D: donor star is a white dwarf
- Mass transfer changes mass ratio:
 - ▣ changes Roche-lobe sizes
 - ▣ can drive further mass transfer

Mass transfer in binary systems (2)

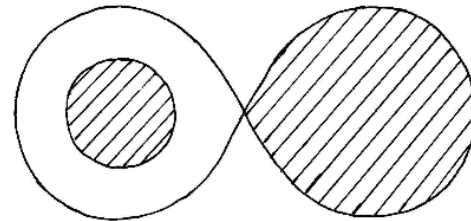
53

□ Describe a binary system as:

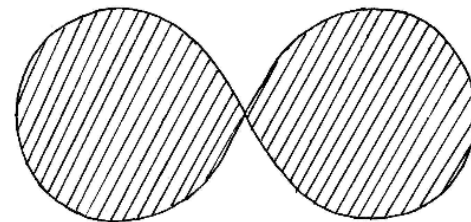
- **Detached:** neither star fills its Roche lobe, both are roughly spherical.
- **Semi-detached:** one star fills its Roche lobe, and is highly distorted. Mass flows onto the other star in the binary.
- **Contact:** both stars fill their Roche lobes - touch at the L_1 point.



DETACHED



SEMI-DETACHED

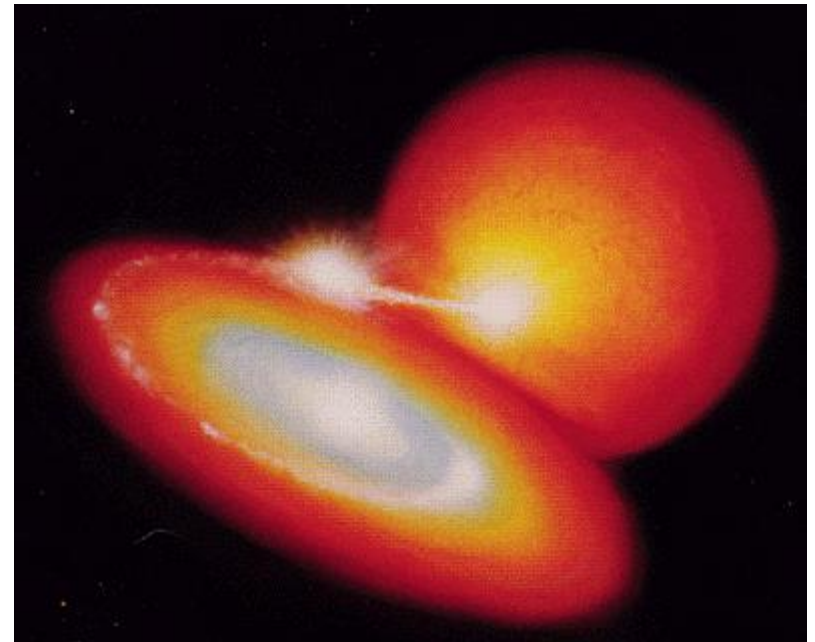


CONTACT

Transfer of matter (1)

54

- In a semi-detached system, gas flowing through L_1 has too much angular momentum to fall directly onto the surface of the other star.
- Gas forms an accretion disk around the mass gaining star, through which the gas slowly spirals in before being accreted.
- This occurs if the accreting star does not have a strong magnetic field.

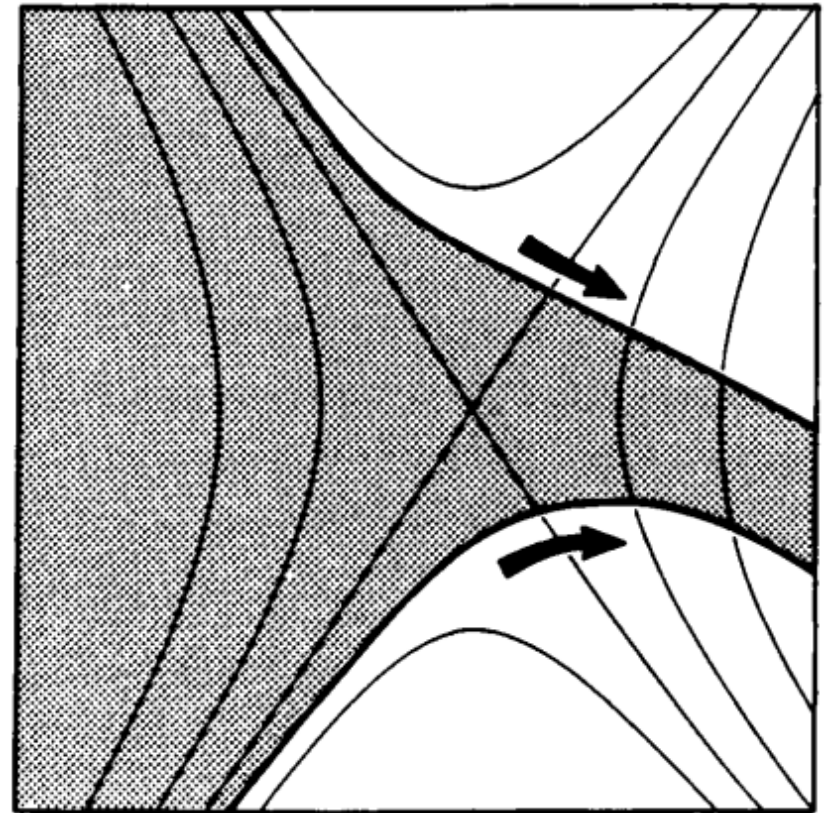


Artist's Conception: Dana Berry, STScI

Transfer of matter (2)

55

- At L_1 gas can escape from the atmosphere of the secondary into the Roche lobe of the primary. The flow resembles the escape of gas through a nozzle into a vacuum
- The flow velocity is approximately the thermal velocity of the atoms in the gas.
- The stream leaving L_1 has a core that is denser than the outer regions; the density profile should be approximately Gaussian.
- Details of the stream lines in the vicinity of L_1 are given by Lubow & Shu (1975).



Transfer of matter (3)

56

- **What happens to the gas after it has flowed through the L_1 point and when it starts to be accelerated towards star 2?**

- The flow velocity through L_1 is roughly equal to the sound speed in the atmosphere of the mass-losing star:

$$c_s \cong 15\sqrt{T_4} \text{ km s}^{-1}$$

where T_4 is in the units of 10^4 K.

Rough
estimate

- T varies from $\sim 3000\text{K}$ to $\sim 30000\text{K}$
- Thus, $c_s \approx 10\text{-}30 \text{ km/s}$

Transfer of matter (4)

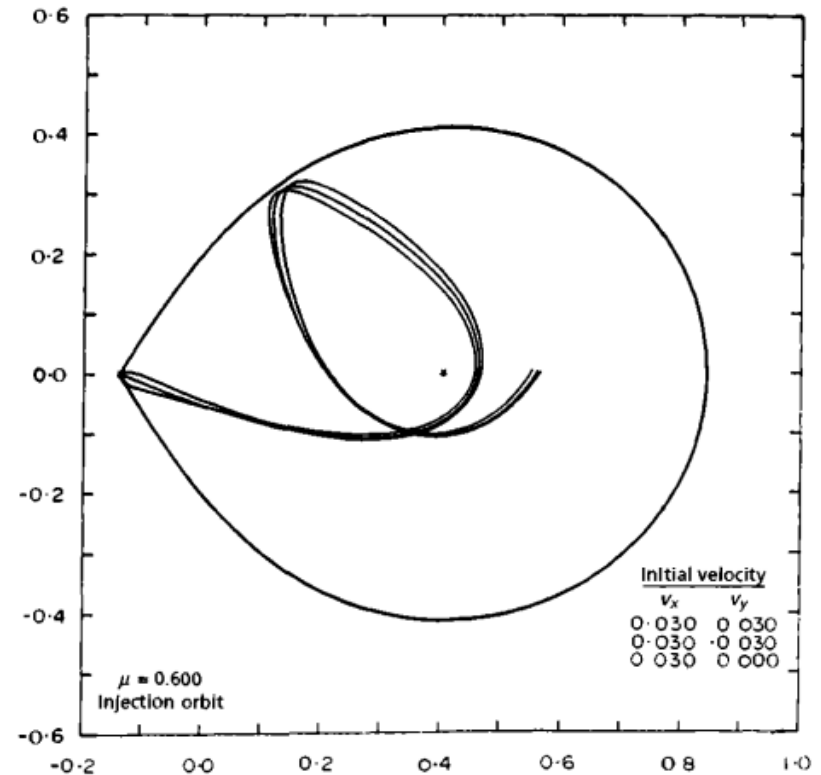
57

- As the stream of gas flows away from L_1 the stream lines are deflected by the Coriolis effect and make an angle with the x-axis that is a function only of q .
- After leaving L_1 the gas particles fall towards the primary, which increases their original sonic velocities to highly supersonic:
compare with the dynamical velocity of the binary system (the orbital velocities of the stars).
- In general, the sound speed of the gas is much less than the dynamical velocities of the stars: $c_s \ll V_{\text{orb}}$

Transfer of matter (5)

58

- The stream expands transversely at the velocity of sound, so pressure forces are soon negligible and the stream trajectory is well described by following the orbits of single particles ejected from L_1 in all directions at sonic velocities.



Transfer of matter (6)

59

- The stream trajectory can be found from integrating the equations of motion for a particle in the rotating binary frame.
- In conserving energy along the trajectory, a particle obeys the equation

$$\frac{1}{2}\dot{r}^2 + \Phi_R = \text{const}$$

- If a particle starts with almost zero velocity ($\dot{r} = 0$) on the Roche lobe, it does not have sufficient energy to cross the lobe at any other point.
- Thus the trajectory lies entirely within the Roche lobe of the primary and whenever the particle approaches the lobe it does so with low velocity.
- The Roche lobes are therefore also known as zero velocity surfaces.

Transfer of matter (7)

60

- Flannery (1975, MNRAS, 170, 325):

The equations of motion are formulated in the conventional RTB problem frame of reference which corotates with the binary, and the physical variables are reduced to the standard dimensionless variables. Scale factors for relevant physical quantities are the following: length, the binary separation A ; mass, the binary total mass M ; time, the inverse of the orbital circular frequency ω^{-1} ; velocity, ωA ; energy, GM/A ; and the angular momentum, ωA^2 . The blue star is designated as star 1 and has mass fraction μ , i.e. $M_1 = \mu M$. With the X axis along the line of centres and the coordinate origin at the centre of mass, the equations of motion are

$$\ddot{x} = 2\dot{y} + x - \mu \frac{(x-x_1)}{r_1^3} - (1-\mu) \frac{(x-x_2)}{r_2^3}, \quad (1)$$

$$\ddot{y} = -2\dot{x} + y - \frac{\mu y}{r_1^3} - (1-\mu) \frac{y}{r_2^3}, \quad (2)$$

where $r_1(r_2)$ is the particle's distance from star 1(2), and dots represent time derivatives. The quantities j_t and r_t defined above are evaluated as



RTB –
restricted
three-body
approximation

Transfer of matter (8)

61

- The stream has a distance of closest approach r_{\min} from the centre of the primary, obtainable from trajectory computations, and approximated to 1% accuracy by

$$\frac{r_{\min}}{a} = 0.0488q^{-0.464} \quad 0.05 < q < 1$$

- If $R_* > r_{\min}$ then the stream strikes the surface of the star directly.
- However, if this is a compact star (a white dwarf, neutron star or black hole), then the stream fails to strike the star directly.
- Instead, the gas flow undergoes self interaction as a consequence of which it **circularizes**.

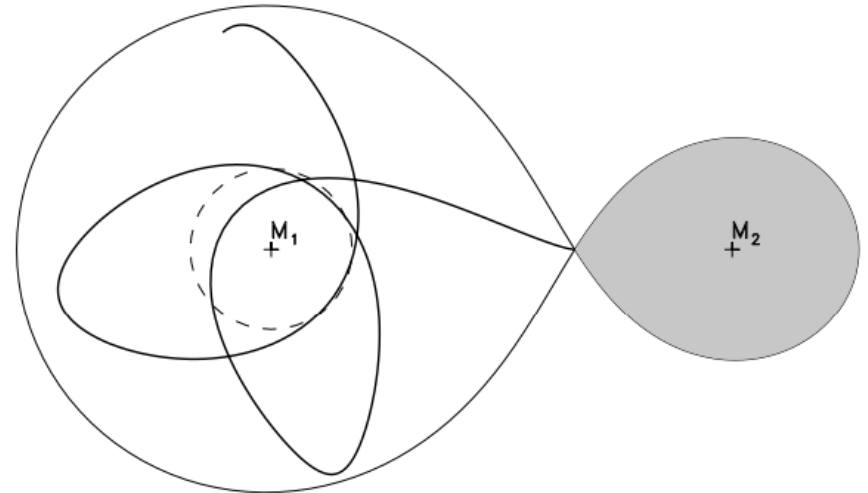
Accretion Disks

Formation of an Accretion Disk,
Tidal limitations,
Boundary layer,
Bright spot,
Stream-Disk overflow

Formation of a Ring (1)

63

- Angular momentum is conserved.
- A circular orbit has the least energy for a given angular momentum → the dissipation will tend to produce a ring of gas.
- Circularization Radius \approx same angular momentum as L_1 .



Formation of a Ring (2)

64

- A circular orbit at a distance R from the primary has a Keplerian velocity

$$V_K(R) = \sqrt{\frac{GM}{R}}$$

- If the gas continues to conserve angular momentum while dissipating energy, the radius of the circularization radius r_{circ} is determined from

$$r_{\text{circ}} V_K(r_{\text{circ}}) \approx \frac{2\pi}{P_{\text{orb}}} R_{L1}^2$$

Formation of a Ring (3)

65

- Then

$$\frac{r_{circ}}{a} = (1 + q) \left(\frac{R_{L1}}{a} \right)^4 \approx (1 + q) (0.5 - 0.227 \log q)^4$$

- A more accurate value (to 1%):

$$\frac{r_{circ}}{a} = 0.0859 q^{-0.426} \quad 0.05 \leq q < 1$$

$$r_{circ} \sim 1.75 r_{min}$$

- If angular momentum was conserved, material would stay in a ring without expanding or accreting onto the primary.

Formation of an Accretion Disk (1)

66

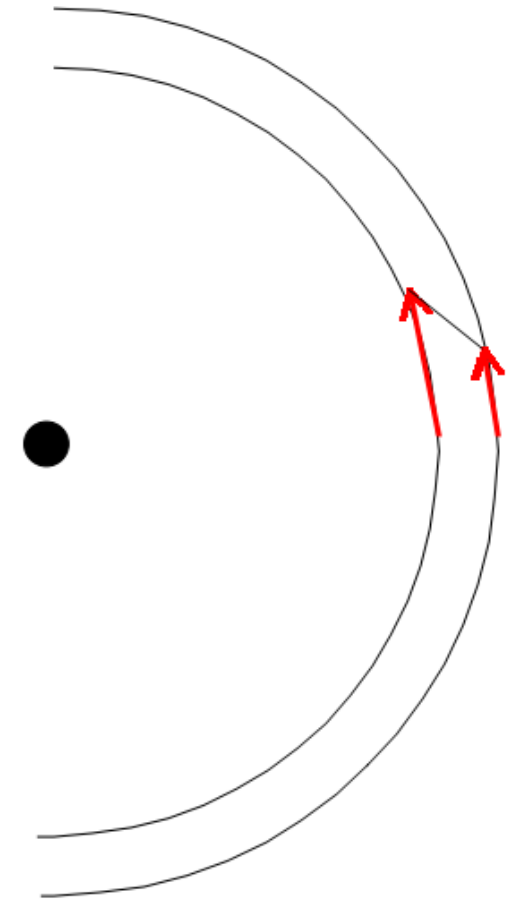
- The ring that is formed has a finite radial extent and rotates differentially.

- Kepler Velocity: $V = \sqrt{\frac{GM}{R}}$

- Differential rotation (Shear):

$$\Delta V = \frac{d}{dR} \left(\sqrt{\frac{GM}{R}} \right) \Delta R = \frac{V}{2} \frac{\Delta R}{R}$$

- Friction:
 - ▣ opposes shear
 - ▣ causes ring to spread inward + outward
 - ▣ Diffusion

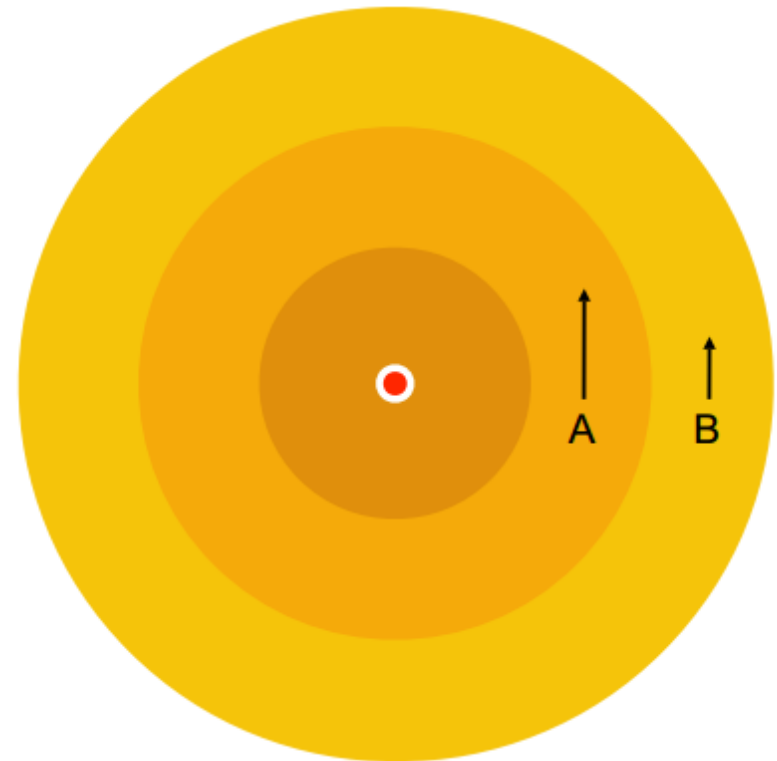


Interacting Binary Stars

Formation of an Accretion Disk (2)

67

- Ring A moves faster than ring B. Friction between the two will try to slow down A and speed up B.
- Angular momentum is transferred from A to B.
- If ring A loses angular momentum, but is forced to remain on a Kepler orbit, it must move inward! Ring B moves outward (which has friction with a ring C, which has friction with D, etc.).
- Disk is formed!



Formation of an Accretion Disk (3)

68

FITdisk

(<https://vitaly.neustroev.net/teaching/tools/fitdisk.zip>)

69

Energetics of accretion

Energetics of accretion (1)

70

- Accretion disks are important in astrophysics as they efficiently transform gravitational potential energy into radiation.
- The gas accreted in a mass transfer binary must lose the gravitational potential energy liberated as it falls toward the mass gaining star. If this energy is radiated, luminosity is:

$$L \approx \frac{GM\dot{M}}{R},$$

where M and R are the mass and radius of the accreting star, and \dot{M} is the mass transfer.

Energetics of accretion (2)

71

- The luminosity of an accretion disk is the bigger the larger the mass flow rate is, the higher the mass of the accretor is, and the more compact the accretor is.
- Compare to the rest mass energy of the gas accreted per unit time:

$$\dot{M}c^2$$

- Efficiency of the accretion process (fraction of the rest mass energy that is radiated):

$$\varepsilon \approx \frac{GM\dot{M}}{R} \times \frac{1}{\dot{M}c^2} = \frac{GM}{Rc^2}$$

Energetics of accretion (3)

72

- Accretion onto a **main sequence star**: as template we take the Sun: $M=1.99 \cdot 10^{33}$ g, $R=6.96 \cdot 10^{10}$ cm:

$$\varepsilon \approx 2 \cdot 10^{-6}$$

- Compare to nuclear fusion of hydrogen to helium. Energy release is $6 \cdot 10^{18}$ erg per gram of hydrogen:

$$\varepsilon_{H \rightarrow He} \approx 7 \cdot 10^{-3} \quad (0.7\%)$$

- Thus, the specific energy output of accretion onto a main sequence star is more than three orders of magnitude less efficient than the hydrogen-helium fusion.
- The absolute values of energy output, i.e., the luminosity, however, depend also on the amount of mass involved in the fusion and the accretion process.

Energetics of accretion (4)

73

$$\varepsilon \approx \frac{GM\dot{M}}{R} \times \frac{1}{\dot{M}c^2} = \frac{GM}{Rc^2}$$

- Accretion onto a **white dwarf**: typical mass 10^{33} g, $R=10^9$ cm:

$$\varepsilon \approx 10^{-4}$$

- Accretion energy is still much smaller - if the accreted hydrogen burns on the surface of the white dwarf can release a lot more energy.
- However, it becomes an interesting energy source in such systems by the sheer fact that nuclear fusion does no longer happen in white dwarfs.

Energetics of accretion (5)

74

- **A neutron star:** typical mass $3 \cdot 10^{33}$ g, $R=10^6$ cm:

$$\varepsilon \approx 0.2$$

$$\varepsilon \approx \frac{GM\dot{M}}{R} \times \frac{1}{\dot{M}c^2} = \frac{GM}{Rc^2}$$

- **A black hole:** The radius of the horizon is given by the Schwarzschild radius: $R_{BH} = R_{Sch} = \frac{2GM}{c^2}$

However, for a non-rotating black hole the innermost stable orbit is $R = 3R_{Sch}$ (for rotating, or Kerr black holes, $R < 3R_{Sch}$). Thus,

$$\varepsilon \approx 1/6$$

- **Very high efficiency - accreting neutron stars and black holes in binaries are luminous sources, normally in X-ray radiation.**

75

Observational Evidence for ADs

Observational Evidence for Accretion Disks (1)

76

- Direct observational evidence for accretion disks in form of a spatially resolved picture of such a disk does not yet exist:
even in the nearest disk-containing systems the angular size of the disk is far below available angular resolution.
- At a distance of $D \sim 50 \text{ pc}$ and with a radius of $r \sim 1 R_{\odot}$, the disk subtends an angle $< 0.2 \text{ mas}$.
- Thus all evidence for accretion disks must necessarily be indirect.

Observational Evidence for Accretion Disks (2)

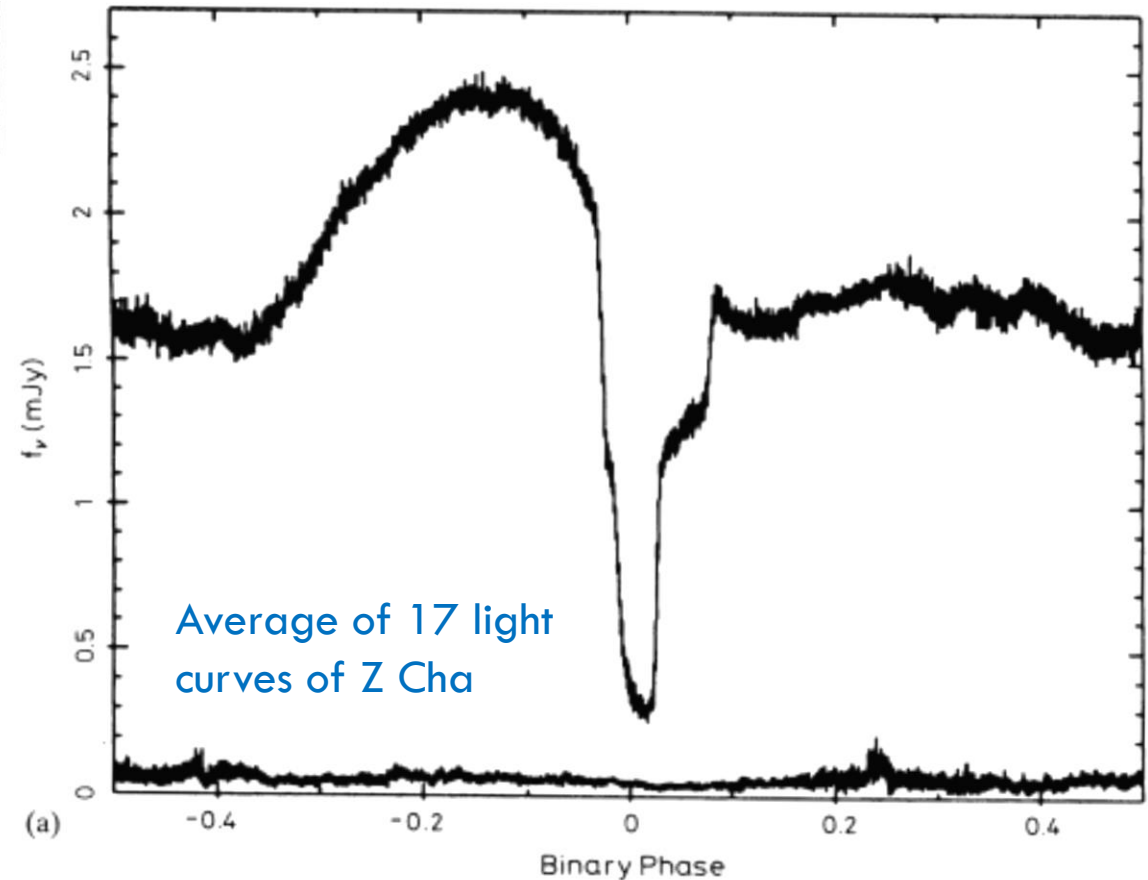
77

- There are two pieces of evidence:
 - ▣ the results of light curve analysis of eclipsing systems
and
 - ▣ the interpretation of the line profiles of the observed spectra.

Light curves of eclipsing CVs (1)

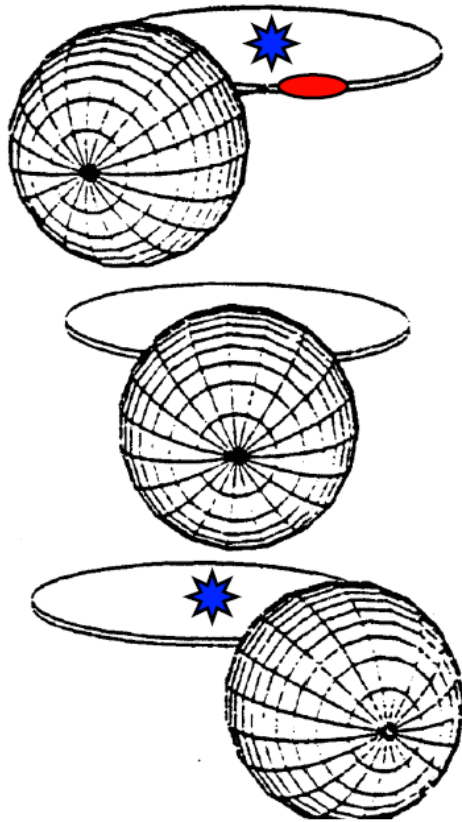
78

Cataclysmic variables (CVs) - binary star systems that have a white dwarf and a low-mass normal star companion. They are typically small – the entire binary system is usually the size of the Earth-Moon system – with an orbital period of 1 to 10 hours.

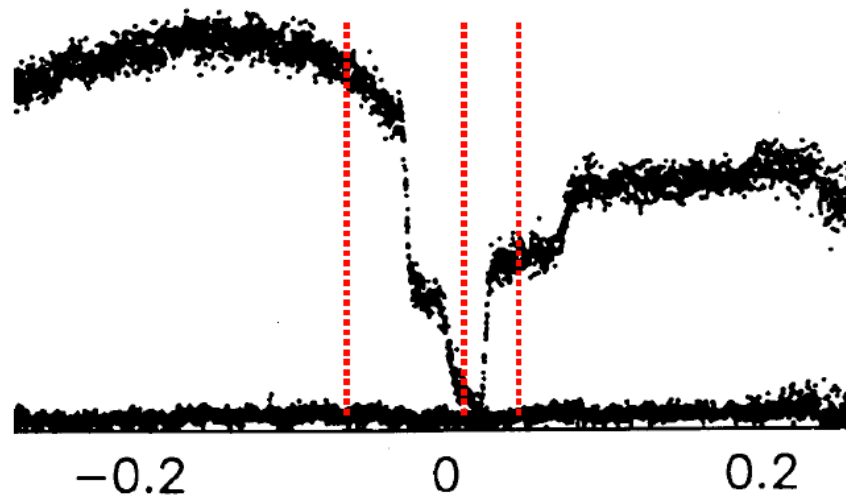


Light curves of eclipsing CVs (2)

79



OY Car in quiescence



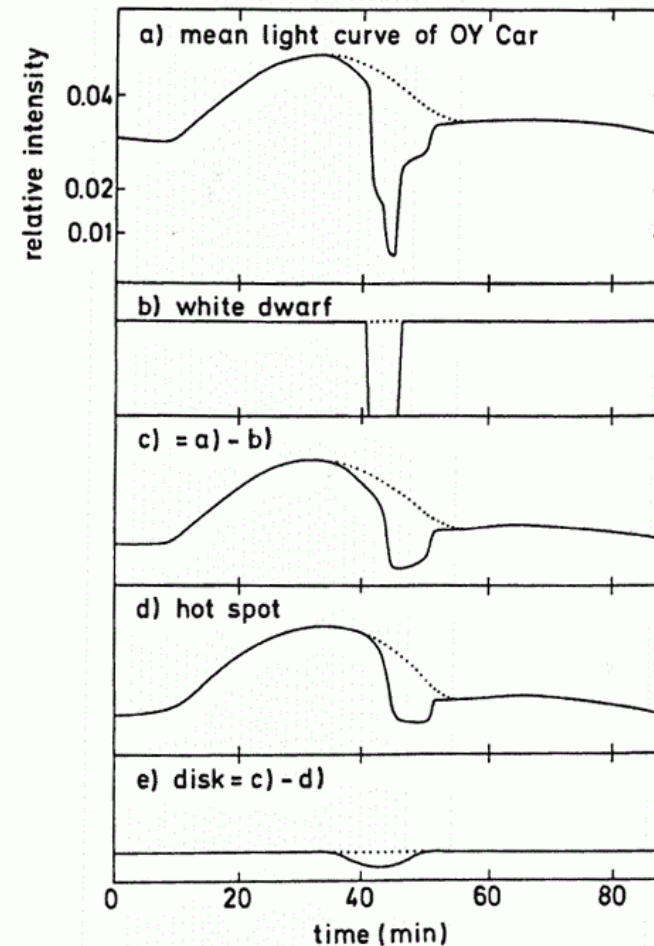
Binary Phase

from Wood et al. 1989,
ApJ, 341, 974

Light curves of eclipsing CVs (3)

80

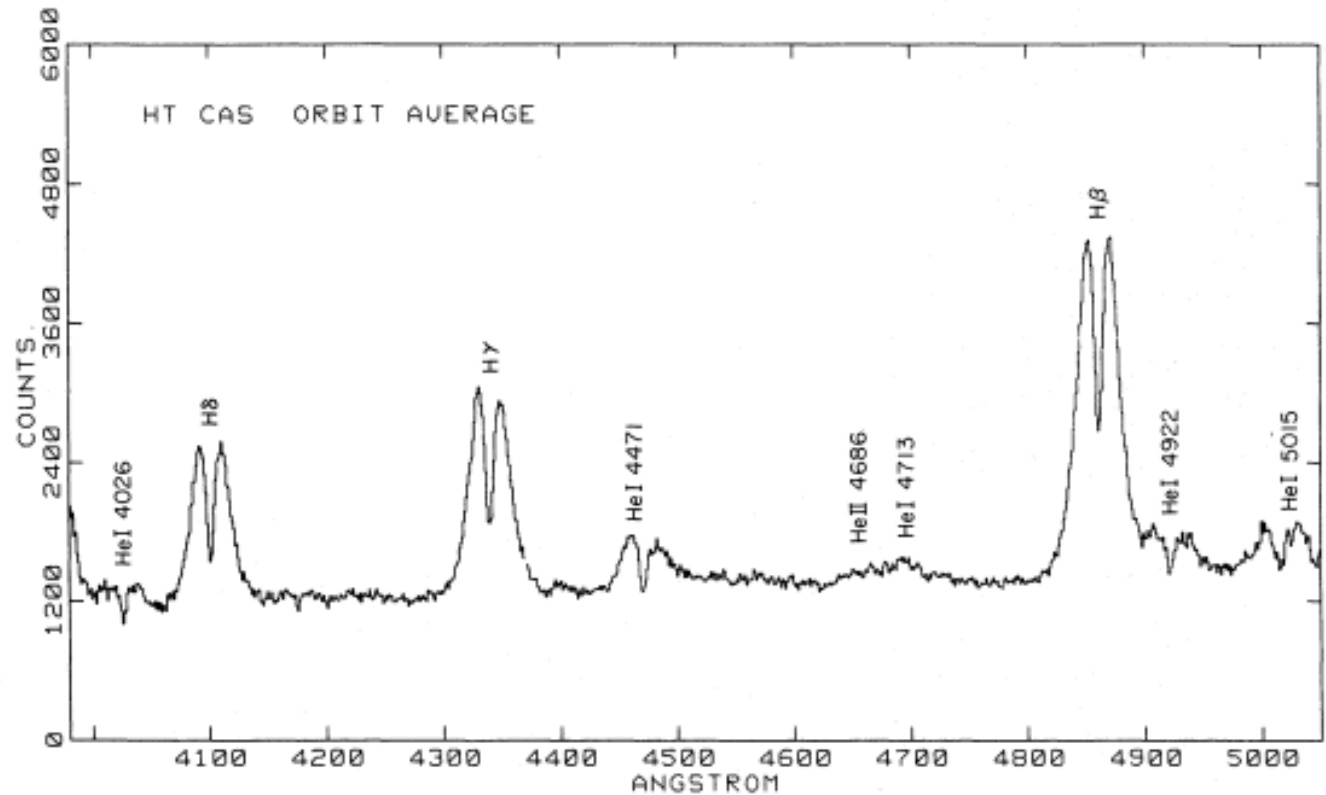
An observed light curve can be decomposed into the various contributions.



Spectroscopy: Emission line profiles (1)

81

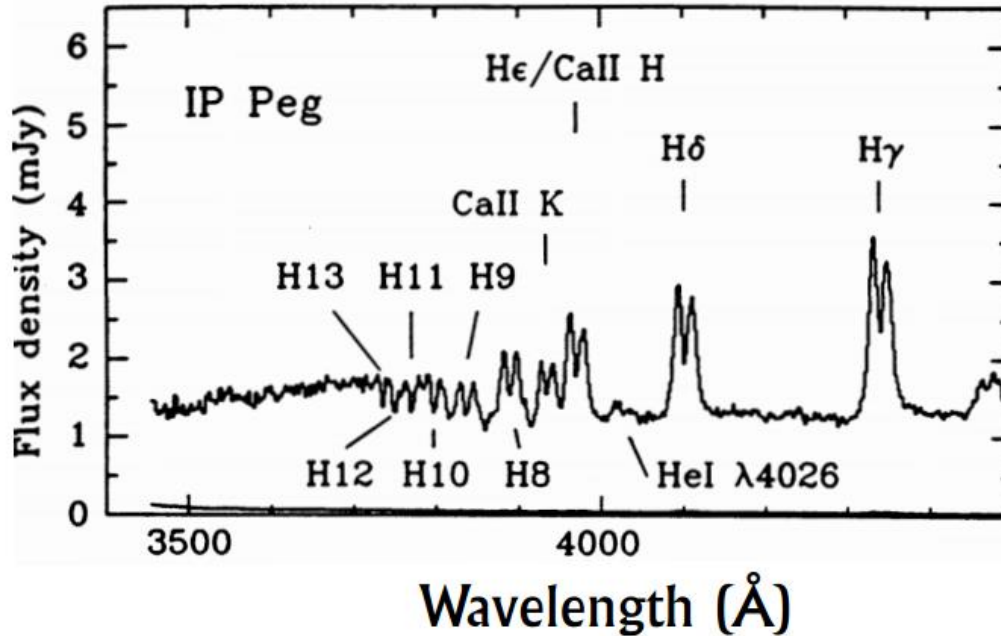
Mean spectrum of HT Cas outside eclipse



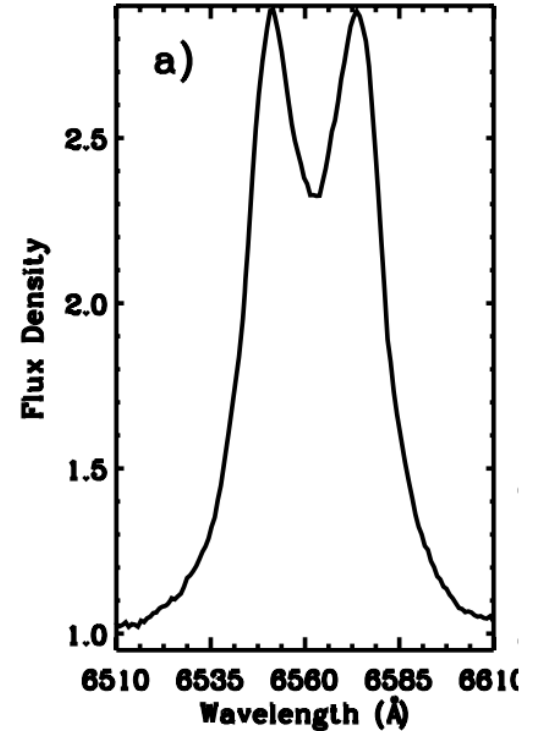
Very broad double-peaked emission lines of nearly the same width. The dominant broadening mechanism is the Doppler shift due to rotation of the accretion disk around the accretor.

Spectroscopy: Emission line profiles (2)

82



IP Peg in low state
from Marsh 1988,
MNRAS, 231, 1117



A 0620-00
Nielsen et al. 2008,
MNRAS, 384, 849

Interacting Binary Stars

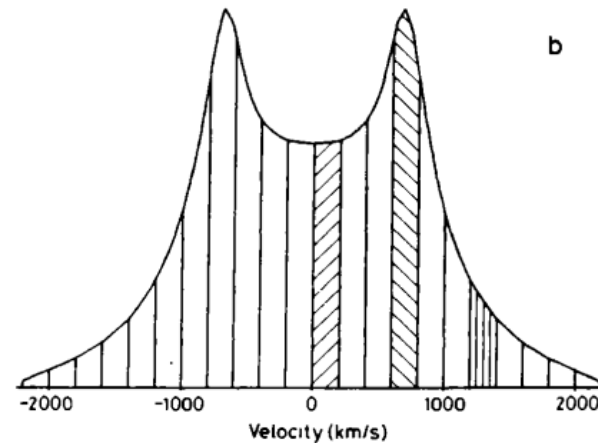
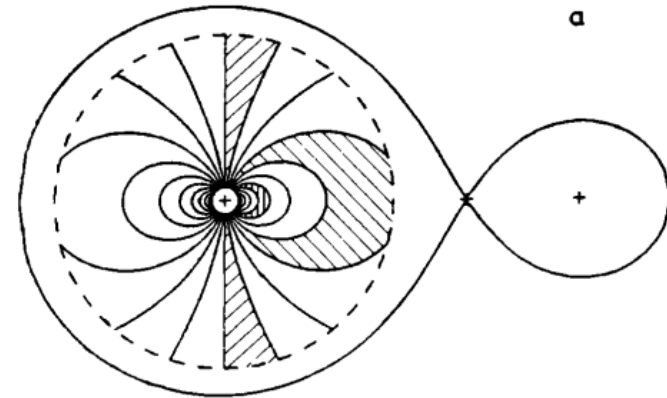
Spectroscopy: Emission line profiles (3)

83

(a) Loci of constant radial velocity in a Keplerian disk in a binary of mass ratio $q = 0.15$ viewed at quadrature

(b) Velocity profile of emission lines from the disk. Emission in the shaded velocity ranges originates in corresponding shaded regions on the disk.

(From Home & Marsh 1986).



Accretion Disks

84

- Accretion disks are important in astrophysics as they efficiently transform gravitational potential energy into radiation.

- **3 Classic Papers:**

- Black hole accretion disks

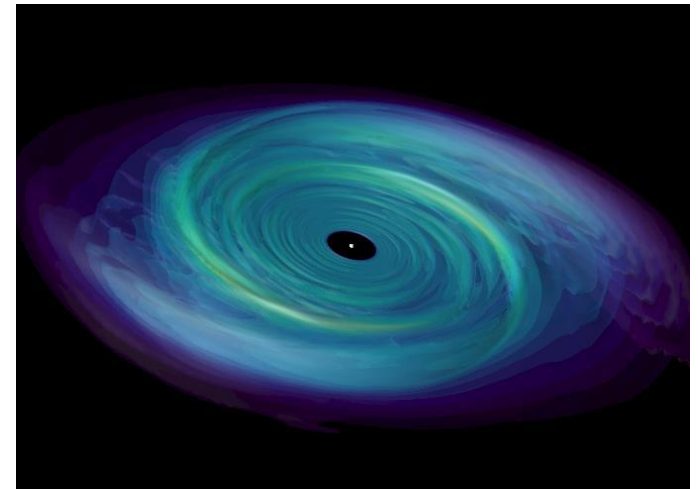
- Shakura & Sunyaev 1973, A&A, 24, 337

- Time-dependent disks

- Lynden-Bell & Pringle 1974, MNRAS, 168, 603

- Gas streams

- Lubow & Shu 1975, ApJ, 198, 383



85

Accretion disk properties

Order-of-magnitude estimates

Order-of-magnitude estimates: Mass flow rates

86

□ Mass flow rates in interacting close binary systems.

As template we take a cataclysmic variable (CV), a binary system with an orbital period of 1 to 10 hours.

The observed disk luminosity of such systems is of order of one solar luminosity $L=3.9 \cdot 10^{33}$ erg/s. Then

$$\begin{aligned} L &\approx \frac{GM\dot{M}}{R} \Rightarrow \dot{M} = \frac{LR_{WD}}{GM_{WD}} = 2.0 \cdot 10^{16} \frac{\text{g}}{\text{s}} \left(\frac{L}{L_{\odot}} \right) \left(\frac{R_{WD}}{10^{-2} R_{\odot}} \right) \left(\frac{M_{WD}}{M_{\odot}} \right)^{-1} = \\ &= \underline{\underline{3 \cdot 10^{-10} \frac{M_{\odot}}{\text{yr}}}} \left(\frac{L}{L_{\odot}} \right) \left(\frac{R_{WD}}{10^{-2} R_{\odot}} \right) \left(\frac{M_{WD}}{M_{\odot}} \right)^{-1} \end{aligned}$$

Order-of-magnitude estimates: Temperatures (1)

87

□ Temperatures of accretion disks.

When one knows the outer radius of a disk and its luminosity one can estimate an average effective temperature of a disk. The luminosity is proportional the radiating area times the fourth power of the (average) temperature (assuming the black body approximation):

$$L_d \approx 2\pi R_d^2 \sigma T_{eff}^4$$

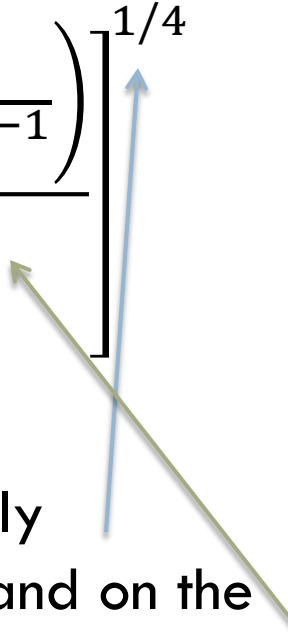
The factor of 2 takes care of the two surfaces of an accretion disk (“top” and “bottom” surface).

Order-of-magnitude estimates: Temperatures (2)

88

□ Temperatures of accretion disks (cont).

With the total disk luminosity of $L \approx GMM\dot{M}/R_{WD}$ we get

$$T_{eff} \approx 10^4 K \left[\frac{\left(\frac{M_{WD}}{M_{\odot}} \right) \left(\frac{\dot{M}}{10^{-9} M_{\odot} \text{ yr}^{-1}} \right)}{\left(\frac{R_{WD}}{10^{-2} R_{\odot}} \right) \left(\frac{R_d}{R_{\odot}} \right)^2} \right]^{1/4}$$


- The average temperature depends only weakly (by its fourth root) on accretor's mass and size and on the accretion rate, but somewhat stronger (by its root) on the disk size

Order-of-magnitude estimates: Temperatures (3)

89

□ Temperatures of accretion disks (cont).

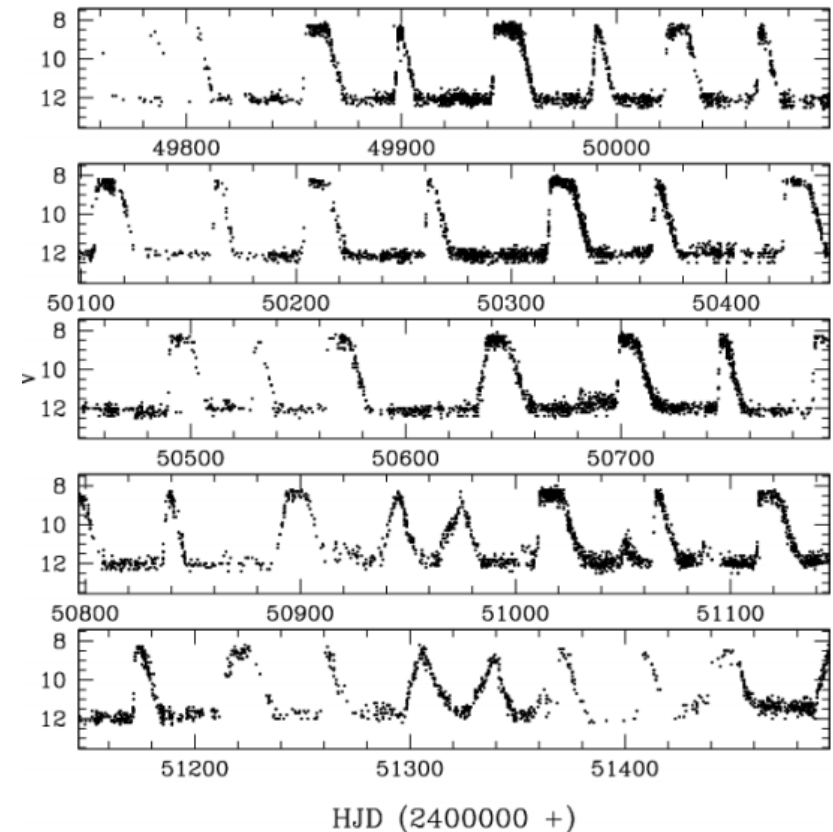
The dependence on the available area shows that the effective temperature cannot be constant throughout the disk. As long as $R_d \gg R_{WD}$, a change of R_d does not alter the luminosity considerably while, at the same time, it strongly changes the available radiating area and thus the effective temperature.

- This leads to the suspicion that the effective temperature in accretion disks decreases with increasing radius. This is the case, indeed.

Order-of-magnitude estimates: Disk masses (1)

90

- **Disk masses in dwarf novae.**
Dwarf novae - a subtype of CVs which exhibits outbursts with a characteristic (though not strict) repetition period of a few ten days.
- The outbursts are caused when the accretion disk reaches a critical temperature, the disk becomes unstable and the gas collapses onto the white dwarf (we will discuss it in detail later).



Order-of-magnitude estimates: Disk masses (2)

91

□ Disk masses in dwarf novae (cont).

The repetition time scale of the outbursts defines the average evolution time scale, i.e. the time scale it takes a particle on average to move through the entire extent of the disk.

- Let us assume an evolution time scale $\tau_{\text{disk}} \approx 10 \text{ days} \approx 10^{-1.5} \text{ yr}$. Together with the mass flow rate we get a disk mass in a dwarf nova:

$$M_{\text{disk,DN}} \approx \dot{M}_{\text{DN}} \tau_{\text{DN}} \approx 10^{-9} M_{\odot} \text{yr}^{-1} 10^{-1.5} \text{yr} \approx 10^{-10.5} M_{\odot} \ll M_{\text{WD}}$$

- Dwarf nova accretion disks have a much smaller mass than the white dwarf about which they move and onto which they accrete. In this respect DN disks are practically **massless**.

Order-of-magnitude estimates: Velocities (1)

92

□ Velocities in dwarf nova disks.

If the disk is practically massless, the particles in the disk move about the centre according to Kepler's third law as long as they move on closed orbits. The azimuthal velocity

$$V_{\phi} = \sqrt{\frac{GM}{R}} = 4.4 \times 10^7 \frac{cm}{s} \left(\frac{M_{WD}}{M_{\odot}} \right)^{1/2} \left(\frac{R}{R_{\odot}} \right)^{-1/2}$$

- At the same time, one can estimate the radial velocity V_R through the disk with which the mass moves

$$V_R \approx \frac{R}{\tau_{\text{disk}}} \approx 7 \times 10^4 \frac{cm}{s} \left(\frac{R}{R_{\odot}} \right)$$

Order-of-magnitude estimates: Velocities (2)

93

□ Velocities in dwarf nova disks (cont.).

Comparing the azimuthal and radial velocities, one finds

$$\frac{V_R}{V_\phi} = 1.6 \times 10^{-3} \left(\frac{M_{WD}}{M_\odot} \right)^{-1/2} \left(\frac{R}{R_\odot} \right)^{3/2} \ll 1$$

- This shows that in accretion disks the motion is almost that of test particles orbiting the centre of the disk in circles, superposed by a slow radial inward drift.

More about Accretion Disks

The angular momentum problem

Basic theory of geometrically thin disks

Formation of a Ring. What next?

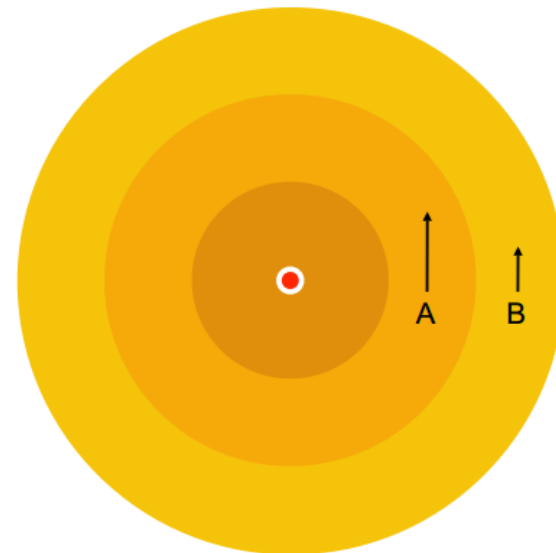
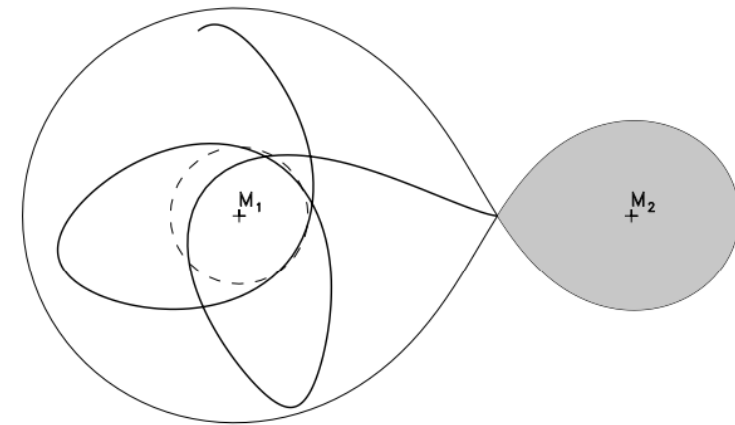
95

- Angular momentum is conserved. A circular orbit has the least energy for a given angular momentum → the dissipation will tend to produce a ring of gas.
- The ring that is formed has a finite radial extent and rotates differentially.

- Differential rotation (Shear):

$$\Delta V = \frac{d}{dR} \left(\sqrt{\frac{GM}{R}} \right) \Delta R = \frac{V}{2} \frac{\Delta R}{R}$$

- Friction causes ring to spread inward & outward.
- Disk is formed!



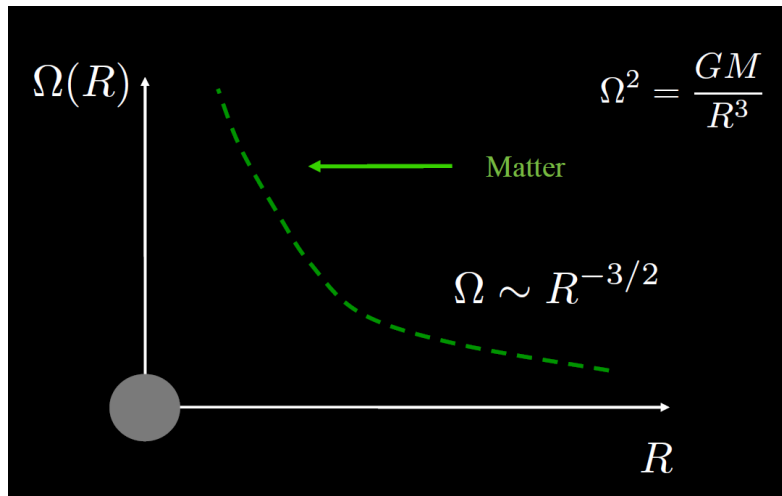
Formation of an Accretion Disk

96

Angular velocity in Keplerian disk
("differential rotation"):

$$\Omega_K = V_K/R = \sqrt{GM/R^3}$$

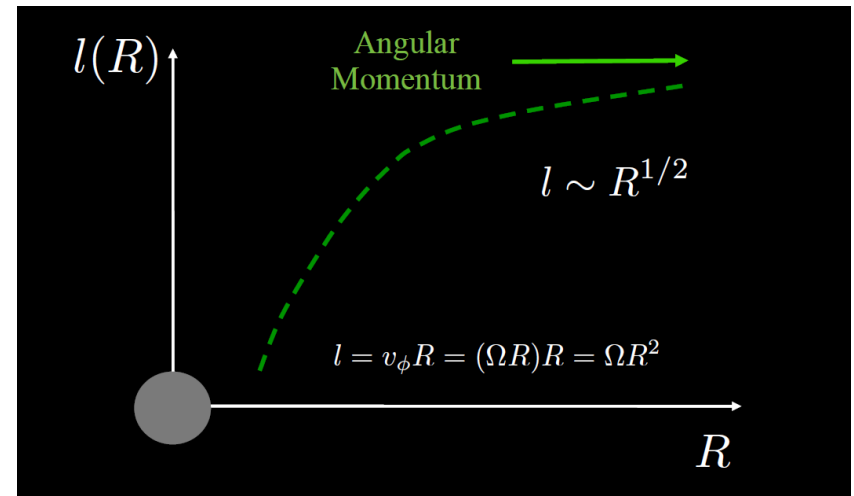
Increases with decreasing R!



Angular momentum per unit mass
("specific angular momentum"):

$$l(R) = RV_K = R^2\Omega_K = \sqrt{GMR}$$

Decreases with decreasing R!



If the disk were a collection of non-interacting particles there would be no accretion.

Gas in the disk must lose angular momentum!

The angular momentum problem

97

How does the accreting matter lose its angular momentum?

- Angular momentum is strictly conserved!
- Gas must shed its angular momentum for it to be actually accreted. Total angular momentum lost when mass moves in unit time from $R + dR$ to R :

$$\frac{dl}{dR} = \dot{M} \cdot \frac{d(R^2 \Omega_K)}{dR}$$

- Suppose that there is some kind of “viscosity” in the disk
 - ▣ Different annuli of the disk rub against each other and exchange angular momentum
 - ▣ Results in **most of the matter moving inwards and eventually accreting**
 - ▣ Angular momentum carried outwards by a small amount of material

Thin Accretion Disks (1)

98

- To start our study of the dynamics of disks, let's first take symmetry considerations and vertical integration of variables, to reduce the dimension of the problem and the number of independent variables:
 - We will assume that the disk is **physically thin**: the height h of the disk in the z direction is much smaller than the extent of the disk in the R direction. It requires that radiation pressure is negligible.
 - We will assume an axisymmetric disk, which means that all quantities are independent of the φ coordinate.
- The idea is to get rid of all z dependencies by integrating the equations through the depth of the disk, so we assumed that the flow is symmetric with respect to the equatorial plane (mirror symmetry about this plane). This procedure allows us to **decouple** the **vertical** and **radial** directions.

Thin Accretion Disks (2)

99

- This implies that rather than dealing with quantities per unit volume, we will deal instead with quantities per unit surface.
- Integrating the density ρ along the z-axis we obtain the surface density, defined as

$$\Sigma(R) \equiv \int_{-\infty}^{+\infty} \rho(R) dz = \int_{-H(R)}^{+H(R)} \rho(R) dz = h\rho$$

- For example, we can now calculate the amount of mass crossing radius R:

$$\dot{M} = 2\pi R \cdot \Sigma \cdot V_R$$

Steady Accretion Disks

100

- We also assume a stationary (**steady**) disk - the physical quantities in a disk do not change with time.
- **Important**, stationarity does not mean that there is no flow, for instance in radial direction in a disk. The only requirement is that this flow proceeds in such a manner that the physical quantities, like the surface density Σ and the radial velocity V_R remain unchanged. In other words: stationarity means that the time derivatives in the equations vanish.
- The disc is assumed to be **optically thick**. This allows the maximum amount of heat to radiate away from the surface of the disk before matter falls into the accreting star.
- Disk **self-gravitation is negligible** so material in differential or Keplerian rotation with angular velocity $\Omega_K(R)$.

Viscous accretion disks (1)

101

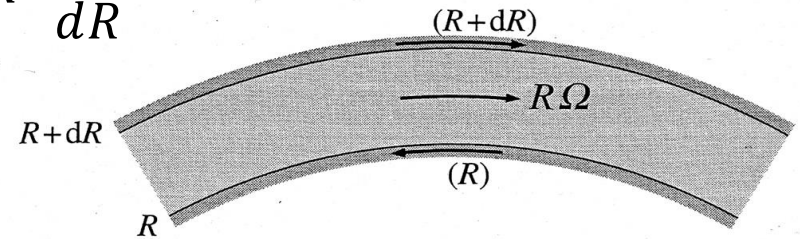
- Consider two consecutive rings on either side of some surface of constant R in the accretion disk and with vertical thickness h , then the outer annulus exerts a viscous force (μ – coefficient of dynamic viscosity):

$$F_{visc} = 2\pi R h \mu R \frac{d\Omega}{dR}$$

- In terms of the kinematic viscosity $\nu = \mu/\rho$

$$F_{visc} = 2\pi \nu \Sigma R^2 \frac{d\Omega}{dR}$$

- This force is acting at a distance R from the centre of rotation, so it will exert a torque by the outer ring on the inner ring

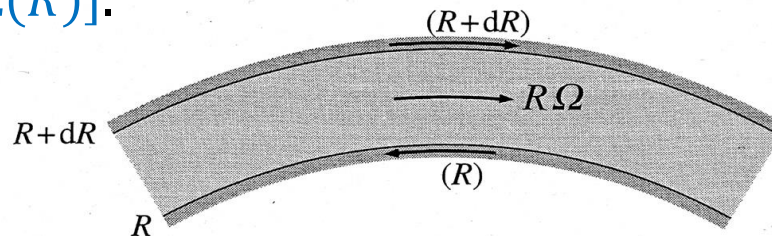


$$Q(R) = F_{visc} R = 2\pi \nu \Sigma R^3 \frac{d\Omega}{dR}$$

Viscous accretion disks (2)

102

- The torque by the outer ring on the inner ring: $Q(R) = 2\pi\nu\Sigma R^3 \frac{d\Omega}{dR}$
- The direction of the torque is such that the fluid at a radius less than R (which is rotating more rapidly) feels a backward torque and loses the angular momentum whereas the fluid at a radius larger than R gains the angular momentum.
- To determine the radial structure of the disk we have to equate this torque to the rate of loss of specific angular momentum.
- Consider a ring located between R and $(R + dR)$.
In unit time, a mass \dot{M} enters the ring at $(R + dR)$ with specific angular momentum $(R + dR)^2[\Omega(R + dR)]$ and leaves at R with specific angular momentum $R^2[\Omega(R)]$.



Viscous accretion disks (3)

103

$$Q(R) = 2\pi\nu\Sigma R^3 \frac{d\Omega}{dR}$$

- Thus, the net angular momentum lost by the fluid per unit time in this ring is

$$\dot{M} \left[\frac{d(R^2\Omega)}{dR} \right] dR$$

- This angular momentum is lost because the torque is acting at both R and $(R + dR)$ whose net effect is $(dQ/dR) dR$. This lead to

$$\dot{M} \left[\frac{d(R^2\Omega)}{dR} \right] dR = - \frac{d}{dR} \left[2\pi\nu\Sigma R^3 \frac{d\Omega}{dR} \right] dR$$

- Using $\Omega_K = \sqrt{GM/R^3}$ and integrating, we get

$$\nu\Sigma\sqrt{R} = \frac{\dot{M}}{3\pi} \sqrt{R} + constant$$

Viscous accretion disks (4)

104

$$v\Sigma\sqrt{R} = \frac{\dot{M}}{3\pi}\sqrt{R} + \text{constant}$$

Constant can be obtained from **no torque boundary condition** at inner edge of disk at $R = R_*$ at which $\frac{dQ}{dR(R_*)} = 0$

Thus, we get

$$v\Sigma = \frac{\dot{M}}{3\pi} \left[1 - \left(\frac{R_*}{R} \right)^{1/2} \right]$$

Viscous accretion disks (6)

105

- All these rings rubbing against one another not only transfer angular momentum, they also make the disk hot. The power that is generated on an annulus takes the schematic form

Power = (torque) \times (relative angular velocity of neighboring annuli)

- Each ring has two plane faces of area $4\pi R dR$, so the radiative dissipation from the disk **per unit area** is

$$D(R) = \frac{Q}{4\pi R} \frac{d\Omega}{dR} = \frac{1}{2} \nu \Sigma \left(R \frac{d\Omega}{dR} \right)^2$$

- Evaluating for circular Keplerian orbits ($\Omega_K = \sqrt{GM/R^3}$):

$$D(R) = \frac{9}{8} \nu \Sigma \frac{QM}{R^3}$$

Viscous accretion disks (7)

106

- We then have:

$$D(R) = \frac{3GM\dot{M}}{8\pi R^3} \left[1 - \left(\frac{R_*}{R} \right)^{1/2} \right] \quad v\Sigma = \frac{\dot{M}}{3\pi} \left[1 - \left(\frac{R_*}{R} \right)^{1/2} \right]$$

and hence the radiation energy flux through the disk faces is
independent of viscosity

- The total disk luminosity is

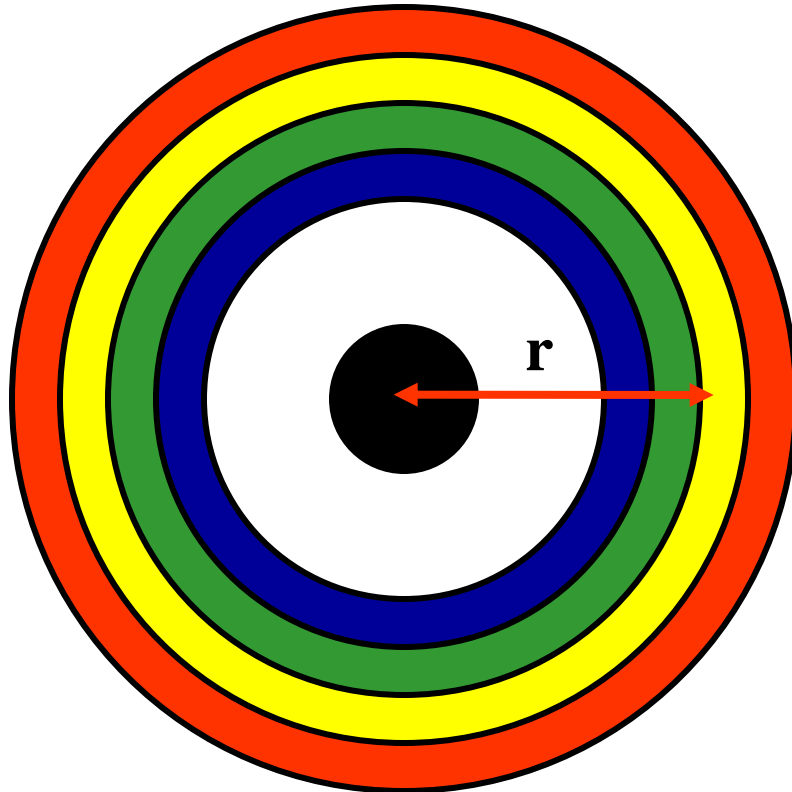
2 sides of a disk


$$L_{disk} = 2 \times \int_{R_*}^{\infty} D(R) \times 2\pi R dR = \frac{GM\dot{M}}{2R_*}$$

i.e., half the gravitational energy released in accreting the gas to radius R_* . The remaining gravitational energy goes into rotational energy, which may be either dissipated in a boundary layer or sucked into a black hole.

AD Temperature Structure (1)

107



- If the accretion disk is optically thick, it can be considered as rings or annuli of blackbody emission.

- Dissipation rate, $D(R)$ is

$$D(R) = \frac{3GM\dot{M}}{8\pi R^3} \left[1 - \left(\frac{R_*}{R} \right)^{1/2} \right]$$

= blackbody flux

$$= \sigma T(R)^4$$

AD Temperature Structure (2)

108

- Thus temperature as a function of radius $T(R)$:

$$T(R) = \left\{ \frac{3GM\dot{M}}{8\pi R^3 \sigma} \left[1 - \left(\frac{R_*}{R} \right)^{1/2} \right] \right\}^{1/4}$$

- and if $T_* = \left(\frac{3GM\dot{M}}{8\pi R_*^3 \sigma} \right)^{1/4}$

- Then for $R \gg R_*$

$$T(R) = T_* \left(R / R_* \right)^{-3/4}$$

AD Temperature Structure (3)

109

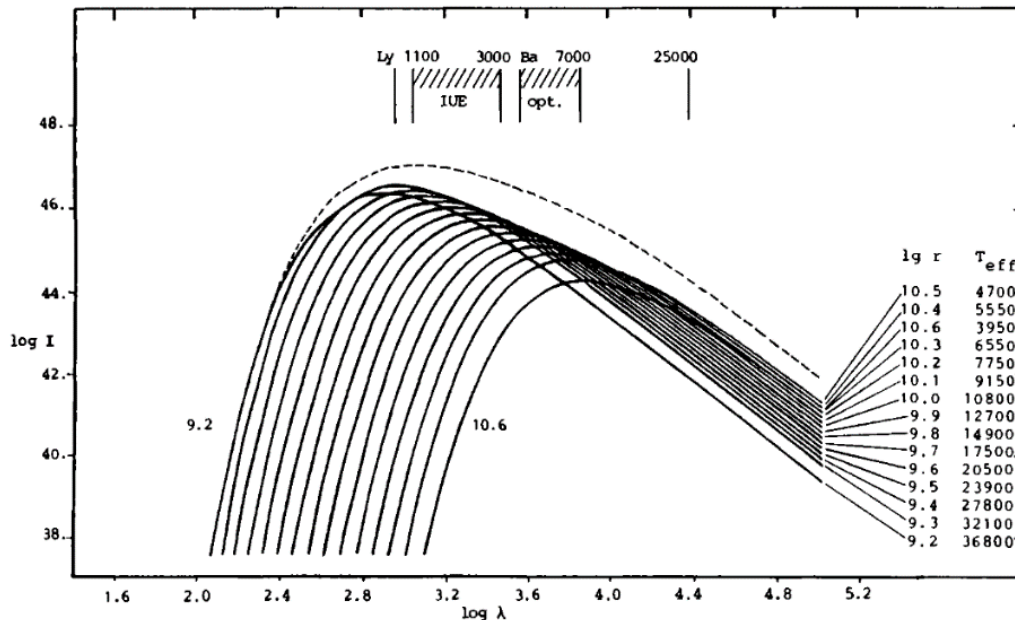
- In dwarf novae in outburst and long-period novalikes, this simple $R^{-3/4}$ radial temperature profile is indeed observed.
- In quiescent dwarf novae a much flatter profile is observed. This is thought to be because the disk does not achieve a steady state in quiescence.

Accretion Disk Spectrum (1)

110

- Integrating the blackbody spectrum over radius gives the predicted spectrum of an optically thick, geometrically thin, steady-state accretion disk

$$S_\lambda \propto \int_{R_{in}}^{R_{out}} B_\lambda[T(R)] 2\pi R dR$$



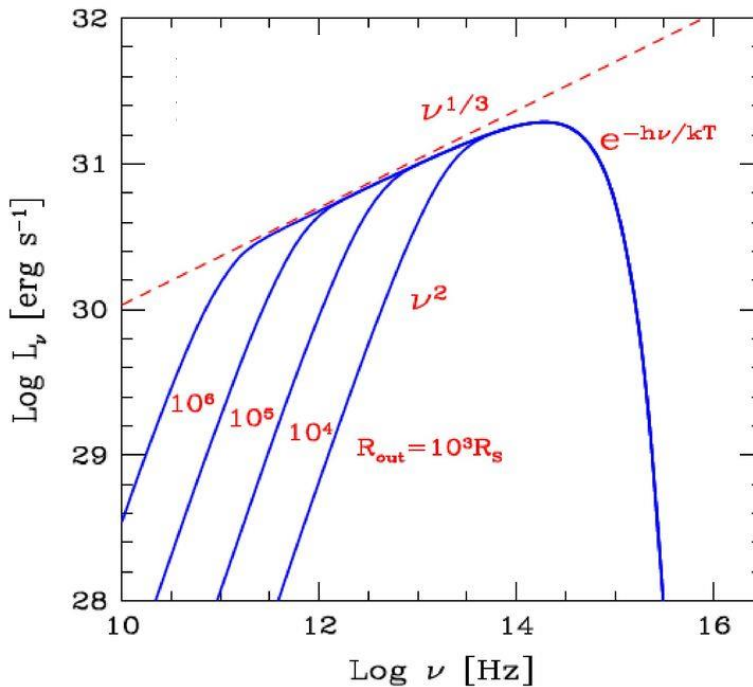
Contributions of BB annuli to the total intensity distribution of an accretion disk.

Accretion Disk Spectrum (2)

111

- The continuum spectrum S_ν (in frequency units) of a disk with different ratios $R_{\text{out}}/R_{\text{in}}$:
$$S_\nu \propto \int_{R_{\text{in}}}^{R_{\text{out}}} B_\nu[T(R)] 2\pi R dR,$$

Spectrum produced by standard geometrically thin, optically thick accretion disk



The spectrum can be divided into three regions:

From the outer edge of the disc we will see the Rayleigh-Jeans tail of T_{outer}

$$S_\nu \propto \nu^2$$

From the inner edge, an exponential cut-off

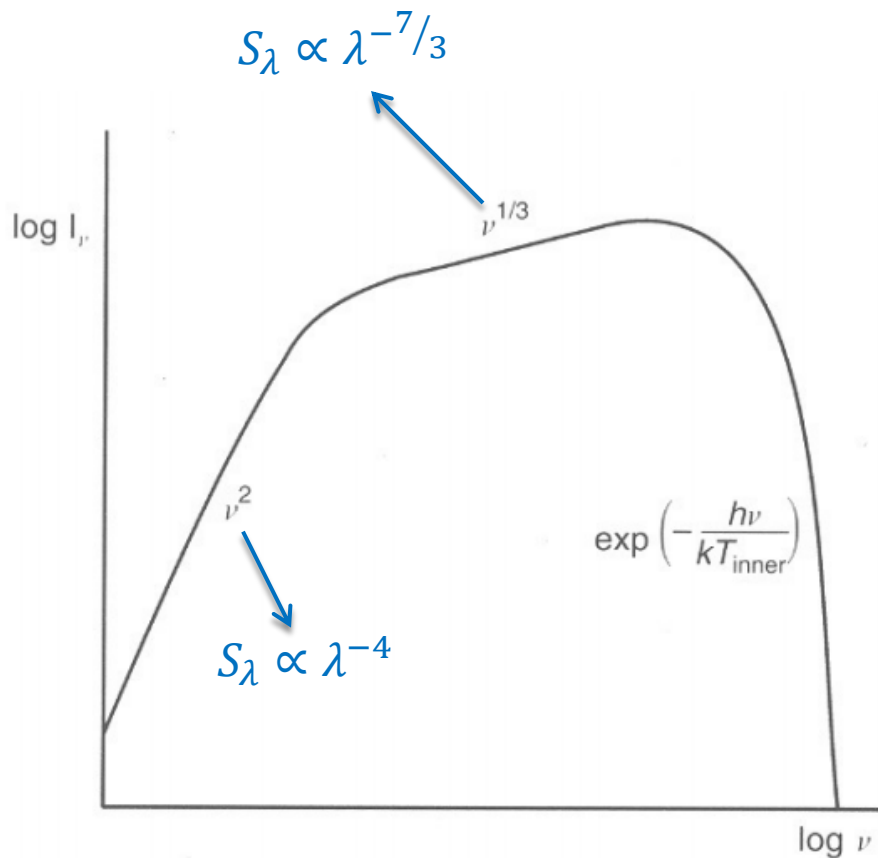
$$S_\nu \propto e^{-h\nu/kT_{\text{inner}}}$$

And the flat part which is sometimes considered a characteristic disc spectrum:

$$S_\nu \propto \nu^{1/3}$$

Accretion Disk Spectrum (3)

112



The flat part is considered a characteristic disc spectrum:

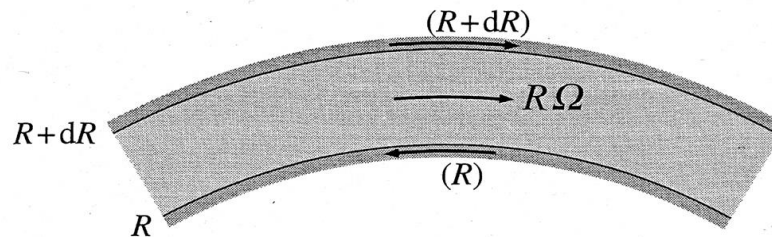
$$S_\nu \propto \nu^{1/3}$$

However! This part of the curve may be **quite short** and the spectrum is not very different from a blackbody, unless T_{out} is appreciably smaller than T_{in} .

AD: Surface Density Evolution (1)

113

- The angular momentum is transferred outwards through the disk by viscous torques.
- The outer parts of the ring will gain angular momentum and will spiral outwards.
- The original ring of matter at $R = R_{\text{circ}}$ will spread to both smaller and larger radii by this process, to form an accretion disk.
- To see it in detail, let's write **the conservation equations** for the mass and angular momentum transport in the disk due to radial drift motion.
- Again, let's consider a ring located between R and $(R + dR)$. Its mass is $\Delta m = 2\pi R \Delta R \Sigma$, and the angular momentum $2\pi R \Delta R \Sigma R^2 \Omega$, where $\Sigma = \rho H$ is the surface density.



AD: Surface Density Evolution (2)

114

- Then, for the mass of the annulus,

$$\begin{aligned} \frac{\partial(2\pi R\Delta R\Sigma)}{\partial t} &= V_R(R, t)2\pi R\Sigma(R, t) - V_R(R + \Delta R, t)2\pi(R + \Delta R)\Sigma(R + \Delta R, t) \\ &\approx -2\pi\Delta R \frac{\partial(R\Sigma V_R)}{\partial R} \end{aligned}$$

- In the limit $\Delta R \rightarrow 0$, we get **the mass conservation equation** (the continuity equation)

$$R \frac{\partial(\Sigma)}{\partial t} + \frac{\partial(R\Sigma V_R)}{\partial R} = 0$$

AD: Surface Density Evolution (3)

115

- The conservation equation of angular momentum is

$$\begin{aligned}
 \frac{\partial}{\partial t} (2\pi R \Delta R \Sigma R^2 \Omega) &= \\
 &= V_R(R, t) 2\pi R \Sigma(R, t) R^2 \Omega(R) \\
 &\quad - V_R(R + \Delta R, t) 2\pi (R + \Delta R) \Sigma(R + \Delta R, t) (R + \Delta R)^2 \Omega(R + \Delta R) \\
 &\quad + Q(R + \Delta R) - Q(R) \\
 &\approx -2\pi \Delta R \frac{\partial}{\partial R} (R \Sigma V_R R^2 \Omega) + \frac{\partial(Q)}{\partial R} \Delta R
 \end{aligned}$$

where $Q(R, t) = 2\pi \nu \Sigma R^3 \frac{d\Omega}{dR}$ is the viscous torque exerted by the outer ring

- In the limit $\Delta R \rightarrow 0$, we get **the angular momentum conservation equation:**

$$R \frac{\partial}{\partial t} (\Sigma R^2 \Omega) + \frac{\partial}{\partial R} (R \Sigma V_R R^2 \Omega) = \frac{1}{2\pi} \frac{\partial(Q)}{\partial R}$$

AD: Surface Density Evolution (4)

116

$$R \frac{\partial(\Sigma)}{\partial t} + \frac{\partial(R\Sigma V_R)}{\partial R} = 0$$
$$R \frac{\partial}{\partial t} (\Sigma R^2 \Omega) + \frac{\partial}{\partial R} (R\Sigma V_R R^2 \Omega) = \frac{1}{2\pi} \frac{\partial(Q)}{\partial R}$$

- If we assume that Ω does not vary significantly with time (a valid approximation), then we can combine our mass conservation and angular momentum conservation equations to yield the following expression:

$$R\Sigma V_R \frac{\partial}{\partial R} (R^2 \Omega) = \frac{1}{2\pi} \frac{\partial(Q)}{\partial R}$$

- Combining it with the mass conservation equation, we get

$$R \frac{\partial \Sigma}{\partial t} = - \frac{1}{2\pi} \frac{\partial}{\partial R} \left[\left\{ \frac{\partial}{\partial R} (R^2 \Omega) \right\}^{-1} \frac{\partial(Q)}{\partial R} \right]$$

AD: Surface Density Evolution (5)

117

- Only now we assume that Ω is Keplerian, $\Omega_K = \sqrt{GM/R^3}$. Then it follows that

$$\begin{aligned}\frac{d\Omega}{dR} &= -\frac{3}{2} \frac{\Omega}{R} \\ Q &= 2\pi\nu\Sigma R^3 \frac{d\Omega}{dR} = -3\pi\nu\Sigma R^2 \Omega \\ \frac{\partial Q}{\partial R} &= -3\pi R^{3/2} \Omega \frac{\partial}{\partial R} (\nu\Sigma R^{1/2})\end{aligned}$$

- We can therefore write **the time evolution of the disk surface density** as

$$\frac{\partial \Sigma}{\partial t} = \frac{3}{R} \frac{\partial}{\partial R} \left[R^{1/2} \frac{\partial}{\partial R} (\nu \Sigma R^{1/2}) \right]$$

(a nonlinear diffusion equation for Σ , because ν may be a function of local variables in the disk)

AD: Surface Density Evolution (6)

118

- The radial velocity follows straightforwardly from the equation of mass conservation:

$$V_R = -\frac{3}{R^{1/2}\Sigma} \frac{\partial}{\partial R} (v\Sigma R^{1/2}) \sim \frac{v}{R}$$

- Finally, the mass flux through the disk at a radius R is simply

$$\dot{M}(R) = 2\pi R\Sigma |V_R| = 6\pi R^{1/2} \frac{\partial}{\partial R} (v\Sigma R^{1/2})$$

- Comparing our expression for the mass flux with that for the evolution of the surface density, we see that

$$\frac{\partial \Sigma}{\partial t} = \frac{3}{R} \frac{\partial}{\partial R} \left[R^{1/2} \frac{\partial}{\partial R} (v\Sigma R^{1/2}) \right] \longrightarrow \frac{\partial \Sigma}{\partial t} = \frac{1}{2\pi R} \frac{\partial \dot{M}}{\partial R}$$

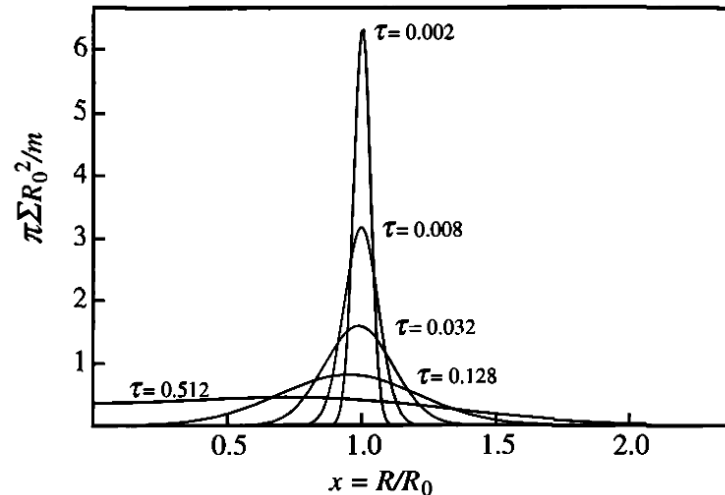
We therefore see that if our accretion disk is in **a steady state**, with $\partial \Sigma / \partial t = 0$, then **the mass flux through the disk is the same at all radii.**

AD: Surface Density Evolution (7)

119

- As an example, the figure shows the spreading of a ring of matter with a Keplerian orbit at $R = R_0$, under the action of viscous torques. The viscosity is assumed to be constant. The typical timescale of the ring's spreading is

$$t_{\text{visc}} \sim R/V_R \sim R^2/\nu$$



- Near the outer edge of the disk $R_{\text{out}} > R_{\text{circ}}$, some other process must finally remove this angular momentum, and it is likely that angular momentum is fed back into the binary orbit through tides exerted by the secondary.

Accretion Disk: vertical structure

120

- It is common to assume that there is no motion in the z -direction, that the gas in the disk is in hydrostatic equilibrium in the vertical direction. This is a reasonable assumption if the timescale to come to equilibrium – typically, the dynamical timescale of the gas – is much shorter than the time that it takes for gas to flow through the disk and onto the central object.
- The hydrostatic equilibrium equation is

$$\frac{1}{\rho} \frac{\partial P}{\partial z} = \frac{\partial}{\partial z} \left[\frac{GM}{(R^2 + z^2)^{1/2}} \right]$$

- For a thin disk ($z \ll R$) this becomes

$$\frac{1}{\rho} \frac{\partial P}{\partial z} = -\frac{GMz}{R^3}$$

Accretion Disk Thickness

121

- We can relate P and ρ via the sound speed in the gas $dP = c_s^2 d\rho$, and then integrate to find that the density in the disk falls off exponentially with height

$$\frac{1}{\rho} \frac{\partial P}{\partial z} = -\frac{GMz}{R^3} \quad \longrightarrow \quad \rho(z) = \rho_0 \exp\left(-\frac{z^2}{2h^2}\right)$$

with a height scale factor given by $h^2 \cong \frac{c_s^2 R^3}{GM}$

- The scale height can be re-written in terms of the rotational velocity:

$$V_{rot} = \sqrt{\frac{GM}{R}} \quad \longrightarrow \quad h^2 \cong \frac{c_s^2 R^2}{V_{rot}^2}$$

- If we have $R \gg h$ we must have $V_{rot}^2 \gg c_s^2$ and so the rotation of the disk is highly supersonic.

Accretion Disk Thickness (cont.)

122

- Lets re-write the scale height again:

$$h^2 \cong \frac{c_S^2 R^2}{V_{rot}^2} \quad \longrightarrow \quad \frac{h}{R} \cong \frac{c_S}{V_{rot}}$$

- Therefore, provided that the disk is cold, and that its rotation is supersonic, our assumption that it is thin is well-justified, since in this case we will have $h \ll R$.
- Note also that for a disk in Keplerian rotation, $\Omega = V_{rot}/R$, and so $c_S = h\Omega$.

Viscosity in an accretion disk

Problem with normal molecular viscosity

Source of anomalous viscosity?

Shakura-Sunyaev α -disk prescription

The magneto-rotational instability

Viscosity (1)

124

- Most important unknown in accretion disk theory: **viscosity**. Even though it dropped out of $T(R)$, it is present in most of other important equations, e.g. in the equation of the time evolution of the disk surface density.

$$\frac{\partial \Sigma}{\partial t} = \frac{3}{R} \frac{\partial}{\partial R} \left[R^{1/2} \frac{\partial}{\partial R} (\nu \Sigma R^{1/2}) \right]$$

- So, what is the source of the kinematic viscosity ν that causes the inward drift of the gas in the accretion disk?
- Viscosity of fluids typically due to molecular interactions (molecular viscosity), the result of thermal collisions between individual gas particles in a hot medium.
- In the case of standard viscosity, the kinematic viscosity is

$$\nu_{mol} \sim \lambda c_s$$

where the mean free path length (in an ionized gas) is

$$\lambda = \frac{1}{n\sigma} = 6.4 \times 10^4 \frac{T^2}{n} \text{ cm}$$

and the speed of sound

$$c_s \sim 10^4 T^{1/2} \text{ cm/s}$$

Viscosity (2)

125

- Then

$$\nu_{mol} \sim \lambda c_s \sim 6.4 \times 10^8 T^{5/2} n^{-1} \text{ cm}^2/\text{s}$$

- For typical values for accretion disks in CVs ($R \sim 10^{10}$ cm, $T \sim 10^4$ K, $n \sim 10^{16}$ cm⁻³):

$$\nu_{mol} \sim 10^3 \text{ cm}^2/\text{s}$$

- This value of the kinematic viscosity yields a viscous accretion time scale of

$$t_{visc} \sim \frac{R^2}{\nu} \sim 10^{17} \text{ sec} \sim 3 \times 10^9 \text{ yr}$$

and the mass will be flowing in at the excruciatingly slow rate of a few cm/yr.

Thus, normal molecular viscosity fails to provide required angular momentum transport by many orders of magnitude!

Viscosity (3)

126

- We therefore see that there must be some additional “anomalous” viscosity present in the disks, with a magnitude that is much larger than the molecular viscosity, in order to explain the observed accretion rates.
- **Then, what gives rise to viscosity?**
- Source of **anomalous viscosity** was a major puzzle in accretion disk studies. Long suspected to be due to some kind of turbulence in the gas...
- If the source of the anomalous viscosity is some form of turbulent process, then we expect that $\nu \sim L_{turb} v_{turb}$, where v_{turb} is the characteristic turbulent velocity and L_{turb} is the size of the largest turbulent eddy. If the turbulence was highly supersonic, then it would rapidly dissipate energy in shocks, and so in practice, we expect that $v_{turb} \sim c_s$. Furthermore, if the turbulence is approximately isotropic, then the size of the largest eddies will not exceed the scale height of the disk, i.e. $L_{turb} \sim h$.



Viscosity (4)

127

- These considerations led [Shakura & Sunyaev \(1973\)](#) to propose the following form for the kinematic viscosity:

$$\nu = \alpha c_s h$$

where c_s is the sound speed, h is the disk scale height (a function of radius), and α is a dimensionless constant.

- α here is a measure of our uncertainty – we expect on general physical grounds that $\alpha < 1$, but it could in principle be very much smaller. Nevertheless, this Shakura & Sunyaev's “ α -disk” prescription allows one to solve for the physical structure of the accretion disk, the mass flow rate, etc., in terms of only this single unknown parameter.
- Typical models of disks have $\alpha \sim 0.01 - 0.1$

The standard α -disk model

128

Astron. & Astrophys. 24, 337–355 (1973)

Black Holes in Binary Systems. Observational Appearance

N. I. Shakura

Sternberg Astronomical Institute, Moscow, U.S.S.R.

R. A. Sunyaev

Institute of Applied Mathematics, Academy of Sciences, Moscow, U.S.S.R.

Received June 6, 1972

Summary. The outward transfer of the angular momentum of the accreting matter leads to the formation of a disk around the black hole. The structure and radiation spectrum of the disk depend, mainly on the rate of matter inflow \dot{M} into the disk at its external boundary. The dependence on the efficiency of mechanisms of angular momentum transport (connected with the magnetic field and turbulence) is weaker. If $\dot{M} = 10^{-9} - 3 \cdot 10^{-8} \frac{M_{\odot}}{\text{year}}$ the disk around the black hole is a powerful source of X-ray radiation with $h\nu \sim 1 - 10 \text{ keV}$

saturated by broad recombination and resonance emission lines. Variability, connected with the character of the motion of the black hole, with gas flows in a binary system and with eclipses, is possible. Under certain conditions, the hard radiation can evaporate the gas. This can counteract the matter inflow into the disk and lead to autoregulation of the accretion.

If $\dot{M} \gg 3 \cdot 10^{-8} \frac{M_{\odot}}{\text{year}}$ the luminosity of the disk around the black hole is stabilized at the critical level of $\sim M \text{ erg}$

The α -disk Model

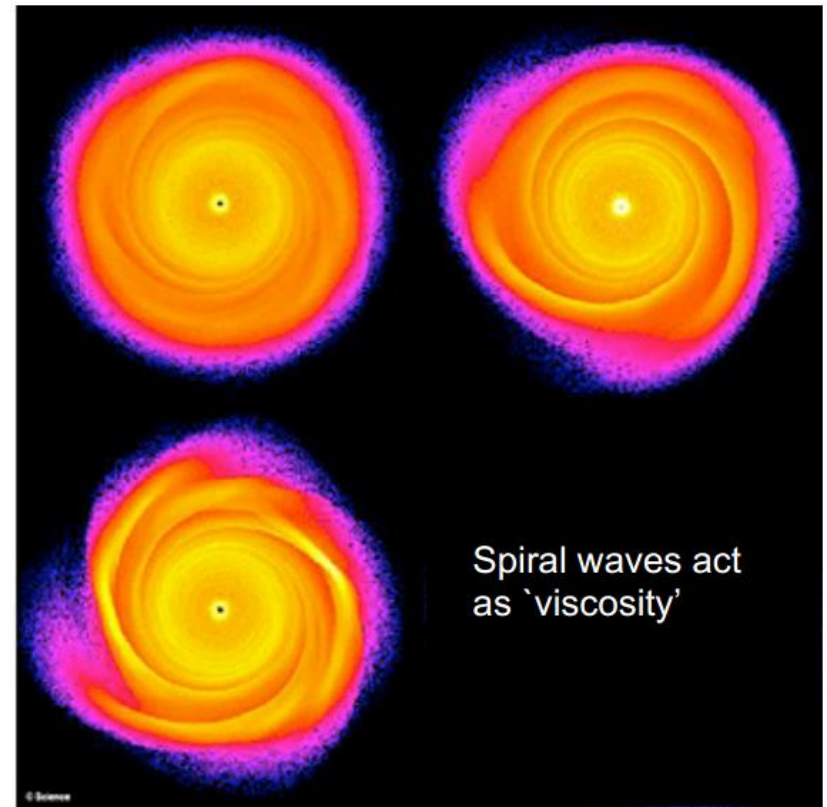
129

- Physics of turbulent viscosity is unknown, however, α prescription yields good agreement between theory and observations.
- For specified α , one can completely solve for the structure of a (steady-state or time-dependent) accretion disk. However, the assumption that α is constant with radius, with time, or from one accretion disk to another is nothing more than **an assumption**.
- 20+ years of accretion disk studies were based on this “alpha-prescription”...
- While the notion of “turbulent viscosity” is intuitively appealing, detailed studies suggest that hydrodynamic mechanisms alone will not produce sustained turbulence in differentially rotating disks.

Anomalous viscosity?

130

- A number of hypotheses have been proposed to explain the much larger *effective* viscosity in accretion disks. The most important of these are:
- (1) A *turbulent viscosity* resulting from random small-scale turbulent fluid motions in the disk, generated by the strong shear in the differentially rotating disk.
- (2) A *magnetic viscosity* associated with the magnetic Lorentz force in a disk containing magnetic fields.
- (3) Nonlinear (spiral) waves or *shocks* in the disk.

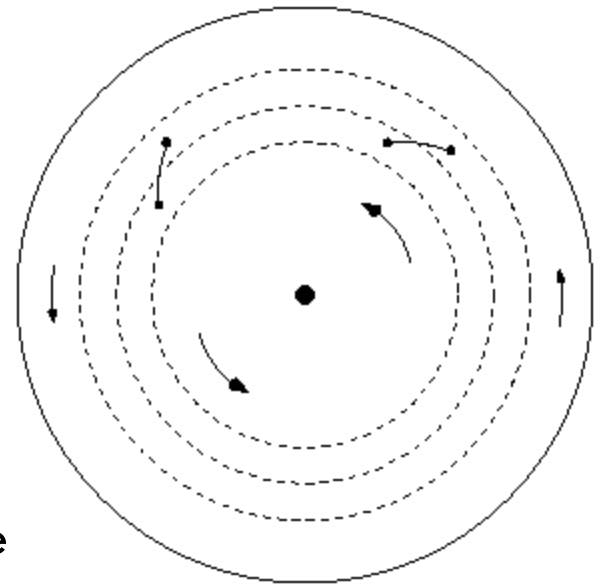


Rice & Armitage

The magneto-rotational instability (1)

131

- Major breakthrough in 1991... The idea of magneto-hydrodynamic (MHD) MHD turbulence was initially discussed by Velikhov (1959) and specifically developed by Steve Balbus and John Hawley (1991, ApJ, 376, 214; 376, 223), who (re)-discovered a powerful magneto-hydrodynamic (MHD) instability
 - ▣ Called magnetorotational instability (MRI)
 - ▣ MRI will be effective at driving turbulence
 - ▣ Turbulence transports angular momentum in just the right way needed for accretion
- Rough idea: MHD instabilities in a differentially rotating, magnetized disk drive turbulence, which in turn produces viscosity.
- Magnetic fields link different annuli and generate MHD turbulence.



The magneto-rotational instability (2)

132

THE ASTROPHYSICAL JOURNAL, 376:214–222, 1991 July 20
© 1991. The American Astronomical Society. All rights reserved. Printed in U.S.A.

A POWERFUL LOCAL SHEAR INSTABILITY IN WEAKLY MAGNETIZED DISKS. I. LINEAR ANALYSIS

STEVEN A. BALBUS AND JOHN F. HAWLEY

Virginia Institute for Theoretical Astronomy, Department of Astronomy, University of Virginia, P.O. Box 3818, Charlottesville, VA 22903

Received 1990 November 1; accepted 1991 January 16

ABSTRACT

In this paper and a companion work, we show that a broad class of astrophysical accretion disk is dynamically unstable to axisymmetric disturbances in the presence of a weak magnetic field. Because of the ubiquity of magnetic fields, this result bears upon gaseous differentially rotating systems quite generally. This work presents a linear analysis of the instability. (The companion work presents the results of nonlinear numerical simulations.) The instability is local and extremely powerful. The maximal growth rate is of order the angular rotation velocity and is *independent* of the strength of the magnetic field, provided only that the energy density in the field is less than the thermal energy density. Unstable axisymmetric disturbances require the presence of a poloidal field component, and are indifferent to the presence of a toroidal component. The instability also requires that the angular velocity be decreasing outward. In the absence of a powerful dissipation process, there are no other requirements for instability. Fluid motions associated with the instability directly generate both poloidal and toroidal field components. We discuss the physical interpretation of the instability in detail. Conditions under which saturation occurs are suggested. The *nonemergence* of the classical Rayleigh criterion for shear instability in the limit of vanishing field strength is noted and explained. The instability is sensitive neither to disk boundary conditions nor to the constitutive fluid properties. Its existence precludes the possibility of internal (noncompressive) wave propagation in a disk. If present in astrophysical disks, the instability, which has the character of an interchange, is very likely to lead to generic and efficient angular momentum transport, thereby resolving an outstanding theoretical puzzle.

Subject headings: accretion — hydrodynamics — hydromagnetics — instabilities

1. INTRODUCTION

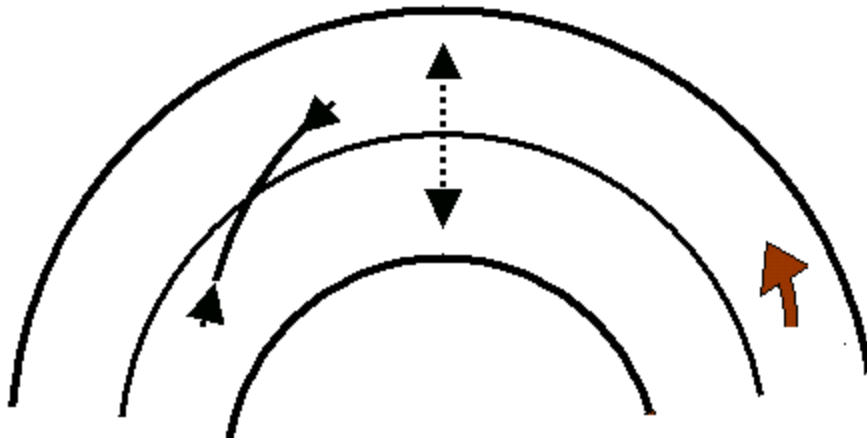
A long-standing challenge to the theory of accretion disks has been to show from first principles a mechanism capable of generating a turbulent viscosity, since the angular momentum transport resulting from the action of ordinary molecular viscosity is extremely inefficient (Pringle 1981). In this work and a companion paper (Hawley & Balbus 1991, hereafter II), we show that accretion disks are subject to a very powerful shearing instability mediated by a *weak* magnetic field of any plausible astrophysical strength. We suggest that this instability is of some relevance to understanding the origin of turbulent viscosity in accretion disks.

It is of course widely appreciated that magnetic fields can play an important role in accretion disk dynamics (e.g., Blandford 1989). In their seminal paper, Shakura & Sunyaev (1973) noted that magnetic turbulence could act as a viscous couple, but argued that nonlinear perturbations would be required to disrupt laminar flow. Magnetic fields have also been invoked, for example, as a source

The magneto-rotational instability (3)

133

- Imagine that a magnetic field line initially connects two neighboring annuli in a radial direction, as shown by the dotted line.
- Because these two annuli have differing angular velocities, the field line will tend to become stretched as the shear proceeds (solid curve).
- The magnetic field will try to oppose the shear, and try to straighten out, which requires speeding up the outer annulus relative to the inner annulus, i.e. transferring angular momentum outward.



However, recent MHD simulations of the magnetorotational instability by Fromang & Papaloizou (2007) demonstrate that turbulent activity decreases as resolution increases.

Thus, the viscosity problem is not yet solved.

134

Standard α -disk model

Properties of the thin, steady-state AD

135

- Thickness: $\frac{h}{R} \cong \frac{c_S}{V_{rot}}$
- Surface density (g/cm²): $\Sigma = \int_{-\infty}^{+\infty} \rho dz = \sqrt{2\pi} \rho_0 h$
- Viscosity (alpha model – hides uncertain physics): $\nu \equiv \alpha c_S h$
- Temperature: $T(R) = T_* (R/R_*)^{-3/4}$
- The radial velocity is highly subsonic:

$$V_R = \frac{\dot{M}}{2\pi R \Sigma} = \frac{3\nu}{2R \left[1 - \left(\frac{R_*}{R} \right)^{1/2} \right]} \sim \frac{\nu}{R} \sim \alpha c_S \frac{h}{R} \ll c_S$$



$$v\Sigma = \frac{\dot{M}}{3\pi} \left[1 - \left(\frac{R_*}{R} \right)^{1/2} \right]$$

- It would be useful to perform slightly more elaborate modeling of α -disks, to find its properties as a function of the radius R , the mass M of the central object, the accretion rate \dot{M} , and the assumed value of α .

Structure of the standard α -disk (1)

136

- Let's combine all the equations of the steady disk:

$$c_S^2 = \frac{P}{\rho}$$

where in general the pressure P is the sum of gas and radiation pressures:

$$P = \frac{\rho k T_c}{\mu m_p} + \frac{4\sigma}{3c} T_c^4$$

μm_p is the mean molecular weight of the gas, σ is the Stefan Boltzmann constant, and the temperature $T(R, z)$ is close to the central temperature $T_C(R) = T(R, 0)$ (assumption).

- As in stars, the vertical energy transport mechanism may be either radiative or convective. We assume that the transport is radiative, and the disk is **optically thick**, i.e.

$$\tau = \rho h \kappa_R(\rho, T_c) = \Sigma \kappa_R \gg 1$$

where k_R is the Rosseland mean opacity.

- Then, the radiation field is locally very close to the **blackbody**.

Structure of the standard α -disk (2)

137

Because of the thin disc approximation, the disc medium is essentially 'plane-parallel' at each radius, so that the temperature gradient is effectively in the z-direction.

Then, the flux of radiant energy through a surface $z=\text{constant}$ is given by

$$F(z) = -\frac{16\sigma T^3}{3\kappa_R \rho} \frac{\partial T}{\partial z} \sim \frac{4\sigma}{3\tau} T^4(z)$$

Recall from Stellar Atmospheres:

Temperature structure of the grey atmosphere

In LTE, the source function is the Planck function, $S(\tau) = B(\tau) = \sigma T^4 / \pi$

$$B(\tau) = \frac{\sigma}{\pi} T^4(\tau) = \frac{3}{4\pi} \left(\tau + \frac{2}{3}\right) F(0)$$

Recall that $F(0) = \sigma T_{\text{eff}}^4$, by definition, so

$$\frac{1}{\pi} \sigma T^4(\tau) = \frac{3}{4\pi} \left(\tau + \frac{2}{3}\right) \sigma T_{\text{eff}}^4 \quad \text{or} \quad T^4(\tau) = \frac{3}{4} \left(\tau + \frac{2}{3}\right) T_{\text{eff}}^4$$

We derived the **temperature dependence on optical depth**.

Note $T(\tau=2/3) = T_{\text{eff}}$ as we obtained earlier, and $T^4(\tau=0) = T_{\text{eff}}^4 / 2$

A complete solution of the grey case, using accurate boundary conditions, without Eddington approximation, leads to a solution only slightly different from this, usually expressed as

$$T^4(\tau) = \frac{3}{4} (\tau + q(\tau)) T_{\text{eff}}^4$$

Here $q(\tau)$ is a slowly varying function (**Hopf function**), with $q = 1/\sqrt{3} = 0.577$ at $\tau=0$ to $q=0.710$ at $\tau=\infty$.

Rosselland mean opacity

$$\frac{1}{\alpha_R} = \frac{\int \frac{1}{\alpha_\lambda} \frac{dB_\lambda}{ds} d\lambda}{\frac{dB}{ds}} \quad \frac{dB}{ds} = \frac{dB}{dT} \frac{dT}{ds} \quad \text{and} \quad \frac{dB}{dT} = \frac{d}{dT} \left(\frac{\sigma}{\pi} T^4 \right) = \frac{4\sigma}{\pi} T^3$$

$$\frac{1}{\alpha_R} = \frac{\int_0^\infty \frac{1}{\alpha_\lambda} \frac{dB_\lambda}{dT} d\lambda}{\frac{4\sigma}{\pi} T^3}$$

Definition of Rosselland mean opacity

The Rosselland mean $1/\alpha_R$ is a weighted (harmonic) mean of opacity, for which there is a corresponding optical depth (**Rosselland depth**):

$$\tau_{\text{Ross}}(s) = \int_0^s \alpha_R(z) dz$$

We hoped for the temperature structure:

$$T^4(\tau) = \frac{3}{4} \left(\tau + \frac{2}{3}\right) T_{\text{eff}}^4 = \frac{3}{4} \left(\tau_{\text{Ross}} + \frac{2}{3}\right) T_{\text{eff}}^4$$

The grey approximation is very good for $\tau_{\text{Ross}} \gg 1$.

Eddington approximation

Structure of the standard α -disk (3)

138

The energy balance equation is

$$\frac{\partial F}{\partial z} = Q^+$$

or

$$F(H) - F(0) = \int_0^H Q^+(z) dz = D(R)$$

If $T_c^4 \gg T^4(H)$, it becomes approximately

$$\frac{4\sigma}{3\tau} T_c^4 = D(R)$$

or, for the effective temperature of the disk:

$$T(R) = \left\{ \frac{3GM\dot{M}}{8\pi R^3 \sigma} \left[1 - \left(\frac{R_*}{R} \right)^{1/2} \right] \right\}^{1/4}$$

Structure of the standard α -disk (4)

139

The basic set of equations governing the accretion disk:

$$\Sigma = \rho H$$

$$\tau = \Sigma \kappa_R(\rho, T_c)$$

$$H = c_s R^{3/2} / (GM)^{1/2}$$

$$P = \rho c_s^2$$

$$v\Sigma = \frac{\dot{M}}{3\pi} \left[1 - \left(\frac{R_*}{R} \right)^{1/2} \right]$$

$$P = \frac{\rho k T_c}{\mu m_p} + \frac{4\sigma}{3c} T_c^4$$

$$v = \alpha c_s H$$

$$\frac{4\sigma T_c^4}{3\tau} = \frac{3GM\dot{M}}{8\pi R^3} \left[1 - \left(\frac{R_*}{R} \right)^{1/2} \right]$$

We can solve it for the eight unknowns $\rho, \Sigma, H, c_s, P, T, \tau, v$ as a function of the radius R , the mass M of the central object, the accretion rate \dot{M} , and the assumed value of α . Then the radial drift velocity v_R can also be obtained.

Structure of the standard α -disk (5)

140

- The above set of equations cannot be solved in a general fashion, because:
 - The pressure has two contributors
 - Different forms of opacity dominate at different locations
- The simplest procedure is to use the most dominant process at each location.
 - When the dominant source of opacity in the disk is free-free absorption, the Rosseland mean opacity $\kappa_R(\rho, T)$ is well approximated by Kramers' law:

$$\kappa_R = 6.6 \text{ cm}^2 \text{ g}^{-1} \left(\frac{\rho}{10^{-8} \text{ g cm}^{-3}} \right) \left(\frac{T}{10^4 \text{ K}} \right)^{-7/2}$$

- At higher temperatures and lower densities, the main source of opacity is Thomson scattering of photons by free electrons, with $\kappa_R = 0.40 \text{ cm}^2 \text{ g}^{-1}$.
- Then, the set of equations has an algebraic solution.

Structure of the standard α -disk (6)

141

- The disk may be composed of a number of distinct regions:
 - Outer disk ($P_{\text{rad}} \sim 0$, and the dominant source of opacity is free-free absorption):

$$R_{\text{bc}} \text{ (cm)} = 2.9 \times 10^8 \dot{M}_{16}^{2/3} M_1^{1/3} f^{2/3}$$

$$H \text{ (cm)} = 1.27 \times 10^8 \alpha^{-1/10} \dot{M}_{16}^{3/20} M_1^{-3/8} R_{10}^{9/8} f^{3/20}$$

$$\rho \text{ (gcm}^{-3}\text{)} = 4.6 \times 10^{-8} \alpha^{-7/10} \dot{M}_{16}^{11/20} M_1^{5/8} R_{10}^{-15/8} f^{11/20}$$

$$v_R \text{ (cms}^{-1}\text{)} = 2.7 \times 10^4 \alpha^{4/5} \dot{M}_{16}^{3/10} M_1^{-1/4} R_{10}^{-1/4} f^{-7/10}$$

$$T \text{ (K)} = 1.4 \times 10^4 \alpha^{-1/5} \dot{M}_{16}^{3/10} M_1^{1/4} R_{10}^{-3/4} f^{3/10}$$

- Middle disk ($P_{\text{gas}} \gg P_{\text{rad}}$, but the opacity is dominated by electron scattering)

$$R_{\text{ab}} \text{ (cm)} = 2.5 \times 10^6 \alpha^{2/21} \dot{M}_{16}^{16/21} M_1^{7/21} f^{16/21}$$

$$H \text{ (cm)} = 8.0 \times 10^5 \alpha^{-1/10} \dot{M}_{16}^{1/5} M_1^{-7/20} R_8^{21/20} f^{1/5}$$

$$\rho \text{ (gcm}^{-3}\text{)} = 1.9 \times 10^{-4} \alpha^{-7/10} \dot{M}_{16}^{2/5} M_1^{11/20} R_8^{-33/20} f^{2/5}$$

$$v_R \text{ (cms}^{-1}\text{)} = 1.0 \times 10^5 \alpha^{4/5} \dot{M}_{16}^{2/5} M_1^{-1/5} R_8^{-2/5} f^{-3/5}$$

$$T \text{ (K)} = 5.9 \times 10^5 \alpha^{-1/5} \dot{M}_{16}^{2/5} M_1^{3/10} R_8^{-9/10} f^{2/5}$$

- Inner disk ($P_{\text{rad}} \gg P_{\text{gas}}$, the opacity is dominated by electron scattering)

$$H \text{ (cm)} = \frac{3\sigma_T \dot{M}}{8\pi c} f = 1.6 \times 10^4 \dot{M}_{16} f$$

$$\rho \text{ (gcm}^{-3}\text{)} = 23 \alpha^{-1} \dot{M}_{16}^{-2} M_1^{-1/2} R_8^{3/2} f^{-2}$$

$$v_R \text{ (cms}^{-1}\text{)} = 44 \alpha \dot{M}_{16}^2 M_1^{1/2} R_8^{-5/2} f$$

$$T \text{ (K)} = 4.2 \times 10^6 \alpha^{-1/4} M_1^{1/8} R_8^{-3/8}$$

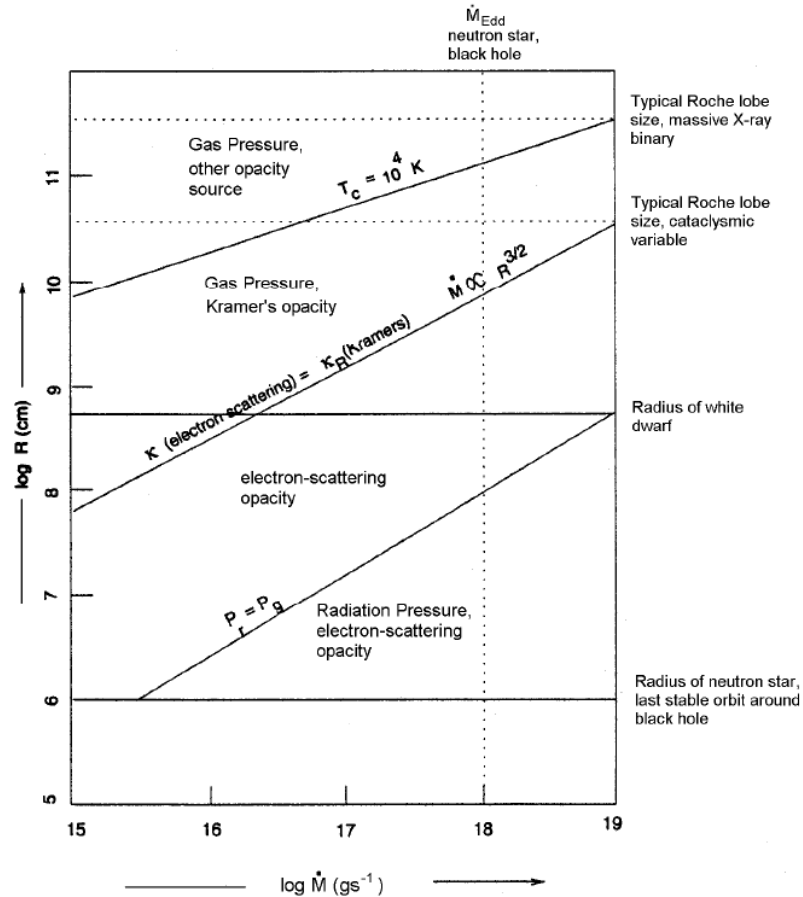
$$f = 1 - (R_*/R)^{1/2}$$

The boundaries between regions

Structure of the standard α -disk (7)

142

The three distinct regions of the accretion disk



Accretion disk typical timescales

143

- Dynamical timescale – the timescale on which inhomogeneities on the disk surface rotate, or hydrostatic equilibrium in the vertical direction is established:

$$t_{dyn} \sim \frac{R}{V_{rot}} \sim \Omega_K^{-1}$$

- Viscous timescale, the timescale on which matter diffuses through the disk under the effect of viscous torques:

$$t_{vysc} \sim \frac{R}{V_R} \sim \frac{R^2}{\nu}$$

- Thermal timescale, the timescale for re-adjustment to thermal equilibrium:

$$t_{th} \sim \frac{\Sigma c_s^2}{D(R)} \sim (h/R)^2 t_{vysc}$$

ADs: confrontation with observation

144

- Inner regions:
 - ▣ closely related to the compact star.
- Outer regions:
 - ▣ radiating predominantly in optical and IR.

- To study the outer regions of the disks observationally, we require that the light in one or more of these parts of the spectrum is dominated by the disk contribution.

Accretion disk: other properties

Tidal Limitation

Boundary Layer

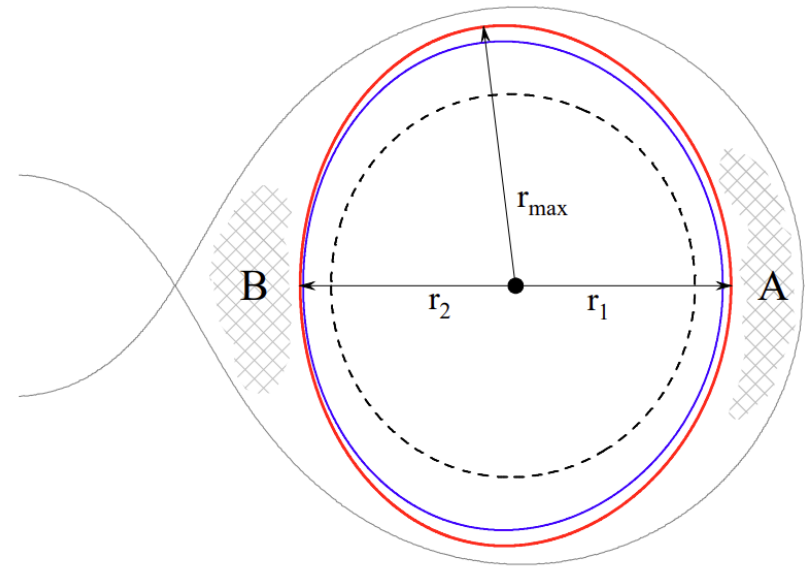
Bright spot

Stream-disk overflow

Accretion disks: Tidal Limitation (1)

146

- For disks that approach R_{L1} in radius the outer parts will be significantly distorted by the gravitational influence of the secondary star. Tidal interaction with the secondary keeps the disk from overflowing the Roche lobe.
- The maximum size of the accretion disk can be found as a largest simple periodic orbit in the restricted three-body problem that does not intersect any other orbit.
- At larger radii intersecting orbits, which are equivalent to tidal shear, will produce dissipation and prevent the disk from growing any larger.



- A different formalism was adopted by Papaloizou & Pringle (1977), with similar results.

Accretion disks: Tidal Limitation (2)

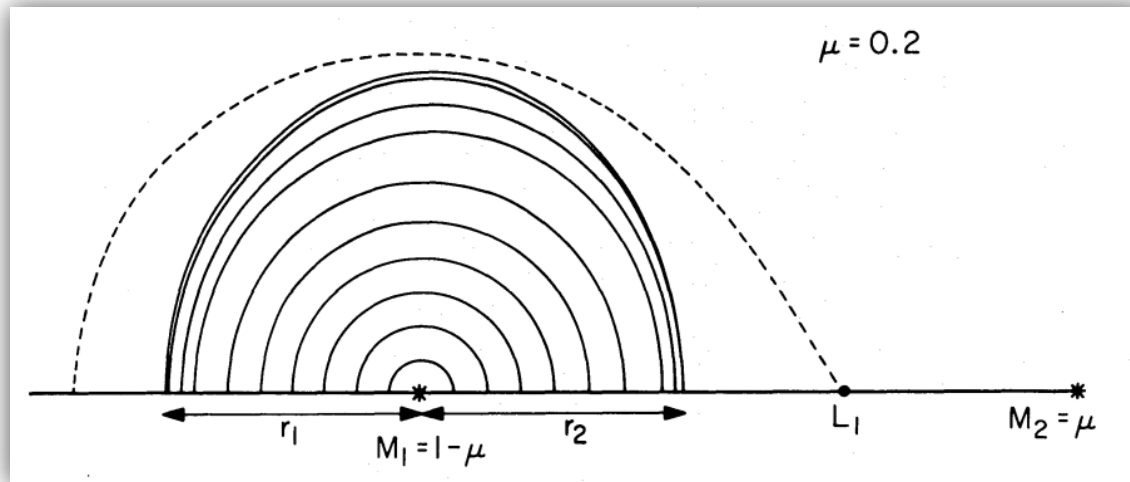
147

- Warner (1995) approximated the tabulated values of r_{\max} calculated by Paczynski (1977):

$$\frac{r_d(\max)}{a} = \frac{0.60}{1 + q} \quad 1\% \text{ accuracy over the range } 0.1 < q < 0.4$$

- Neustroev & Zharikov (2020):

$$\frac{r_d(\max)}{a} = 0.353 + 0.271e^{-3.045 \cdot q} \quad 1\% \text{ accuracy over the range } 0.03 < q < 0.7$$



Accretion disks: Tidal Limitation (3)

- It is commonly accepted that the actual radius of a disk is the result of competition between disk viscosity, effects of the mass transfer stream (which adds matter of low specific angular momentum to the outer edge of the disk) and tidal dissipation.
- Until recently, there was general consensus that variations in the outer disk radius play an important role in understanding the structure and evolution of accretion disks. These variations are predicted by various models of discs (see e.g. Smak 1984; Lasota 2001; Hameury & Lasota 2005).
- However, more and more evidence appear in favor of the idea that the disk radius in cataclysmic variables during many years of observations remains consistently large, close to r_{\max} (see, e.g., Neustroev & Zharikov, 2020, A&A, 642, A100).

Accretion disks: Boundary Layer (1)

149

- The required Keplerian angular velocity Ω_K cannot be maintained at the inner edge of the disk if it is to join smoothly to a **non-magnetic** accreting star spinning at below the break-up velocity $\Omega_K(R)$.
- The region over which gas moving at Keplerian velocities in the disk is decelerated to match the star angular velocity ω_* is called the **boundary layer** (BL).
- If the star spins more slowly than the break-up value, the BL must release a large amount of energy as the accreting matter comes to rest at the stellar surface. Some of this is used to spin up the star, but there remains an amount to be dissipated.

Accretion disks: Boundary Layer (2)

150

- From conservation of energy and angular momentum it can be shown (Kley 1991) that the energy released in the BL is

$$L_{BL} = \frac{GM_*\dot{M}}{2R} \left(1 - \frac{\omega_*}{\Omega_K}\right)^2 = L_d \left(1 - \frac{\omega_*}{\Omega_K}\right)^2$$

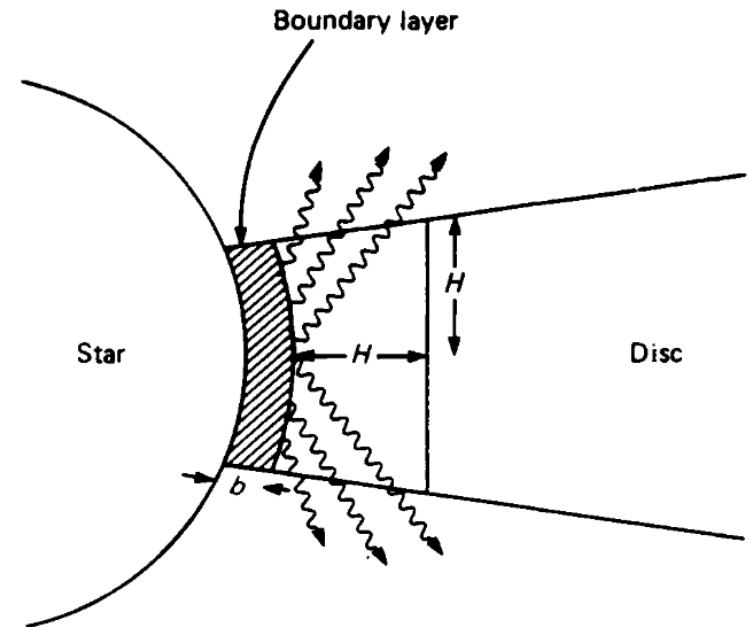
where L_d is the total accretion disk luminosity.

- For $\omega_* \ll \Omega_K$ this is one-half of the total accretion luminosity.

Accretion disks: Boundary Layer (3)

151

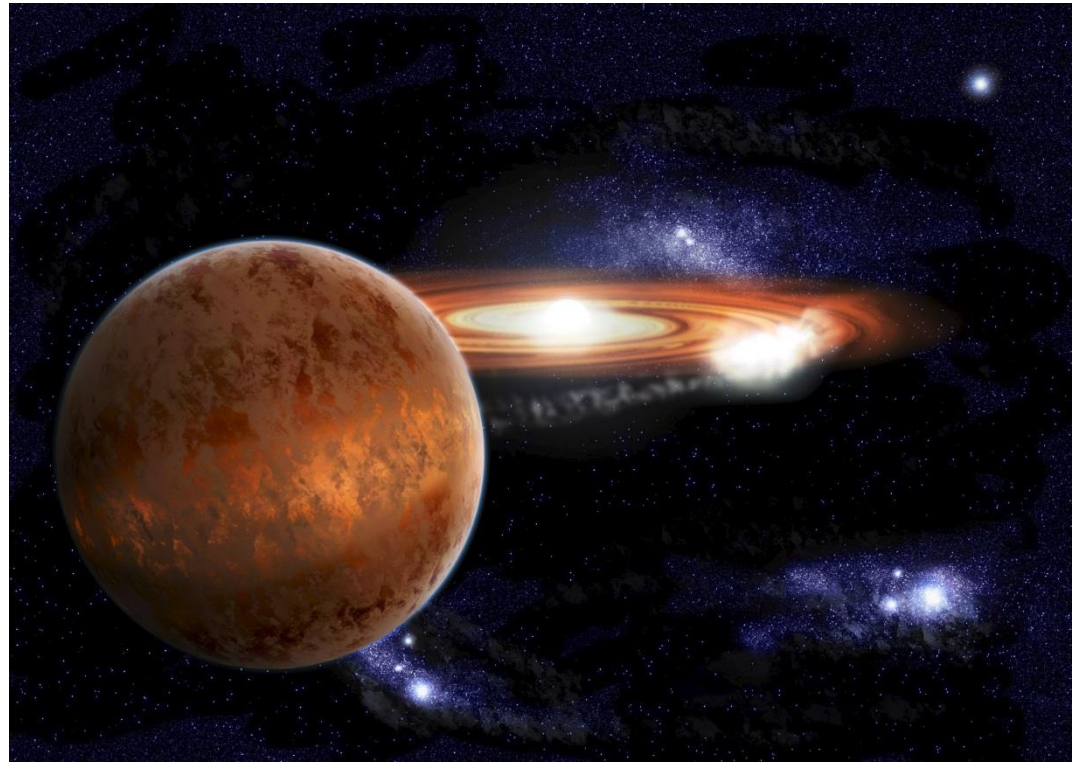
- Where the luminosity of the BL appears in the spectrum depends on its optical thickness.
- The bulk of the radiation from an optically thick BL should be emitted in the soft X-ray and EUV regions.
- An optically thin BL should radiate in hard X-rays, with energies ~ 20 keV.



Accretion disks: Bright spot (1)

152

The gas stream impacts onto the outer rim of an accretion disk at supersonic speeds, creating a shock-heated area that may radiate as much or more energy at optical wavelengths as all the other components (primary, secondary, disk) combined.



Accretion disks: Bright spot (2)

153

- If the bulk of the stream flow impacts at the rim bright spot, its luminosity will be given approximately by the energy released on allowing mass to fall at a rate \dot{M}_2 from infinity to a distance r_d from the primary:

$$L_{BS} \approx \frac{GM_1\dot{M}_2}{r_d}$$

This is an upper limit:

(i) the fall is from L_1 not ∞ (ii) the stream meets the rotating disk edge obliquely

- Compare with the luminosity of the accretion disk, through which mass is flowing at a rate \dot{M}_d :

$$L_d \approx \frac{GM_1\dot{M}_d}{2R_1}$$

- Sometimes $L_{BS} > L_d \rightarrow \dot{M}_d < \dot{M}_2$

Accretion disks: Bright spot (3)

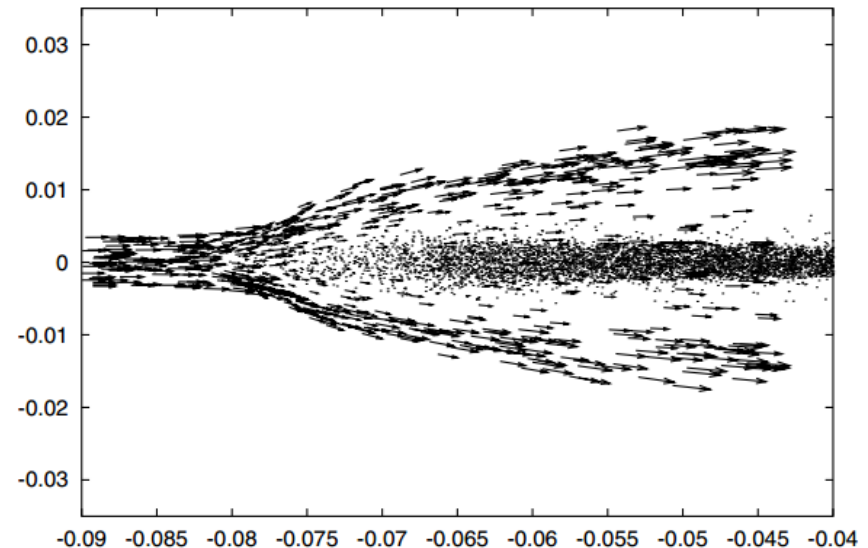
154

- The location of the bright spot is obviously determined by the intersection of the stream trajectory with the outer edge of the disk.
- Can be used to measure q and the disk radius (position of the bright spot can be derived from eclipse observations).

Stream-disk overflow (1)

155

- Part of the stream can flow over the rim of the disk and continue approximately along the single particle trajectory over the face of the disk until it impacts the disk at a later time.

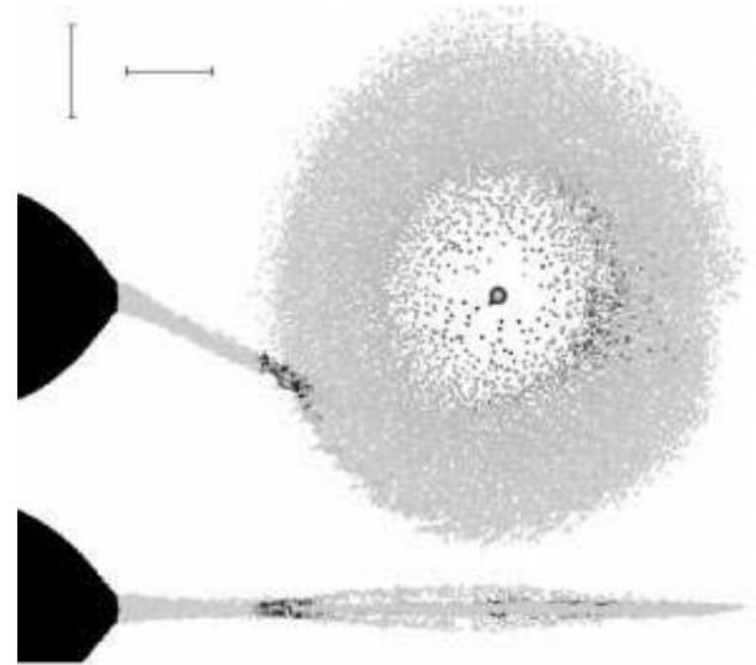


Stream-disk impact region
(from Kunze, Speith and Hessman, 2001)

Stream-disk overflow (2)

156

- The ultimate impact point for stream material continuing over the face of the disk is in the vicinity of the point of closest approach to the primary, creating there a **second** bright spot at a position $(r, \alpha) \approx (r_{\min}, 148^\circ)$.
(Lubow, 1989)

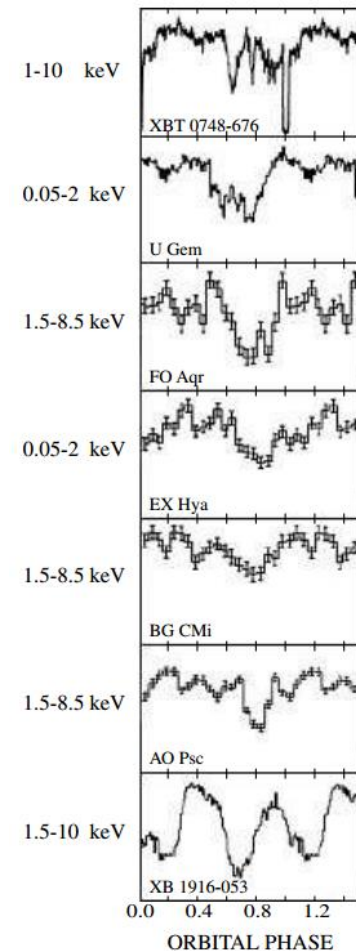


Stream-disk impact region
(from Kunze, Speith and Hessman, 2001)

Stream-disk overflow (3)

157

- The stream overflow can cause the X-ray absorption dips observed in cataclysmic variables (CVs) and low-mass X-ray binaries (LMXBs) around orbital phase 0.7, if the inclination is at least 65° .



Orbital phase-folded X-ray light curves
(Hellier et al, 1993)

Stream-disk simulations (1)

158

- If the impact region is optically thick, so that the energy of impact is not quickly radiated, then part of the stream bounces off the disk and is sprayed into the Roche lobe;
- The denser core of the stream can penetrate into the edge of the disk releasing its kinetic energy at optical depths greater than unity, thus locally heating the rim, increasing its scale height and causing a bulge that runs around the edge of the disk for typically half the perimeter;
- The stream overflow.

Stream-disk simulations (2)

159

- **However!** Bisikalo et al.:
- *"The interaction between the stream from the inner Lagrange point and the disk is shockless"*
- *"A region of enhanced energy release is formed due to the interaction between the circum-disk halo and the stream and is located beyond the disk, and the resulting shock is fairly extended."*
- *Instead of "a bright spot" – "a hot line"*

Close Binary Stars

Existence Of Accretion Disks In Close Binary Systems

The zoo of close binary systems

Cataclysmic Variables (CVs)

Low-Mass X-ray Binaries (LMXBs)

High-Mass X-ray Binaries (HMXB)

Contact Binaries

Symbiotic Stars, etc

Existence Of Accretion Disks In Close Binaries

161

- Members of close binary systems might undergo mass transfer at different stages in their evolution.
- In an evolution which starts with both components on the main sequence, it is always the more massive star evolves faster and thus fills its critical Roche lobe first and starts transferring mass to its companion.
- In many cases, the primary's remnant after the first mass transfer will later become a compact star.
- If in such a system at a later time the secondary starts transferring mass back to the now compact primary, this will almost invariably result in the formation of an accretion disk around it.

Existence Of Accretion Disks In Close Binaries

- We expect the formation of an accretion disk wherever the specific angular momentum of material flowing towards a star is so high that it cannot directly fall on it.
- The more compact and therefore the smaller this star, the better is the chance for the formation and persistence of an accretion disk.
- Apart from the frequent combination compact star/main sequence star we find also binaries with a larger separation containing a compact star and a star which has reached a more advanced evolutionary stage (e.g. GK Per or some long-period low-mass X-ray binaries).
- The closest systems are the ones which consist of two compact stars.
- Besides the accretion via Roche lobe overflow there is also the possibility of accretion from a stellar wind. This is particularly relevant for detached systems consisting of an O/B star and a neutron star or a black hole (massive X-ray binaries).

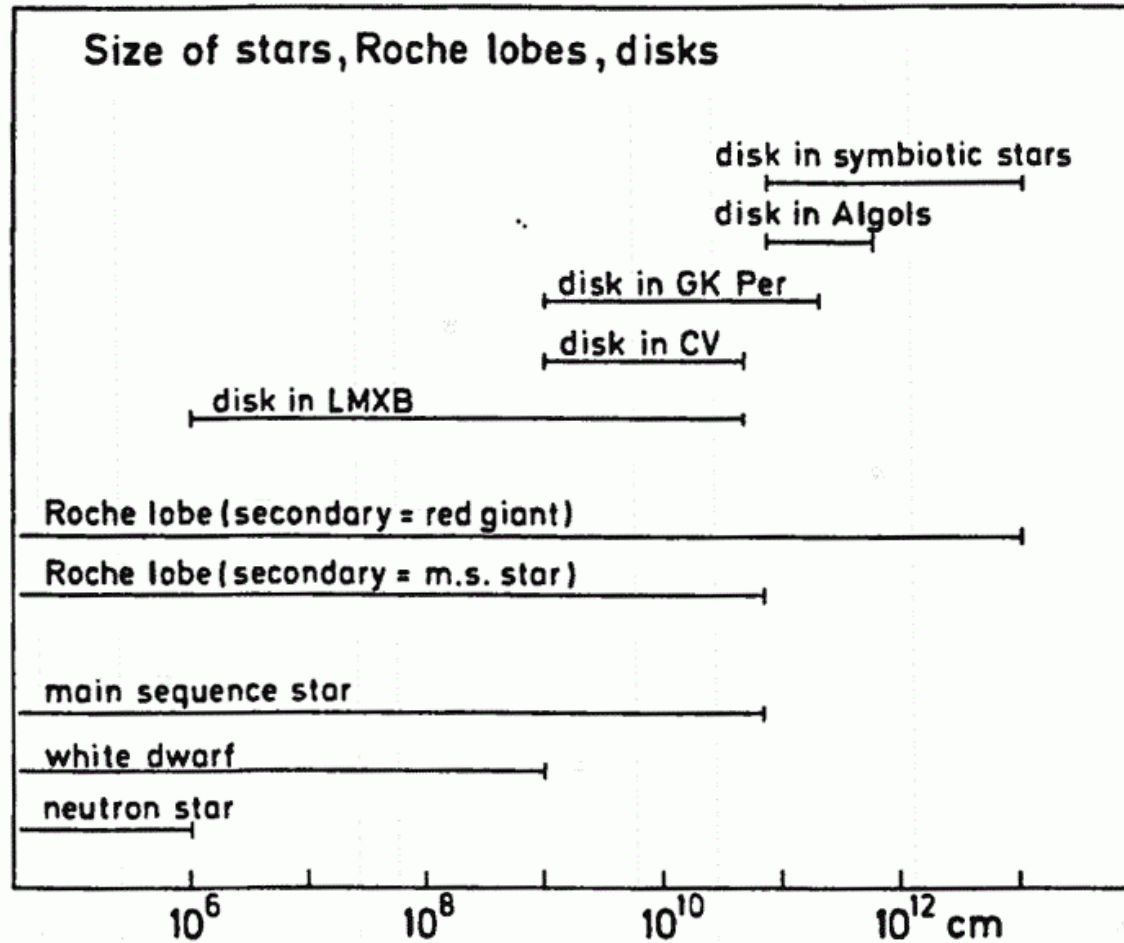
The zoo of close binary systems

secondary \ primary	main-sequence star ^{*)}	evolved star ^{**)}	white dwarf	neutron star or black hole
main-sequence star ^{*)}	[binary T Tauri stars] [RS CVn stars] Algols (AD) (TAD) {W UMa stars = contact systems}	symbiotic stars Type I as e.g. CI Cyg, Z And, AR Pav (AD) Algols (AD), (TAD)	^{*)} main-sequence star or slightly evolved ^{**)} evolved star, but not yet a compact star [] detached systems	
evolved star ^{**)}	[Wolf-Rayet binaries] [binary planetary nebulae]		(AD) evidence for an accretion disk (TAD) evidence for a transient accretion disk	
white dwarf	[pre-cataclysmic binaries] non-magnetic CVs: UX UMa stars (AD) dwarf novae (AD) DQ Her stars (AD) AM Her stars	long period CVs as GK Per (AD) recurrent nova (AD) symbiotic stars (AD) symbiotic novae (AD)	[double white dwarfs] AM CVn stars (AD)	
neutron star or black hole	massive X-ray binaries (AD) (wind accretion) low mass X-ray binaries (AD) HZ Her/Her X-1 (AD) SS 433 (AD)	long period low mass X-ray binaries (AD)	[binary pulsars] 4U1820-30 (AD)	[binary pulsars]

Comments: in semi-detached systems the mass gaining star is listed as the primary
in detached systems the more evolved star is listed as the primary

Accretion Disks In Close Binaries

164



Accretion Disks In Close Binaries

165

- **HMXBs:**
 - ▣ The donor stars are O or B giants or supergiants, $L_{\text{opt}} \sim 10^{37} - 10^{38}$ erg/s, much higher than the UV and optical luminosity of the disks.
- **LMXBs and CVs:**
 - ▣ The donor stars are late type, low-mass, faint stars, the accreting compact stars are neutron stars (black holes) and white dwarfs respectively.
 - ▣ The processes of mass transfer are similar in these two types of systems, but $L_{\text{opt,LMXB}} \geq 100 L_{\text{opt,CV}}$
 - ▣ This means that re-absorption of X-rays in LMXB disks is very important.
- **CVs are the best candidates for testing the theory of steady (and unsteady) thin disks.**

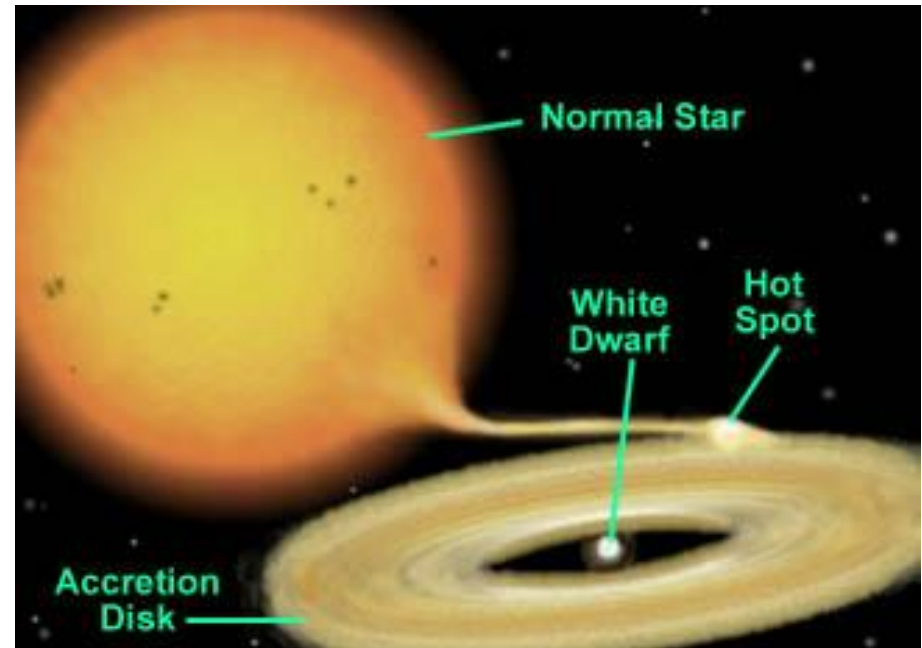
166

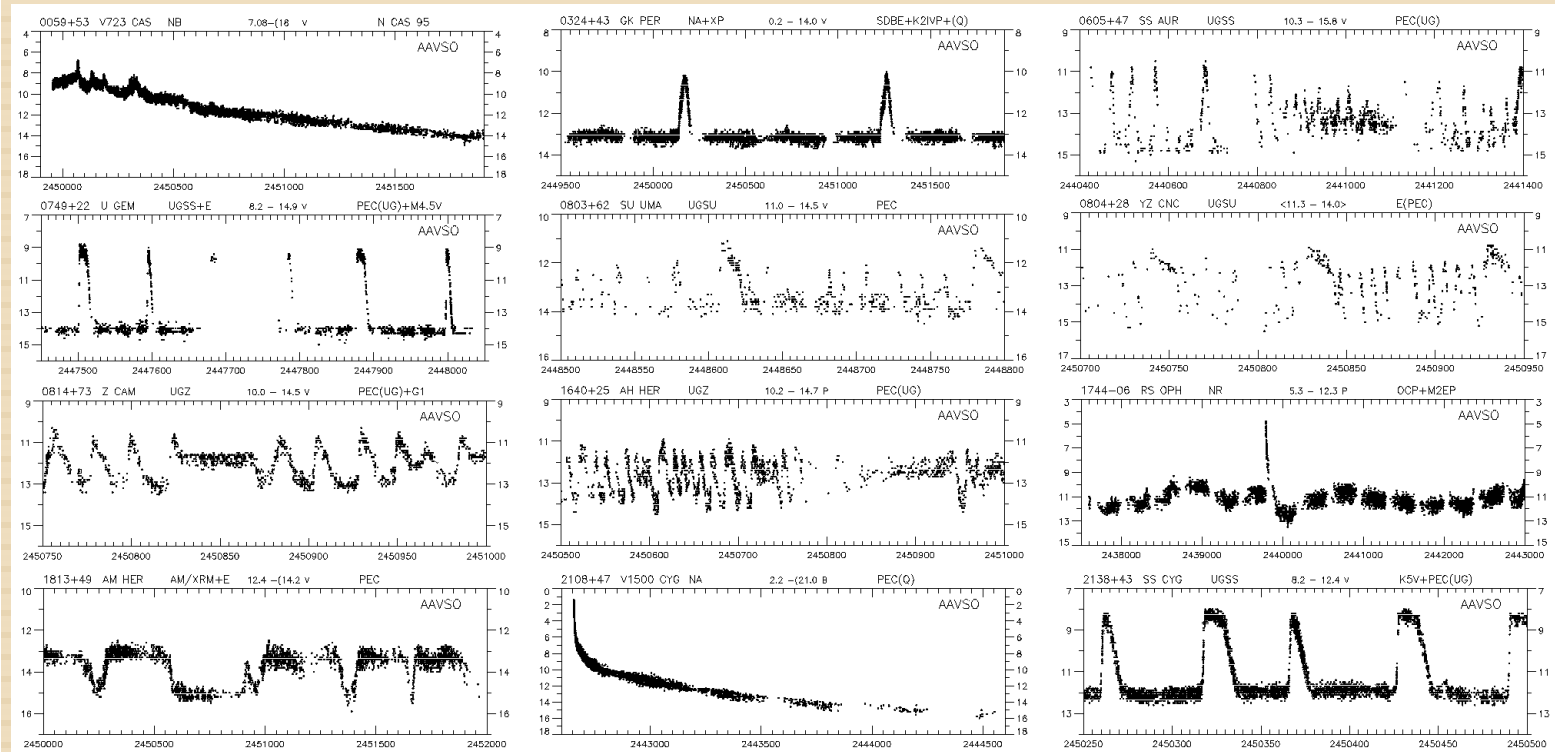
Cataclysmic Variables

Cataclysmic Variables

167

- Compact close binary systems;
- Red dwarf-type (Sun-like) star – secondary, and a white dwarf – primary;
- Due to evolution, the red star is losing matter to the white dwarf star via an accretion disk (usually but not always);
- Thousands of CVs are known.





168

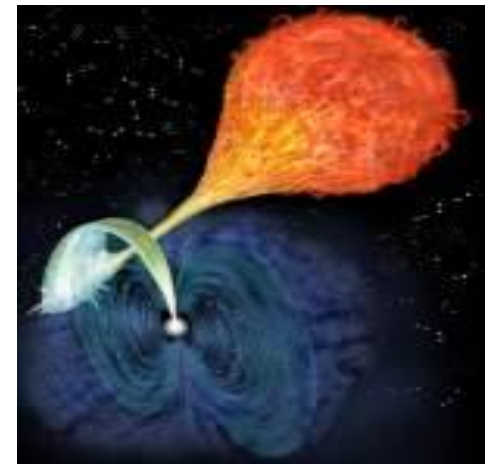
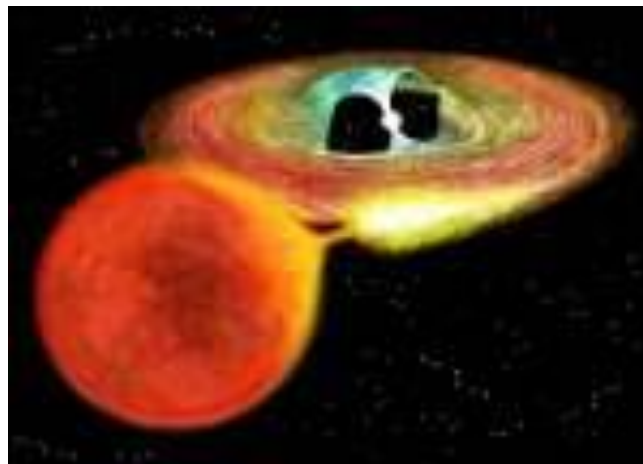
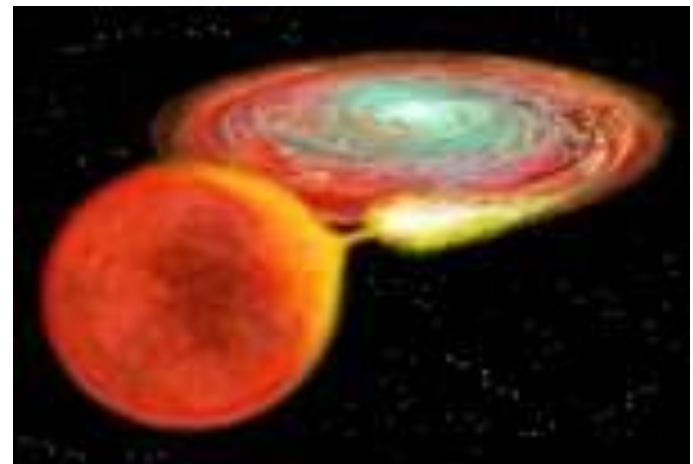
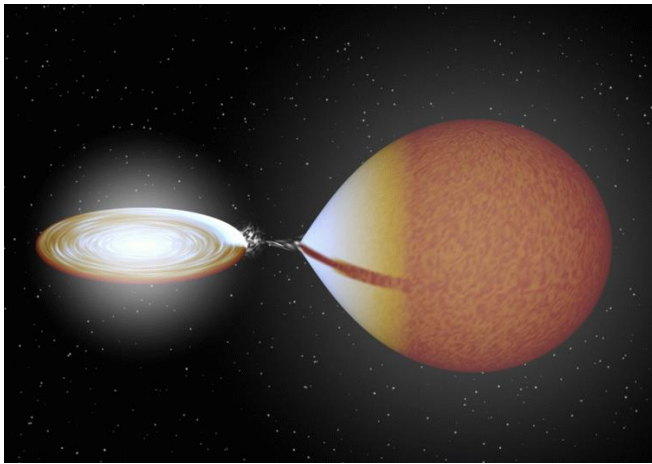
The Many Faces of Cataclysmic Variables

The classification of CVs is rooted in the historical observations of these objects, which concentrated, for obvious reasons, on the spectacular outbursts that characterise these stars and lend them their name.

Interacting Binary Stars

Classification of CVs (1)

169



Interacting Binary Stars

Classification of CVs (2)

170

- The fundamental observational characteristic of CVs is their variability.
- CVs vary on many different time scales, from long-term variations of years, down to short-term variability of seconds:
 - Long-term variability
 - Classical Nova Eruptions
 - Dwarf Nova Eruptions
 - Variability on orbital timescales
 - Orbital variability
 - Superhumps
 - Short-term variability
 - White Dwarf Spin Period
 - QPO
 - Non-Radial Pulsations
 - Flickering

Classical Novae Eruptions (1)

171

- **Classical novae (CN)** have, *by definition*, only one observed eruption. The range from pre-nova brightness to maximum brightness is from 6 to greater than 19 magnitudes and is strongly correlated with the rate at which the nova fades after maximum.
- **Recurrent novae (RN)** are, *by definition*, previously recognized CN that are found to repeat their eruptions, implying a nova recurrence time scale of approximately 10 years – 100 years.

Classical Novae Eruptions (2)

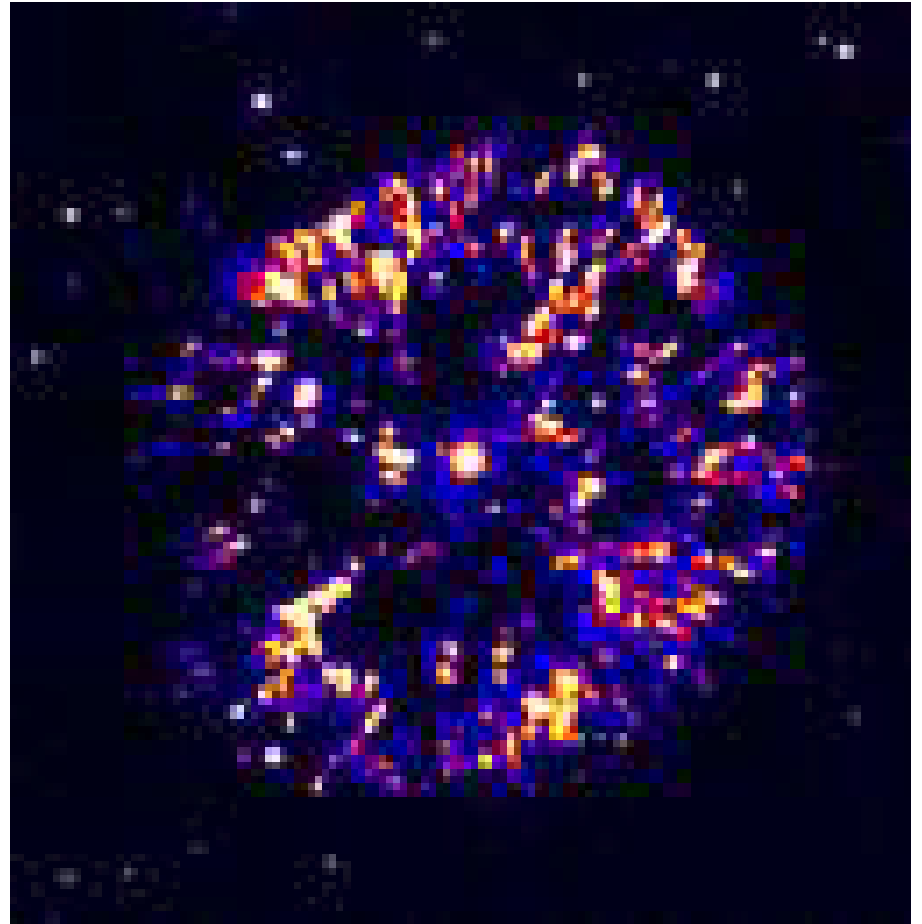
172

- Observationally, CN with more massive WDs are brighter during the eruptions, but decline faster, compared to CN with lower WD masses. They are therefore divided into classes depending on how fast they fade.
- The speed class usually being defined by the quantity t_2 , which is defined as the time it takes for the nova to decline 2 mag below maximum brightness.
 - ▣ The largest amplitude eruptions, of shortest duration, are in very **fast novae** ($t_2 < 10$ days). They decline with a rate up to 0.2 mag d^{-1} .
 - ▣ The lowest amplitudes, in eruptions that may last for years (a decline rate of $0.008 - 0.013 \text{ mag d}^{-1}$), are in the **slow novae** ($t_2 > 150$ days).

Classical Novae Eruptions (3)

173

- The nova eruption is due to the accumulation of hydrogen-rich material from the secondary star on the surface of the white dwarf.
- As material is accumulated, the temperature and density of this layer eventually become high enough to start nuclear fusion in a runaway manner.

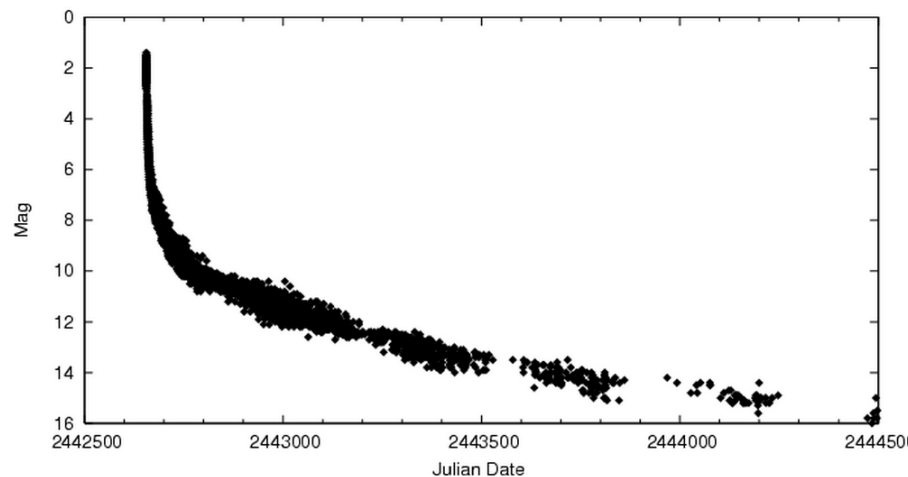


Interacting Binary Stars

Classical and Recurrent Novae (1)

174

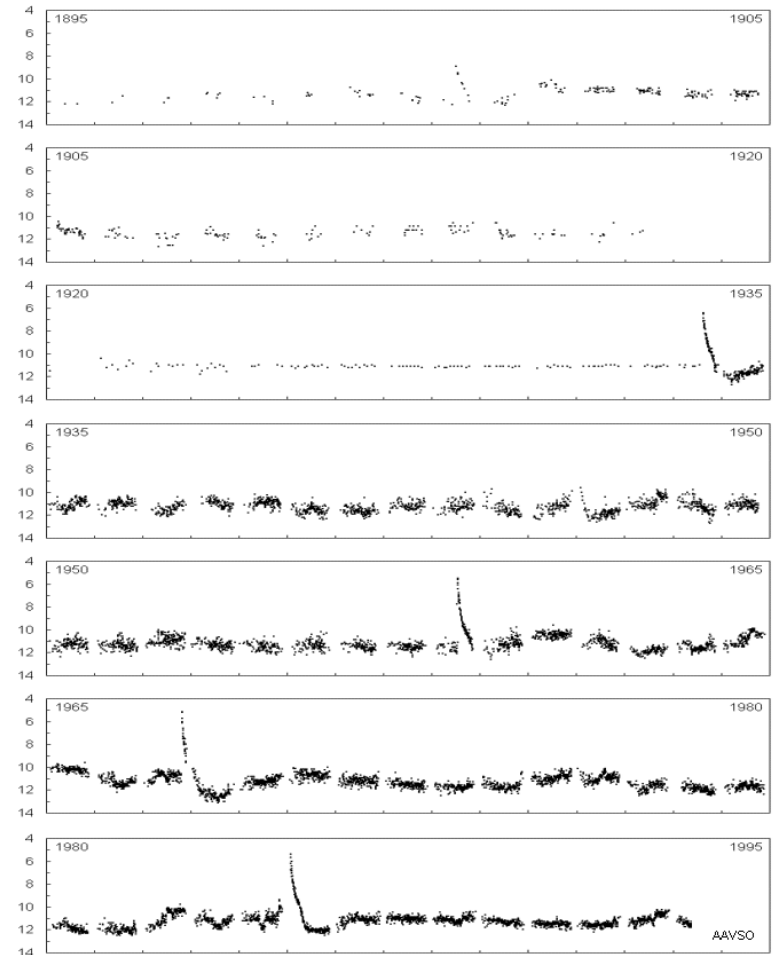
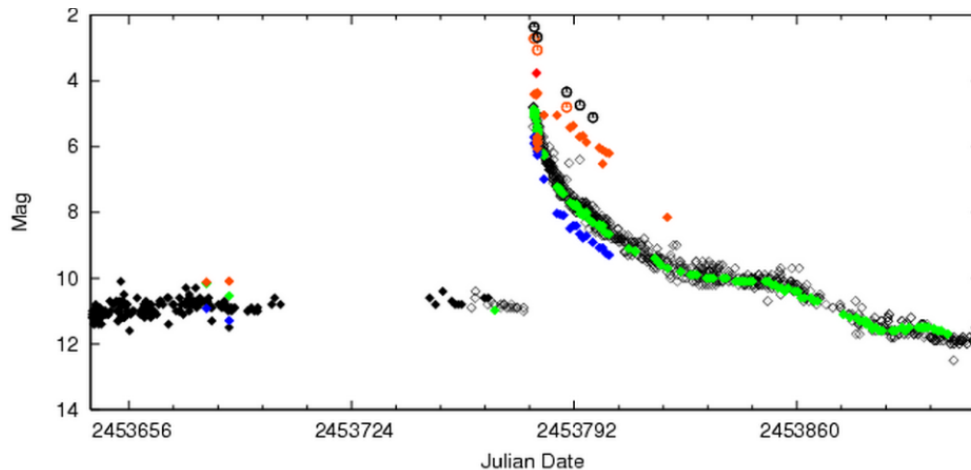
- **V1500 Cygni** or **Nova Cygni 1975** was a bright nova occurring in 1975. It had the second highest intrinsic brightness of any nova of the 20th Century, exceeded only by CP Puppis in 1942.
- V1500 Cyg was discovered on August 29 and reached 1.7 mag on the next day. It remained visible to the naked eye for about a week, and 680 days after maximum the star had dimmed by 12.5 magnitudes.



Classical and Recurrent Novae (2)

175

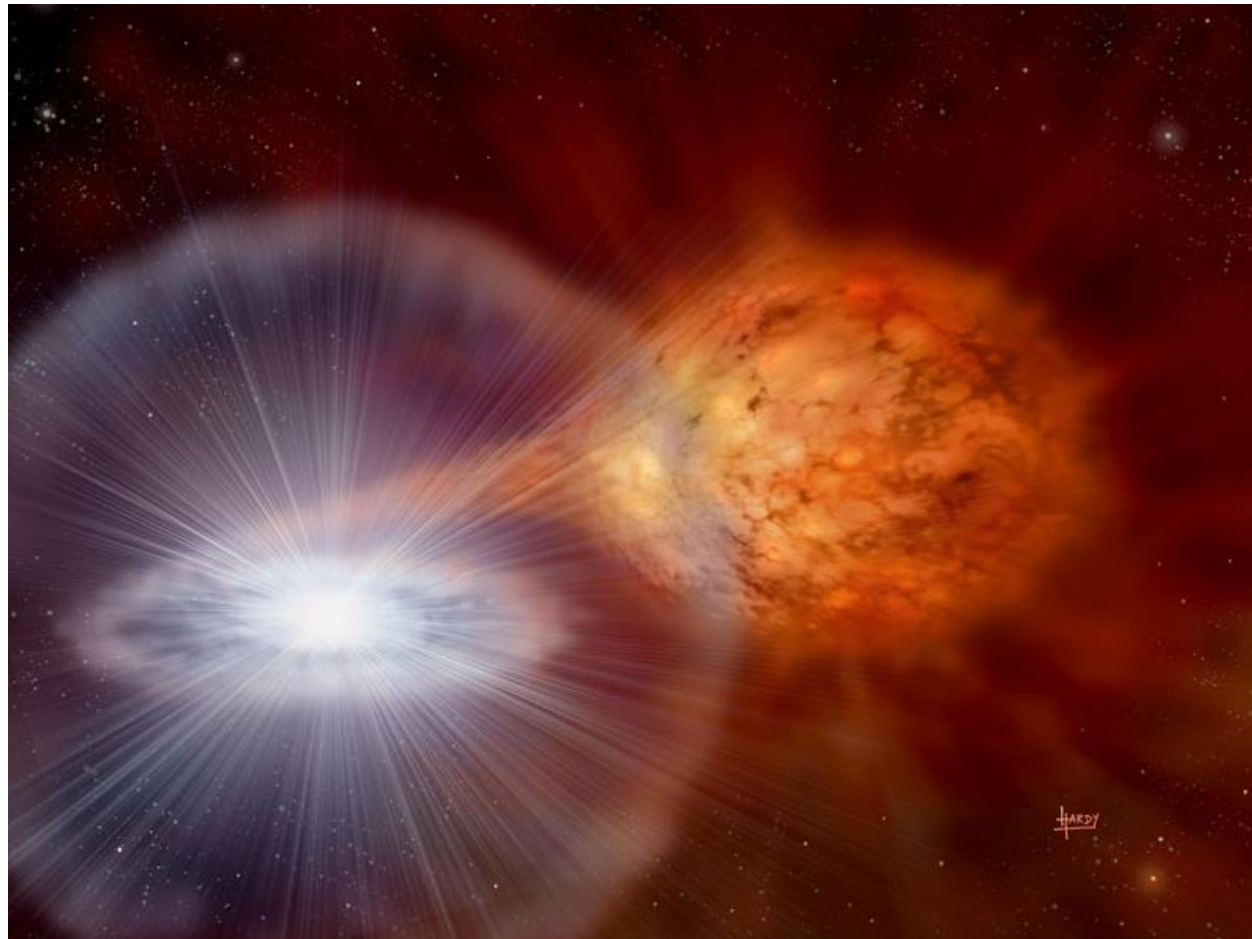
- ❑ **RS Ophiuchi** (*RS Oph*) is a **RN** erupted in 1898, 1933, 1958, 1967, 1985, and 2006 and reached about 5 mag on average.
- ❑ In its quiet phase it has an apparent magnitude of about 12.5.



Interacting Binary Stars

Classical and Recurrent Novae (3)

176



Explosions from White Dwarf Star RS Oph
Illustration Credit & Copyright: David A. Hardy & PPARC

Interacting Binary Stars

Classical and Recurrent Novae (4)

177

- In theory, the expected mass required to ignite the hydrogen layer on the WD surface should be roughly equal to the total mass of the expelled nova shell. A WD of mass $1 M_{\odot}$ will need to accumulate $\approx 10^{-4} M_{\odot}$, before ignition.
- Assuming an accretion rate of $\dot{M} \sim 10^{-9} M_{\odot} \text{ yr}^{-1}$, the time scale between two such eruptions is about $\sim 10^4 - 10^5$ years.
- A nova recurrence time scale of < 100 years can only occur for systems which have a high accretion rate (of order $10^{-7} M_{\odot} \text{ yr}^{-1}$) and a massive WD ($M_1 > 1 M_{\odot}$).
- In RNe, the WD is expected to gain more mass between eruptions than it ejects during them. This could make the already high WD mass exceed the Chandrasekhar limit ($M_{\text{CH}} \approx 1.4 M_{\odot}$). Therefore, RNe are considered as candidate supernova Type Ia progenitors.

Dwarf Nova Outbursts (1)

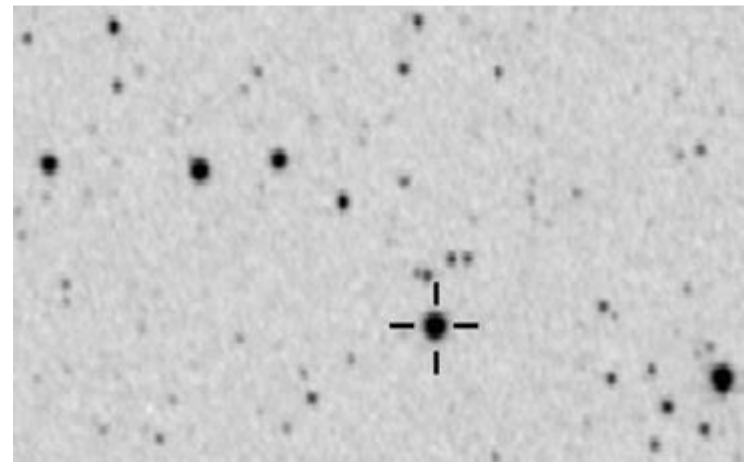
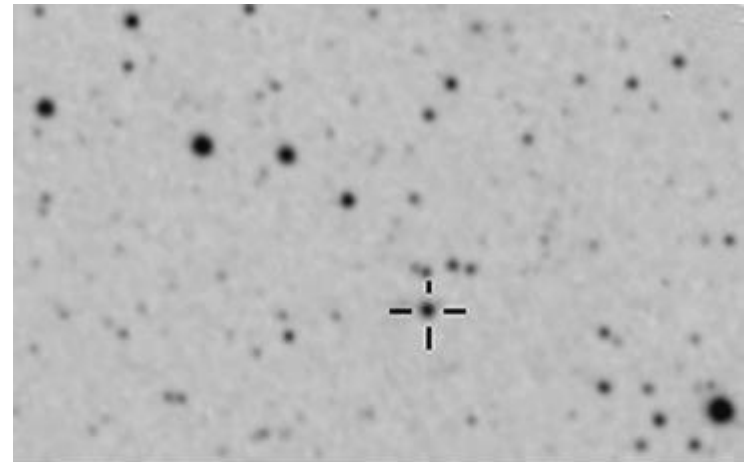
178

- **Dwarf nova (DN)** eruptions are less violent than the CN eruptions. DNe have outbursts of typically 2-5 mag, with some rare objects (e.g., WZ Sge) with up to 8 mag range.
- However, they occur more frequently: the interval between outbursts is from ~ 10 d to tens of years with a well-defined time scale for each object; the duration of normal outbursts is $\sim 2-20$ d, correlated with interval between outbursts.
- The DN outburst is reasonably well understood as a release of gravitational energy, caused by a temporary large increase in mass transfer rate through the disk.

Dwarf Nova Outbursts (2)

179

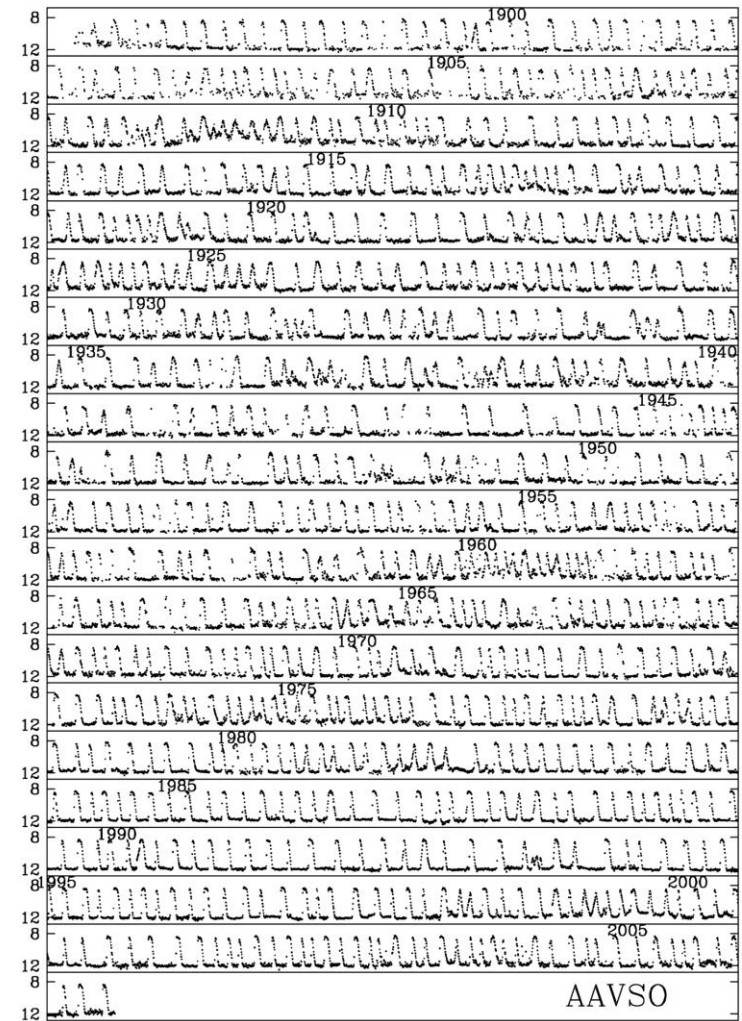
- Since its discovery in 1896, **SS Cygni** has undoubtedly been one of the most observed variable stars in the night sky.
- It undergoes frequent and regular brightness outbursts every 7-8 weeks, rising from 12th magnitude to 8th magnitude for, typically, 1–2 days.



Dwarf Nova Outbursts (3)

180

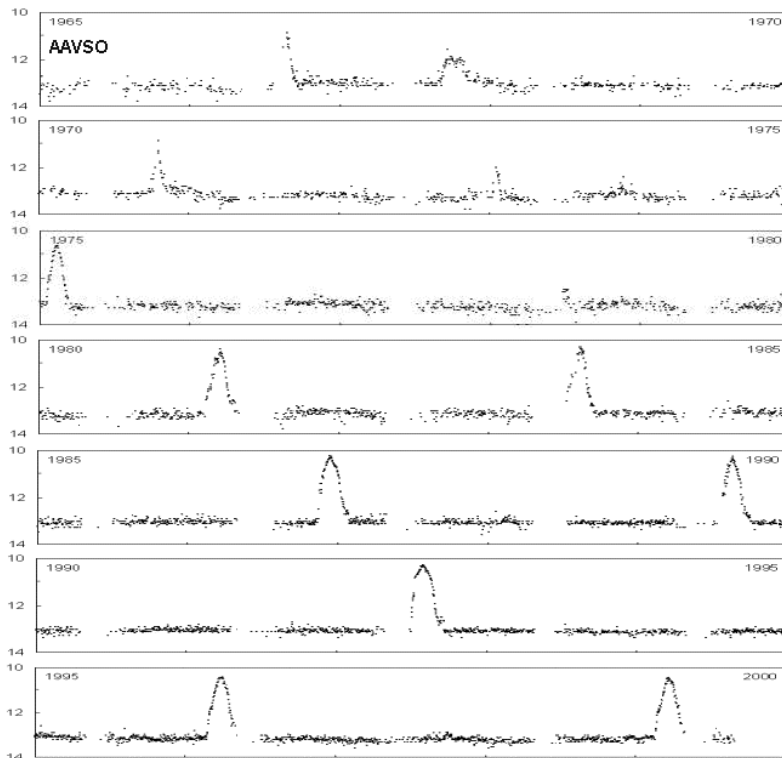
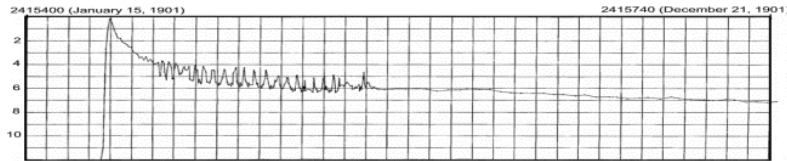
- The 1896 discovery of SS Cyg proved to be only the second star of the dwarf nova type, with U Gem being the first of the class with its discovery in 1855.
- In the past century, not a single outburst of SS Cyg has been missed.



SS Cyg (27 Sep 1896–30 July 2006)

Dwarf Nova Outbursts (4)

181



- A few CNe also show DN outbursts.
- **GK Persei (Nova Persei 1901)** was a bright nova occurring in 1901 (max ~ 0.2 mag). After fading into obscurity at about 12 mag, GK Per began displaying infrequent outbursts of 2-3 mag, occurring about every three years. Thus, GK Persei has changed from a CN to a typical DN.

Dwarf Novae

182

- There exist three distinct subtypes of dwarf novae:
- **SU Ursae Majoris** stars exhibit superoutbursts in addition to regular outbursts;
- **Z Camelopardalis** stars show protracted standstills about 0.7 mag below maximum brightness, during which outbursts cease for intervals of tens of days to years;
- **U Geminorum** stars are the dwarf novae that are neither Z Cam nor SU UMa stars.

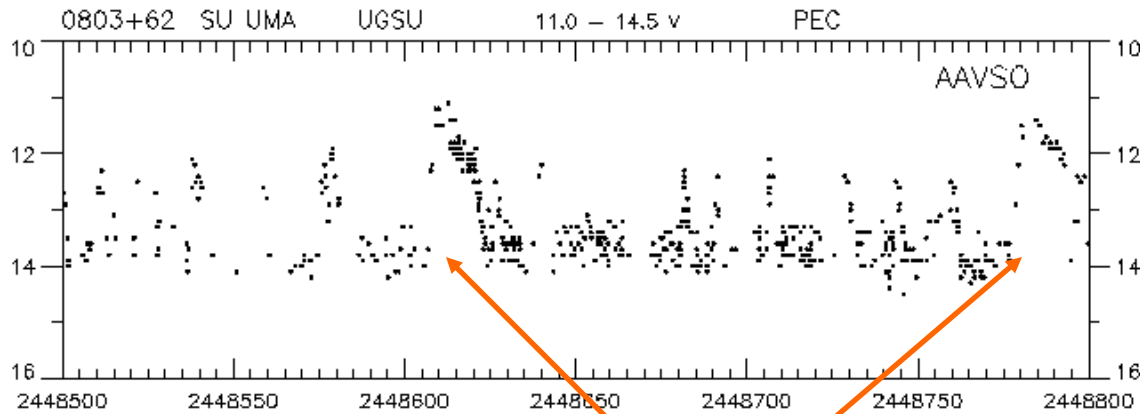
Dwarf Novae: SU UMa stars (1)

183

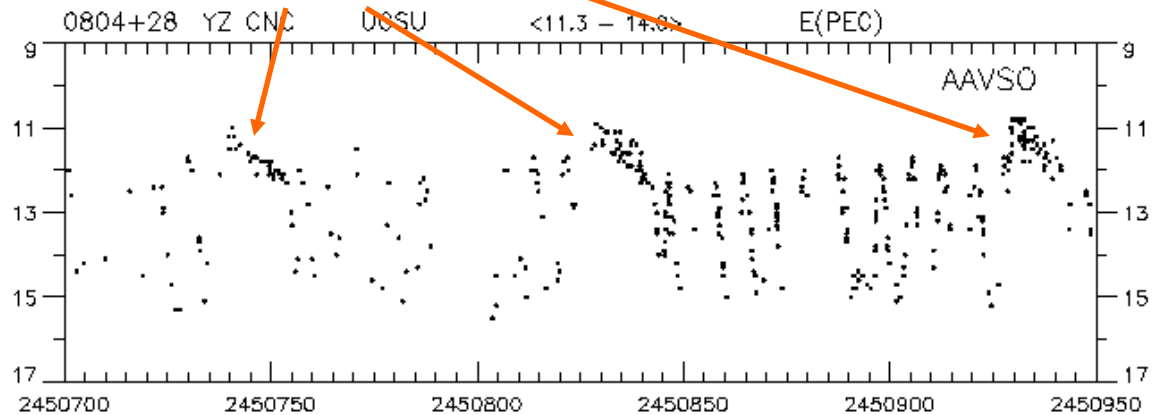
- Narrow outbursts of about 1-2 days;
- The superoutbursts are approximately 0.7 mag brighter than normal outbursts and of longer duration (for ~ 5 times the duration of an ordinary outburst);
- The superoutbursts often appear to be triggered by normal outbursts, as a pause before maximum superoutburst brightness is achieved.
- Superhumps seen during superoutbursts;
- Subtype: WZ Sagittae

Dwarf Novae: SU UMa stars (2)

184



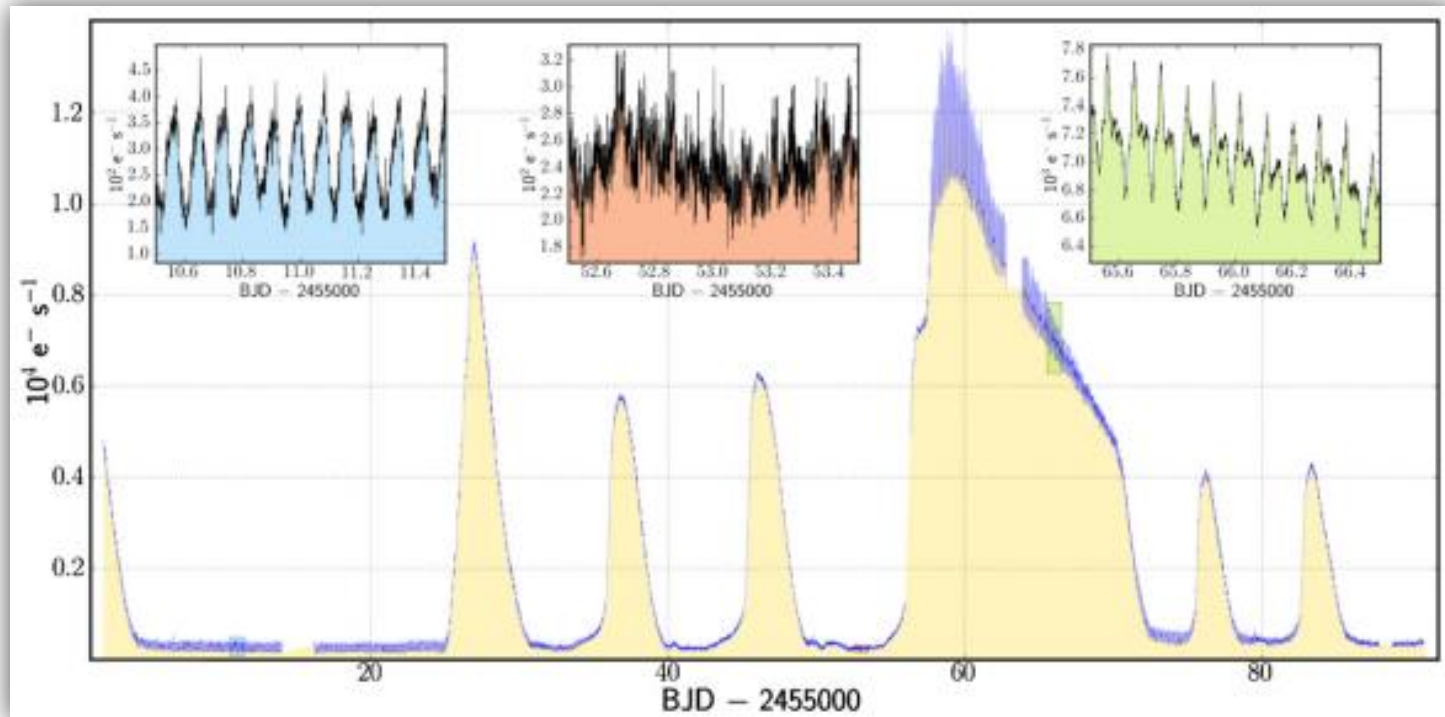
Superoutbursts



Interacting Binary Stars

Dwarf Novae: SU UMa stars (3)

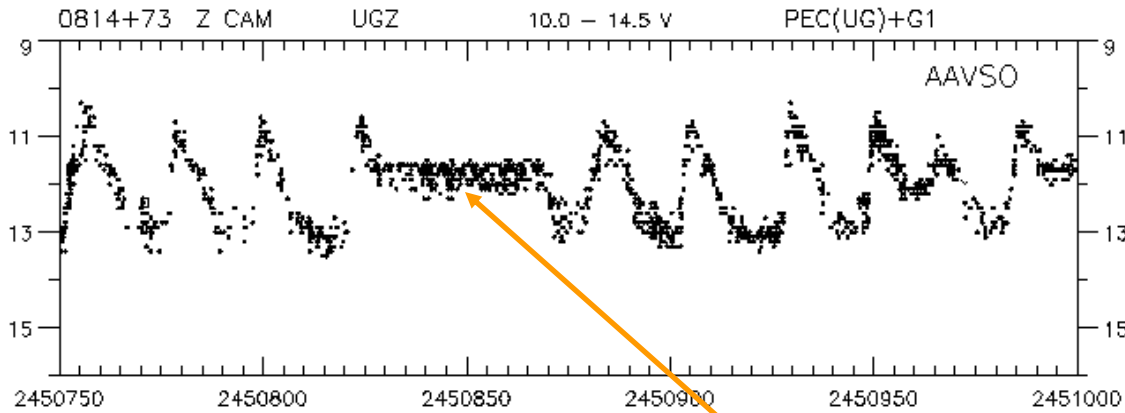
185



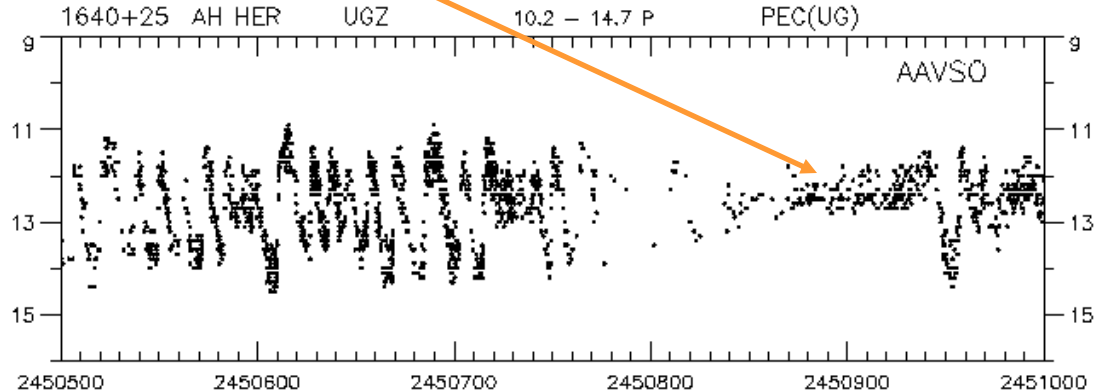
Kepler light curve of V344 Lyrae showing several normal outbursts and one superoutburst (from Still et al. 2010).

Dwarf Novae: Z Cam stars (1)

186



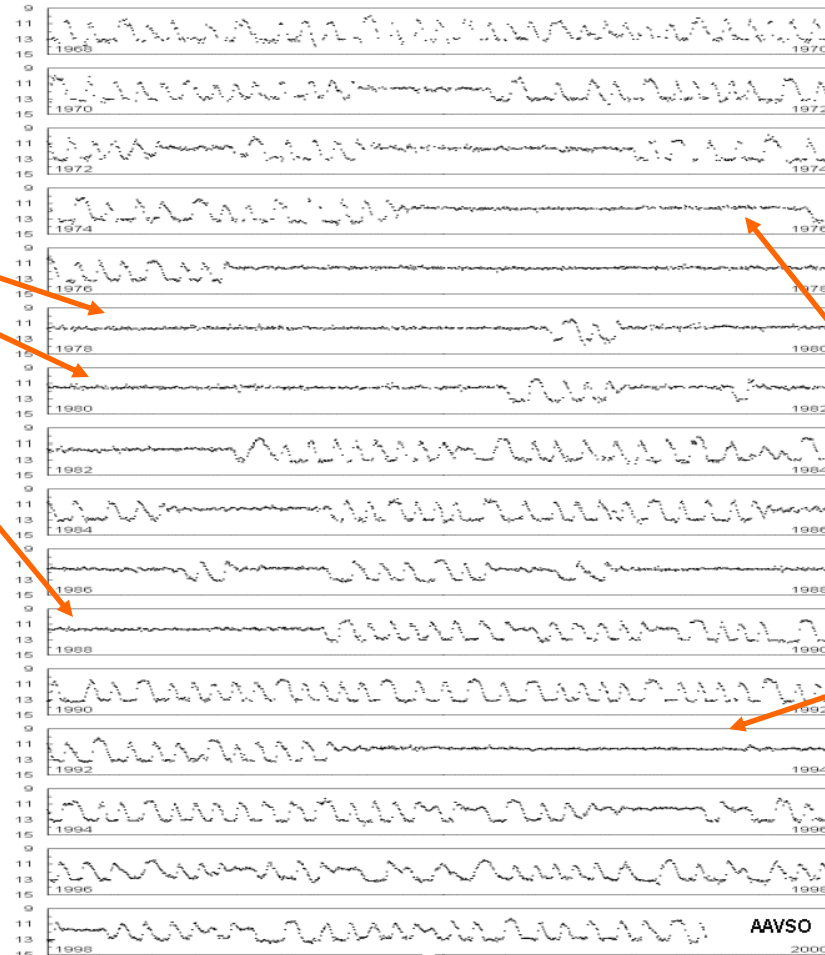
Standstill



Interacting Binary Stars

Dwarf Novae: Z Cam stars (2)

Z Camelopardalis



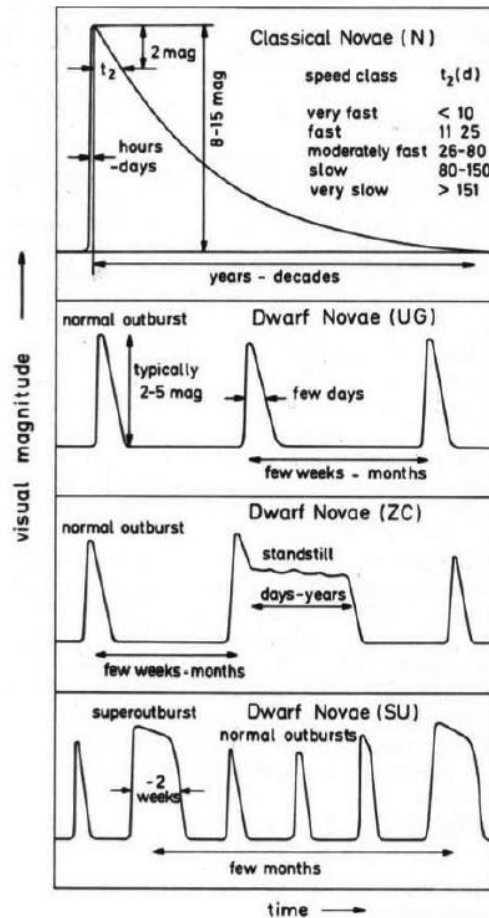
Standstill

Standstill

Outbursts of CNe and DNe

188

The eruption behaviour of CNe and DNe.



Dwarf Nova Outbursts (5)

189

- Several CNe also show DN outbursts.
- The distinction between RN and DN is made spectroscopically: in RN and CN a substantial shell is ejected at high velocities; in DN no shell is lost.



GK Persei: Nova of 1901.

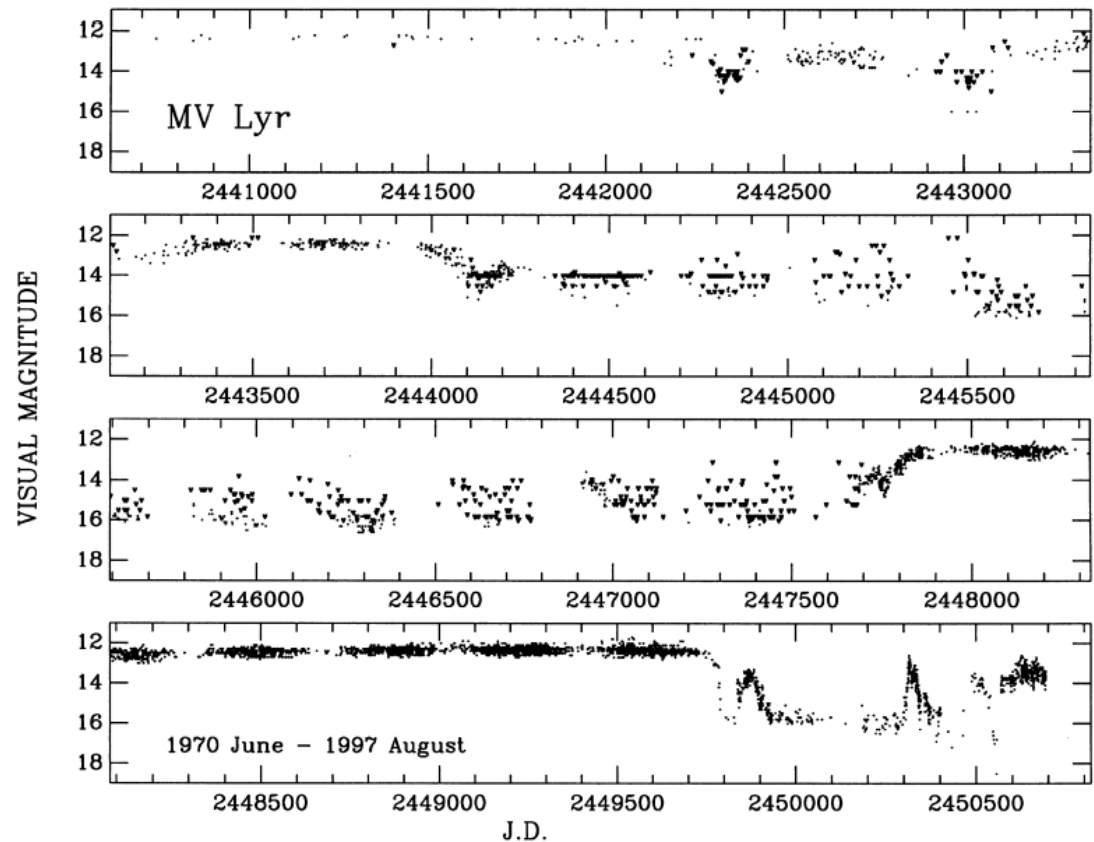
Nova-like variables

- **Nova-like** variables include all the '*non-eruptive*' CVs.
- Perhaps, the NLs include pre-novae and post-novae stars, for all of which our observational baseline (typically ~ 1 century) is too short to reveal their cataclysms.
- In addition, the **VY Scl** stars are included, which show occasional reductions in brightness from an approximately constant maximal magnitude, caused by temporary lowering of the rate of mass transfer from the secondary.
- Similar to CN in terms of light changes and spectral features.
- Magnetic CVs are usually included among the NLs (except for the few that are already recognized as CN or other defined types).

VY Sculptor

191

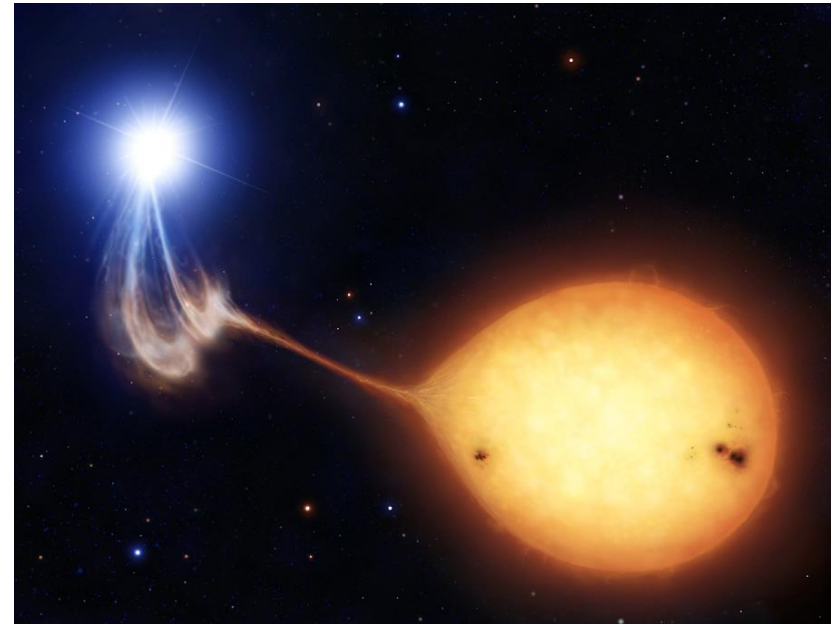
□ Anti-Dwarf Nova



Polars (AM Her stars)

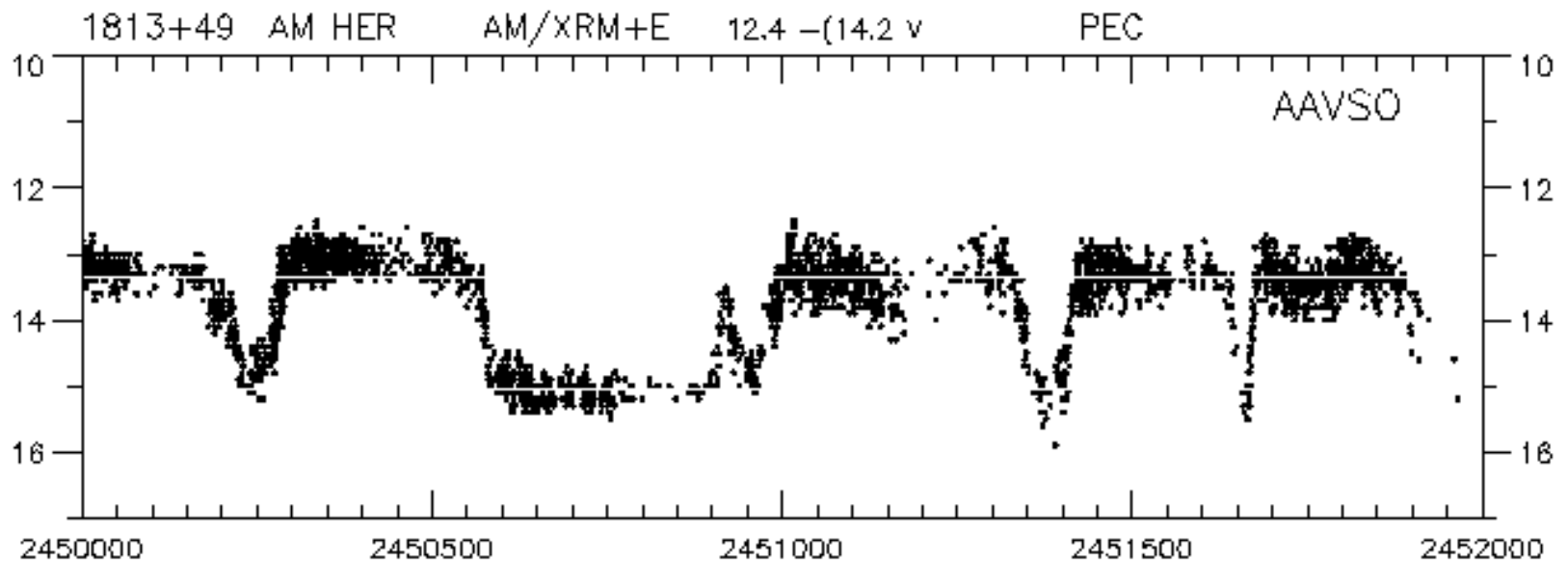
192

- A White dwarf has magnetic field of 10-100 mega Gauss;
- Accretion columns, instead of an accretion disk;
- Synchronous rotation ($P_{\text{spin}} = P_{\text{orb}}$);
- Source of hard X-ray, extreme UV, UV, as well as optical wavelengths.



Polars (AM Her stars)

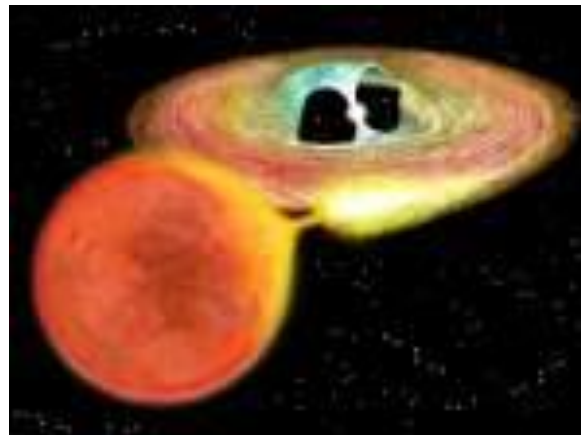
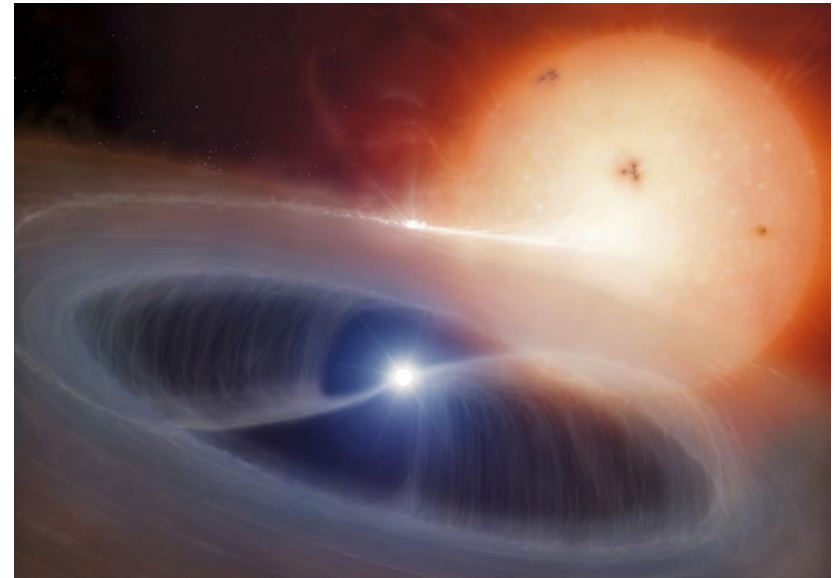
193



Intermediate Polars (DQ Her stars)

194

- White dwarf has magnetic field of 1-10 mega Gauss;
- Accretion disk yields to accretion column near white dwarf;
- Rotation not synchronous;
- Source of hard X-ray, UV, as well as optical wavelengths.



Interacting Binary Stars

195

CVs: Distribution of Orbital Periods

CVs: Distribution of Orbital Periods (1)

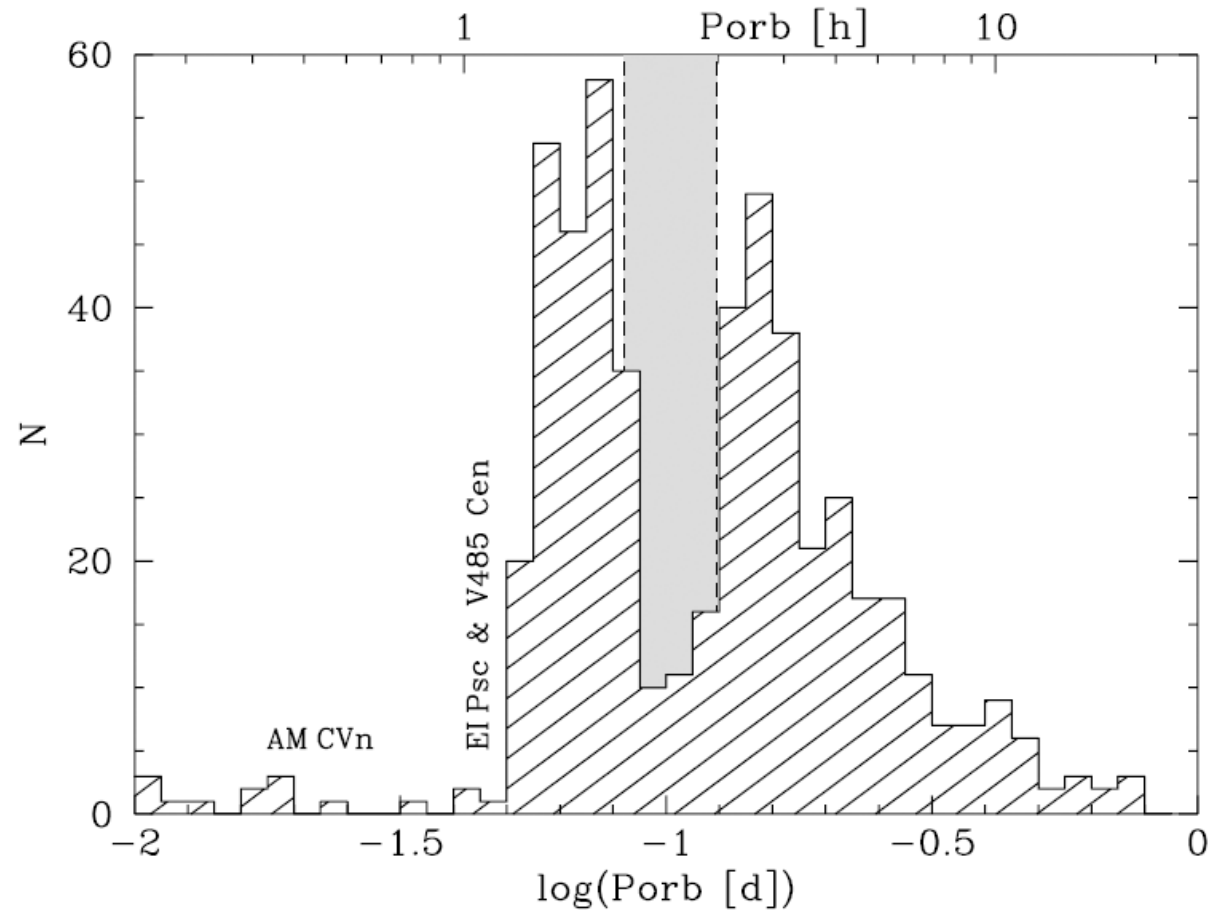
196

- The orbital period P_{orb} of a CV is **the most easily** (and precisely) determined global parameter.
- On its own, P_{orb} reveals something about the scale of the binary.
- As the period of a CV changes on the mass transfer timescale, the distribution of CVs as a function of their orbital period is an important marker of their evolutionary status.

CVs: Distribution of Orbital Periods (2)

197

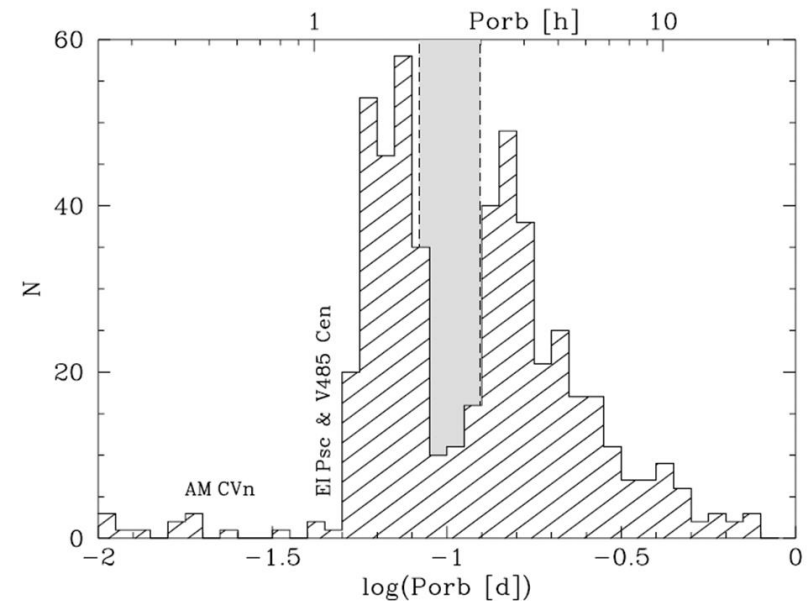
Figure shows the orbital period distribution of 531 CVs from Ritter & Kolb (2003, V7.3).



CVs: Distribution of Orbital Periods (3)

198

- Distinctive features in this distribution:
 - the 2-3 h **period gap**;
 - a sharp cut-off at ~ 80 min: the **minimum period**;
 - a dwindling number of the systems at long P_{orb} : **the long-period cut-off**.
 - ~~□ there is approximately the same number of systems above and below the period gap.~~

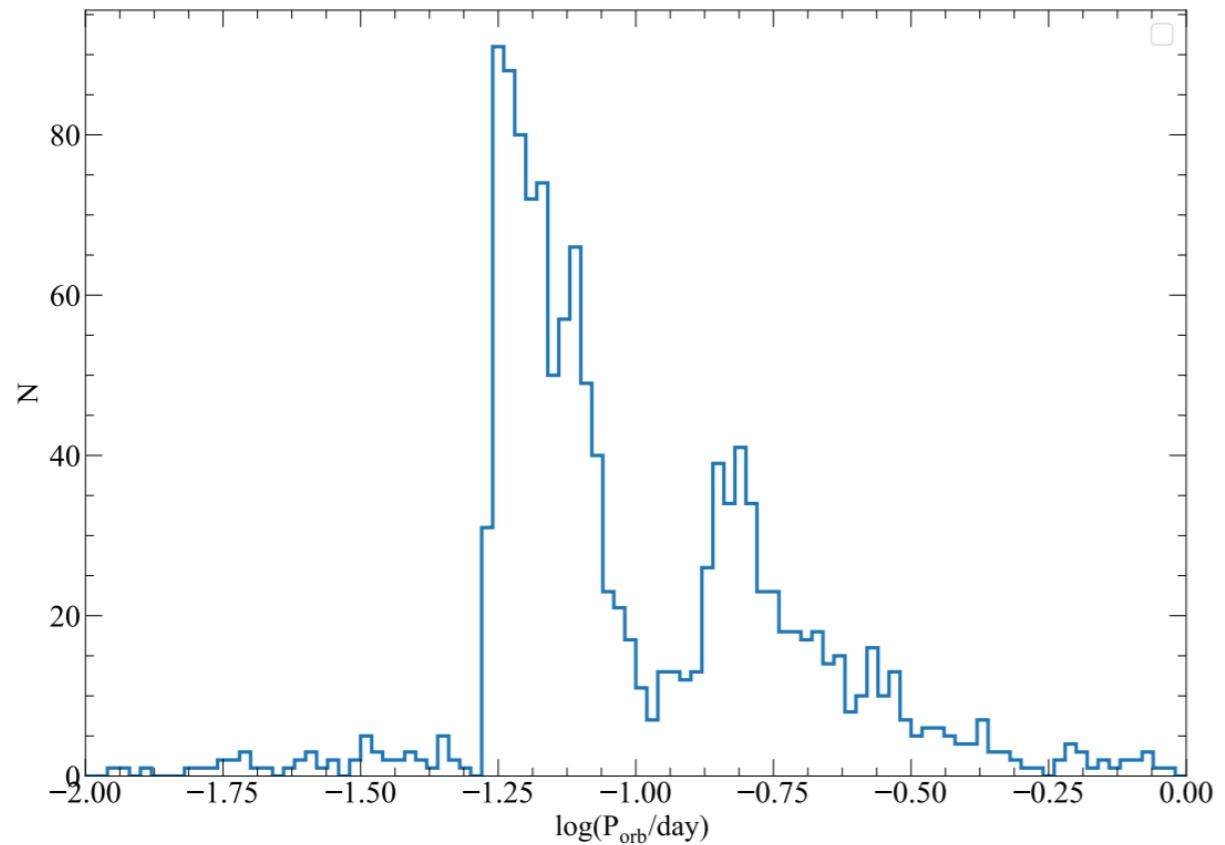


Not anymore, and that is good! We will discuss it later

CVs: Distribution of Orbital Periods (4)

199

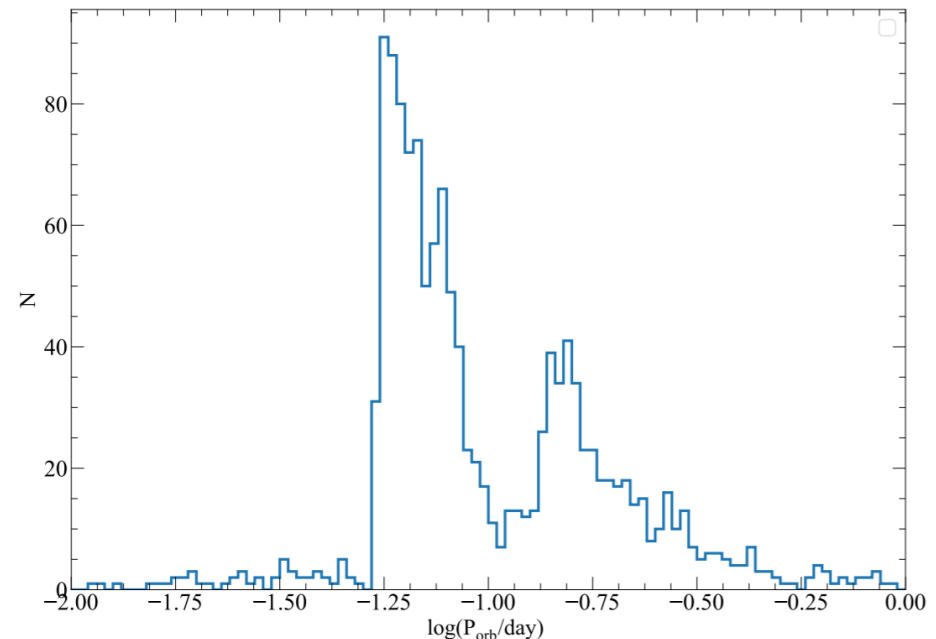
The current population of CVs to date with known orbital periods is ~ 1400 .



CVs: Distribution of Orbital Periods (5)

200

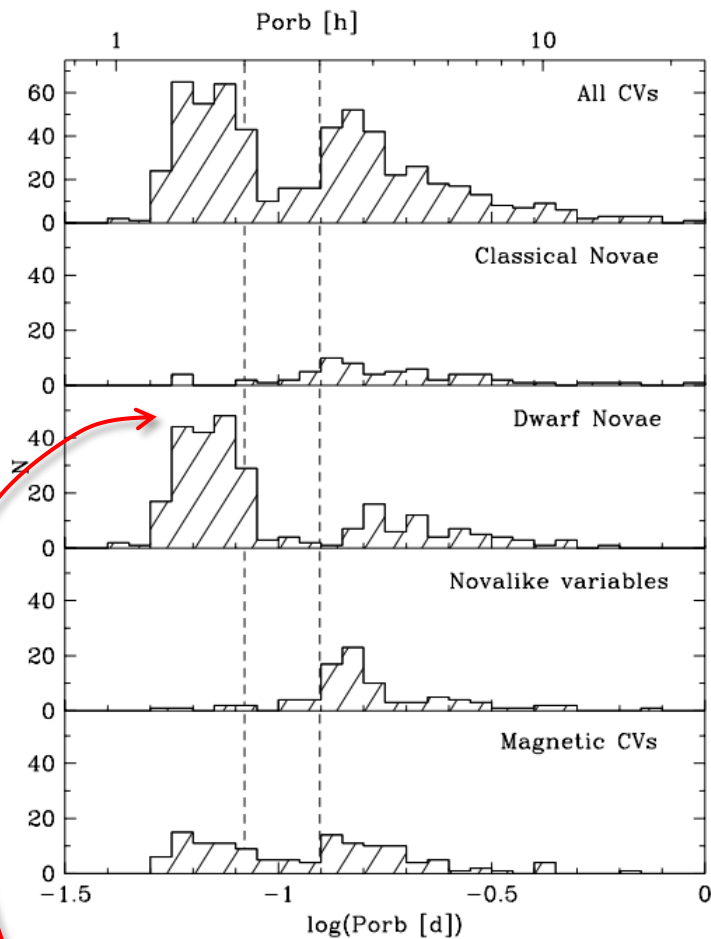
- Distinctive features in this distribution:
 - ▣ the 2-3 h **period gap**;
 - ▣ a sharp cut-off at ~ 80 min: the **minimum period**;
 - ▣ a dwindling number of the systems at long P_{orb} : the **long-period cut-off**.



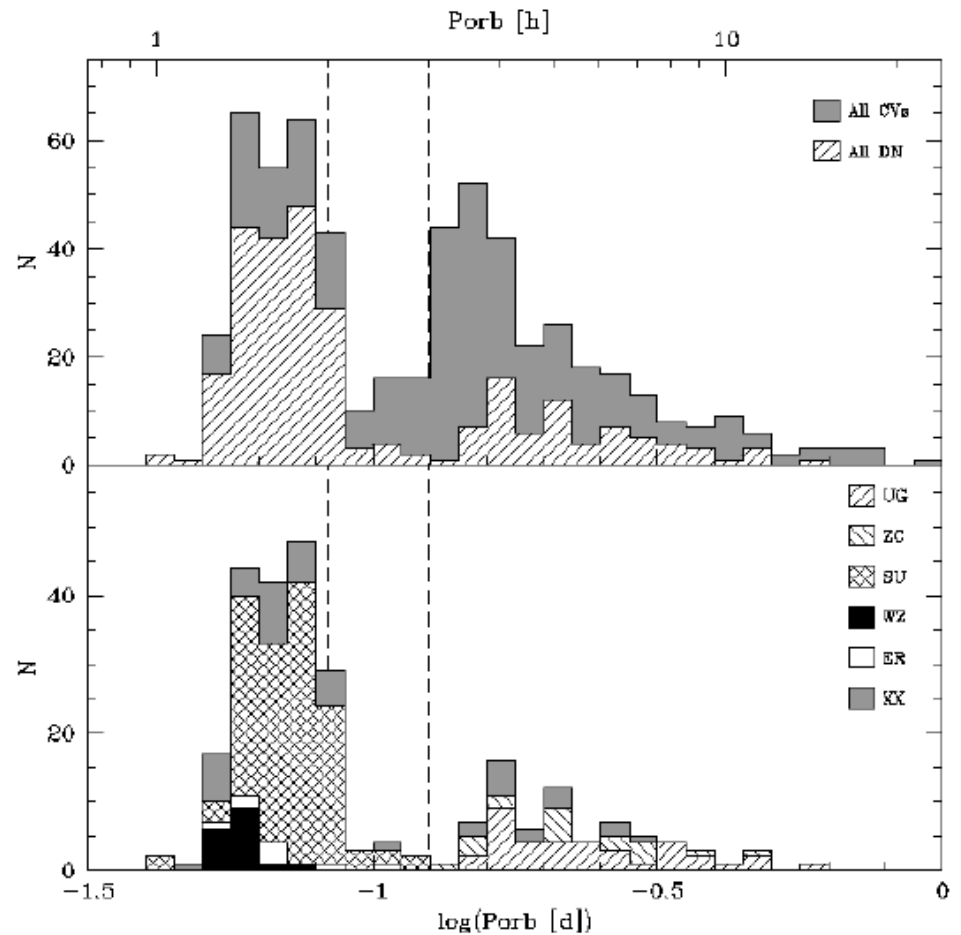
Interacting Binary Stars

CVs: Distribution of Orbital Periods (6)

201



Slightly outdated plots



Interacting Binary Stars

CVs: Distribution of Orbital Periods (7)

202

- Other features in this distribution:
 - ▣ Most non-magnetic novae have P_{orb} above the period gap;
 - ▣ Most of the SU UMa stars lie below the period gap; very few exceptions lie just at the high end of the gap;
 - ▣ All definite U Gem and Z Cam stars lie above the gap;
 - ▣ Almost all NLs lie above the period gap;
 - ▣ Most VY Scl stars have $3.2 < P_{\text{orb}}(\text{h}) < 4.0$;
 - ▣ Most polars have $P_{\text{orb}} < 4.6$ h, with little evidence for a period gap, although there is a minimum frequency near $P_{\text{orb}} \sim 3$ h. Polars concentrate towards shorter orbital periods.
 - ▣ Most of the definite intermediate polars have their P_{orb} above the gap.

CVs: Distribution of Orbital Periods (8)

203

- The existence of the gap and the minimum P_{orb} result from the way in which the secondary responds to mass loss. We will discuss it later.
- The significance of some of the correlations between P_{orb} distribution and CV type is not fully understood.

CVs: Distribution of Orbital Periods (9)

204

Kepler's third law gives : $4\pi^2 a^3 = GMP^2$

$$M_1 = m_1 M_\odot, \quad M_2 = m_2 M_\odot, \quad M = M_1 + M_2 = m M_\odot \quad q = \frac{M_2}{M_1}$$

$$\begin{aligned} a &= 3.53 \times 10^{10} m_1 (1 + q)^{1/3} P_{\text{hr}}^{2/3} \text{ cm} \\ &= 2.9 \times 10^{11} m_1 (1 + q)^{1/3} P_{\text{day}}^{2/3} \text{ cm} \\ &= 1.5 \times 10^{13} m_1 (1 + q)^{1/3} P_{\text{yr}}^{2/3} \text{ cm} \end{aligned}$$

P_{orb} of 1-10 h imply component separations ~ 0.5 -3 times the radius of the Sun.

CVs: Distribution of Orbital Periods - 10

205

$$\frac{R_2}{a} = \frac{2}{3^{4/3}} \left(\frac{q}{1+q} \right)^{1/3} = 0.462 \left(\frac{M_2}{M_1 + M_2} \right)^{1/3} \quad \text{Paczyński}$$

Hence:
$$\bar{\rho} = \frac{M_2}{\frac{4}{3}\pi R_2^3} \cong 110 P_{hr}^{-2} g \text{ cm}^{-3}$$

For Main Sequence secondaries:

$$\bar{\rho} = \frac{3M_2}{4\pi R_2^3} \cong \frac{3M_{\odot}}{4\pi R_{\odot}^3 m_2^2} \cong 1.4 m_2^{-2} g \text{ cm}^{-3}$$

$$m_2 \cong \frac{R_2}{R_{\odot}}$$

$$m_2 \cong 0.11 P_{hr}$$

Stars with densities of typical lower main sequence stars can fill their Roche lobes.

Systems with $P_{orb} > 10$ h must contain evolved secondaries.

$$R_2 \cong 7.9 \times 10^9 P_{hr} \text{ cm}$$

CVs: Distribution of Orbital Periods - 11

206

- The stream has a distance of closest approach r_{\min} from the centre of the primary, obtainable from trajectory computations, and approximated to 1% accuracy by
$$\frac{r_{\min}}{a} = 0.0488q^{-0.464} \quad 0.05 < q < 1$$
- If $R_* > r_{\min}$ then the stream strikes the surface of the star directly.
- From Kepler's third law, the stream will not impact on the WD:

$$P_{orb} > 0.44 \frac{q^{0.7}}{(1+q)^{1/2}} m_1^{-1/2} h$$

Satisfied by all
known CVs



Accretion Disk!!!

Observational evidence for ADs in CVs

Light curves of eclipsing Cataclysmic Variables.

Eclipse Mapping

Emission lines from accretion disks

Trailed spectra

Principle of Doppler Tomography

Single peaked emission lines

The wind from an accretion disk.

Accretion Disks in CVs (1)

208

- Direct observational evidence for accretion disks in in form of a spatially resolved picture of such a disk does not yet exist:
even in the nearest disk-containing systems the angular size of the disk is far below available angular resolution.
- At a distance of $D \sim 50 \text{ pc}$ and with a radius of $r \sim 1 R_{\odot}$, the disk subtends an angle $< 0.2 \text{ mas}$.
- Thus all evidence for accretion disks must necessarily be indirect.

Accretion Disks in CVs (2)

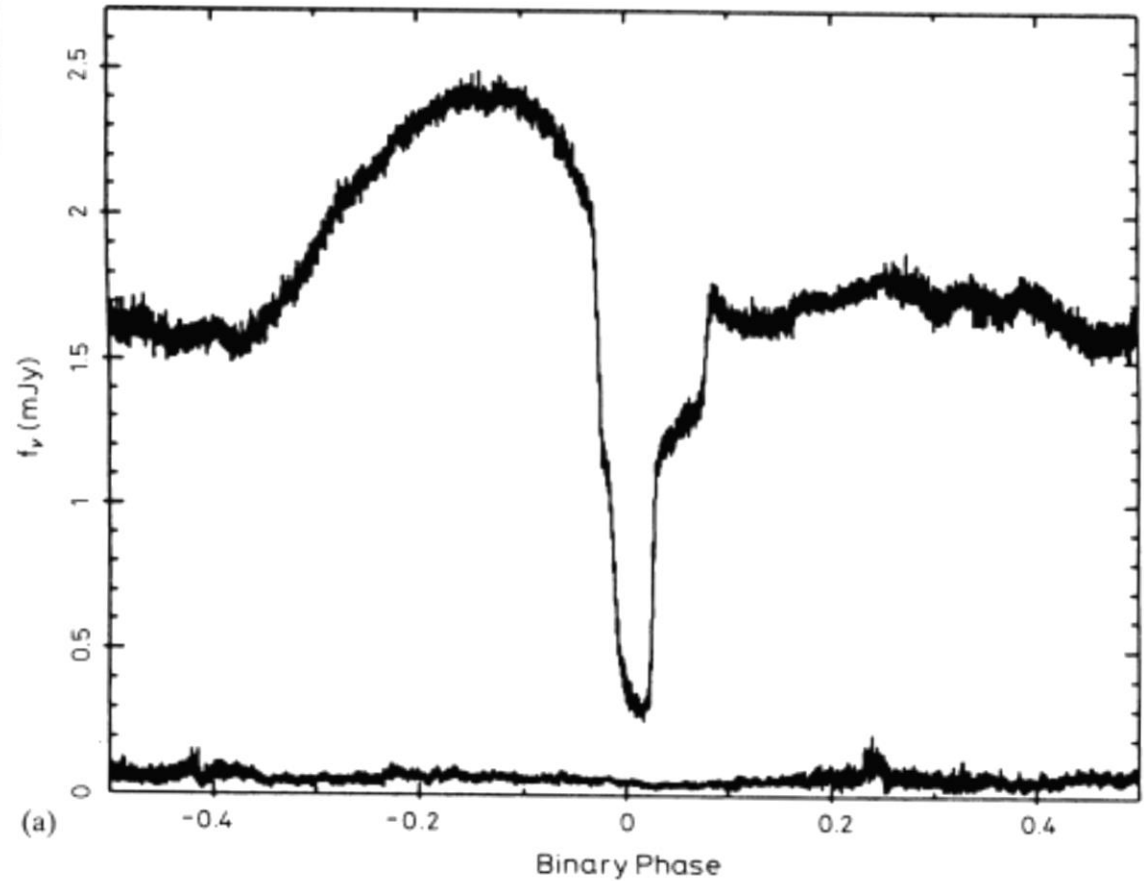
209

- There are two pieces of evidence:
 - ▣ the results of light curve analysis of eclipsing systems
and
 - ▣ the interpretation of the line profiles of the observed spectra.

Light curves of eclipsing CVs (1)

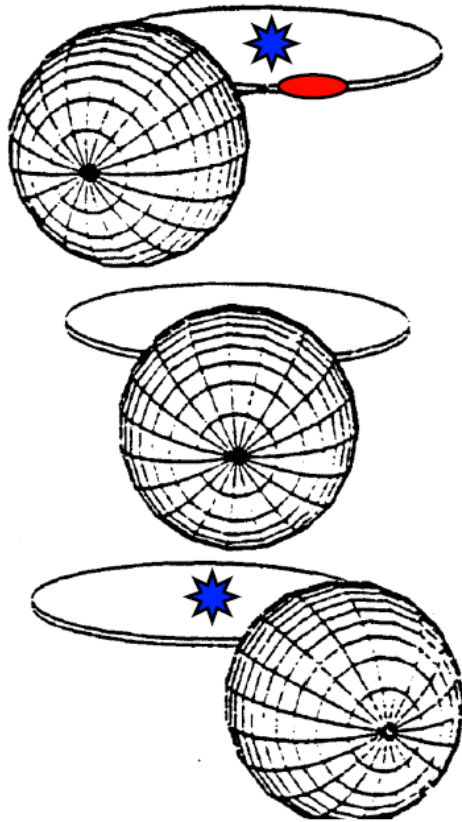
210

Average of 17 light curves of Z Cha

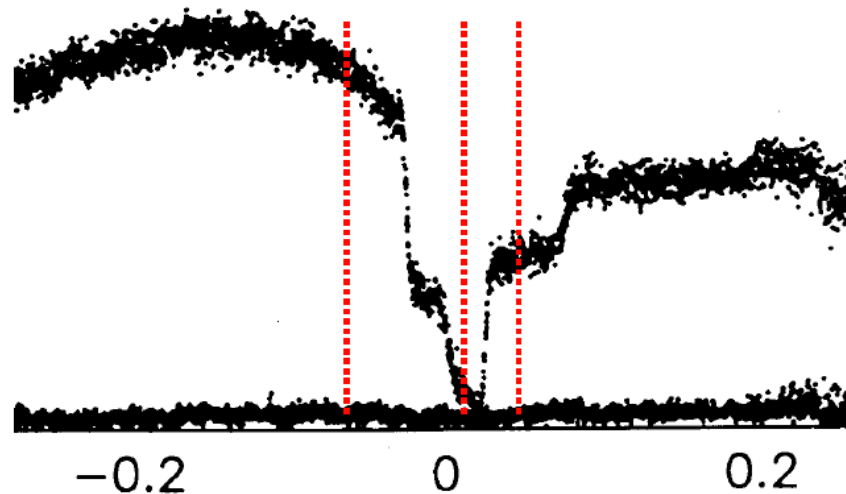


Light curves of eclipsing CVs (2)

211



OY Car in quiescence



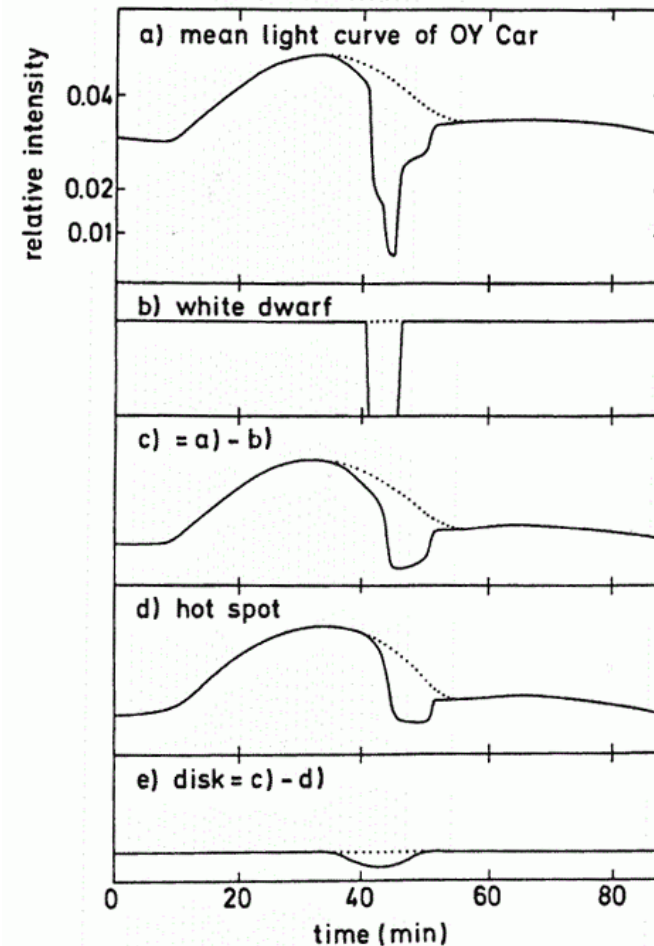
Binary Phase

from Wood et al. 1989,
ApJ, 341, 974

Light curves of eclipsing CVs (3)

212

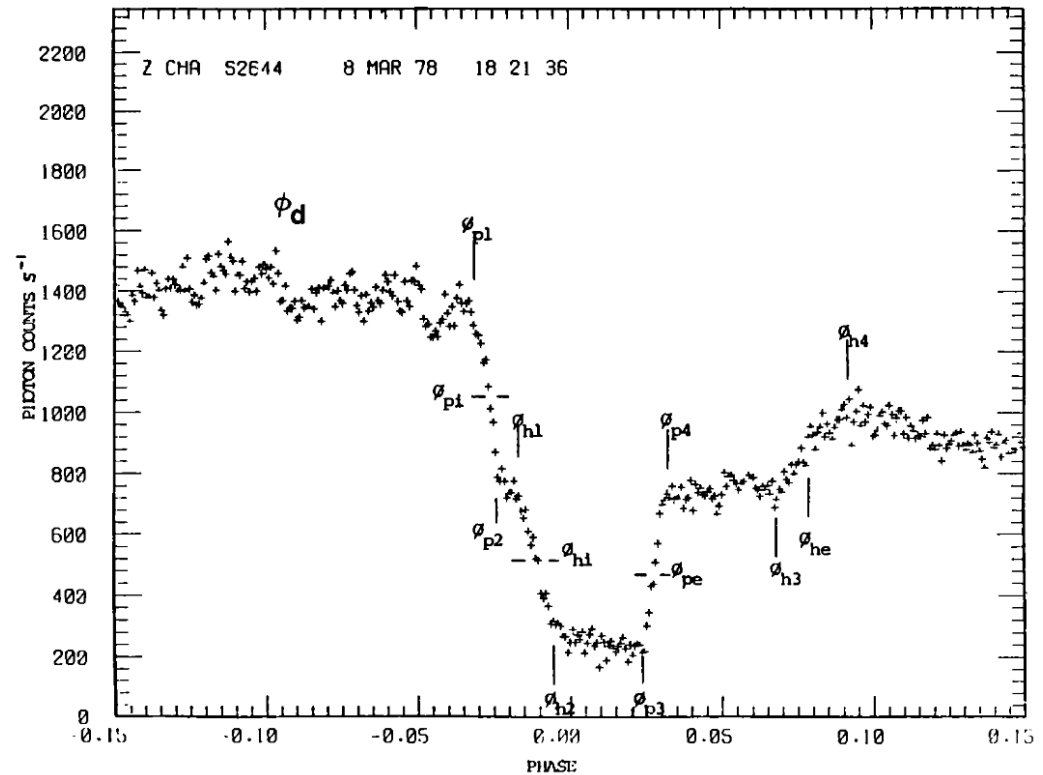
An observed light curve can be decomposed into the various contributions.



Light curves of eclipsing CVs (4)

213

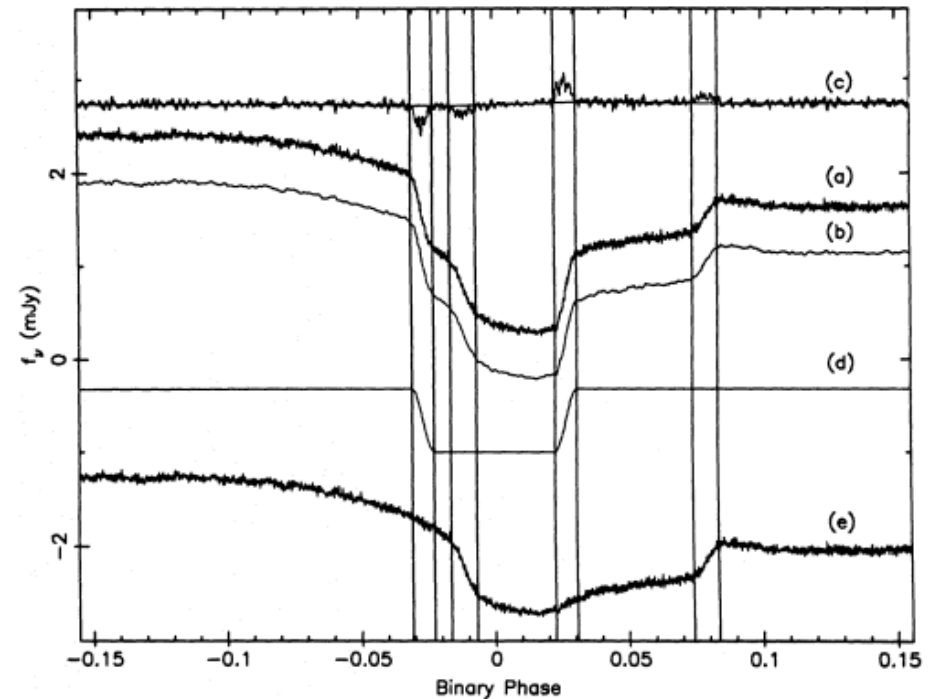
- Eclipse light curve of Z Cha with contact phases marked.
 - ϕ_d is the probable beginning of eclipse of the disk.
- (From Cook & Warner 1984).



Light curves of eclipsing CVs (5)

214

- Decomposition of an average of 17 eclipse light curves of Z Cha. (from Wood et al. 1986):
- (a) Original light curve.
- (b) Smoothed light curve.
- (c) Derivative of smoothed light curve with spline fit.
- (d) Reconstructed white dwarf eclipse, symmetrized about mid-eclipse.
- (e) Original light curve minus white dwarf light curve.

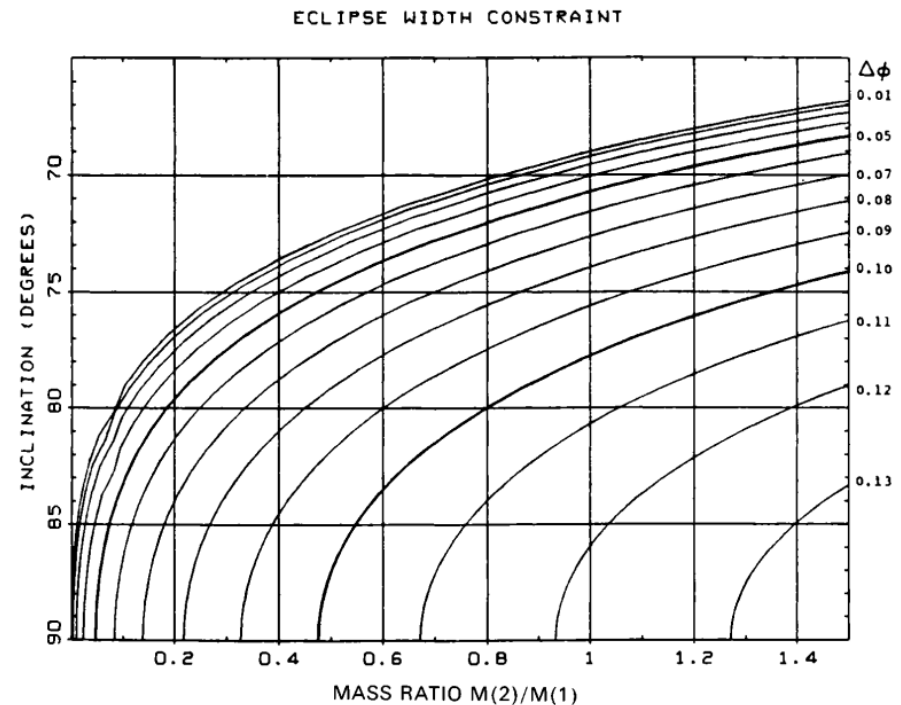


The vertical lines show the contact phases of the white dwarf and the bright spot.

Eclipse Analysis (1)

215

- The duration $\Delta\phi$ of total eclipse of the primary is a function only of q and i .
- For Roche geometry this function is not expressible in analytical form, but is available in tabular and graphical form.



Eclipse Analysis (2)

216

- Approximate results are obtained by ignoring the distorted shape of the secondary:

$$\sin^2 i \approx \frac{1 - [R_L(2)/a]^2}{\cos^2 2\pi\phi_p}$$

where $\pm\phi_p$ is the phases of mid-immersion and mid-emergence of the primary.

- The radius of the disk may be found from its first and last contact points, occurring at phases $\pm\phi_d$. To first order, for deep eclipses,

$$r_d/a = \tan 2\pi\phi_d - \tan 2\pi\phi_p$$

Eclipse Analysis (3)

217

- General formulae that relate the observed eclipse contact points to the structure of the system:

Smak 1971, Acta Astronomica, 21, 15;

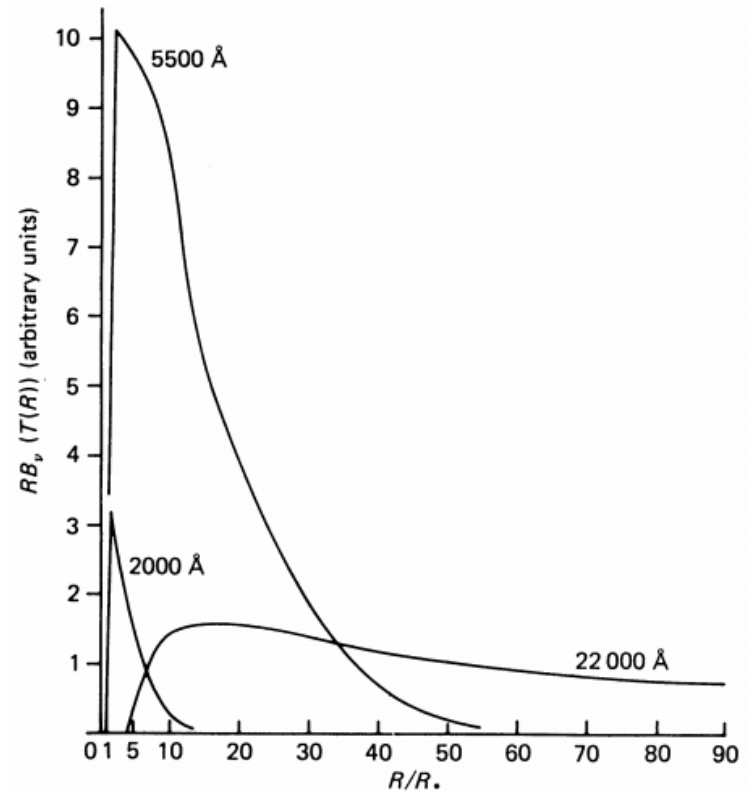
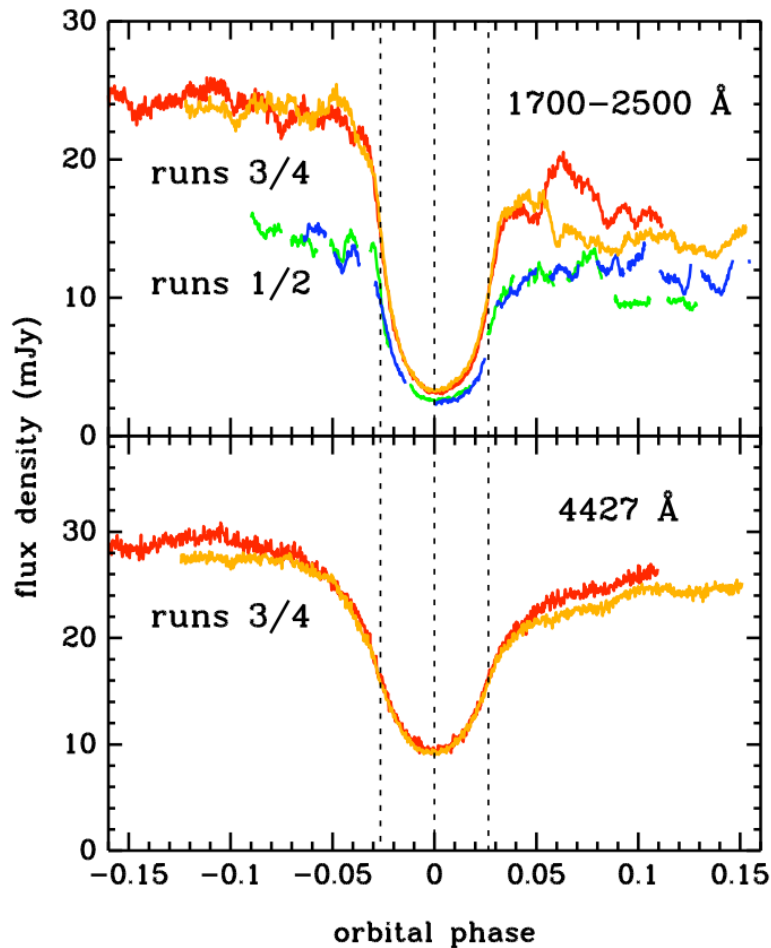
Smak 1979, Acta Astronomica, 29, 309;

Lin 1975, MNRAS, 170, 379;

Robinson, Nather & Patterson, 1978, ApJ, 219, 168

Light curves vs wavelength

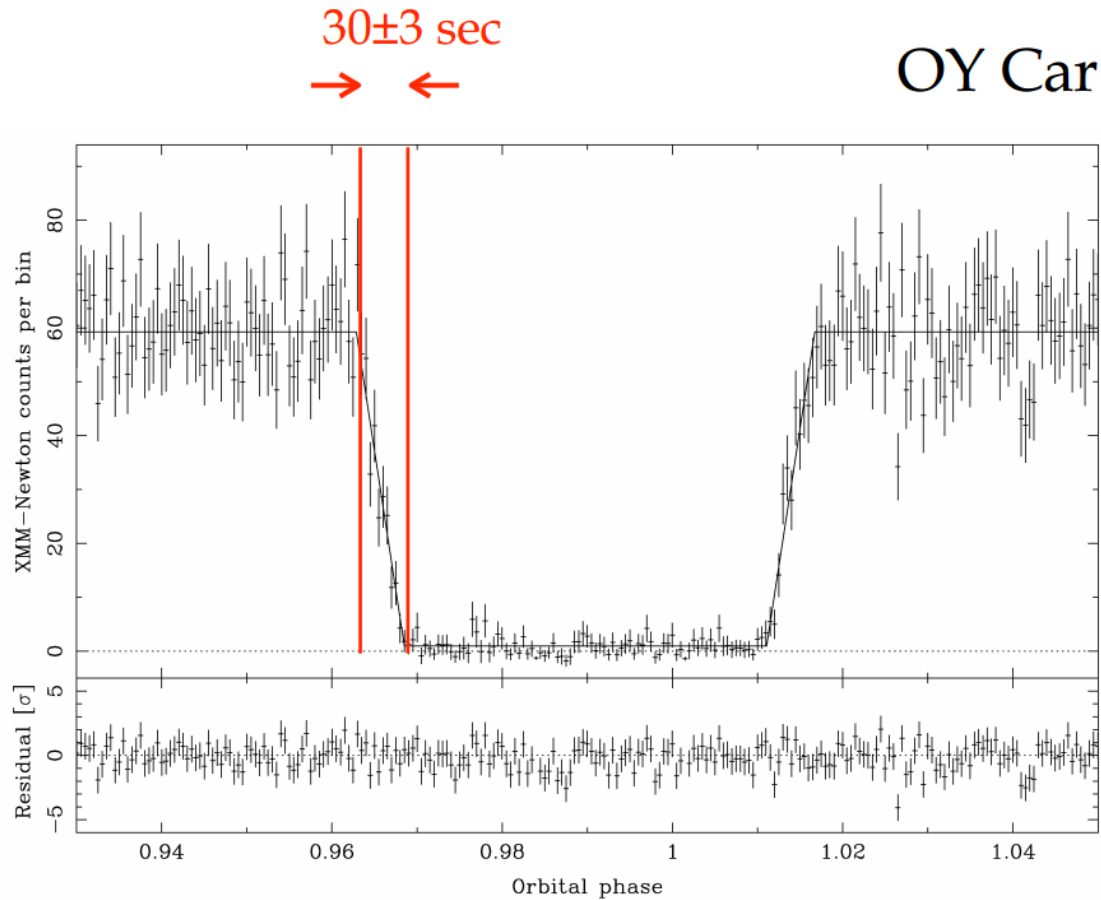
218



UX UMa in UV and Optical
(from Baptista et al. 1998)

X-Ray eclipse of the boundary layer

219



Clues from eclipse light curves

220

- Dwarf Novae in quiescence:
 - ▣ Clear signature of bright spot and white dwarf
 - they contribute most of the light
 - ▣ Very shallow disk eclipse
 - small contribution from disk to total light
- Dwarf Novae in outburst and Nova-Likes
 - ▣ Disk is the primary source of light, white dwarf and bright spot not clearly seen
 - ▣ Very broad and deep disk eclipse

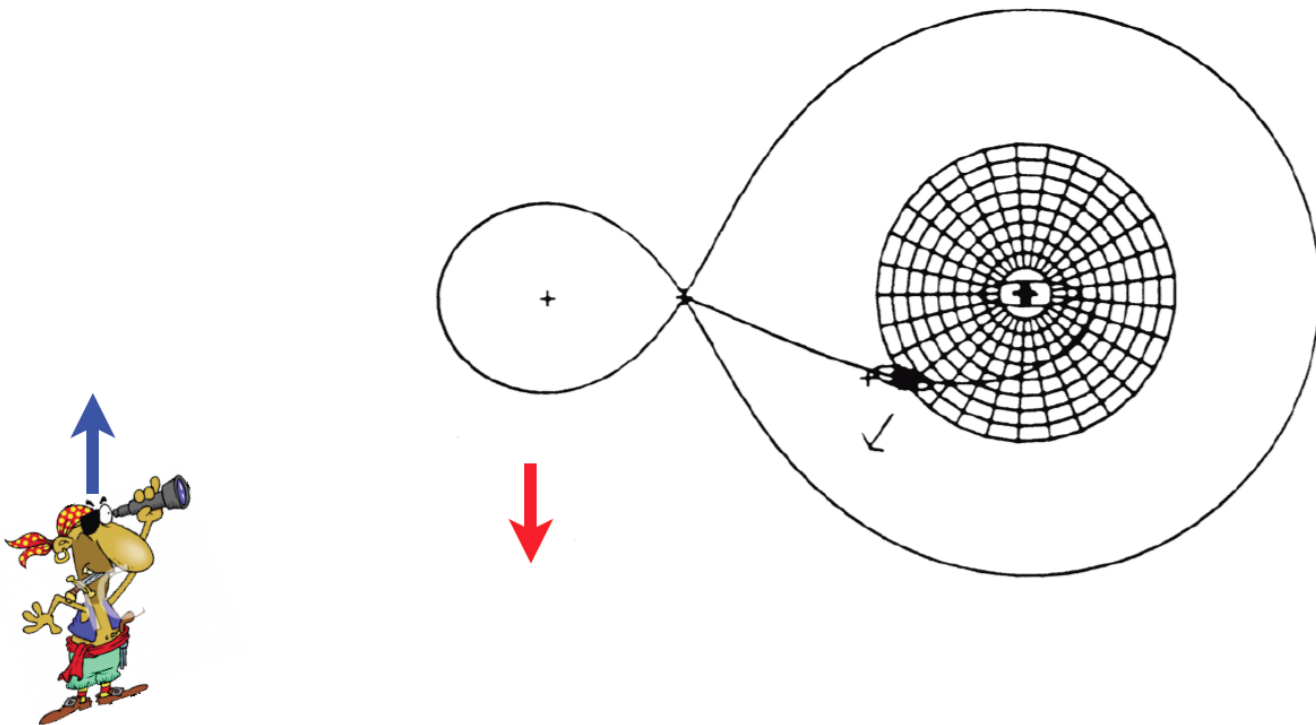
Eclipse Mapping

221

- Eclipse Mapping is an indirect imaging technique that provide spatially resolved observational constraints on accretion disks on angular scales of micro arcseconds.
- Eclipse Mapping assembles the information contained in the shape of the eclipse into a map of the accretion disk surface brightness distribution.

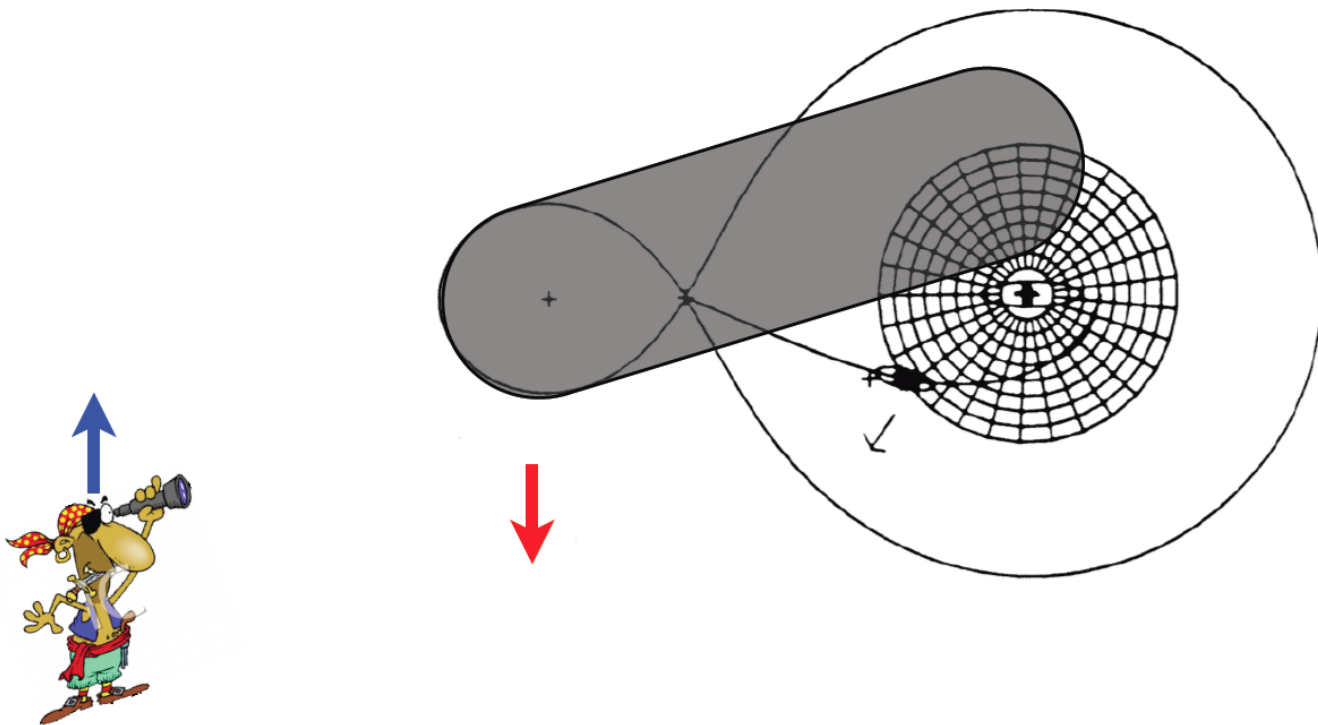
Eclipse Mapping: The basic principle (1)

222



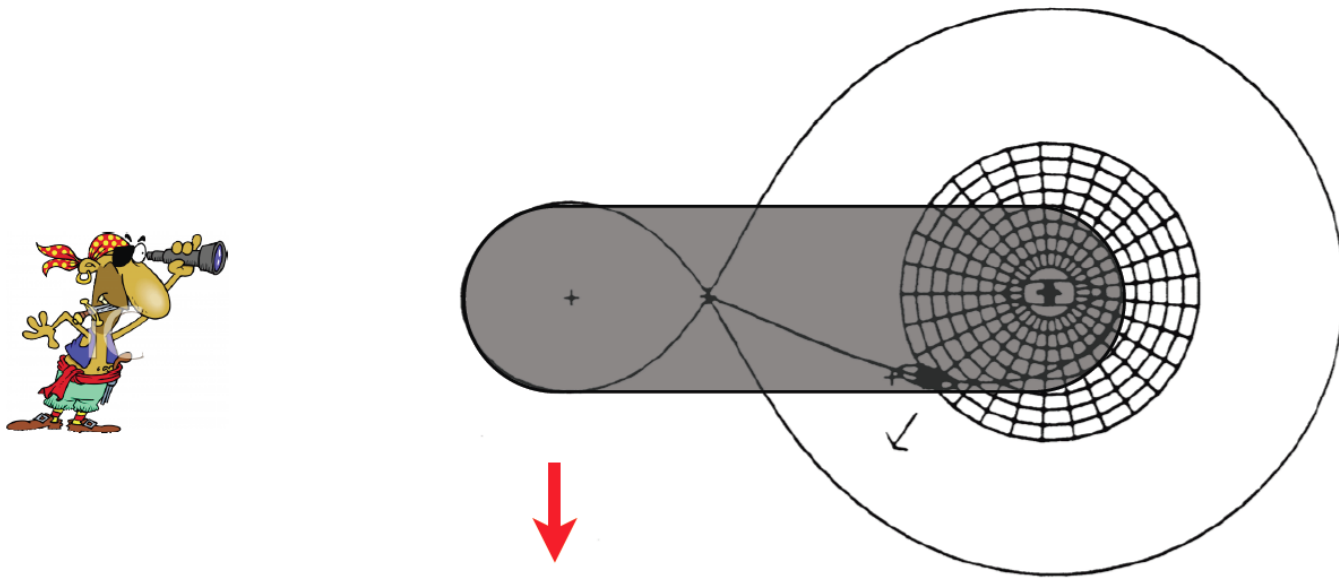
Eclipse Mapping: The basic principle (2)

223



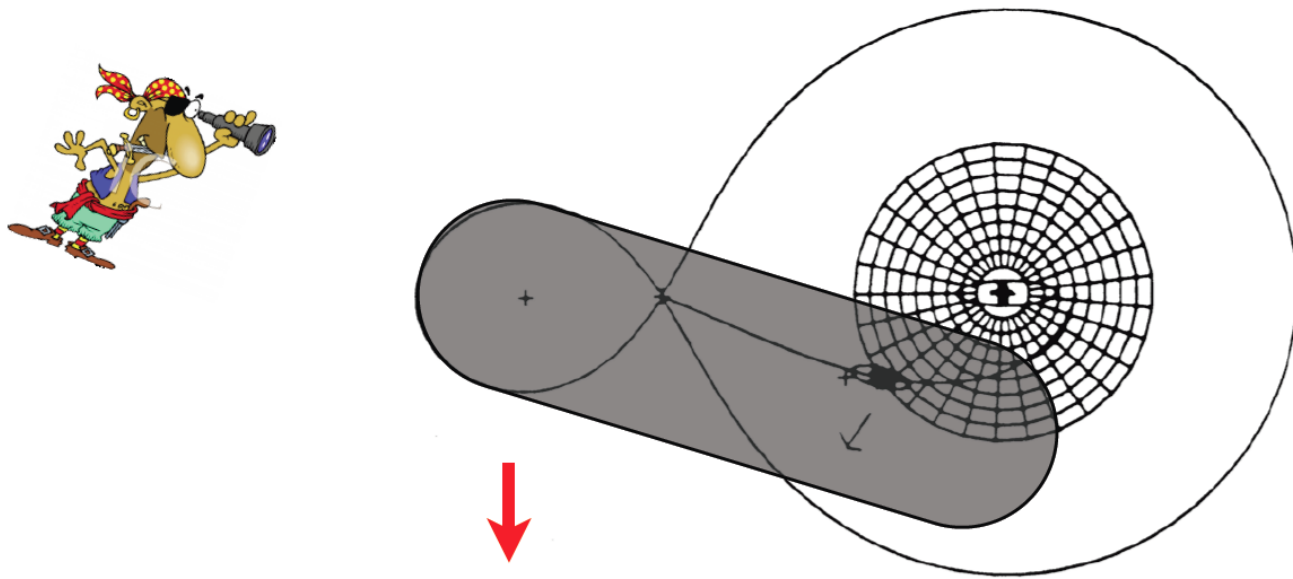
Eclipse Mapping: The basic principle (3)

224



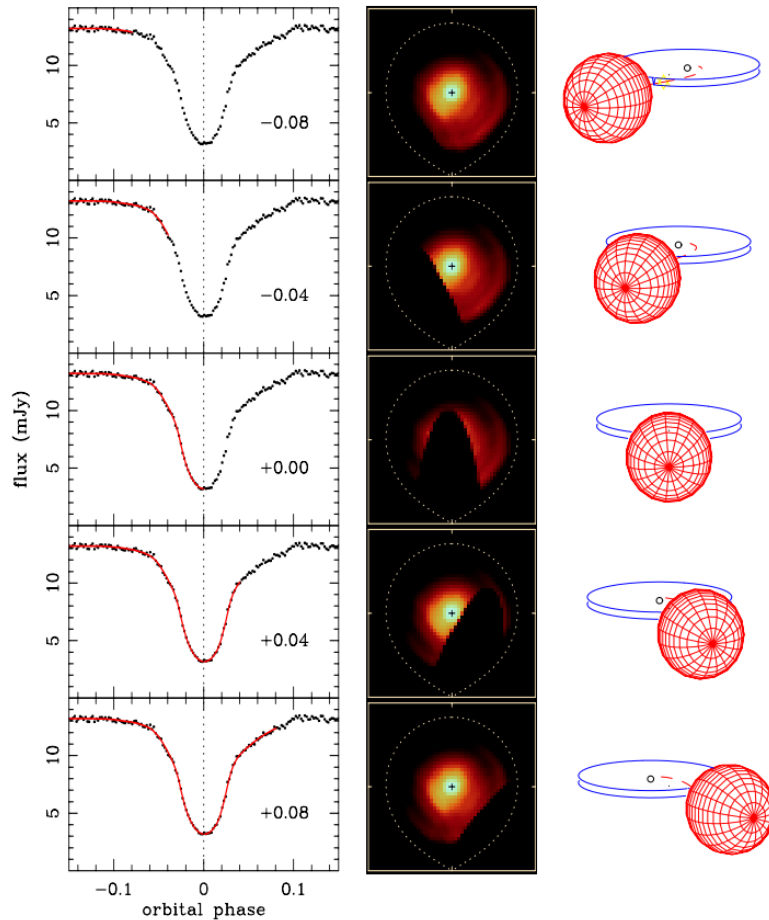
Eclipse Mapping: The basic principle (4)

225



Eclipse Mapping: The basic principle (5)

226

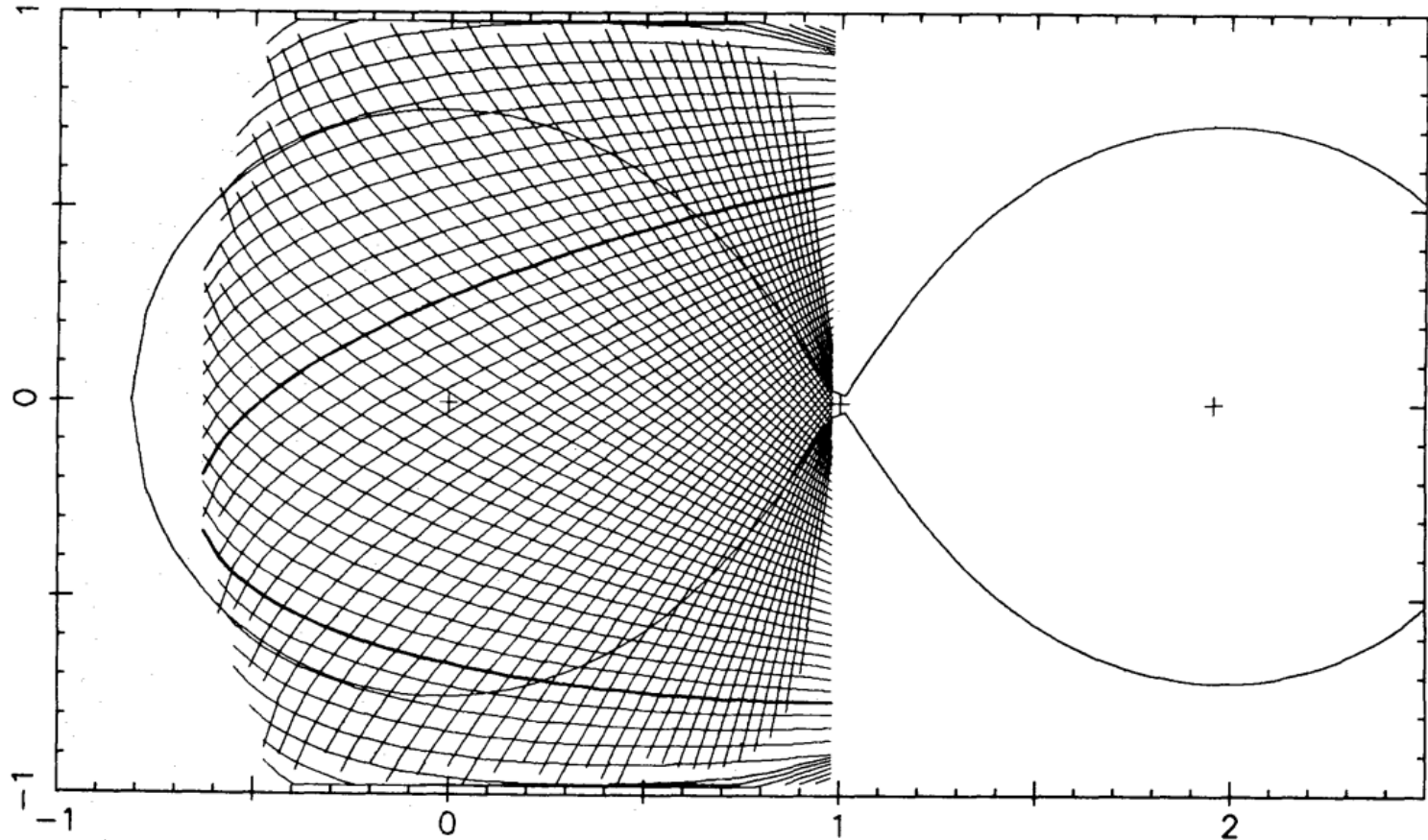


- Simulation of a disk eclipse ($q = 0.3; i = 78^\circ$).

Eclipse Mapping: The basic principle (6)

227

$$q = 0.9 \quad \Delta\phi = 0.081$$



Interacting Binary Stars

Eclipse Mapping (1)

228

- Recover 2D surface brightness of the disk from the 1D eclipse light curve.
- Not enough constraints to solve the problem uniquely. Need help!
- Resort to maximum entropy method to incorporate expectations/prejudices, e.g.,
 - azimuthal symmetry
 - uniformity or smoothness

Eclipse Mapping (2)

229

How is this done in practice?

□ Synthesize eclipse light curve from assumed 2D image of the disk. Iteratively adjust its surface brightness to satisfy two constraints:

□ Good fit to the light curve (via χ^2 test)

$$\chi^2 = \sum_{i=1}^n \left(\frac{F_i - M_i}{\sigma_k} \right)^2$$

□ Close resemblance to “default” image; maximum entropy constraint

$$S = - \sum_{k=1}^{N^2} I_k \ln \left(\frac{I_k}{D_k} \right)$$

Eclipse Mapping (3)

230

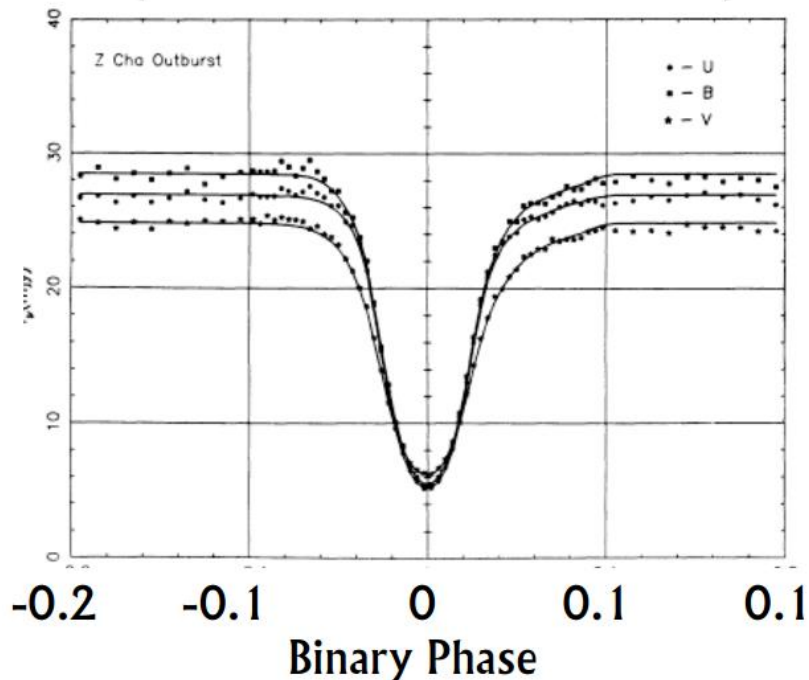
Requirements and assumptions:

- Need to know the parameters of the binary in order to reconstruct the geometry correctly.
- Must assume that disk is static.
- Initial implementation assumed flat disk.
Current versions allow for 3-D structure.
- Default map may influence the results. Need to carry out tests to verify results.
- Reconstruction of physical parameters (e.g., temperature) is only as good as the adopted model.

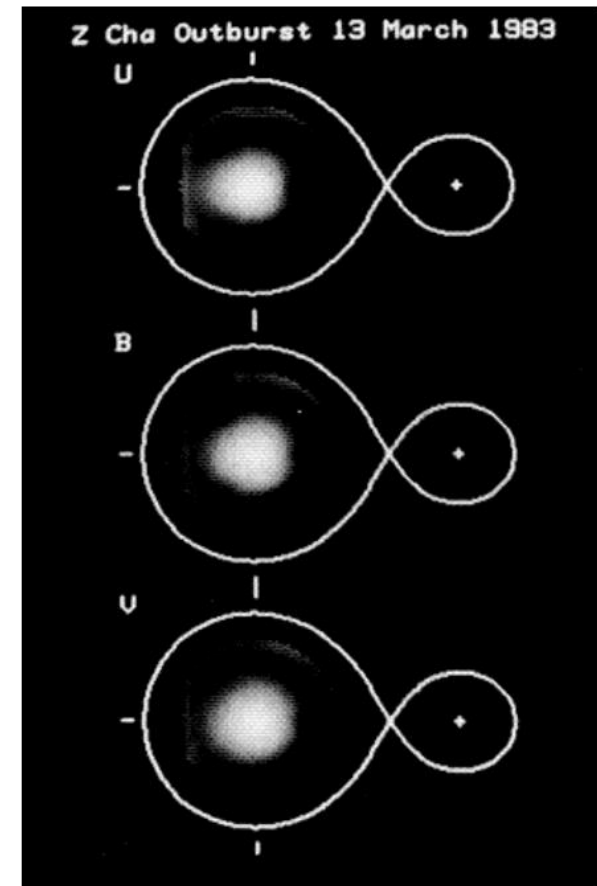
Eclipse Mapping: Early Applications

231

Eclipse maps of Z Cha in outburst.

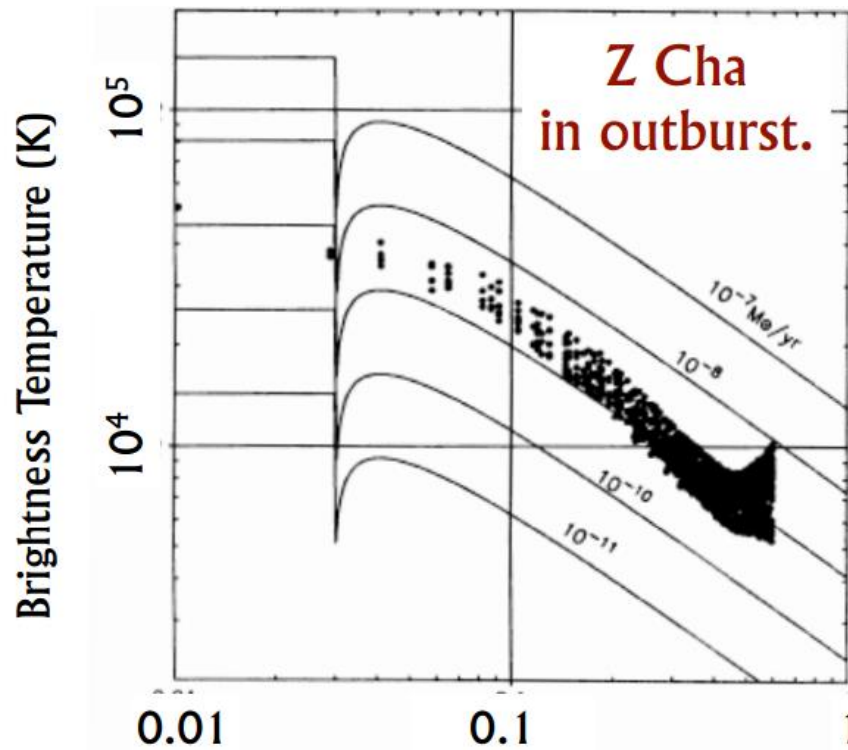


Horne & Cook, 1985,
MNRAS, 214, 307

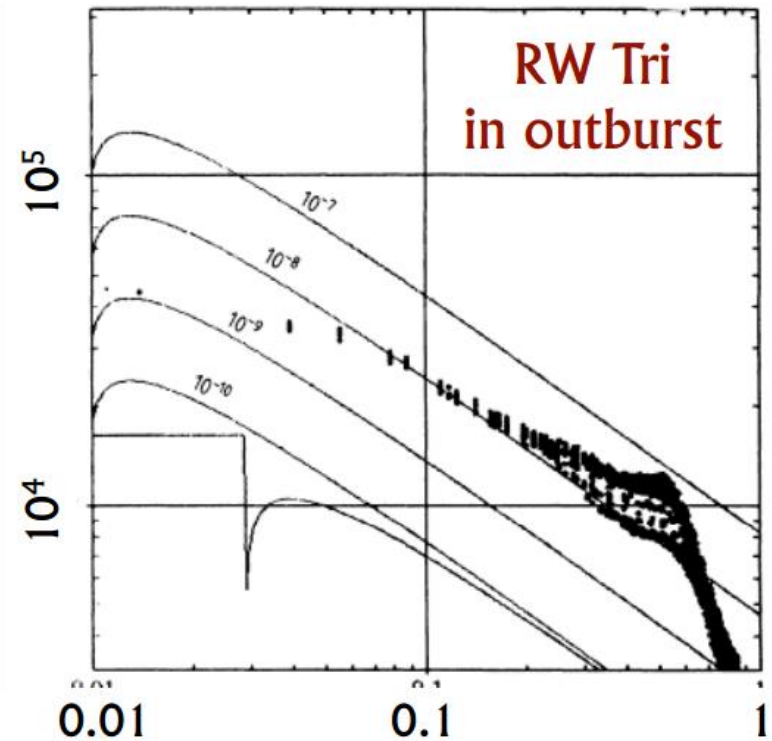


Radial brightness profile of the disk (1)

232



Horne & Cook, 1985,
MNRAS, 214, 307

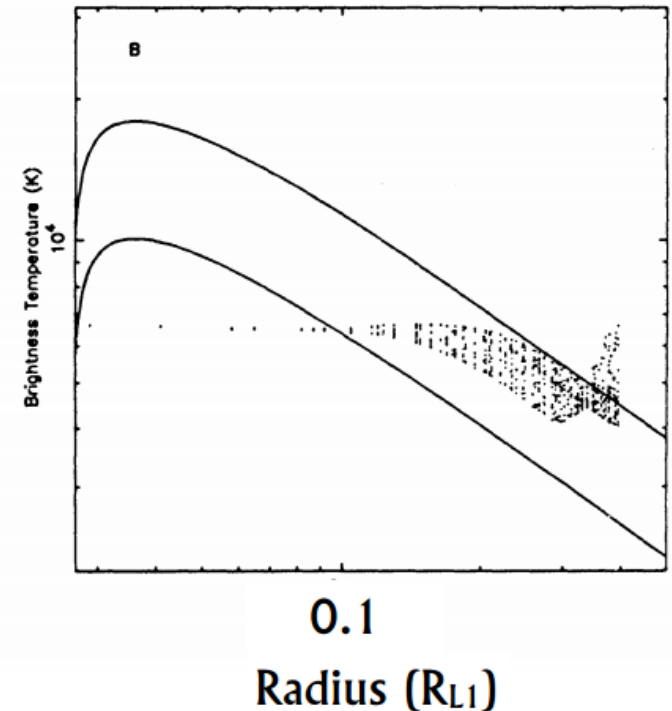
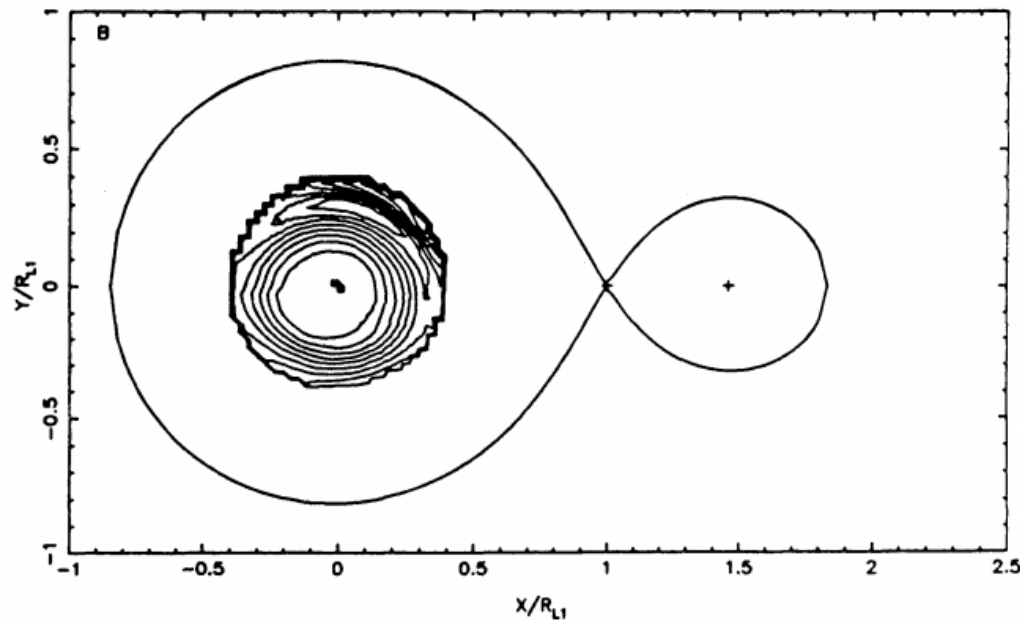


Horne & Stiening, 1985,
MNRAS, 216, 933

Radial brightness profile of the disk (2)

233

HT Cas in quiescence



Wood et al. 1992, ApJ, 385, 294

Eclipse Mapping: Early Applications

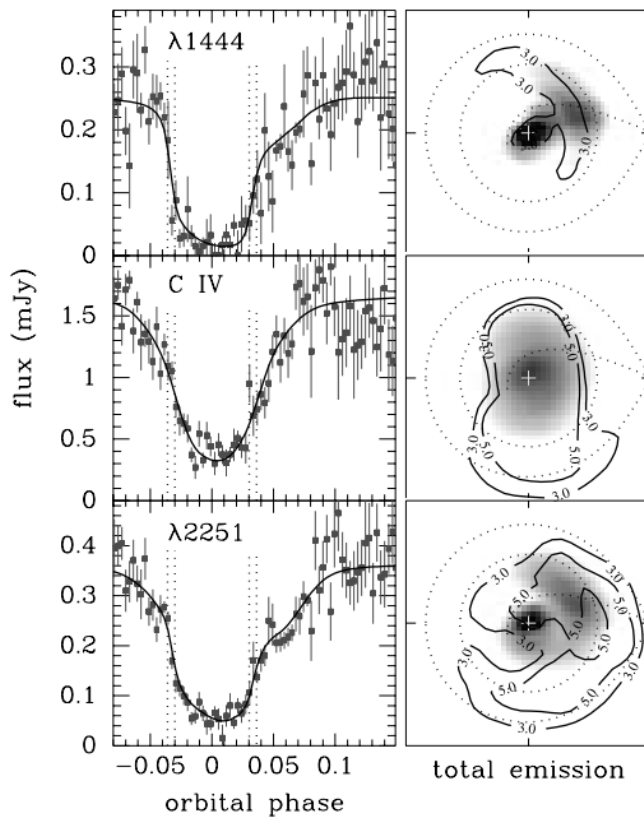
234

- Accretion disks in outbursting dwarf novae and in long-period novalike variables closely follow the expected radial dependence of temperature with radius for a steady-state disk, $T \propto R^{-3/4}$.
- However, in the short period quiescent dwarf novae the radial temperature profile is essentially flat.
- This suggests that the quiescent disks are far from being in a steady-state.
- **Also!** The SW Sex stars (a group of mostly eclipsing novalike variables that display a number of unexplained phenomena): the radial temperature profiles are noticeably flatter than the $T \propto R^{-3/4}$.

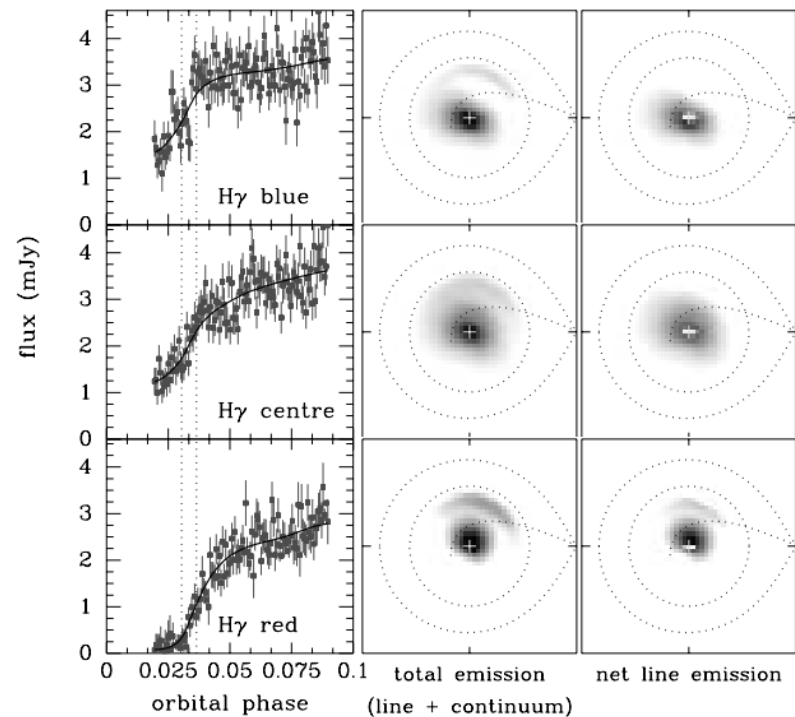
Spectral Mapping: V2051 Oph in quiescence (1)

235

C IV and UV continuum



sections of the H γ line

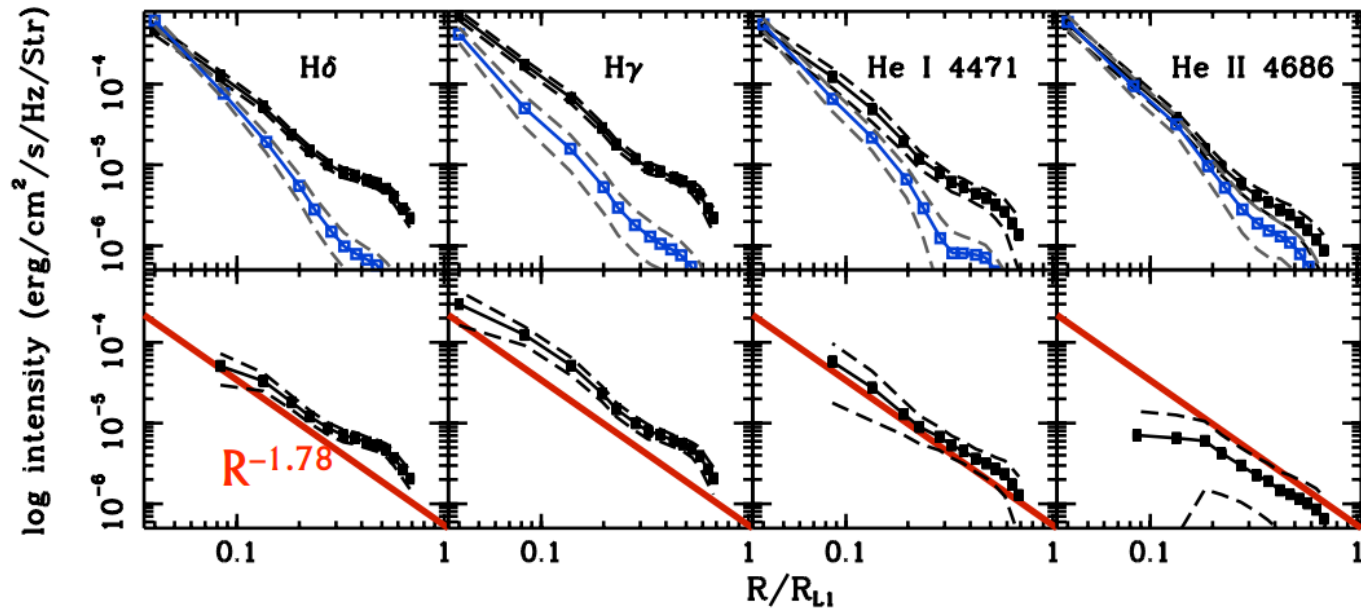


from Saito & Baptista 2006,
AJ, 131, 2185

Spectral Mapping: V2051 Oph in quiescence (2)

236

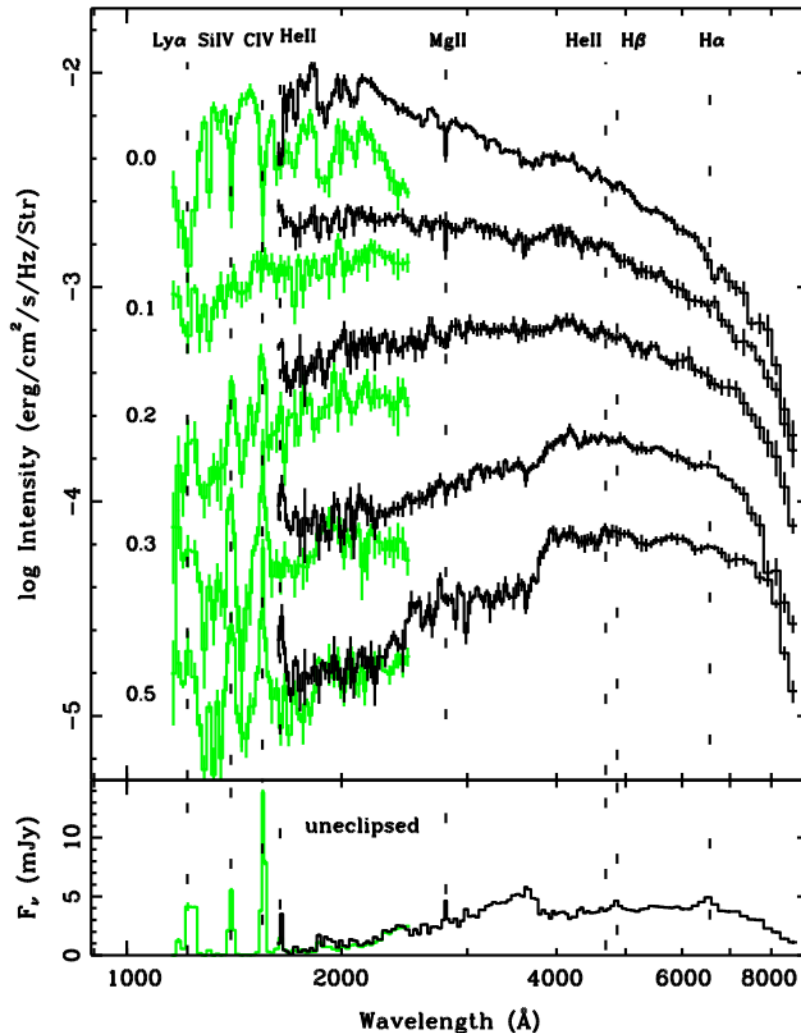
Emissivity profiles of continuum and emission lines



from Saito & Baptista 2006, AJ, 131, 2185

Spectral Mapping: UX UMa in high state (1)

237



Radially resolved spectra
of the disk
(pioneered by Rutten et al
1993, Nature, 362, 518)

Eclipse mapping of UX
UMa with HST/FOS spectra

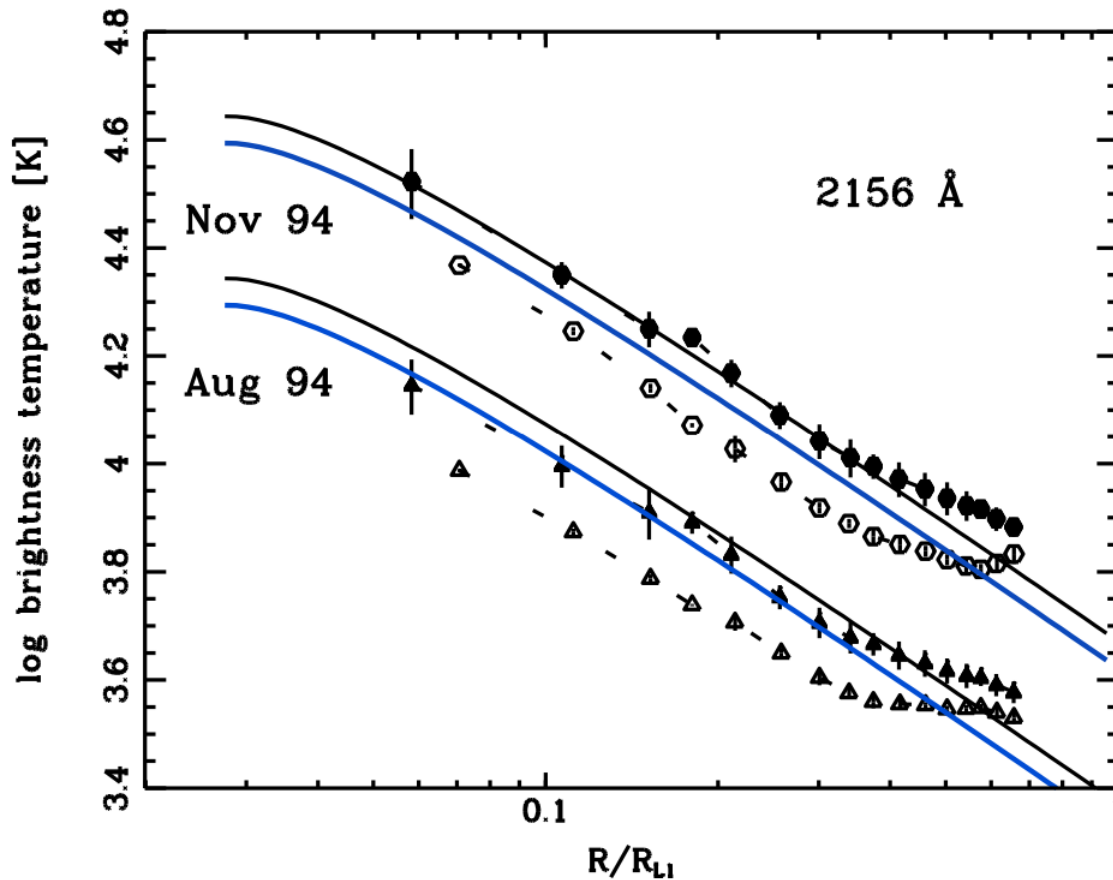
Spectrum gets redder and
lines go to emission in
outer disk

from Baptista et al 1998,
MNRAS, 298, 1079

Spectral Mapping: UX UMa in high state (2)

238

- Brightness temperature profile of the disk:



Lessons from eclipse mapping

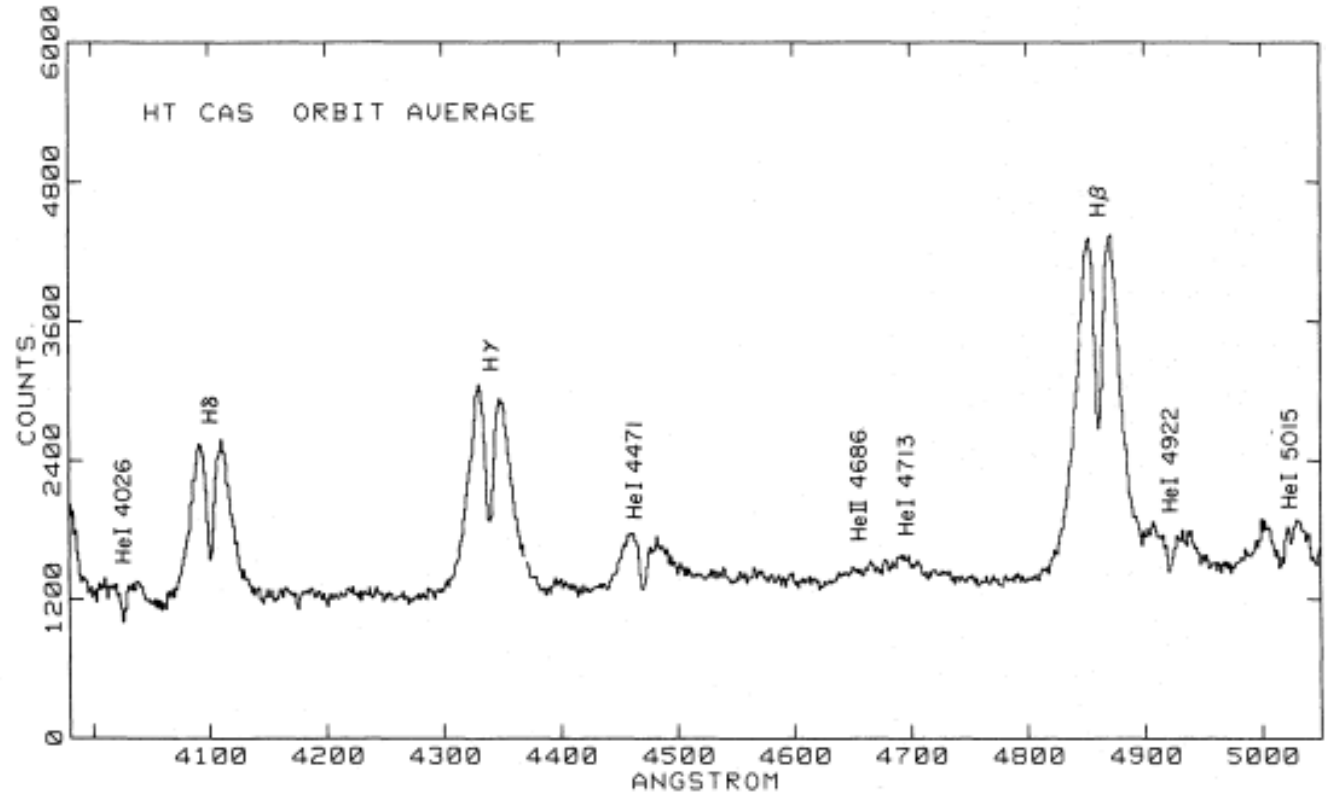
239

- CVs in high state \rightarrow α -disk models?
- Spatially-resolved disk spectra in qualitative agreement with theoretical expectations.
- Temperature profiles not in quantitative agreement with the predictions of disk models.
 - ▣ Irradiated disk models may be able to do better. (Orosz & Wade 2003, ApJ, 593, 1032)
 - ▣ We see emission lines! Optically thin gas? Where is the source of the emission lines?

Spectroscopy: Emission line profiles (1)

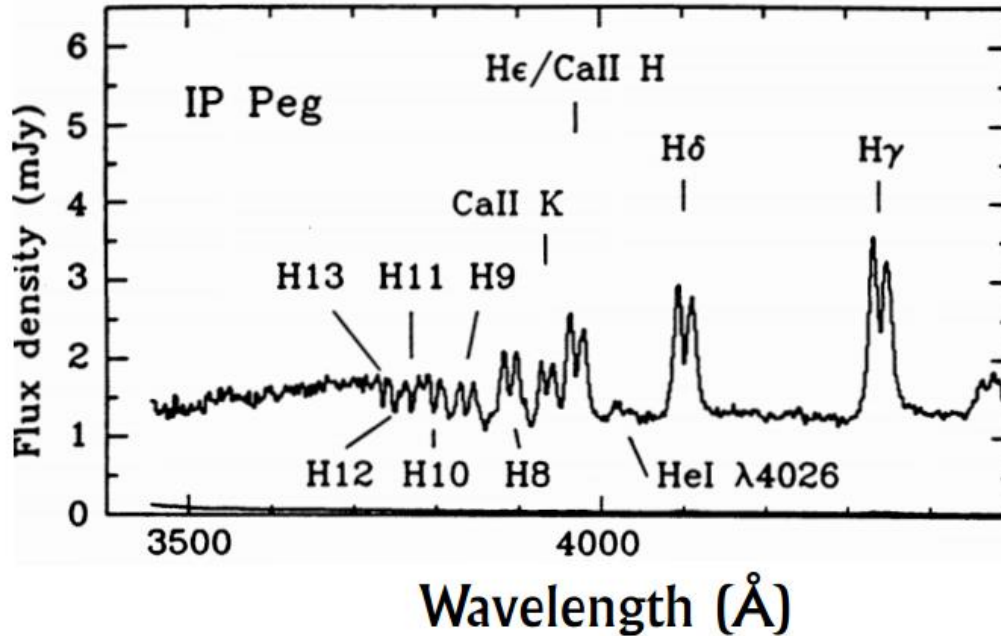
240

Mean spectrum of HT Cas in quiescence outside eclipse

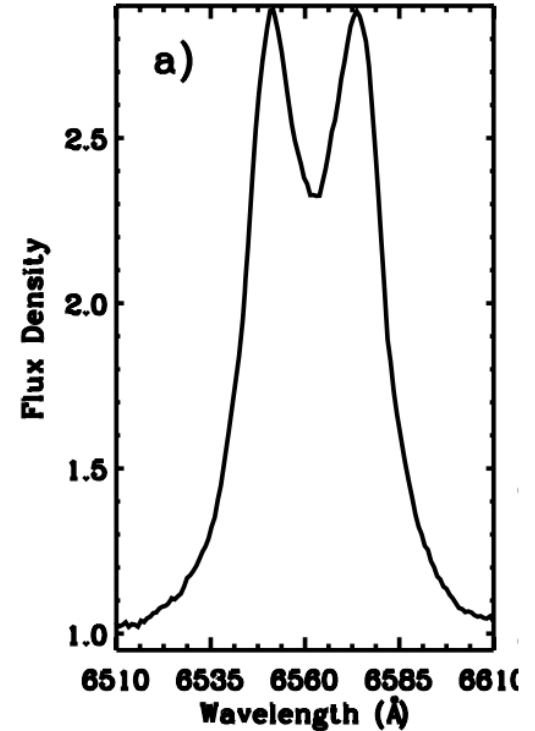


Spectroscopy: Emission line profiles (2)

241



IP Peg in low state
from Marsh 1988,
MNRAS, 231, 1117



A 0620-00
Nielsen et al. 2008,
MNRAS, 384, 849

Interacting Binary Stars

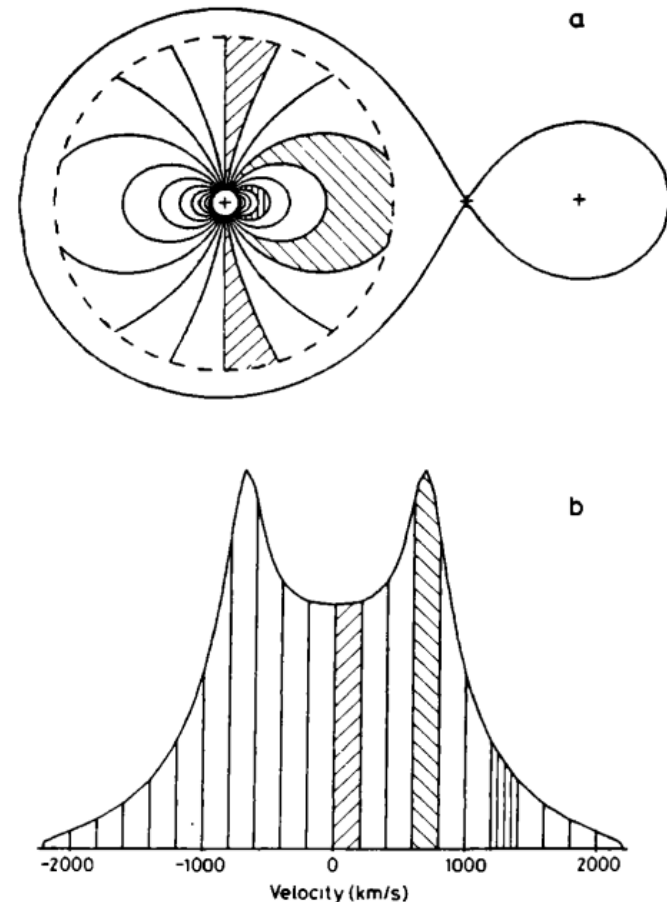
Spectroscopy: Emission line profiles (3)

242

(a) Loci of constant radial velocity in a Keplerian disk in a binary of mass ratio $q = 0.15$ viewed at quadrature

(b) Velocity profile of emission lines from the disk. Emission in the shaded velocity ranges originates in corresponding shaded regions on the disk.

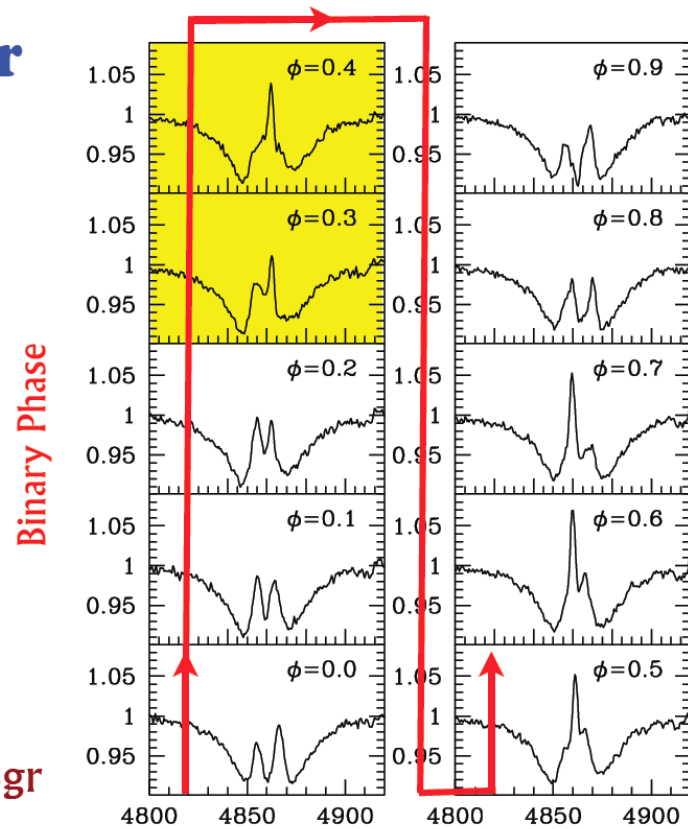
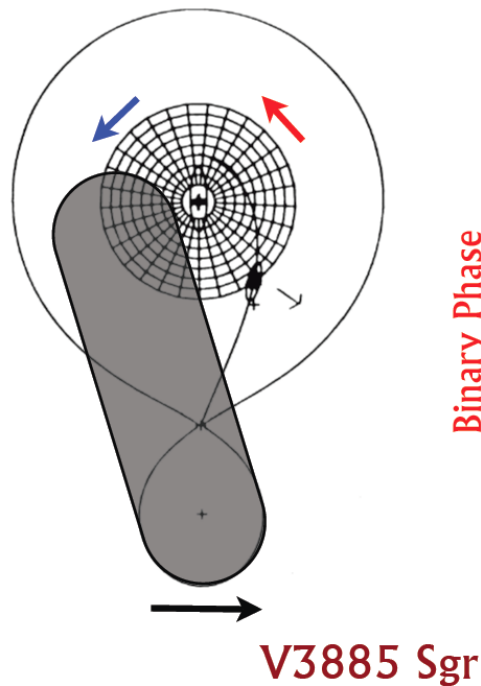
(From Home & Marsh 1986).



Spectroscopy: Emission line profiles (4)

243

Eclipse behavior

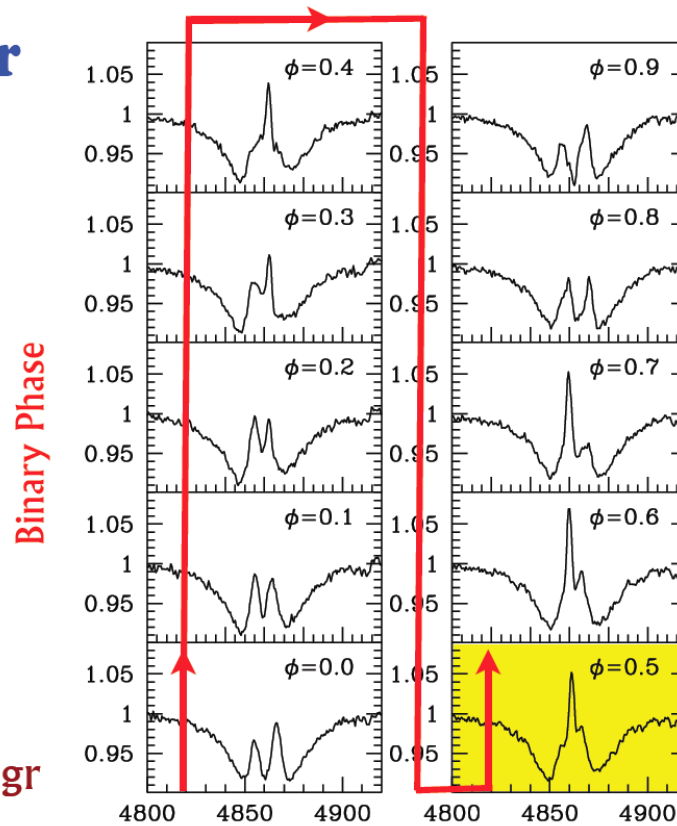
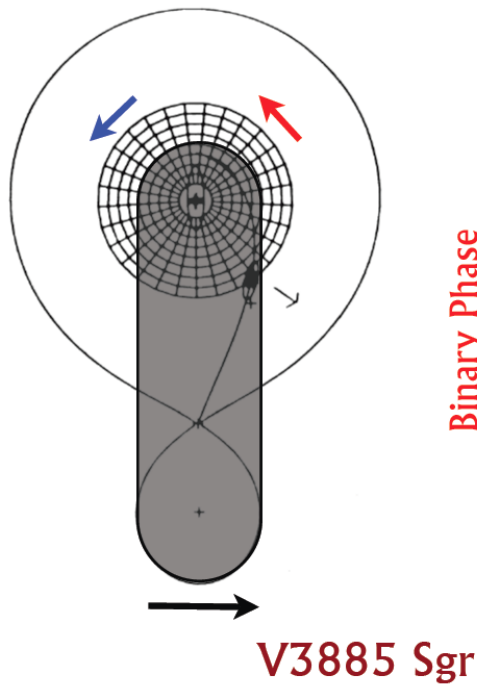


Hartley et al. 2005, MNRAS, 363, 286

Spectroscopy: Emission line profiles (5)

244

Eclipse behavior

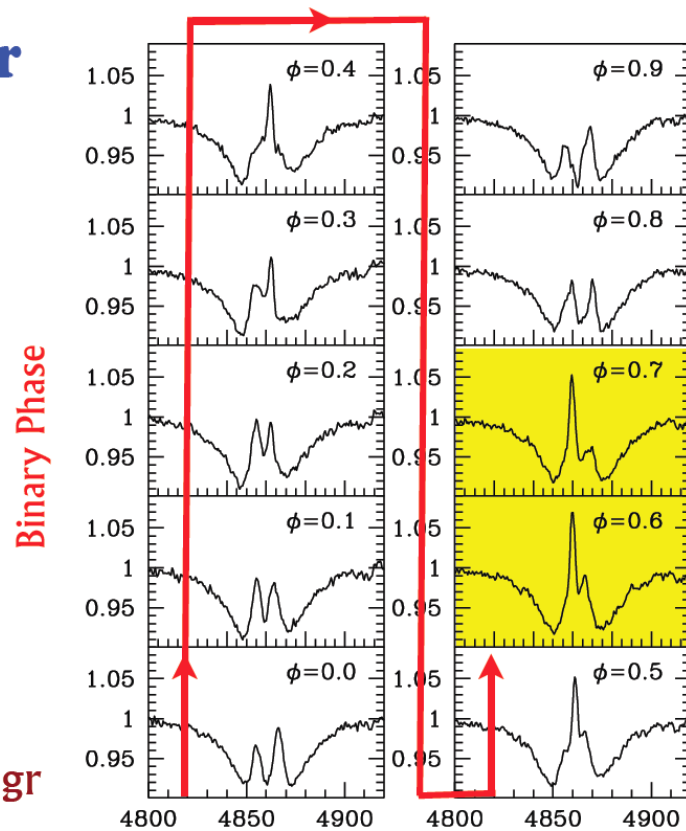
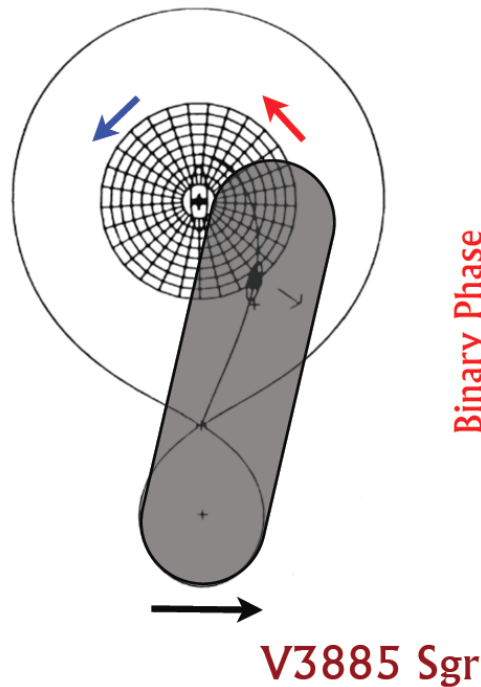


Hartley et al. 2005, MNRAS, 363, 286

Spectroscopy: Emission line profiles (6)

245

Eclipse behavior

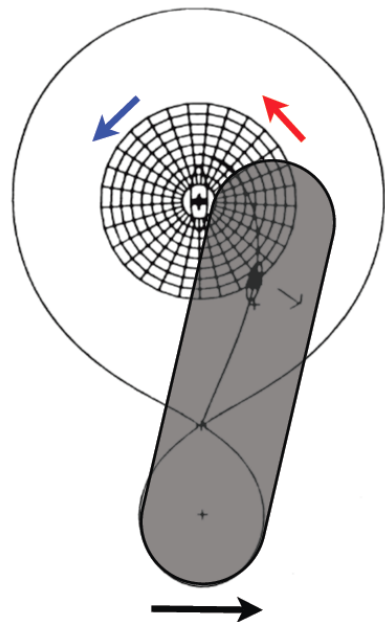


Hartley et al. 2005, MNRAS, 363, 286)

Spectroscopy: Emission line profiles (7)

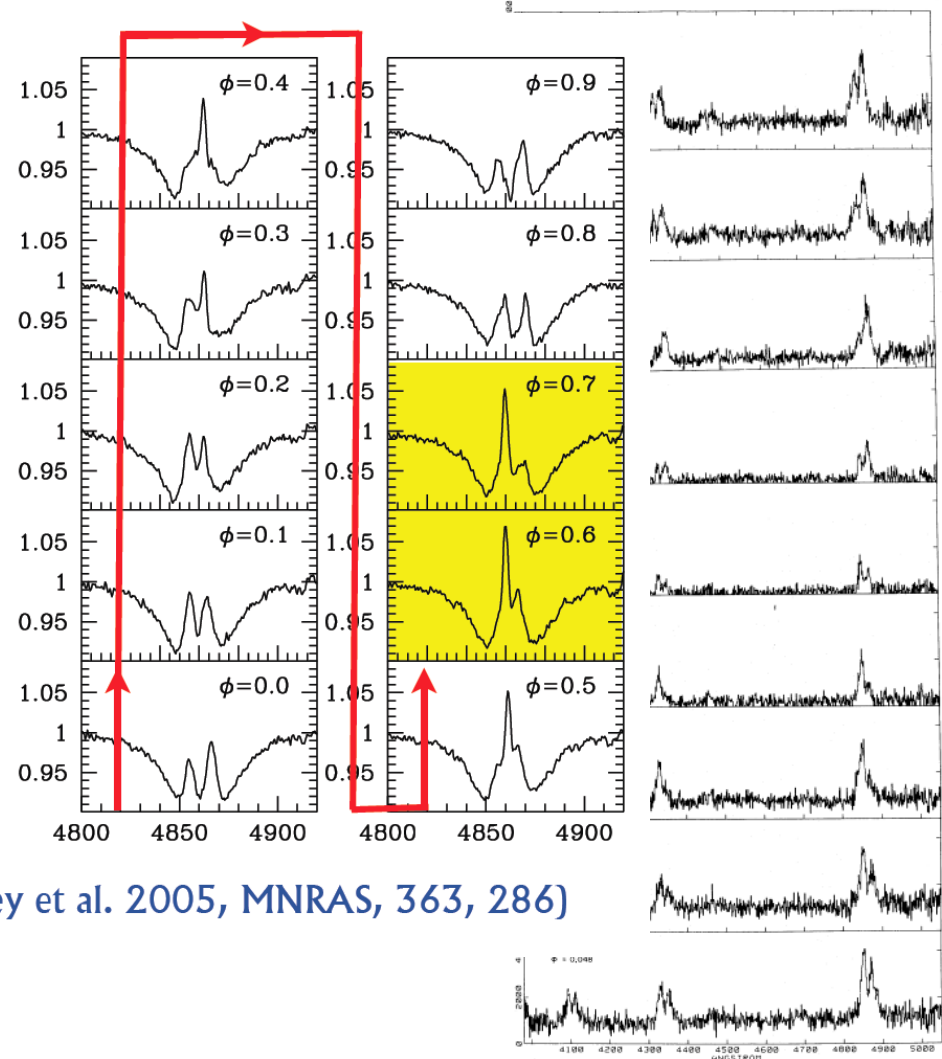
246

Eclipse behavior



V3885 Sgr

Binary Phase

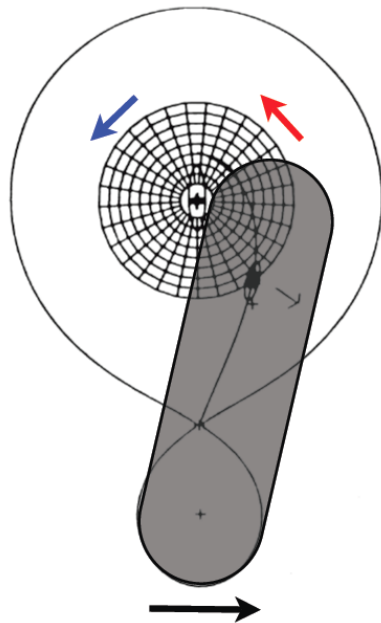


Hartley et al. 2005, MNRAS, 363, 286)

Spectroscopy: Emission line profiles (8)

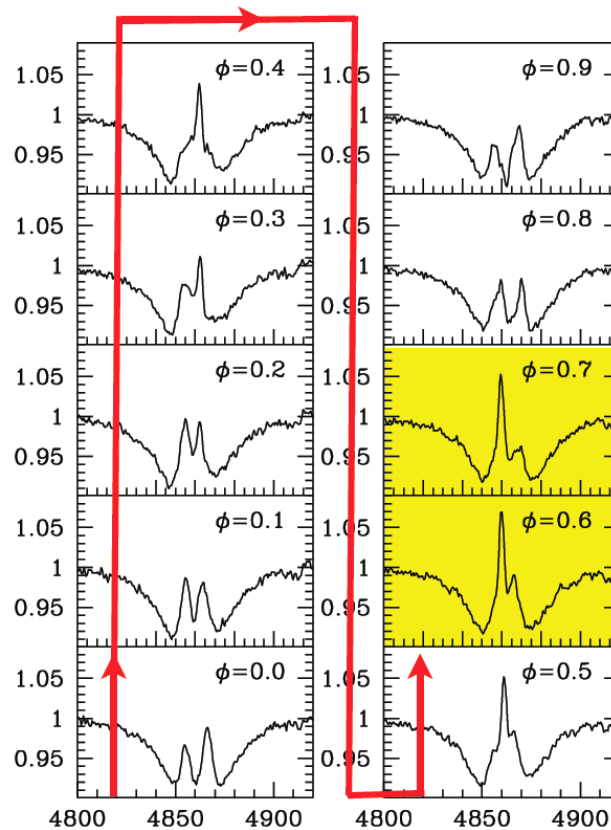
247

Eclipse behavior

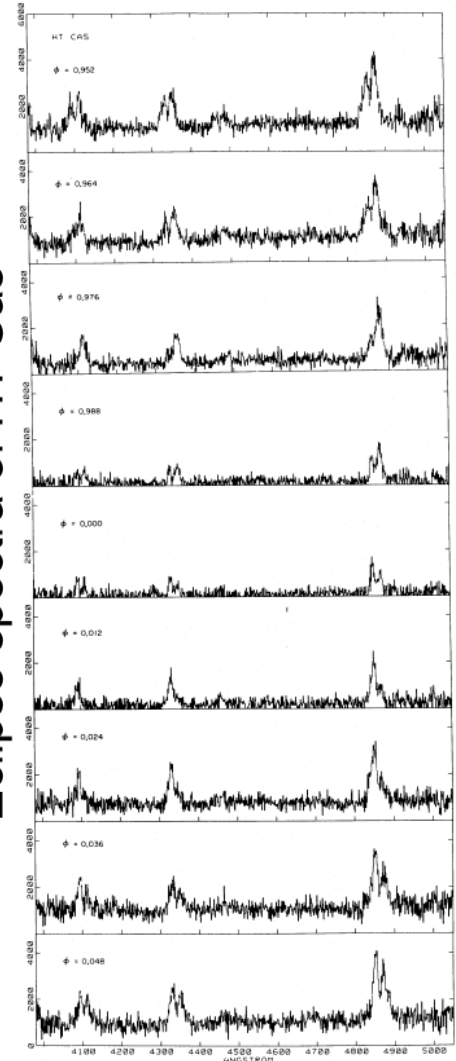


V3885 Sgr

Binary Phase



Eclipse spectra of HT Cas



Hartley et al. 2005, MNRAS, 363, 286

Modelling emission line profiles (1)

248

□ Smak (1969, 1981):

The emission line profile in terms of the dimensionless radial velocity u is:

$$F(u) \sim \int_{r_1}^{r_z} \frac{r^{3/2} f(r) dr}{(1 - u^2 r)^{1/2}}$$

where $r_z = \min(1, u^{-2})$

$f(r)$ is the density distribution of the emitting atoms. Good assumption $f(r) \sim r^{-\alpha}$.

Here α is not the Shakura & Sunyaev viscosity prescription.

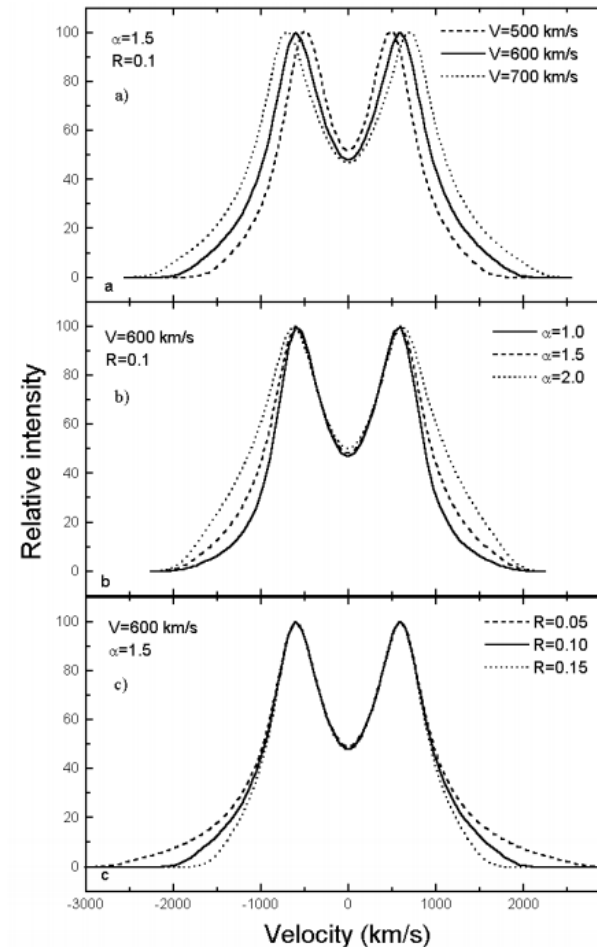
For specific values of α the integral can be expressed **analytically**.

- If you want to compare the modelled profiles with observations – Do not forget to convolve with the instrumental profile!

Modelling emission line profiles (2)

249

- **The shapes of the profiles:**
The accretion disk parameters basically affect different parts of line profiles on the whole, and therefore they can be determined unambiguously:
 - The velocity of the outer rim of the accretion disk V defines the distance between the peaks in the lines;
 - The shape of the line profile depends on the parameter α ;
 - The extent of the wings is determined by r_1 .

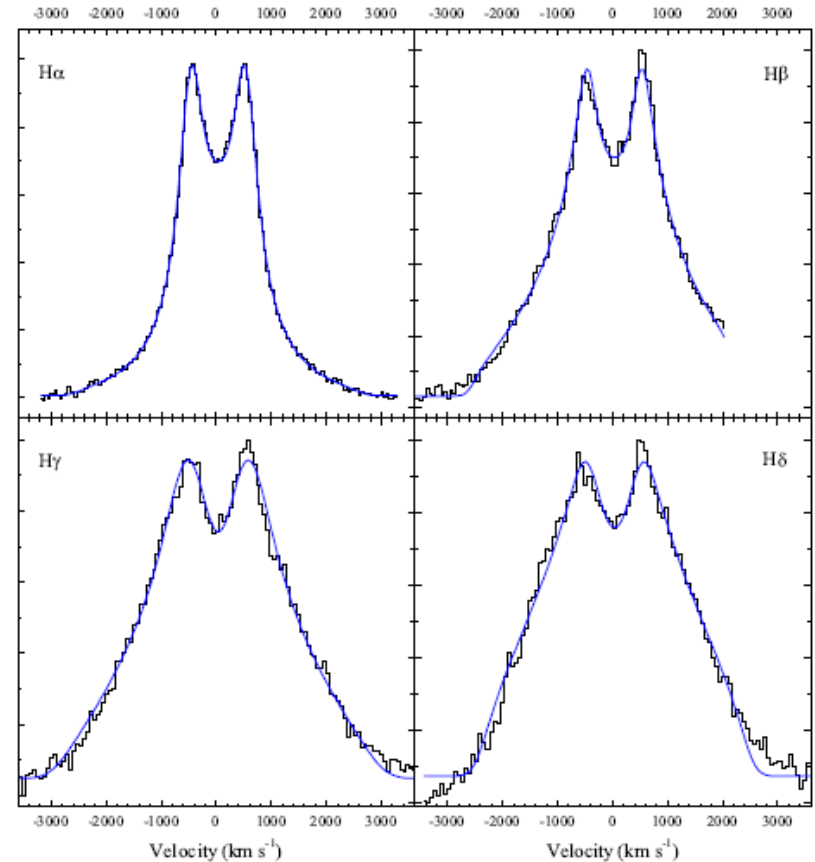


From Borisov & Neustroev, 1998

Modelling emission line profiles (3)

250

- **The shapes of the profiles:**
The accretion disk parameters basically affect different parts of line profiles on the whole, and therefore they can be determined unambiguously:
 - The velocity of the outer rim of the accretion disk V defines the distance between the peaks in the lines;
 - The shape of the line profile depends on the parameter α ;
 - The extent of the wings is determined by r_1 .



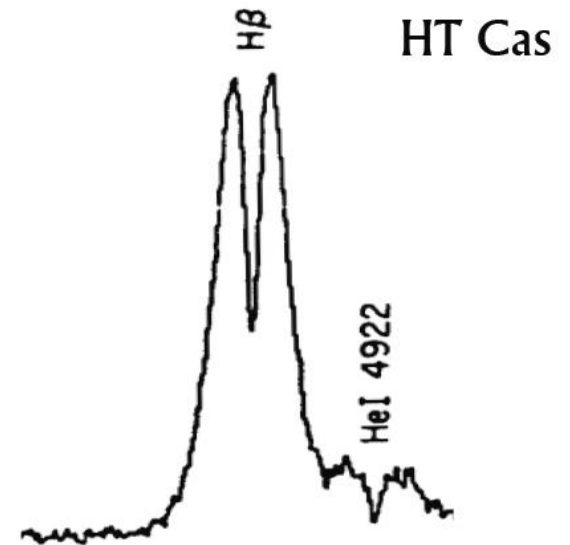
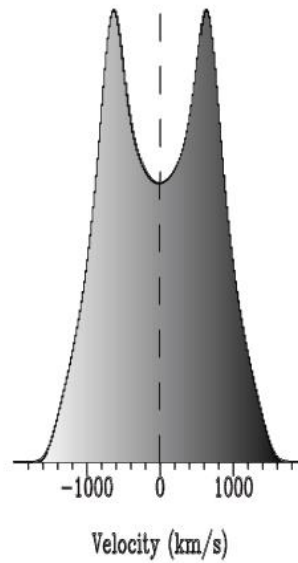
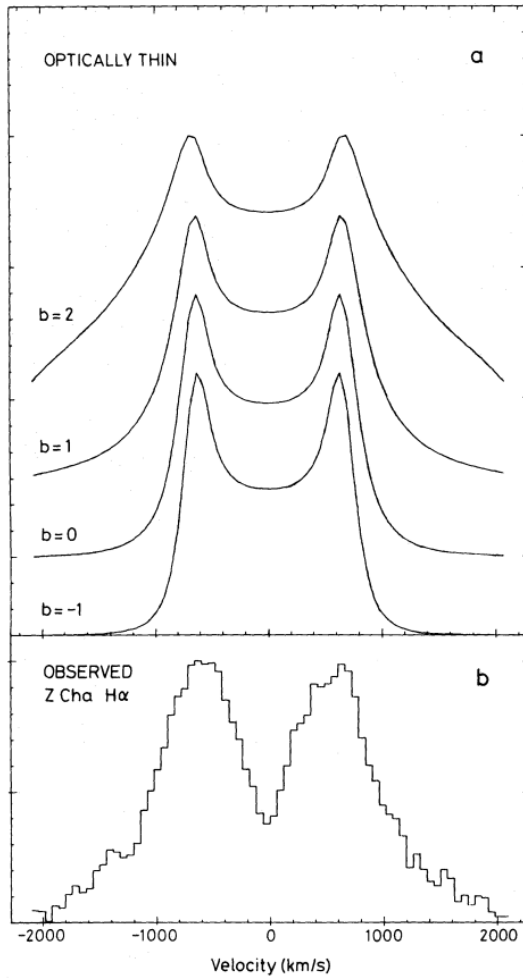
Observations!



Interacting Binary Stars

Spectroscopy: Emission line profiles (9)

251

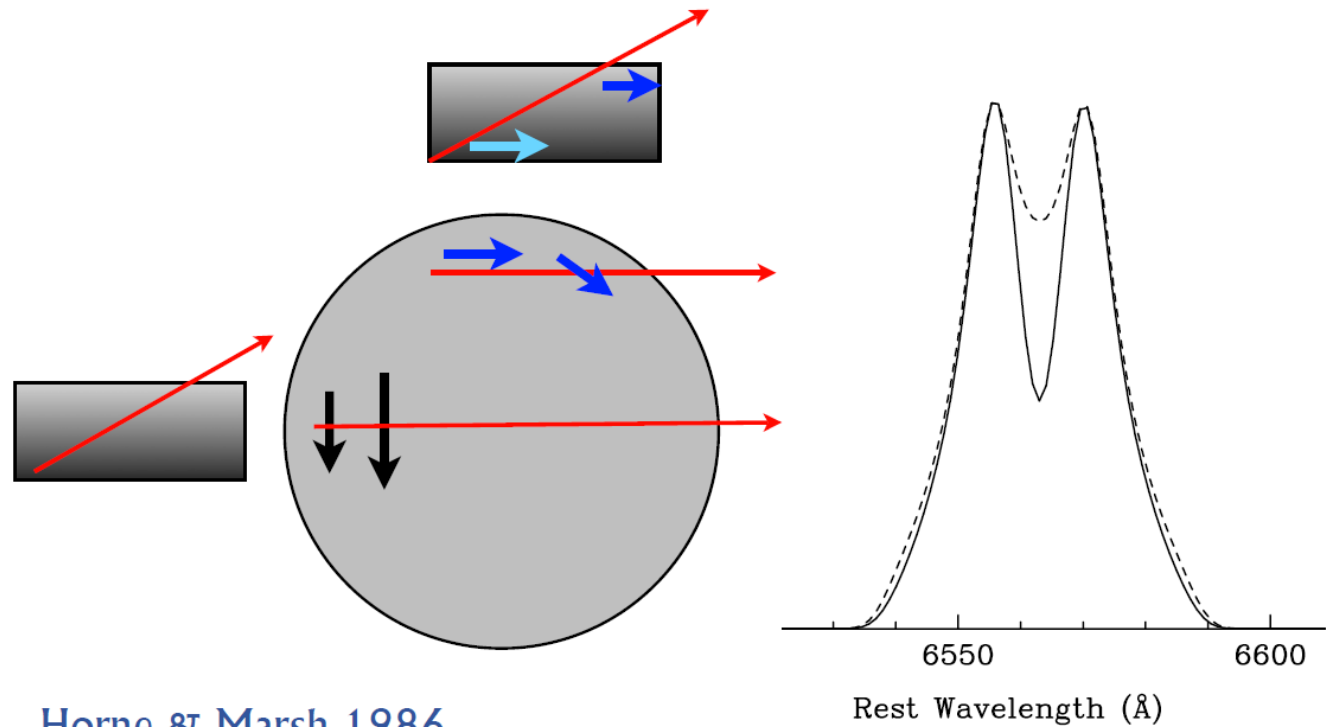


Interacting Binary Stars

Radiative transfer effects

252

The importance of shear:



Horne & Marsh 1986,
MNRAS, 218, 761

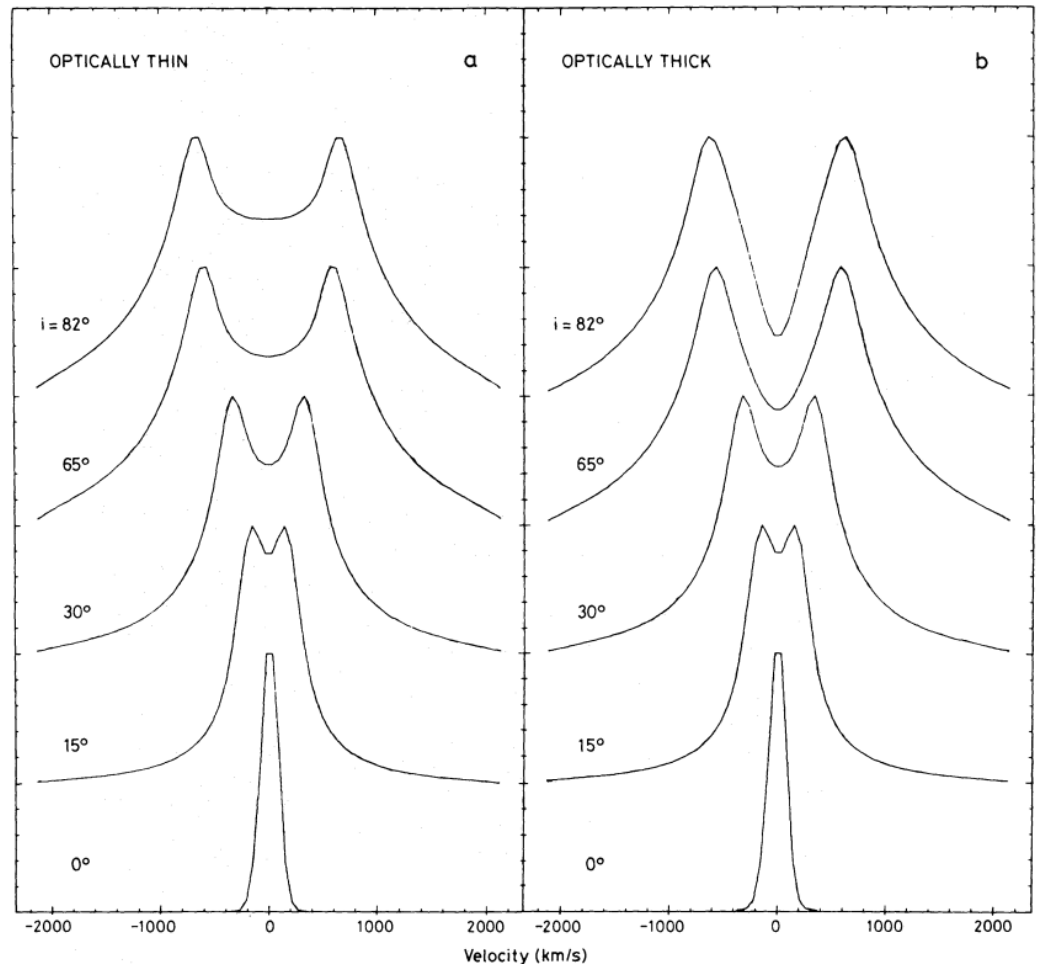
Interacting Binary Stars

Modelling emission line profiles (4)

253

Synthetic line profiles for optically thin and optically thick emission lines covering a range of inclinations.

(Horne & Marsh 1986, MNRAS, 218, 761)



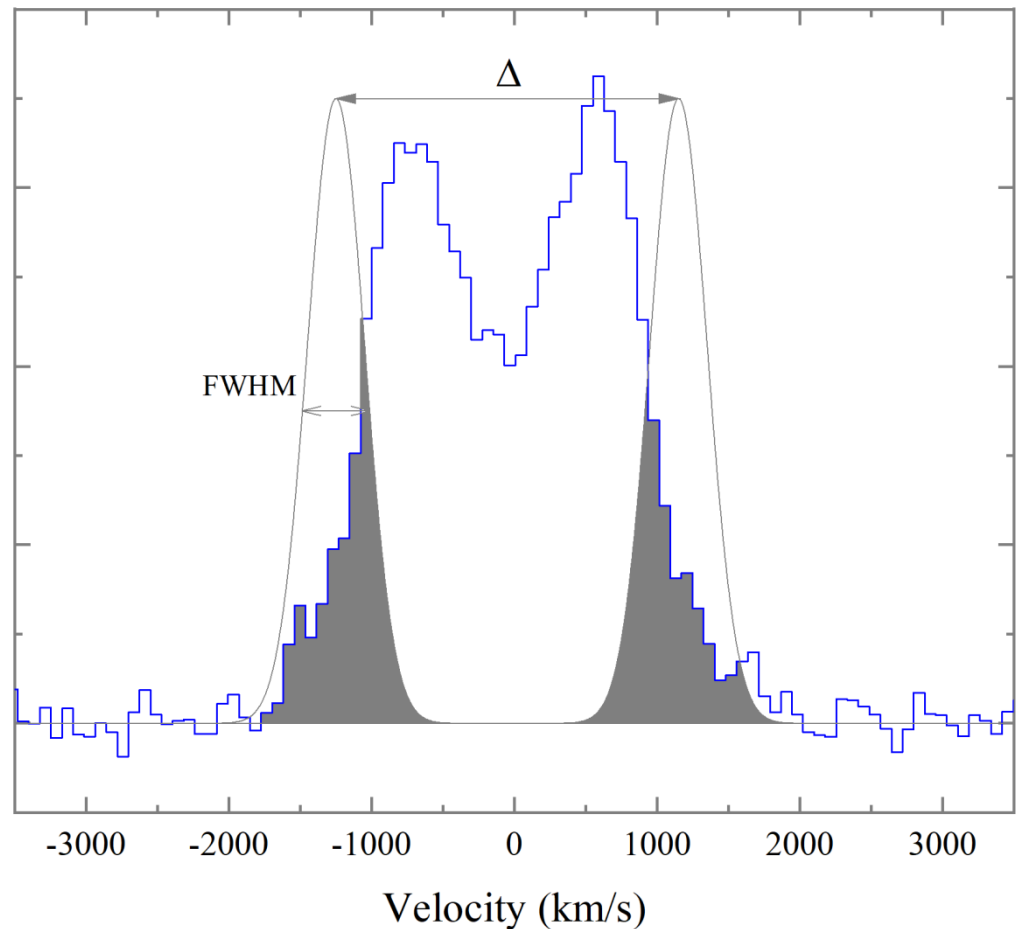
Radial velocity measurements

254

Double-peaked emission lines from an accretion disk are usually very broad.

A “normal”, single-Gaussian fit doesn't work.

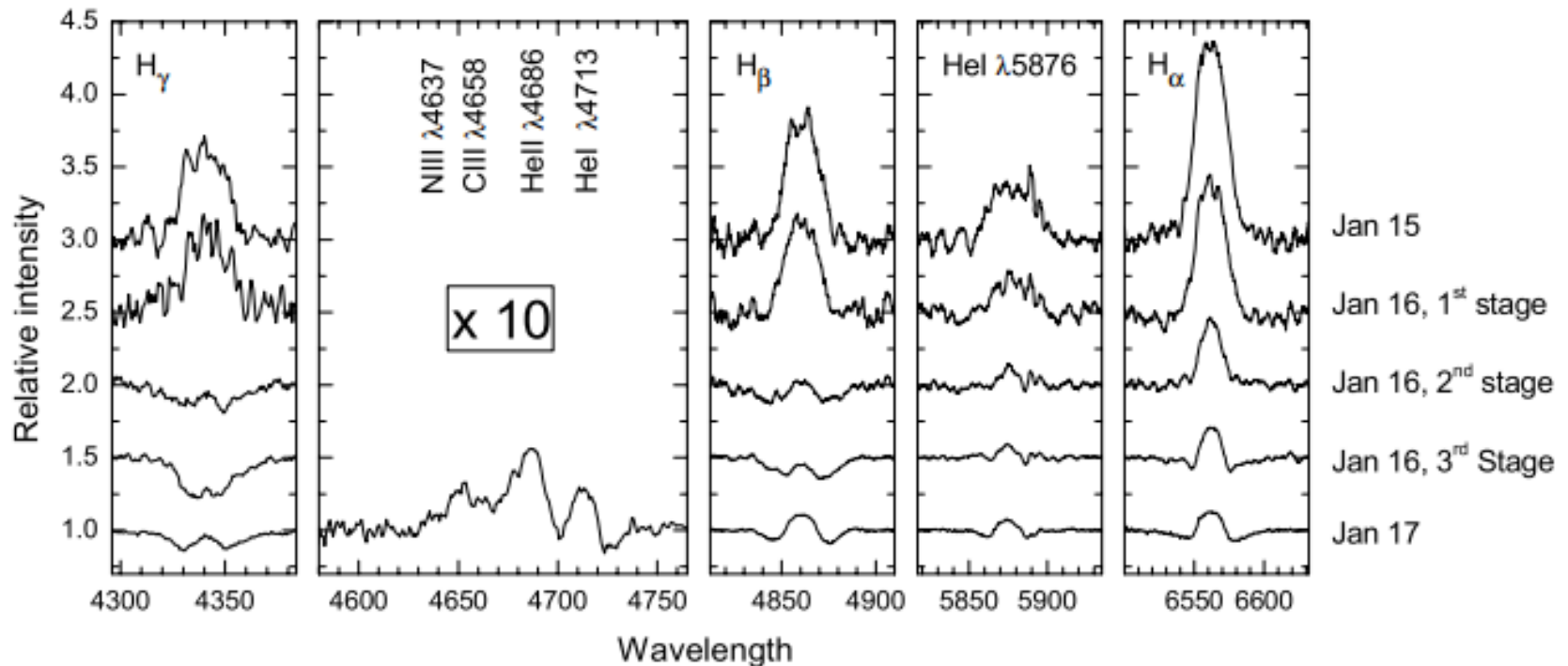
Instead, we can use the double-Gaussian method by Schneider & Young (1980) and later refined by Shafter (1983).



Something changes in outburst!

255

BZ Uma from the quiescent to outburst state (Neustroev et al., 2005)



Source of power for the lines

256

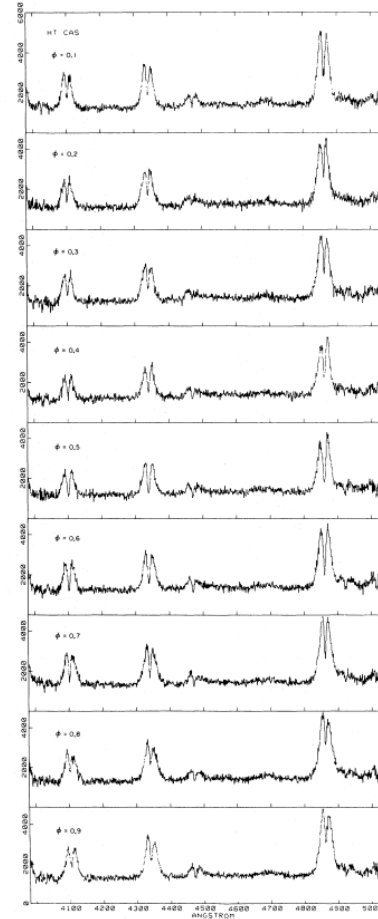
- Local Energy Dissipation
 - ▣ Emission from optically thin disk in LTE
Williams 1980, ApJ, 235, 939
 - ▣ Coronal loops over the disk, analogous to solar magnetic loops
Horne & Saar 1991, ApJ, 374, L55
- Photoionization
 - ▣ CVs in high state:
Horne & Marsh 1990, ApJ, 349, 593
- **There is still no good theory explaining the cause and properties of Accretion disk emission lines.**

Spectral orbital variability

257

Spectra of HT Cas
in quiescence
at various orbital
phases

Young et al. 1981

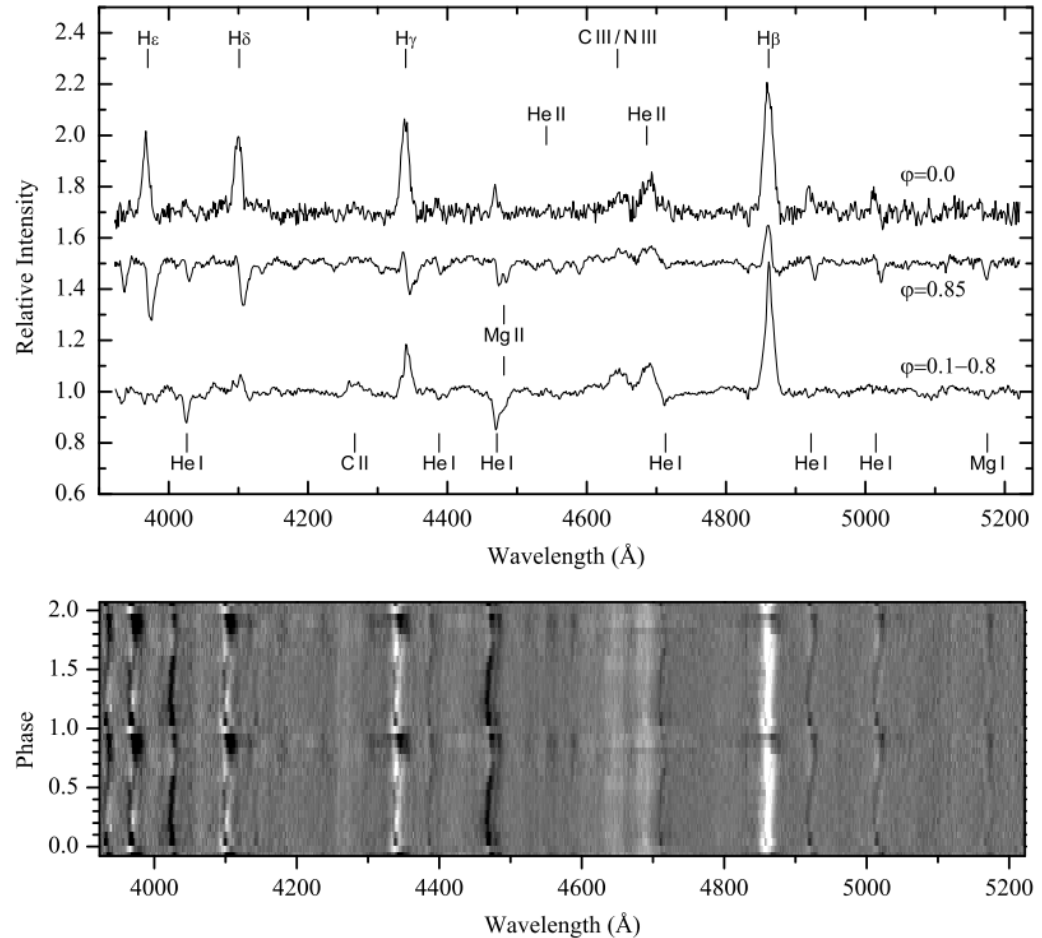


Trailed spectra (1)

258

UX UMa

Neustroev et al.
2011



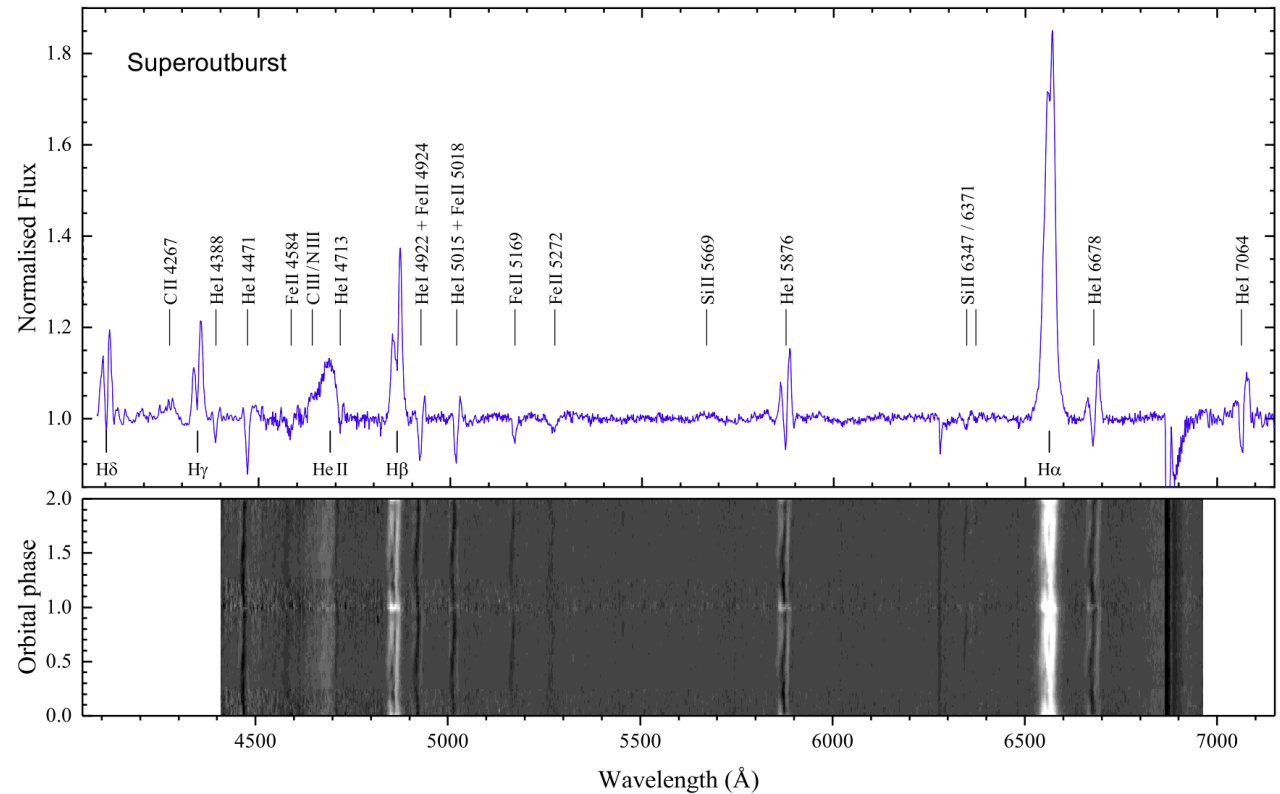
Interacting Binary Stars

Trailed spectra (2)

259

HT Cas

Neustroev & Zharikov
2020



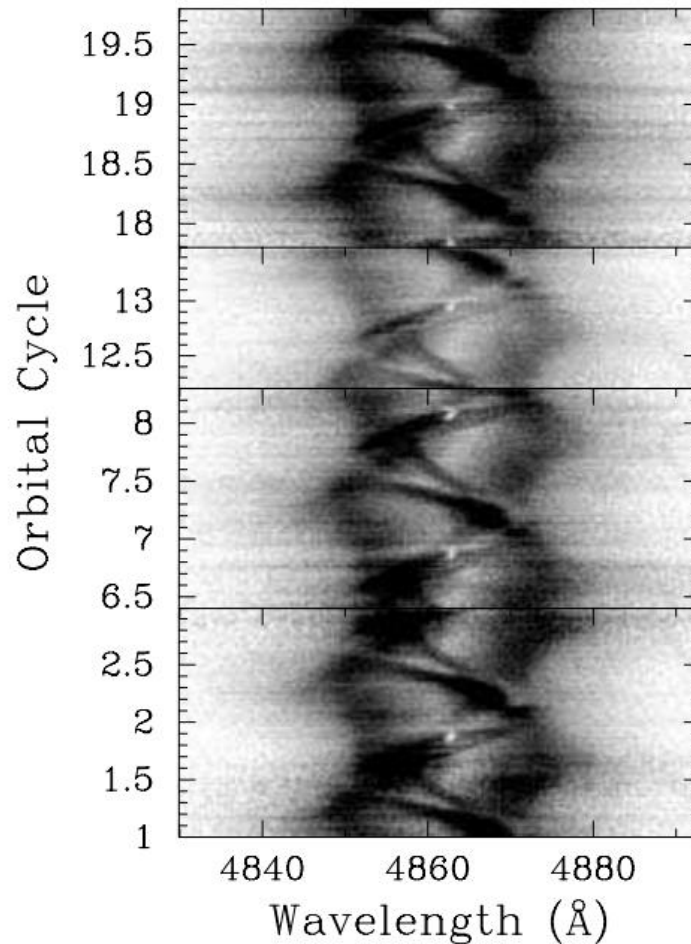
Trailed spectra (3)

260

U Gem:

Trailed H α spectra
without phase binning.

From Unda-Sanzana et al. 2006



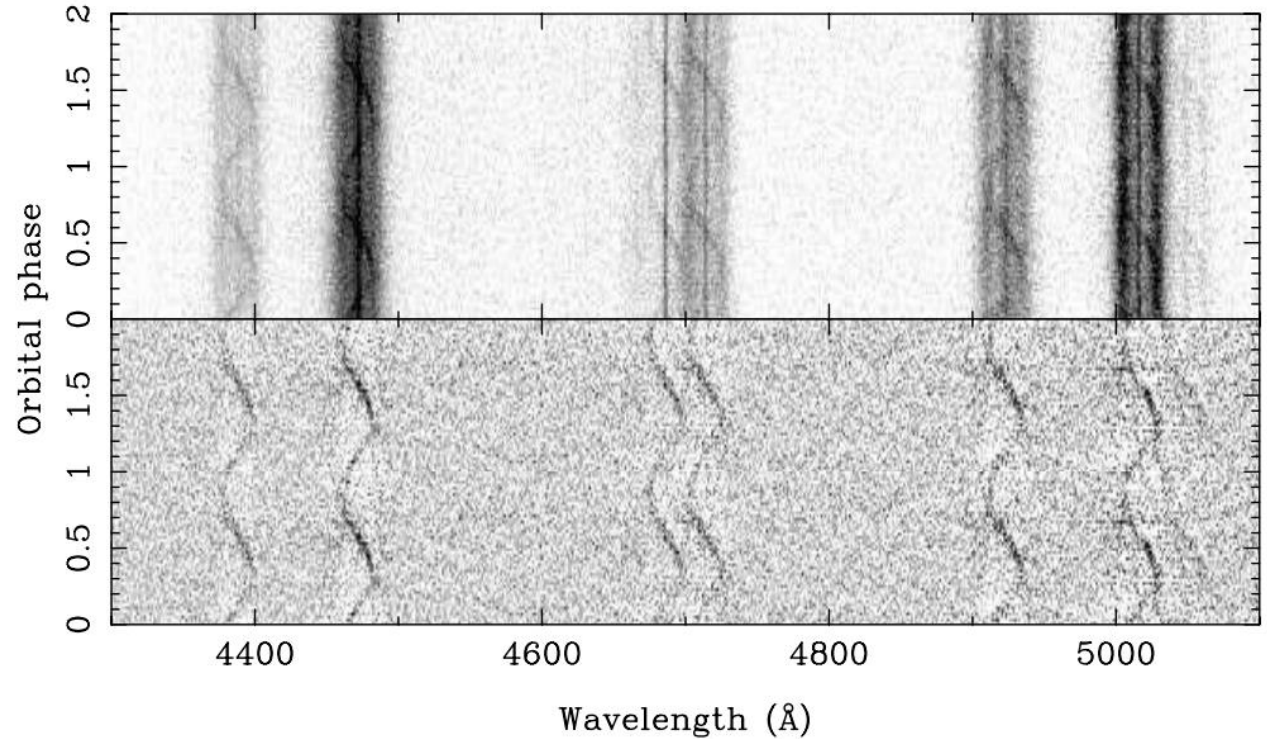
Interacting Binary Stars

Trailed spectra (4)

261

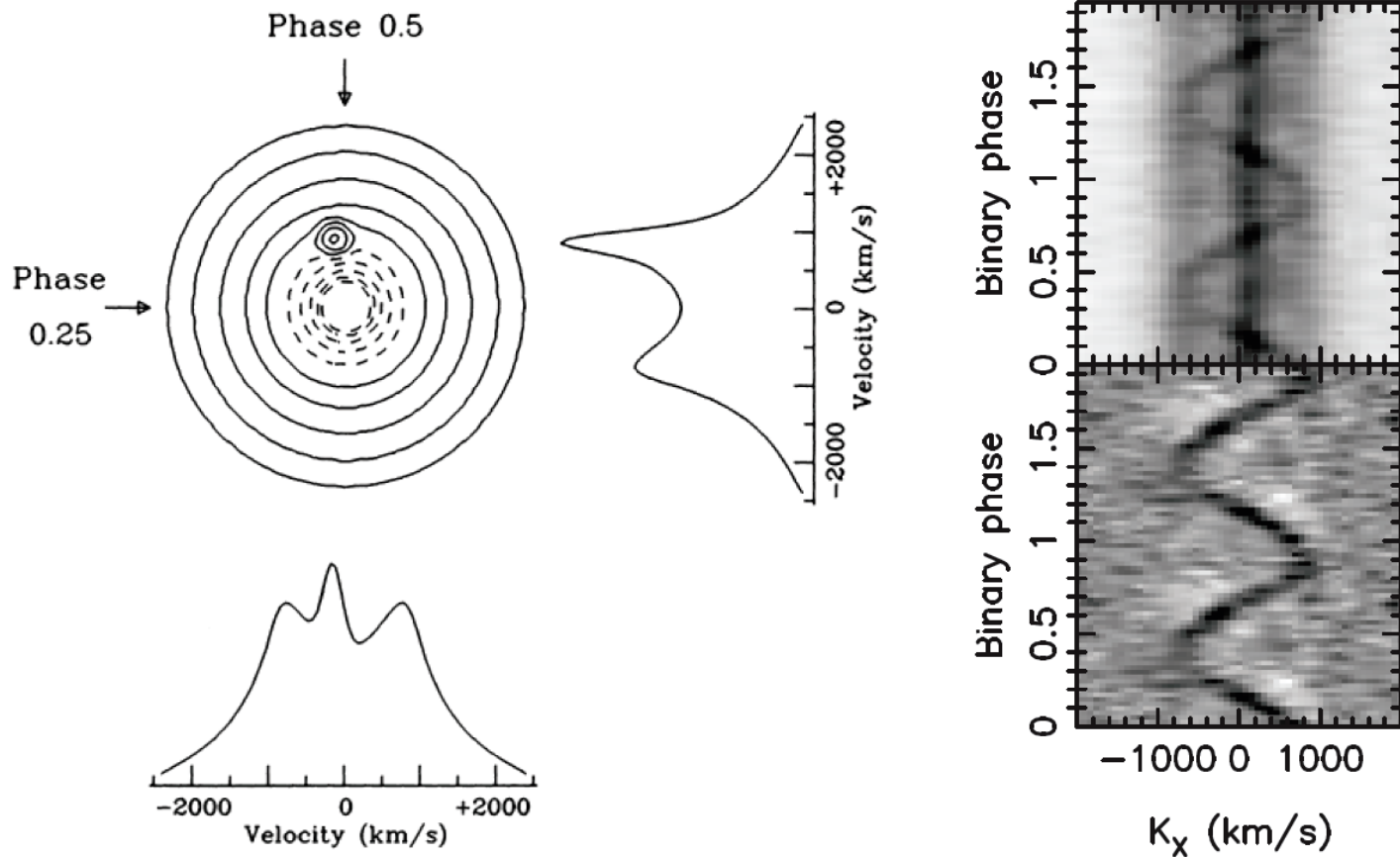
GP Com:

Marsh T. 1999



Principle of Doppler Tomography

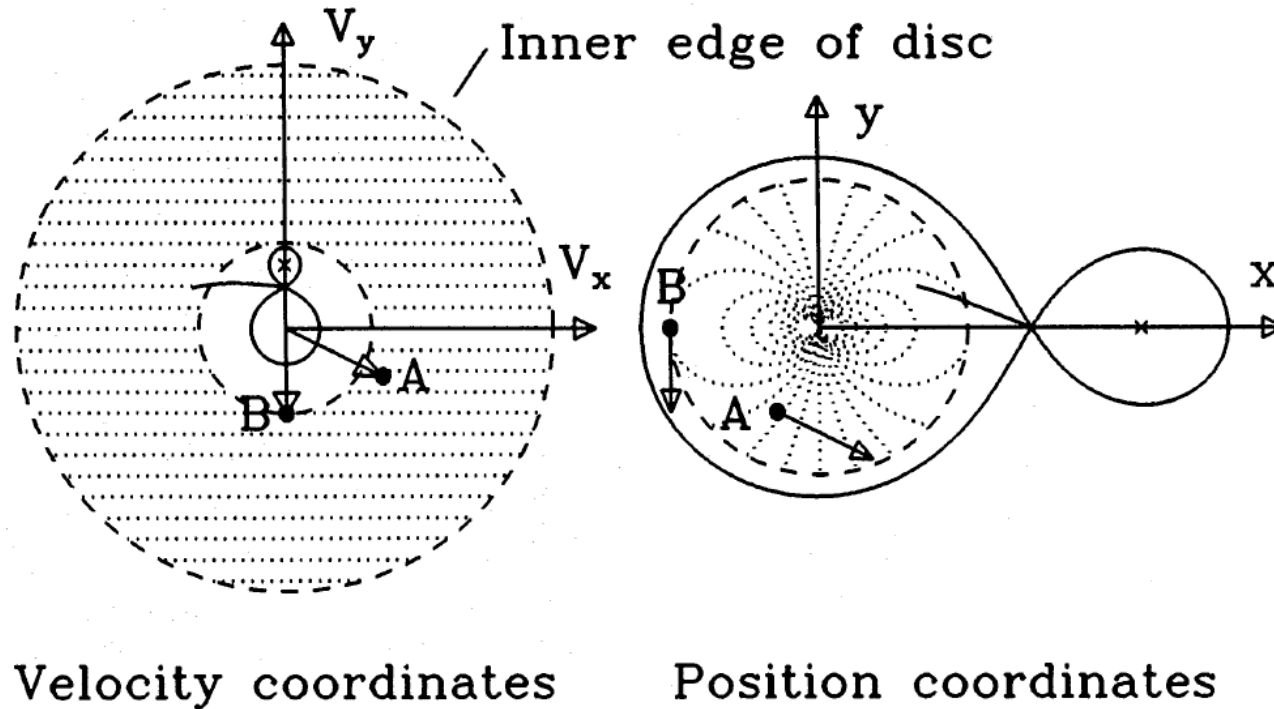
262



from Marsh & Horne 1988, MNRAS, 235, 269

Principle of Doppler Tomography

263



from Marsh & Horne 1988, MNRAS, 235, 269

Computing Doppler maps

264

- ✦ Observed line profile at binary phase ϕ in terms of parameters in binary frame

$$f(V, \phi) = \iiint I(V_x, V_y, V_z) g(V - \gamma + V_x \cos \phi - V_y \sin \phi + V_z) dV_x dV_y dV_z$$

line intensity
in disk frame

local line
profile

projected
velocities

- ✦ Assume no vertical motions, replace local profile, $g(V)$, by its Fourier transform, $G(s)$, and invert

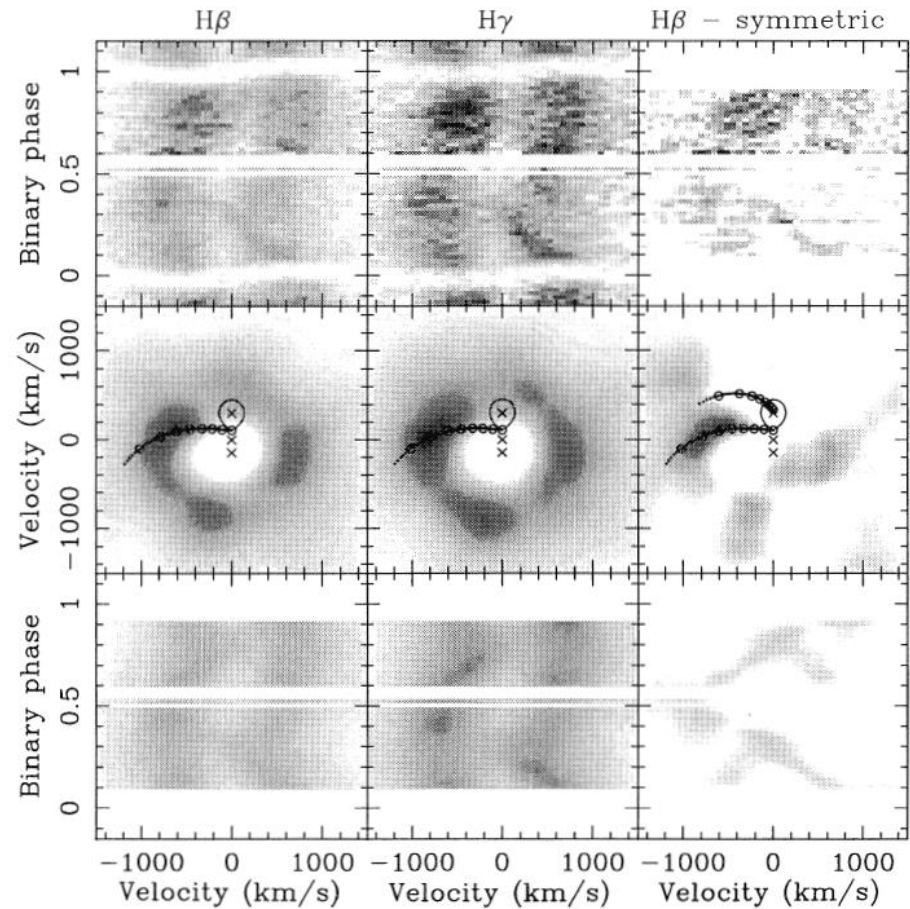
$$I(V_x, V_y) = \int_0^{2\pi} \int_0^\infty \frac{s}{G(s)} \int f(V, \phi) \exp[-i2\pi s(V - \gamma + V_x \cos \phi - V_y \sin \phi)] dV ds d\phi$$

- ✦ Alternative: maximum entropy inversion

Tomography: Early Applications (1)

265

IP Peg: Quiescence

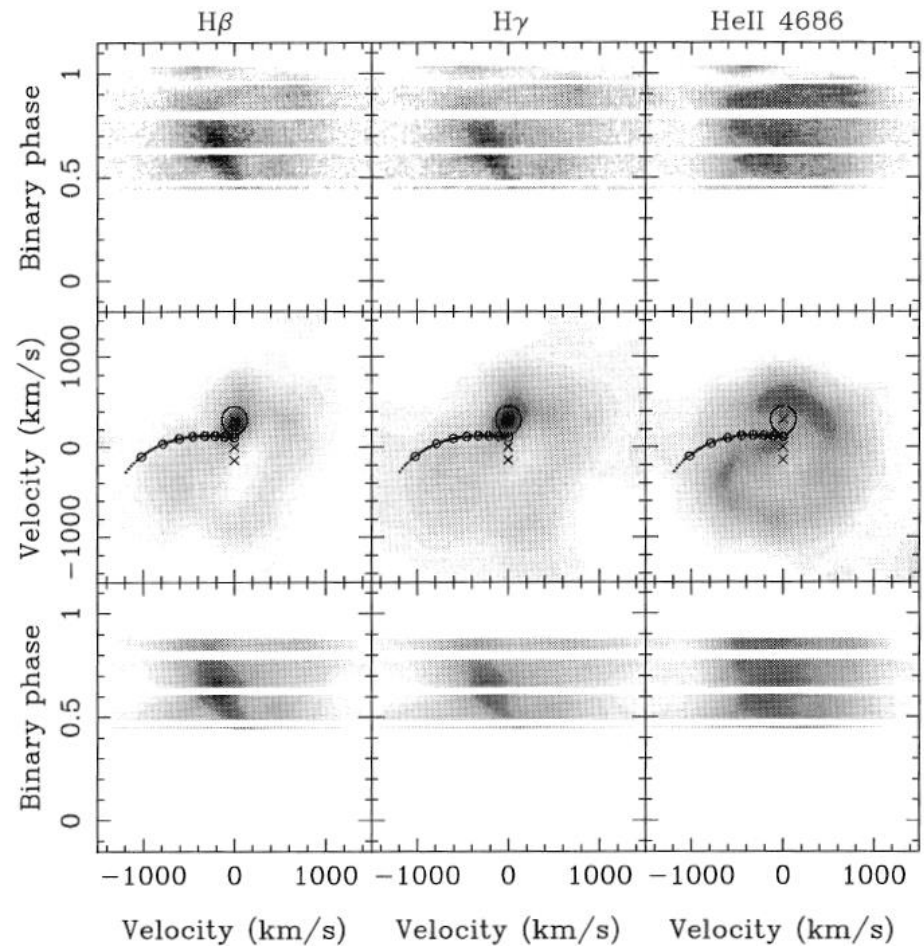


Horne & Marsh 1990, ApJ, 349, 593

Tomography: Early Applications (2)

266

IP Peg: Outburst

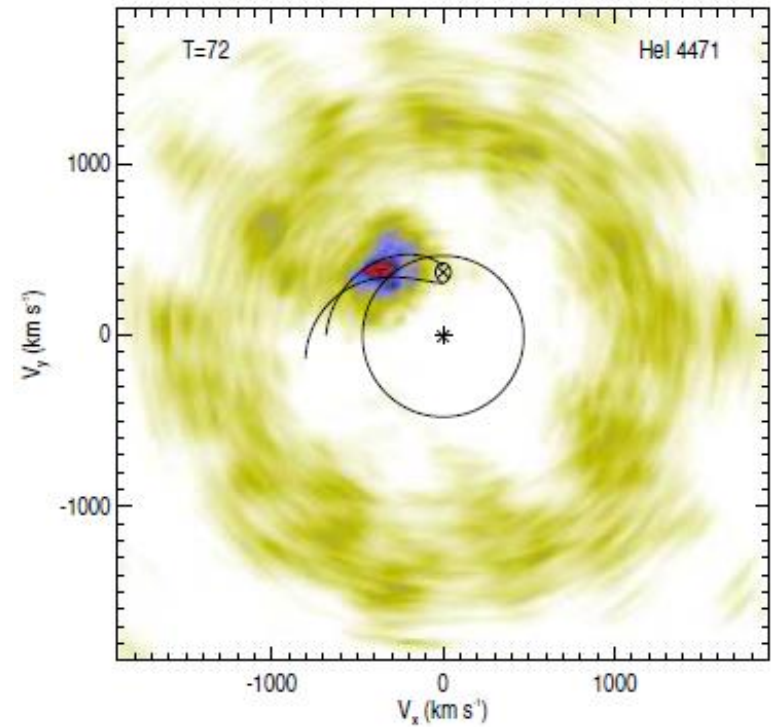
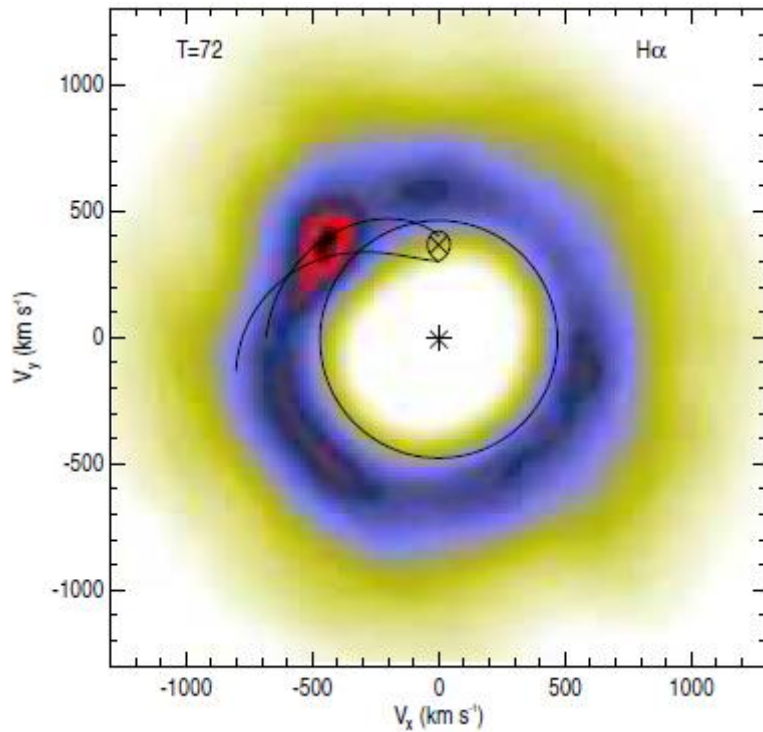


Horne & Marsh 1990, ApJ, 349, 593

Tomography: Expected structures (1)

267

Disk ring and a hot spot



Tomography: Expected structures (2)

268

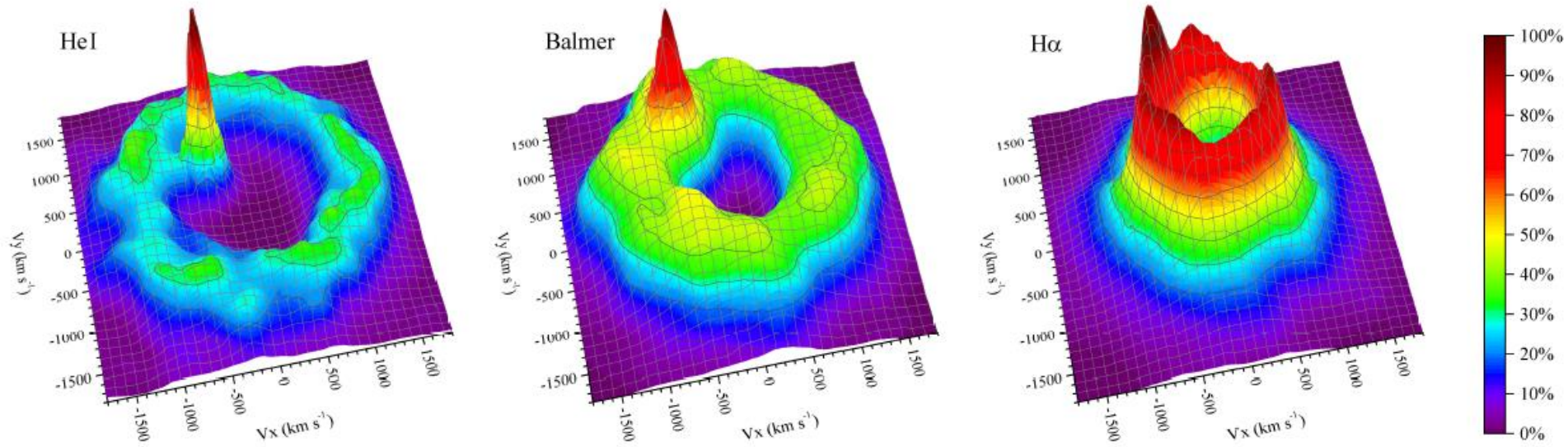


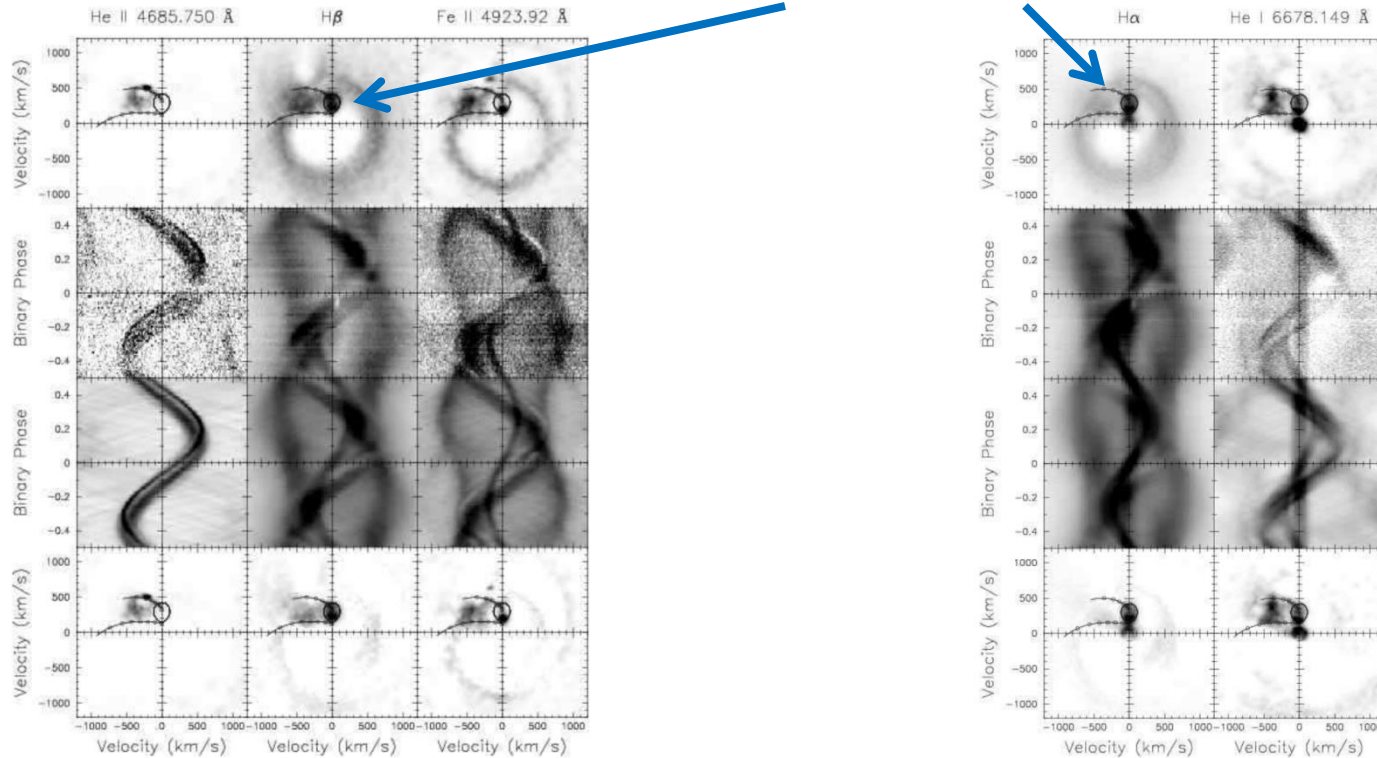
Figure 9. The H α tomogram and the averaged higher order Balmer and He I maps from the $T=72$ data set in 3D representation (see text for detail).

Tomography: Expected structures (3)

269

Disk ring and a hot spot

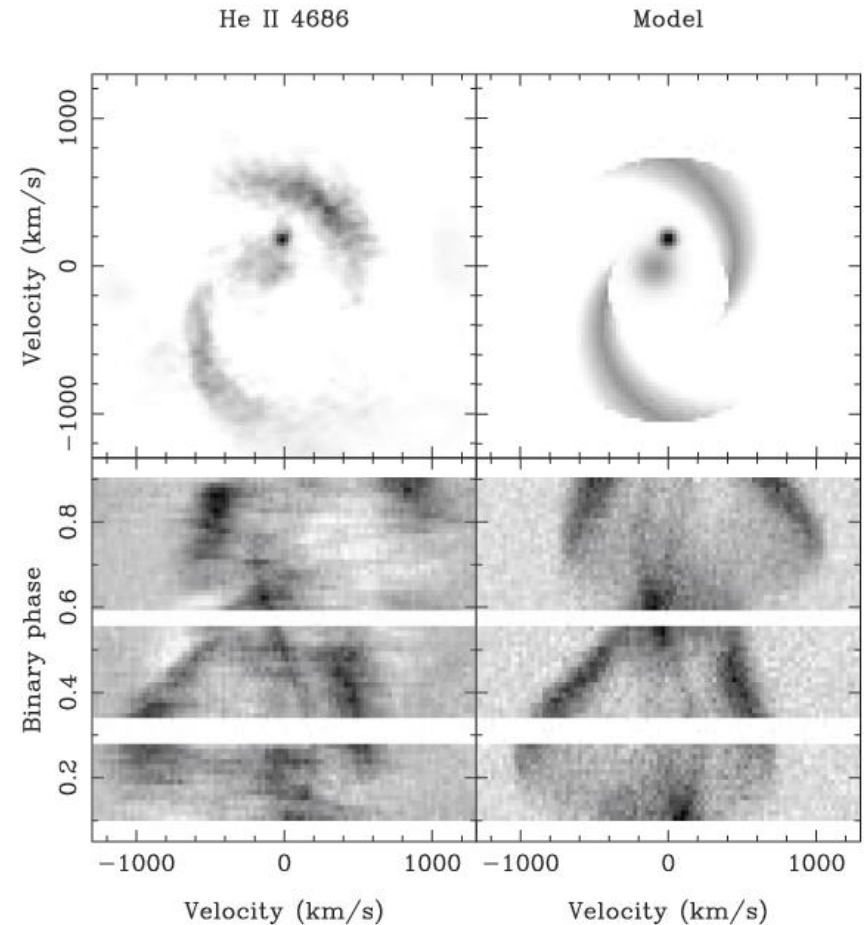
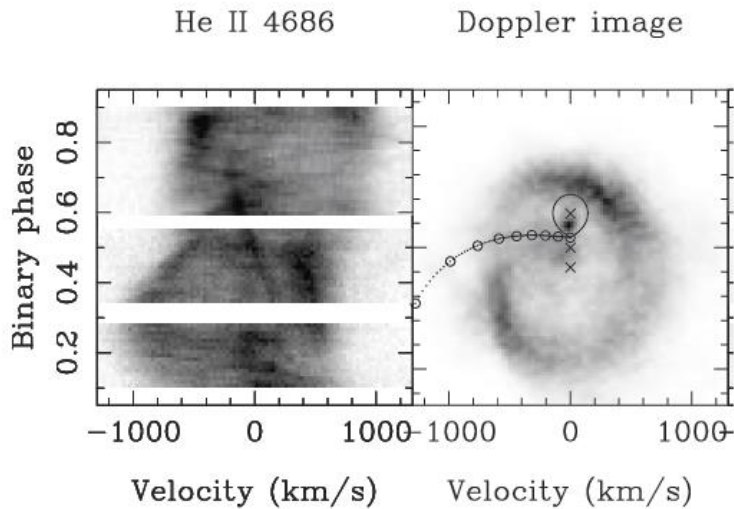
Donor star!



Tomography: Spiral Arms

270

IP Peg: Outburst



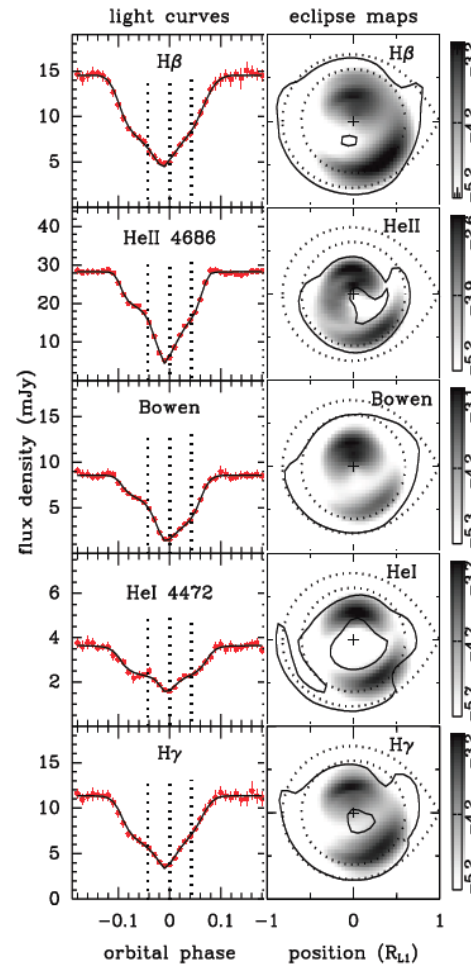
Harlaftis et al. 1999, MNRAS, 306, 348

Confirmation from eclipse mapping

271

Eclipse maps in selected emission lines of IP Peg in outburst

Detection of spiral structure



Baptista et al. 2005, A&A, 444, 201

What's a problem with spiral arms?

272

- Predicted by theory (Sawada et al. 1986)
- Angular momentum transport mechanism.
- Observed around peak of outburst:
 - ▣ IP Peg (DN) — Harlaftis et al. 1999
 - ▣ WZ Sge (DN) — Kuulkers et al. 2002
 - ▣ SS Cyg (DN) — Steeghs et al. 2001
 - ▣ U Gem (DN) — Groot et al. 2001

 - ▣ V 3885 Sgr (NL) — Hartley et al. 2005
 - ▣ UX UMa (NL) — Neustroev et al. 2011
- Sometimes observed in quiescence.

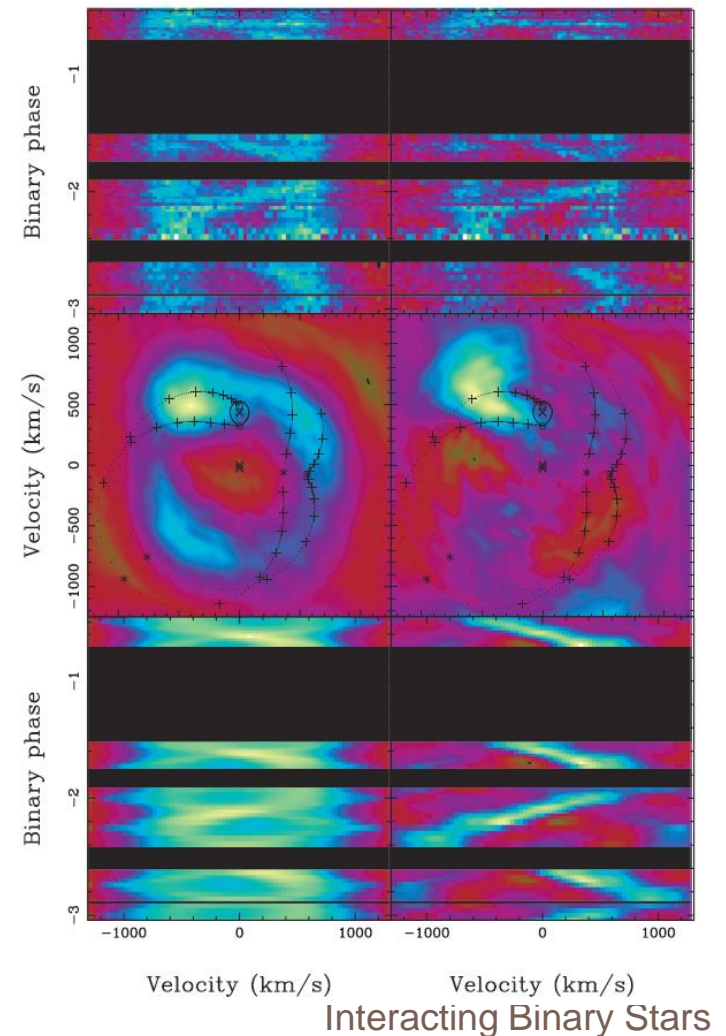
Tomography: unusual structures (1)

273

Disk eccentricity:

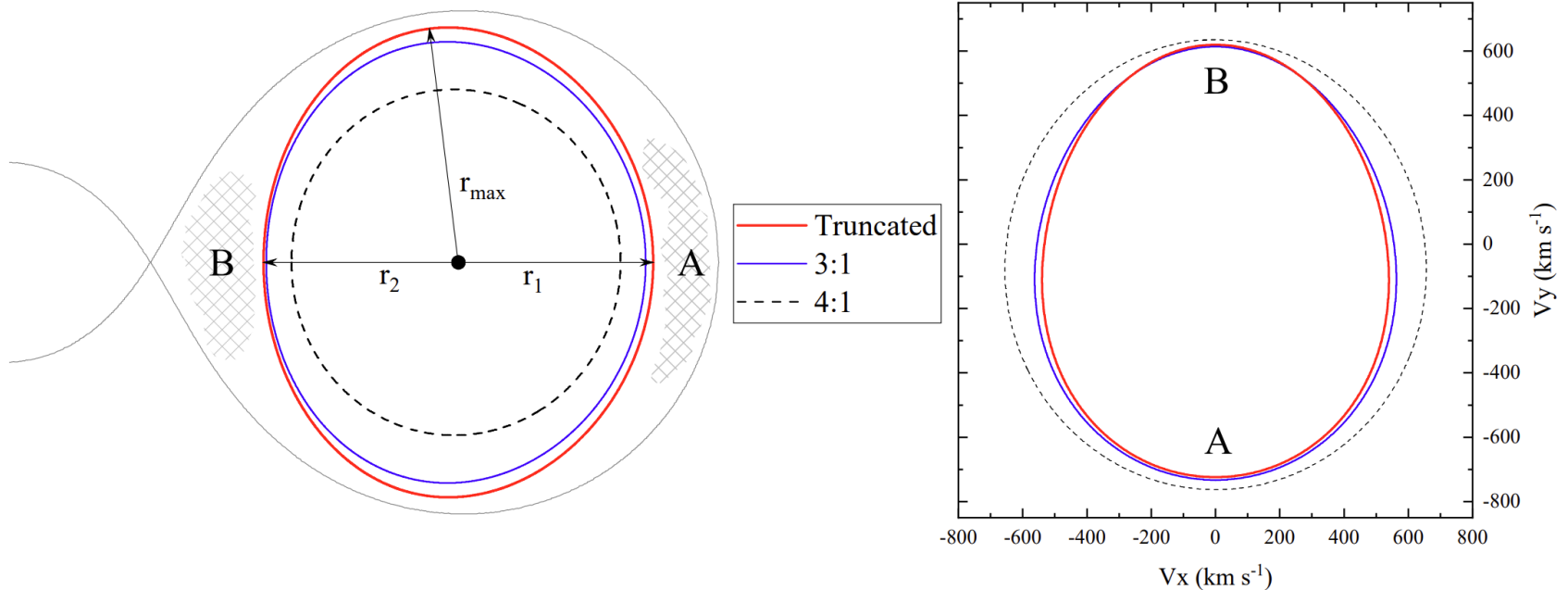
- ❑ Tidal perturbation of the disk by the secondary star at $q < 0.25$
- ❑ Proposed to explain “superhumps” in CVs (Whitehurst 1988; Lubow 1991)

Figure from Nielsen et al. 2008, MNRAS, 384, 849



Tomography: unusual structures (2)

274



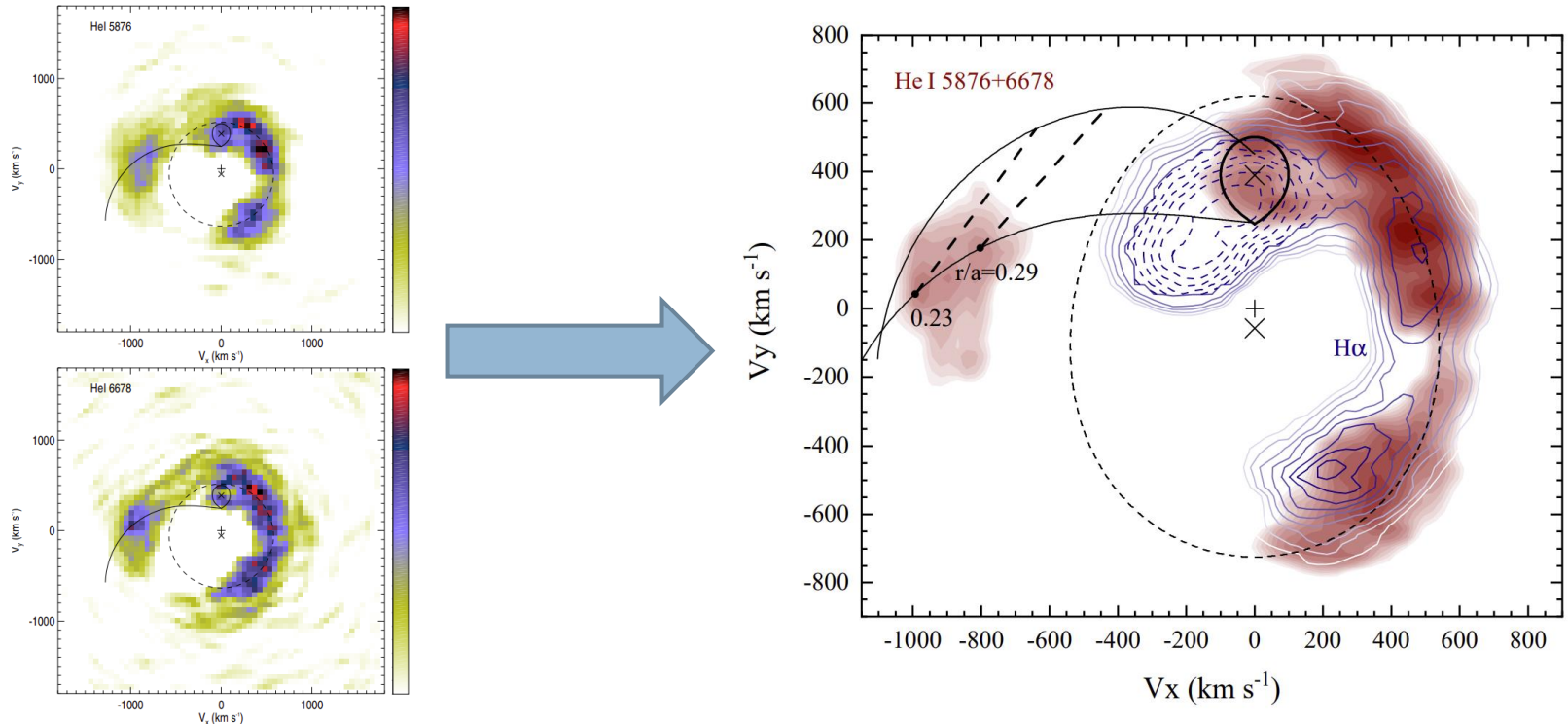
Unusual, but explained: disk elongation:

Tidal perturbation of the disk by the secondary star

Neustroev & Zharikov.: 2020, A&A, 642, A100

Tomography: unusual structures (3)

275



Unusual, but explained: disk elongation:

Tidal perturbation of the disk by the secondary star

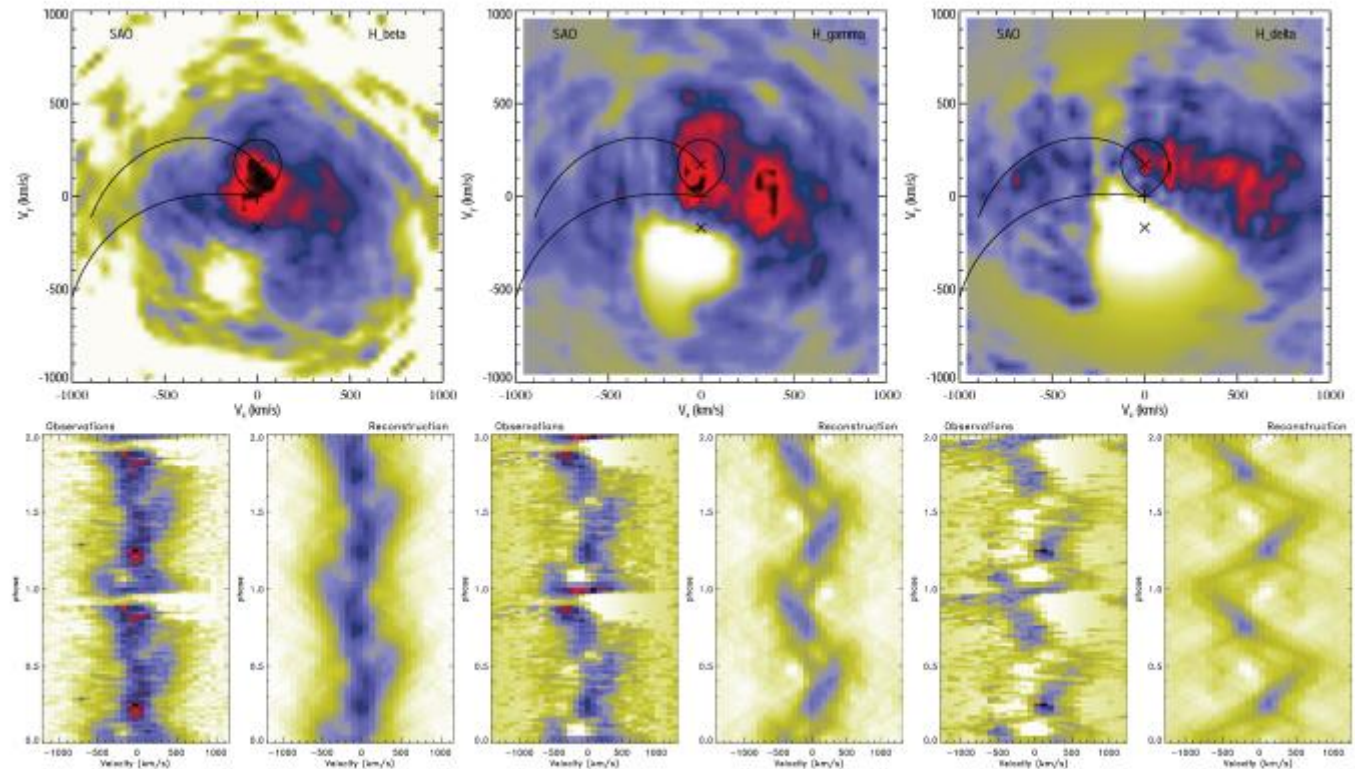
Neustroev & Zharikov.: 2020, A&A, 642, A100

Tomography: Unusual/Unexpected structures (1)

276

Dark spot:

Disk
overflow?



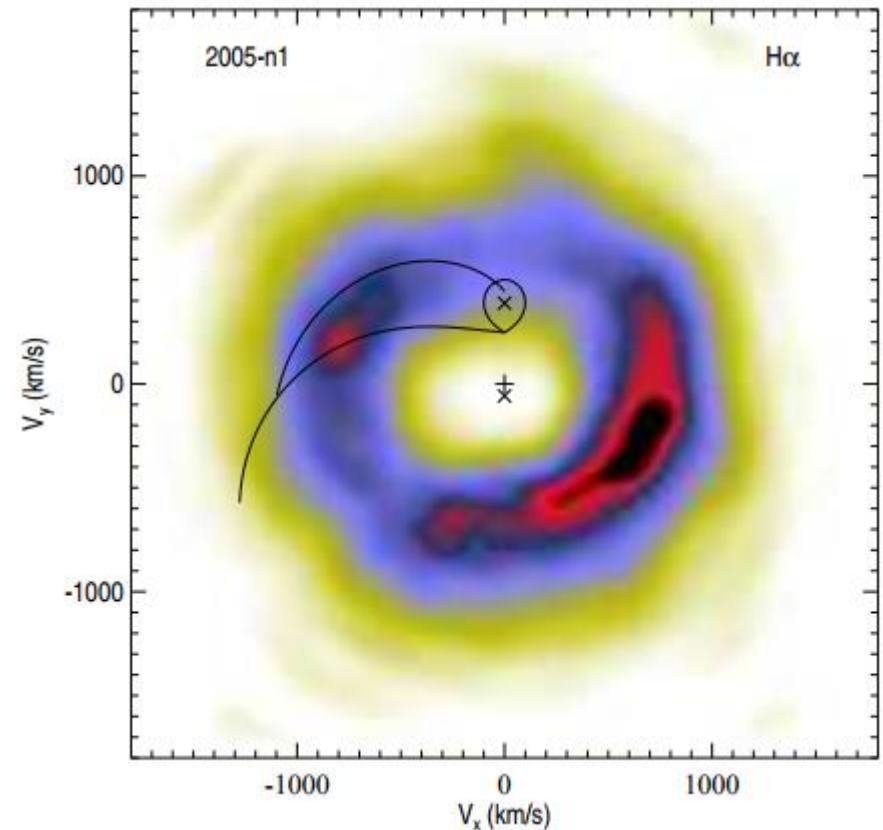
UX Uma:

Tomography:

Unusual/Unexpected structures (2)

277

HT Cas:
Bright spot on
the opposite side of
the disk



Neustroev et al.: 2016, A&A, 586, A10

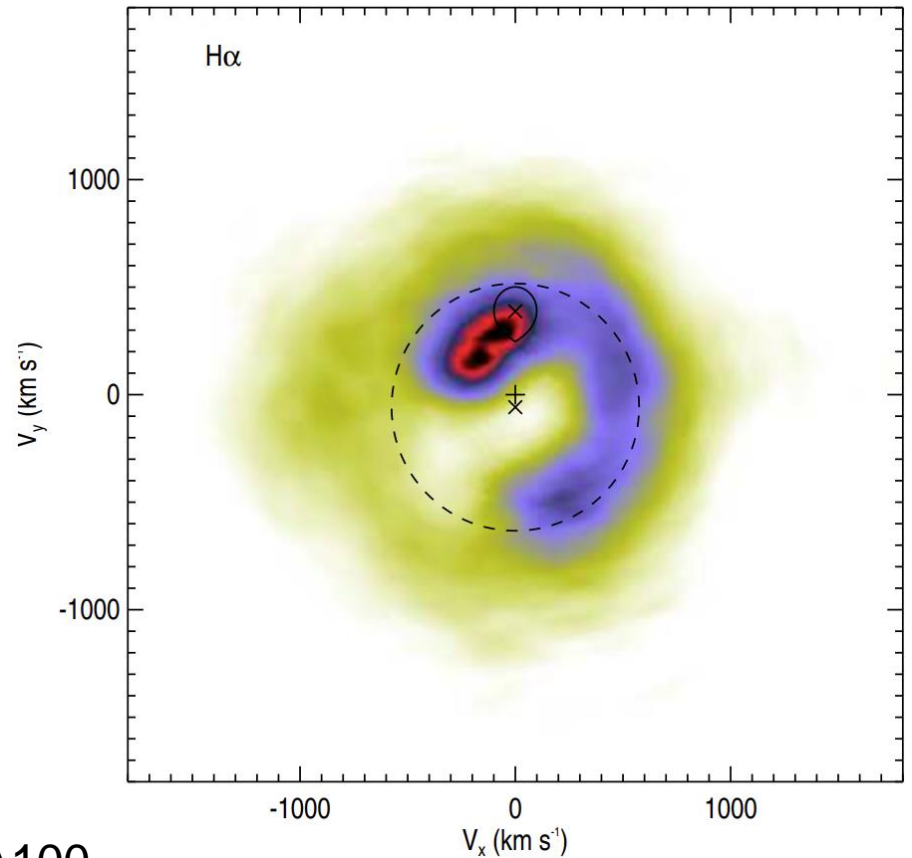
Interacting Binary Stars

Tomography:

Unusual/Unexpected structures (3)

278

HT Cas:
a horseshoe structure
during
the superoutburst



Neustroev & Zharikov.: 2020, A&A, 642, A100

Interacting Binary Stars

Single Peaked Lines?

279

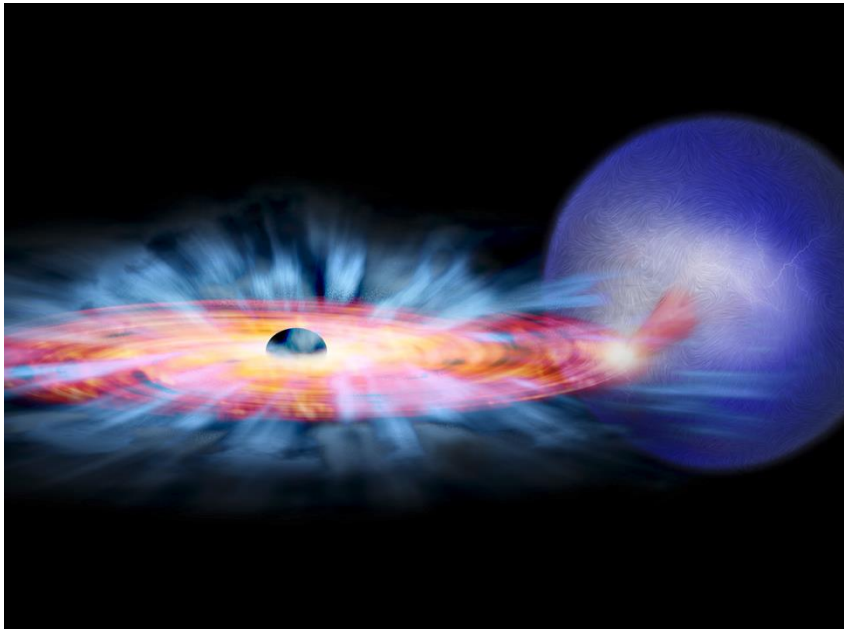
- Why do the lines change from double-peaked to single-peaked during outburst?
- Why some eclipsing NLs show single-peaked profiles?
- Do single-peaked lines still come from the disk?

“The answer is blowin’ in the wind”
— Dylan, B.1962, *Special Rider Music*

How do we know there are outflows?

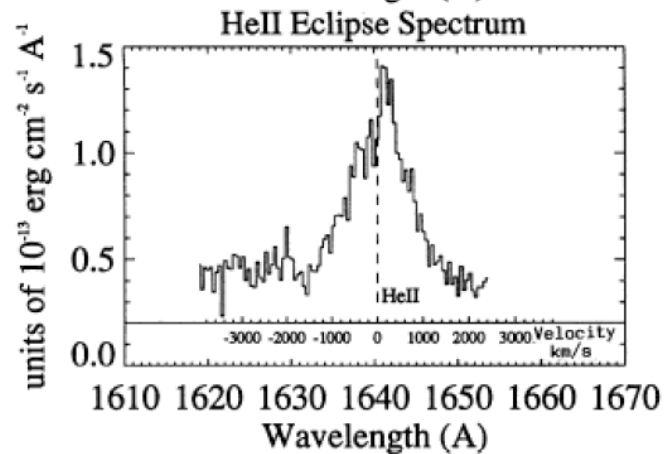
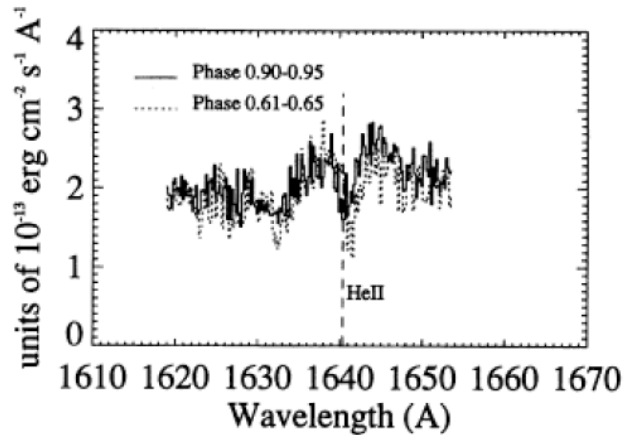
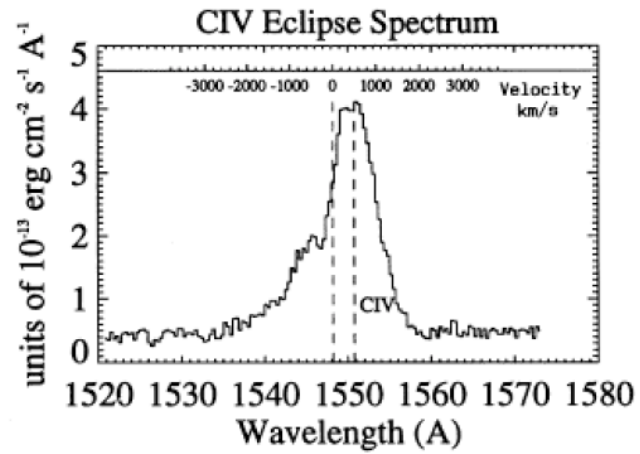
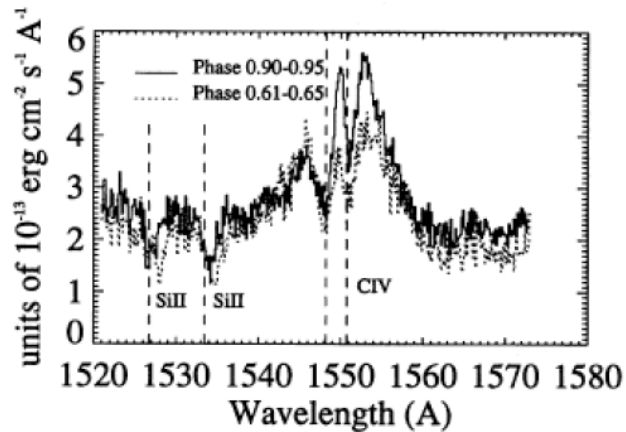
280

- Blueshifted absorption lines in the UV spectra of CVs (P-Cygni profiles)
- Residual flux during eclipse (vertically extended gas)



The Wind of UX UMa

281



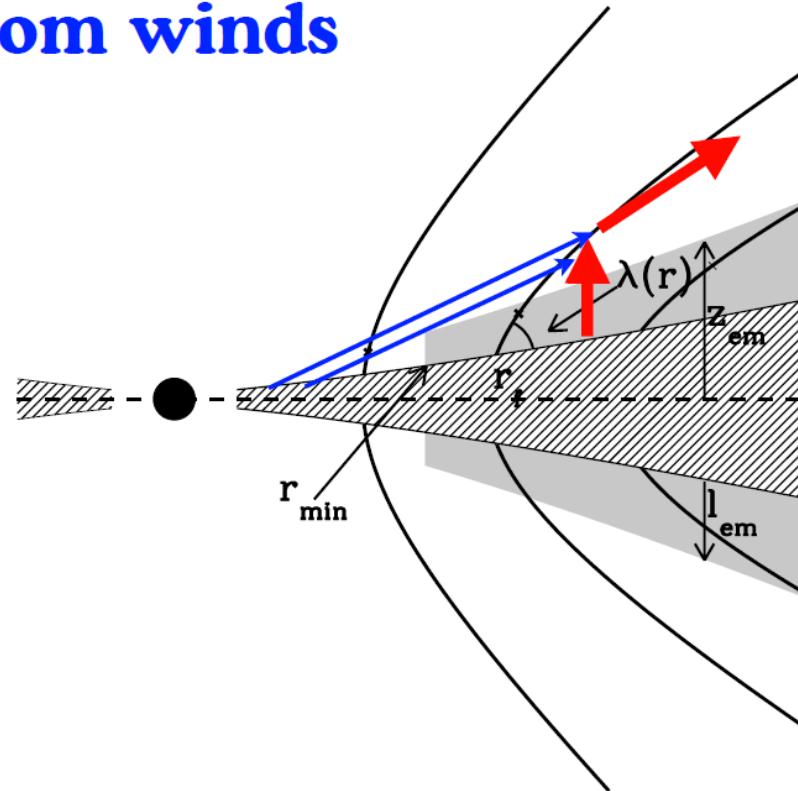
figures from Mason et al. 1995, MNRAS, 274, 271

The Wind

282

Emission lines from winds

- ◆ Dense layer at the base emits the lines.
- ◆ Powered by photoionization
- ◆ $v_r \ll v_\phi$
but
 $dv_r/dr \gg dv_\phi/dr$



from Murray et al. 1995,
ApJ, 451, 498

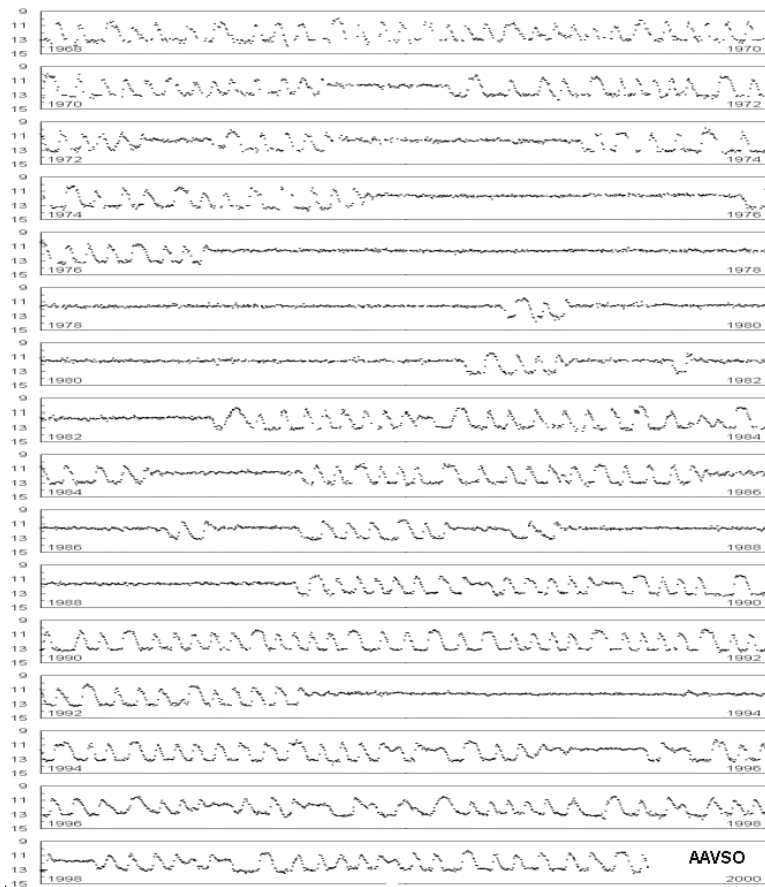
283

Dwarf Nova Outbursts

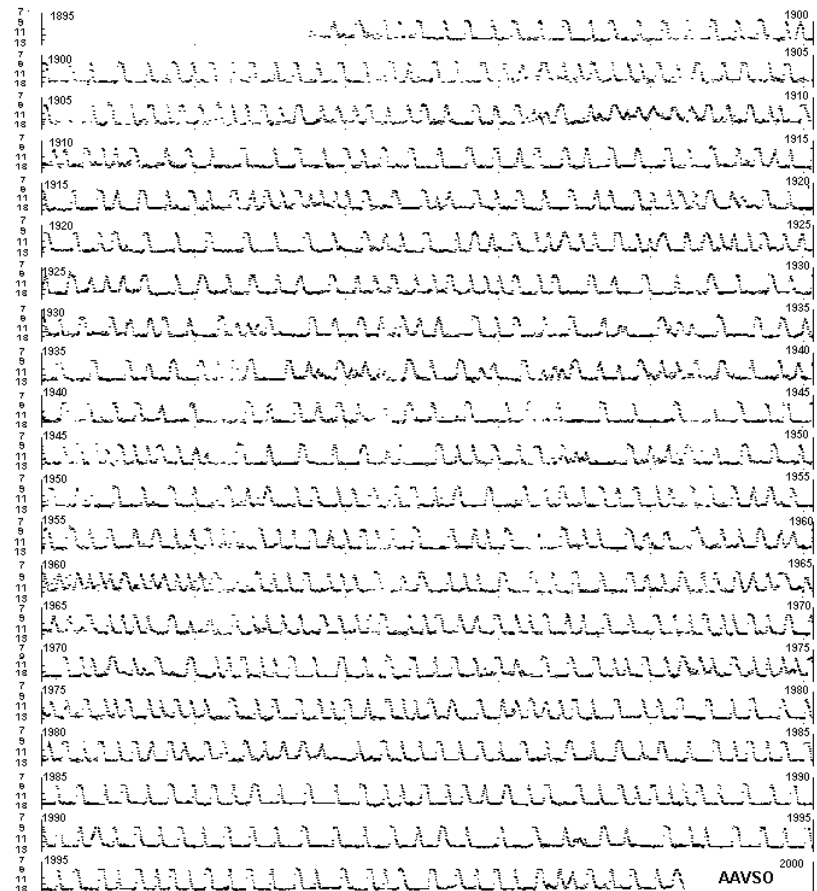
Dwarf Nova Outbursts

284

Z Camelopardalis

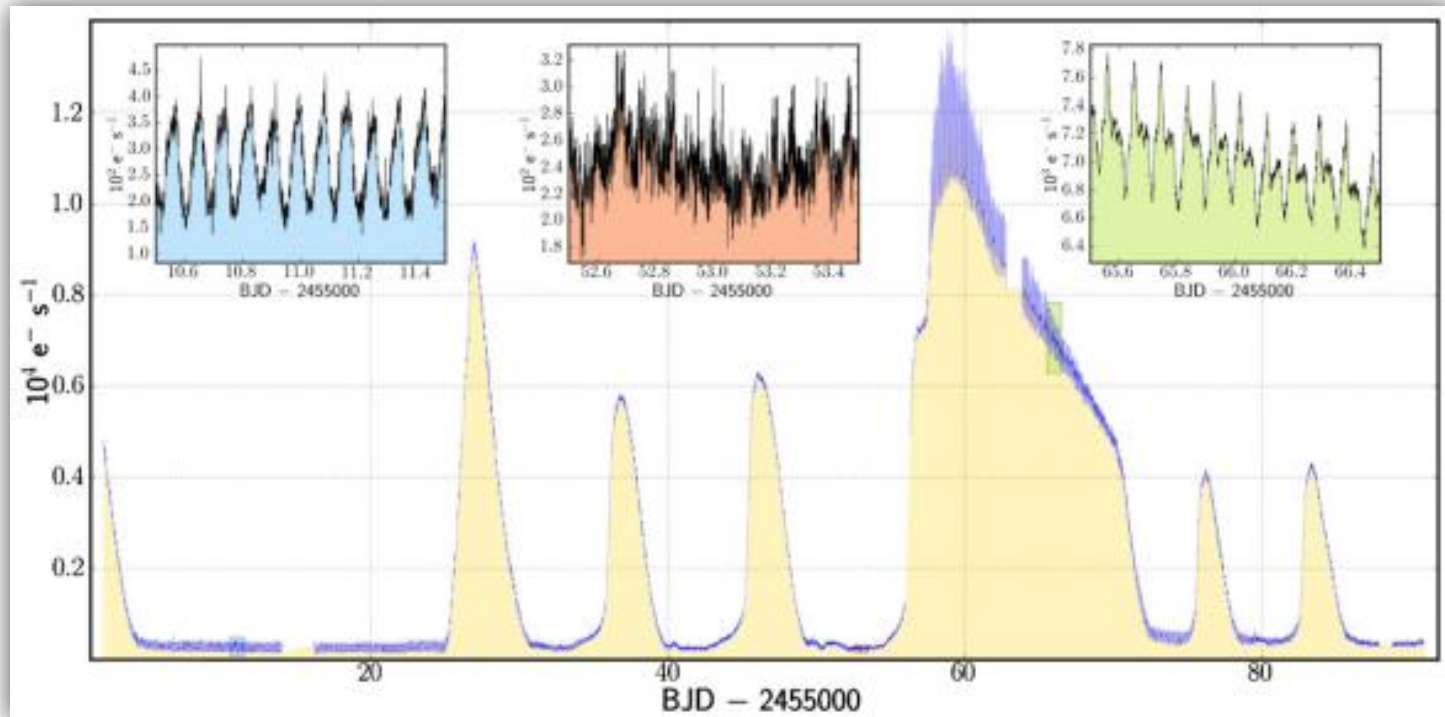


SS Cygni



Dwarf Nova Superoutbursts

285

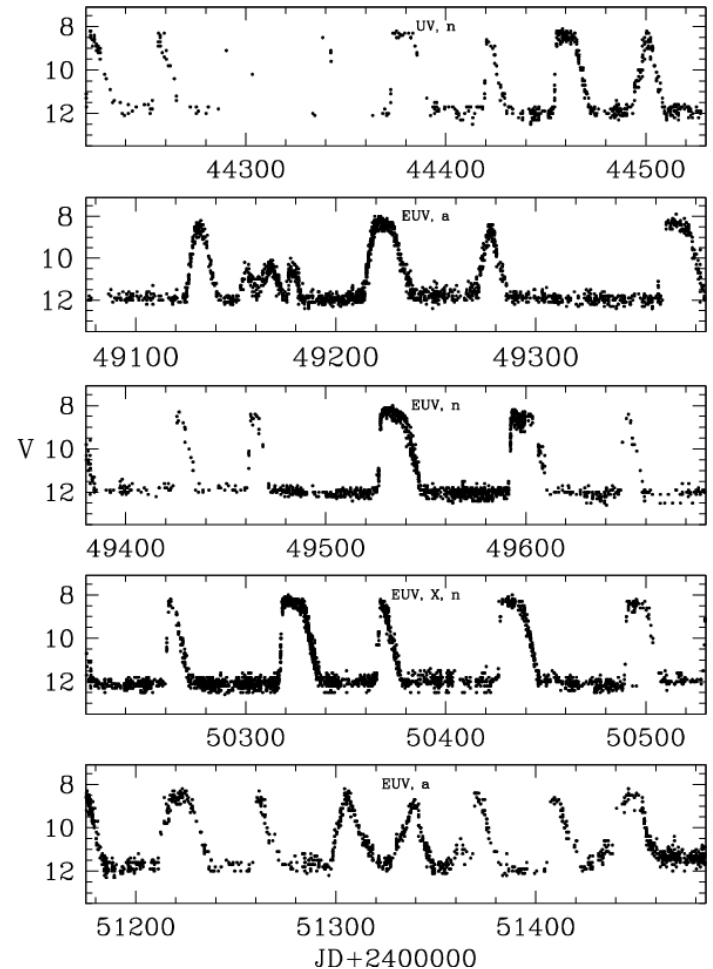
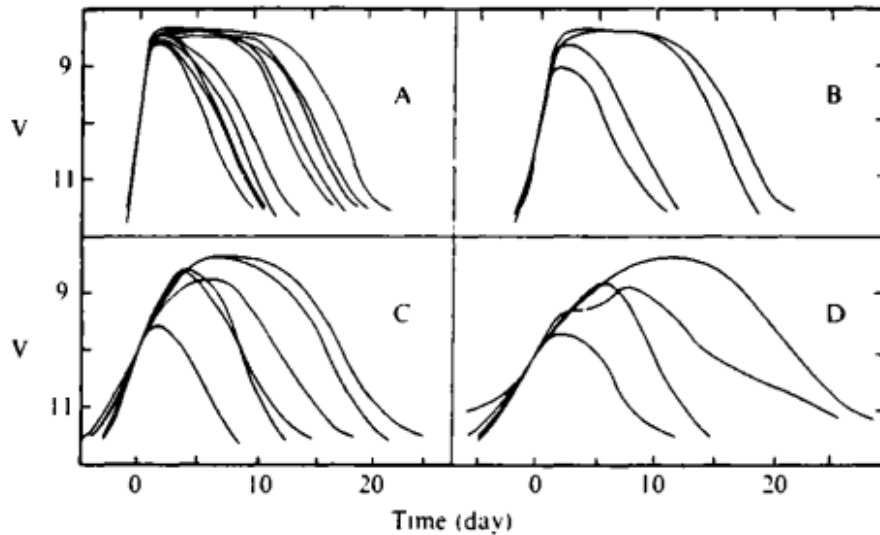


Kepler light curve of V344 Lyrae showing several normal outbursts and one superoutburst (from Still et al. 2010).

DN Outbursts: Properties and Correlations (1)

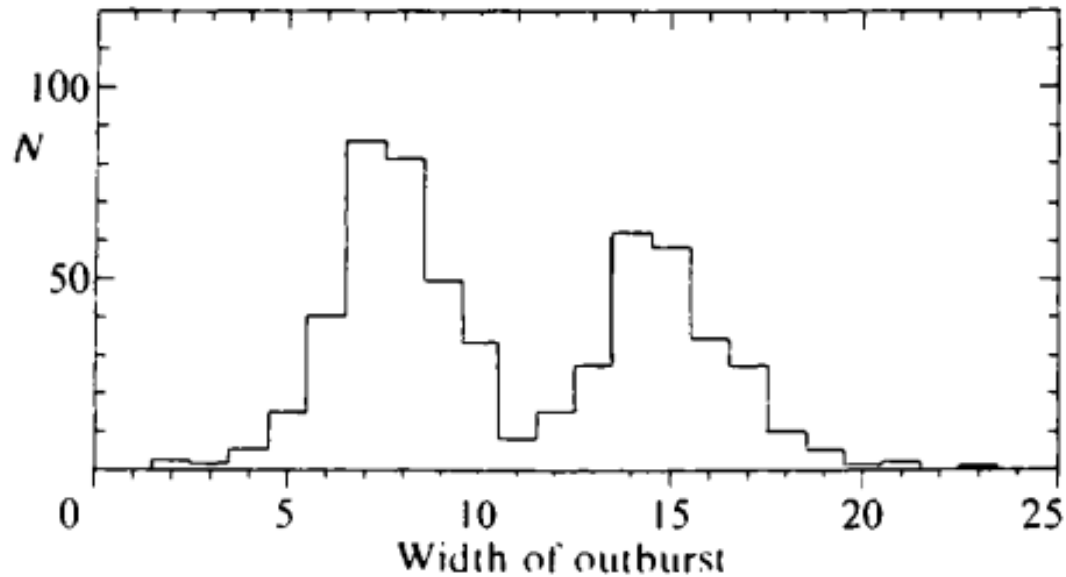
286

□ Outbursts of SS Cyg: Short, Long, and Slow-Rise



DN Outbursts: Properties and Correlations (2)

287

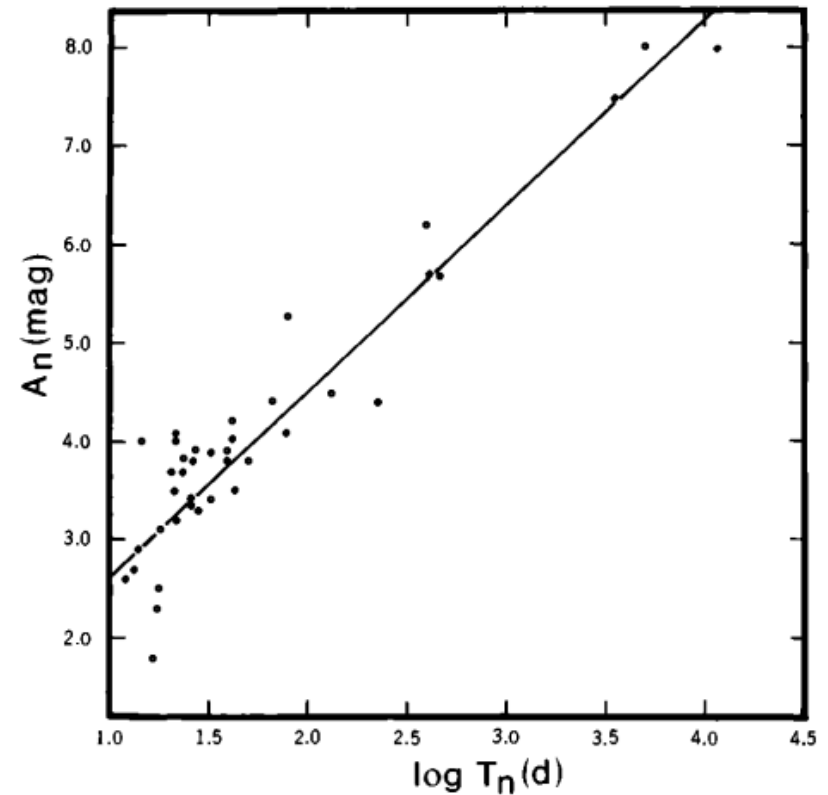


Bimodal distribution of outburst widths of SS Cyg.
From Bath & van Paradijs (1983).

DN Outbursts: Properties and Correlations (3)

288

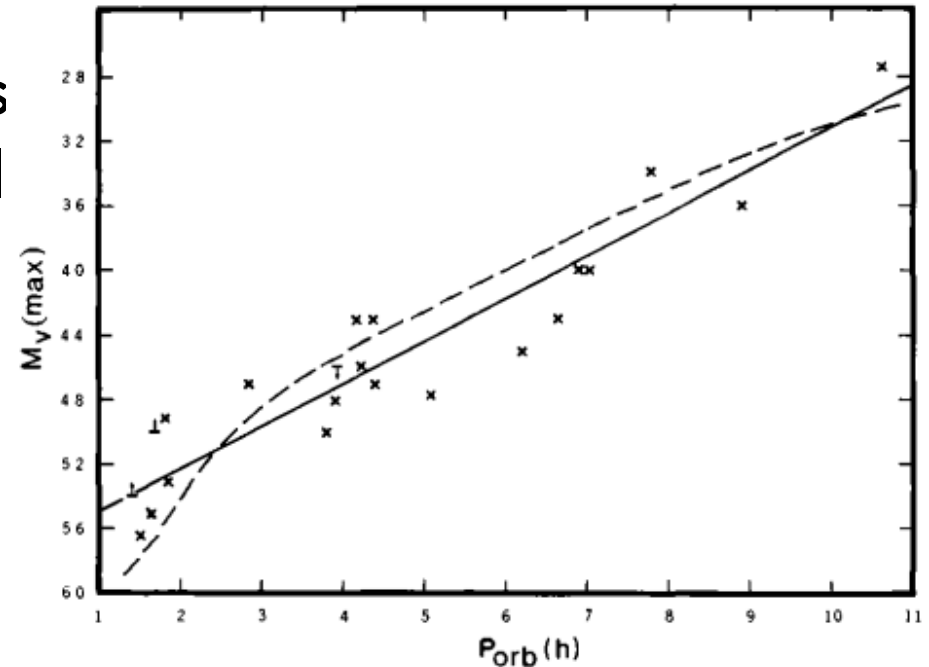
- Corrected outburst amplitude versus outburst interval for dwarf novae.



DN Outbursts: Properties and Correlations (4)

289

- Absolute visual magnitude of DN disks at maximum of normal outbursts - orbital period relation.
- The solid line represents equation



$$M_V(\max) = 5.74 - 0.259P_{orb}(h) \quad P_{orb} \lesssim 15 \text{ h.}$$

(Warner 1987)

DN Outbursts: Properties and Correlations (5)

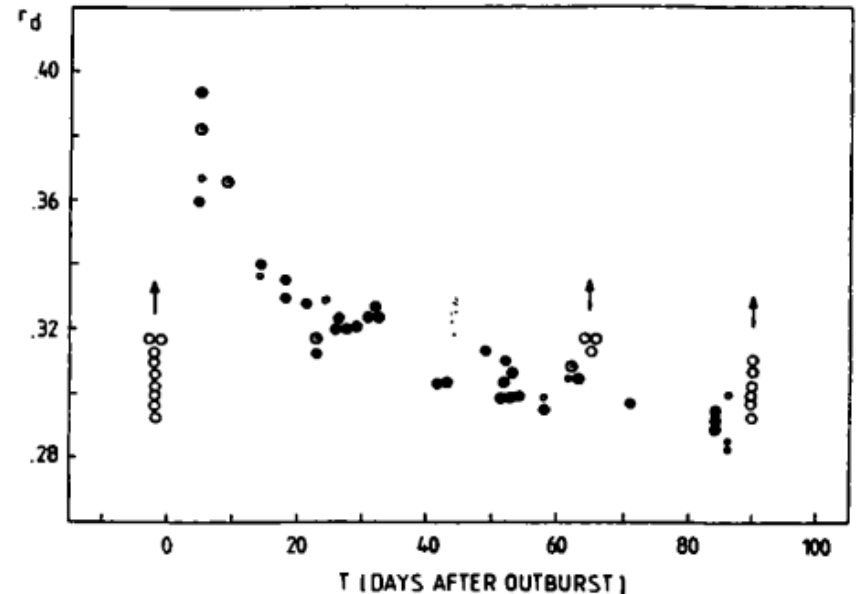
290

- Variation of disk radius r_d in U Gem, as a function of days after outburst.

r_d is in units of the orbital separation a .

- **Warning!**

r_d is measured from the position of the hot spot.

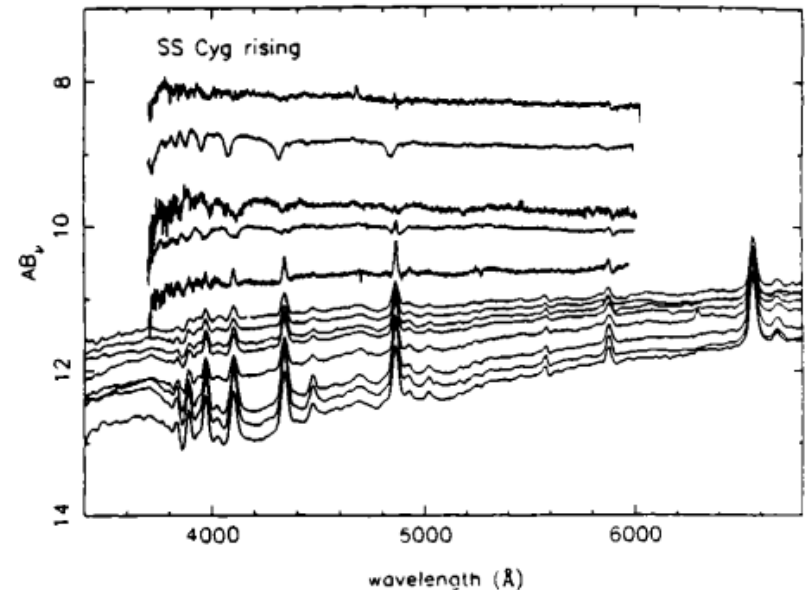


DN Outbursts: Properties and Correlations (6)

291

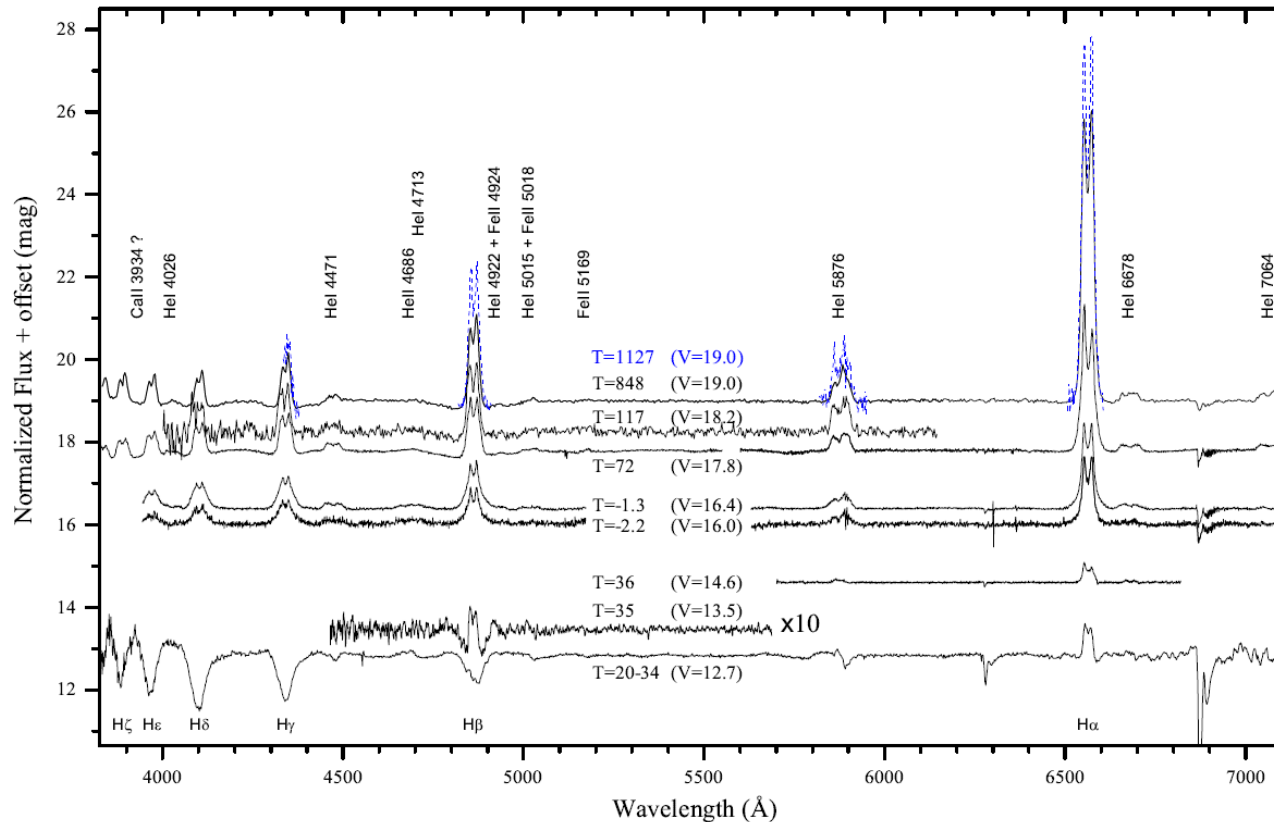
- Spectral changes in SS Cyg from quiescence (lowest spectrum) to maximum of outburst (uppermost spectrum).

(From Horne 1991).



DN Outbursts: Properties and Correlations (7)

292

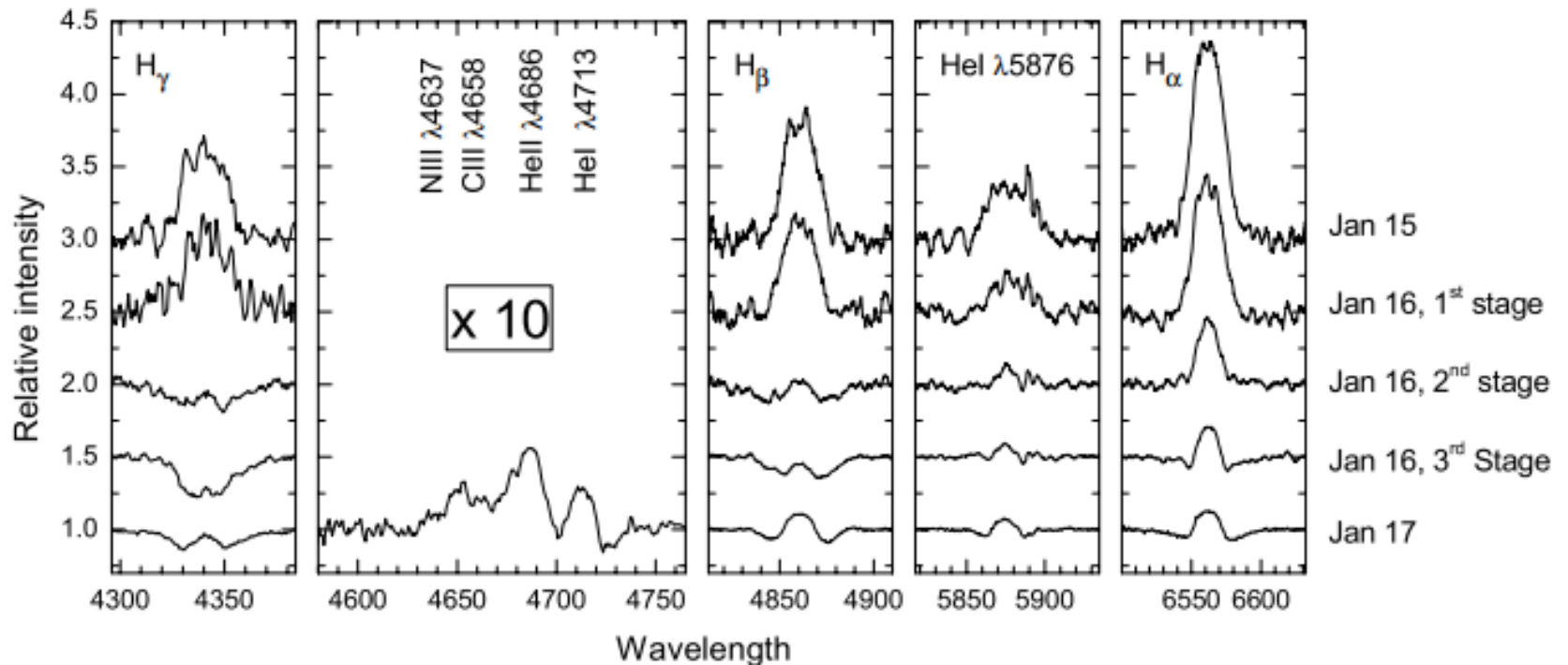


Spectral changes in SSS122222 from quiescence (uppermost spectrum) to maximum of superoutburst (lowest spectrum).
(From Neustroev 2017).

DN Outbursts: Properties and Correlations (8)

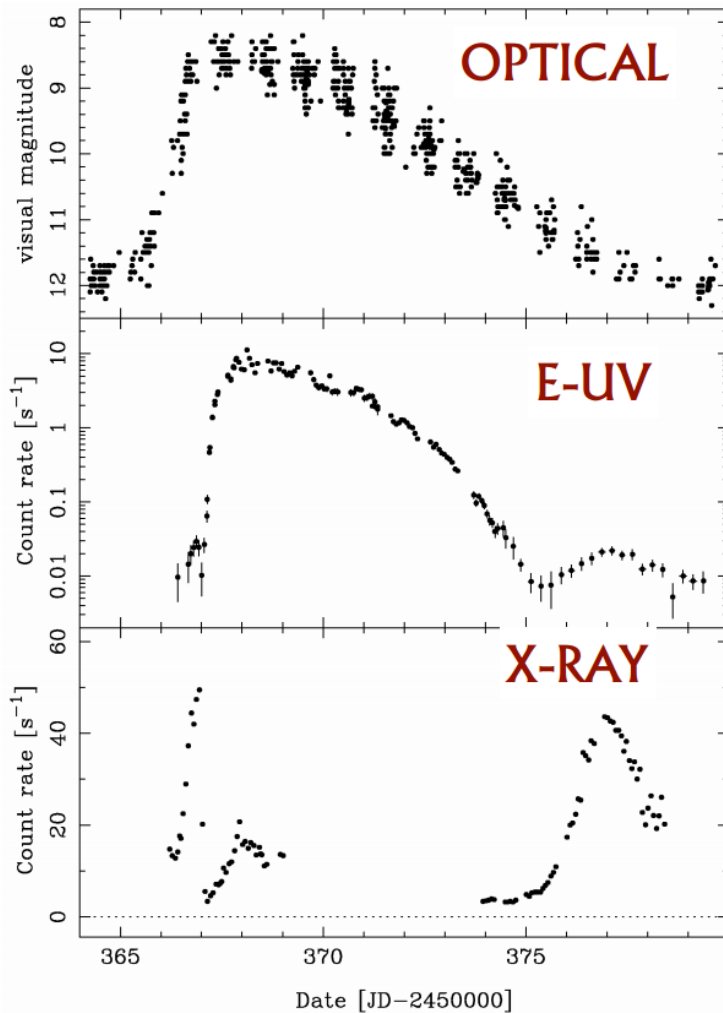
293

BZ Uma from the quiescent to outburst state (Neustroev et al., 2005)



DN Outbursts: Properties and Correlations (9)

294



- Observations of SS Cyg through a dwarf nova outburst
- Change in density of boundary layer
opt. thin \leftrightarrow opt. thick

(from Wheatley et al. 2003)

Dwarf Nova Outbursts (1)

295

- **Two models were proposed in the 1970s:**
 1. The mass-transfer instability model (MTI model)
→ Bath (1973).

The mass-transfer rate from the secondary star is thought to be unstable and the mass-accretion rate onto the white dwarf is variable accordingly.

Dwarf Nova Outbursts (2)

296

- **Two models were proposed in the 1970s:**
 2. The disk-instability model (DI model)
→ Osaki (1974).

The mass-transfer rate from the secondary star is thought to be constant but the alternation of outburst/quiescence is caused by (some unknown at that time) instabilities within accretion disks; mass is stored within the disk during quiescence and, when it reaches some critical amount, it is suddenly accreted onto the white dwarf due to some instability, which explains an outburst.

Dwarf Nova Outbursts (3)

297

- The models fiercely competed in the 1970s.
- However, a very promising instability mechanism in accretion disks was discovered around 1980.
- On the other hand, there are several reasons to be dissatisfied with the MTI model.

Now the MTI model is out of favour

Dwarf Nova Outbursts (4)

298

- There are several reasons to be dissatisfied with the MTI model:
 - ▣ There is the fact that no high mass-transfer rate systems show DN outbursts.
 - ▣ There is no evidence from bright spot luminosities for increased mass-transfer rate during or before outbursts.
 - ▣ Polars do not have disks, and do not show DN outbursts.

Dwarf Nova Outbursts (5)

299

- A thermal instability of accretion disks based on the **bi-stable** nature of accretion disks with the disk temperature around 10^4 K where the hydrogen changes from an ionized state to a neutral state, and it is called the "thermal instability" or the "thermal limit cycle instability."
- The DI model is now widely accepted by both theoreticians and observers

Thermal limit cycle instability (1)

300

- The key property is viscosity.
- An accretion disk acts as a mass transfer channel between the mass-losing star and the white dwarf.
- The rate of mass flow through the disk, \dot{M}_d , is set by the viscosity, and will in general not be equal to the rate of mass transfer from the secondary, \dot{M} .
- If $\dot{M}_d < \dot{M}$, then mass will build up in the disk.
- If $\dot{M}_d > \dot{M}$ mass will drain out of the disk.

Thermal limit cycle instability (2)

301

- From calculations of the vertical structure of the accretion disk we can obtain the surface density Σ for given radius r and \dot{M}_d (or equivalently averaged viscosity $\Sigma\bar{\nu}$ or T_{eff}).
- The vertical structure of accretion disks depends on whether energy transport is largely by radiation or largely by convection, and at temperatures around 10^4 K two solutions are possible – a convective solution with a low mass flow rate and a radiative solution with a high mass flow rate.

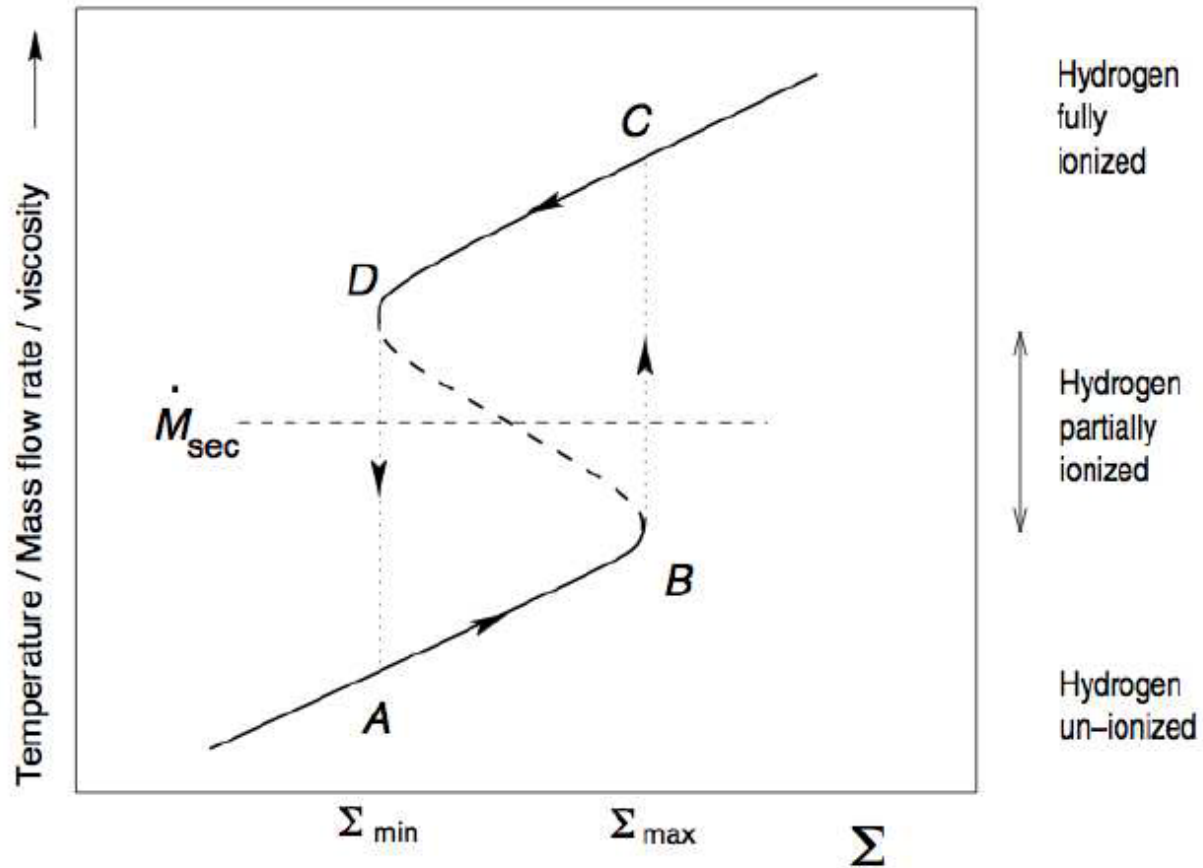
Thermal limit cycle instability (3)

302

- In the range of temperatures at which hydrogen **recombines**, the resulting dramatic reduction of opacities makes the disk thermally and viscously **unstable**:
a surface density – (averaged) viscosity relation $\Sigma - \Sigma \bar{\nu}$ is double-valued for a range of density.
- At a given radius, the disk thermal equilibria form an S – shaped curve, the middle branch of which represents unstable solutions.

Thermal limit cycle instability (4)

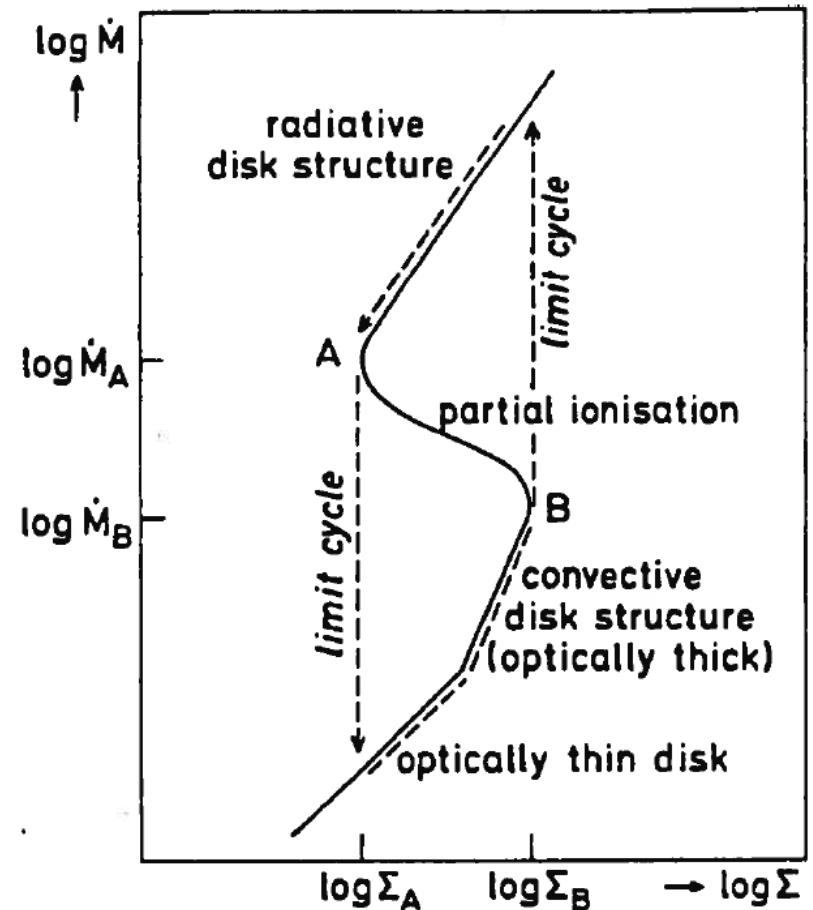
303



Thermal limit cycle instability (5)

304

- Outburst triggers at small R (inside-out front propagation) / large R (outside-in) for small / large \dot{M}_d
- Heating wave switches disk to outburst state
- Cooling wave switches disk to quiescent state



Thermal limit cycle instability (6)

305

Outburst properties:

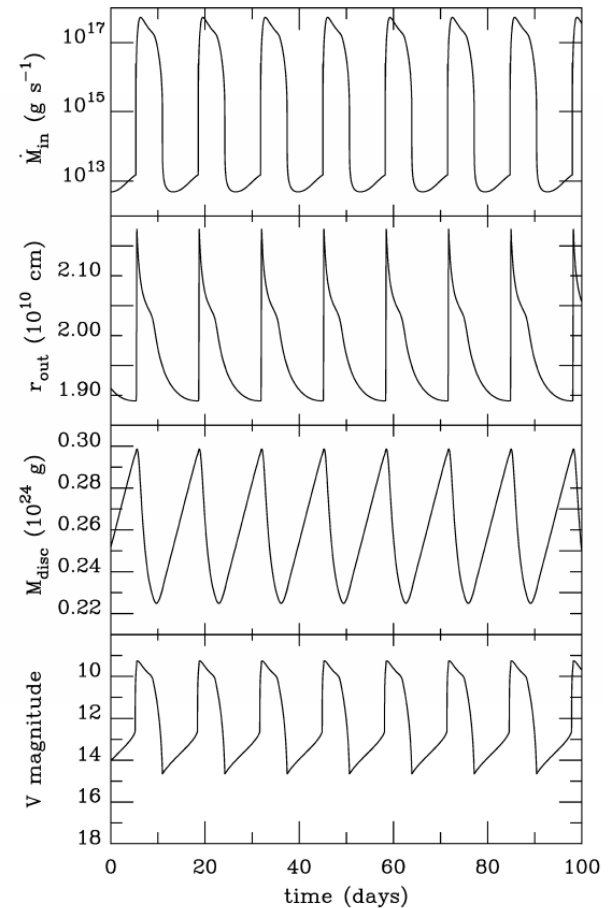
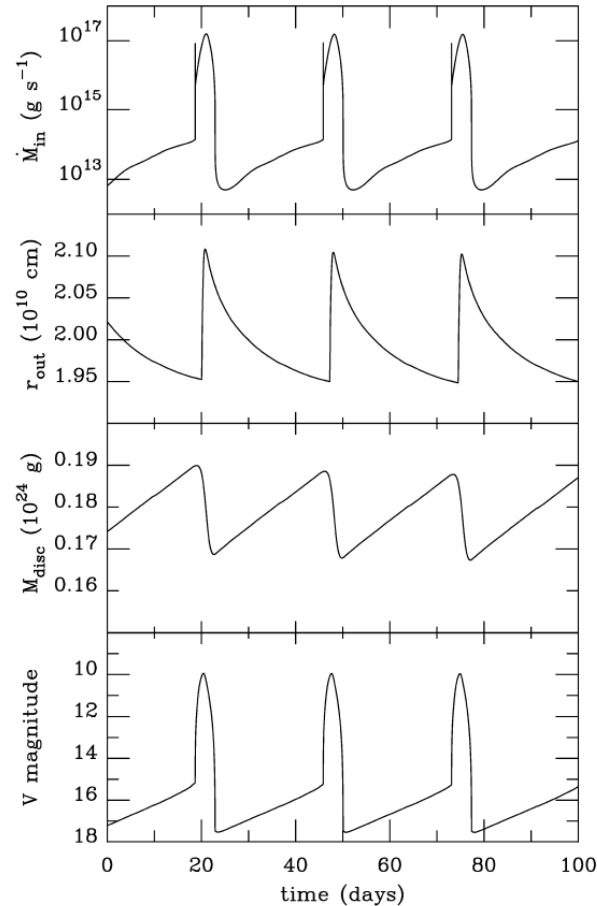
$$M_1 = 0.6 M_{\text{sun}}$$

$$\alpha_{\text{cold}} = 0.04, \alpha_{\text{hot}} = 0.20$$

$$\dot{M} = 10^{16} \text{ g/s (left)}$$

$$\dot{M} = 10^{17} \text{ g/s (right)}$$

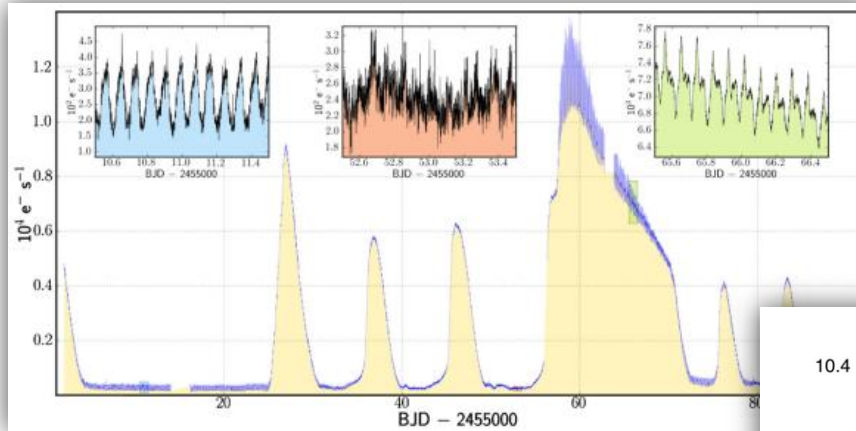
(Hameury et al.,
1998).



Interacting Binary Stars

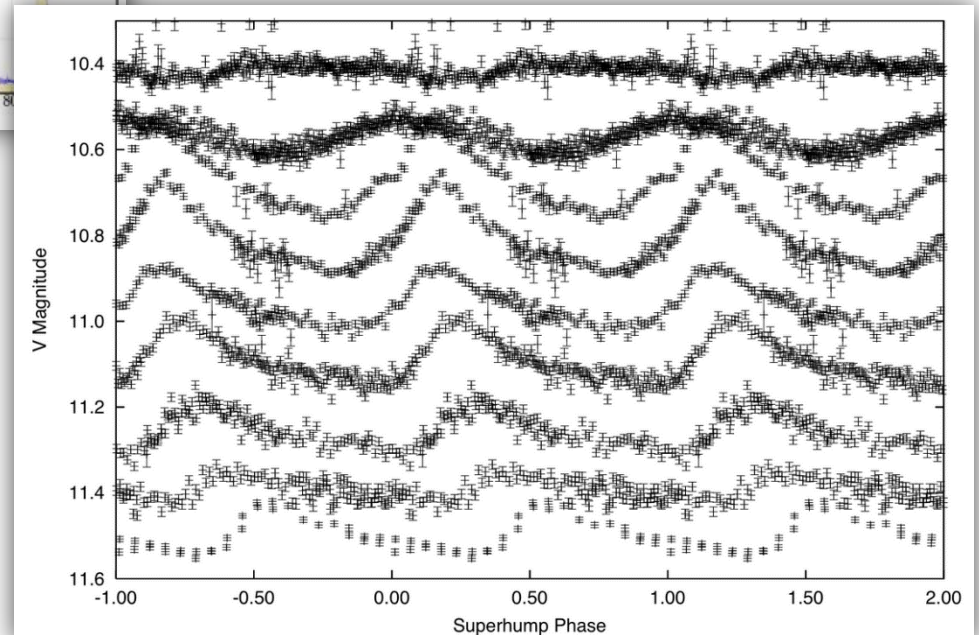
Superoutbursts and Superhumps (1)

306



The duration of a superoutburst is several times longer than those of normal outbursts. The maximal brightness is about 1 mag brighter than those of normal outbursts.

Superhumps resembles in shape orbital humps in quiescence, but have a much larger (~ 100 times) luminosity (a few tenths of magnitude during superoutbursts). The period of light variation is a few per cent longer than the orbital period.



Interacting Binary Stars

Superoutbursts and Superhumps (2)

307

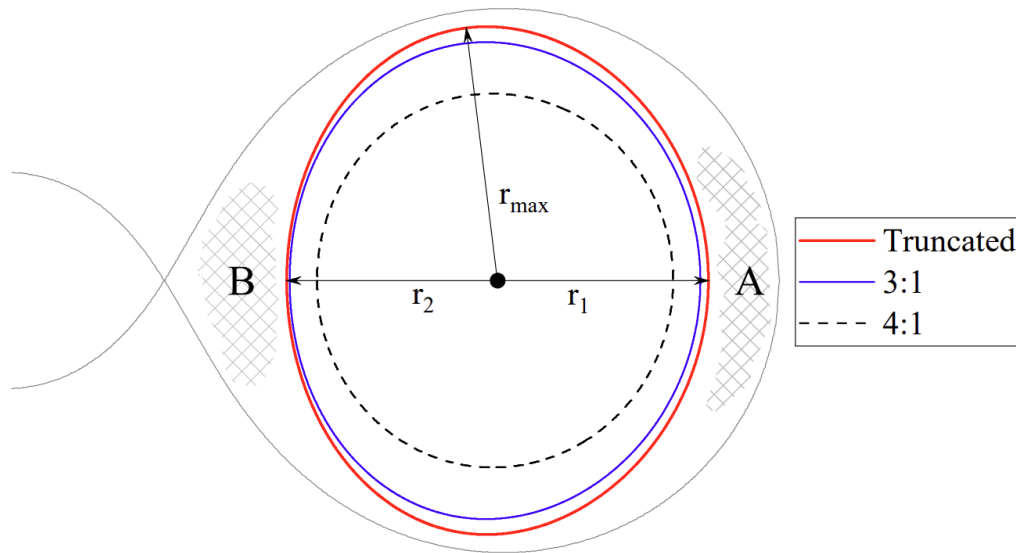
- Mass is transported inwards through a disk, so angular momentum must be transported outwards.
- So what happens to the angular momentum at the outer edge?



Superoutbursts and Superhumps (3)

308

- For disks that approach R_{L1} in radius the outer parts will be significantly distorted by the gravitational influence of the secondary star. Tidal interaction with the secondary keeps the disk from overflowing the Roche lobe.



Superoutbursts and Superhumps (4)

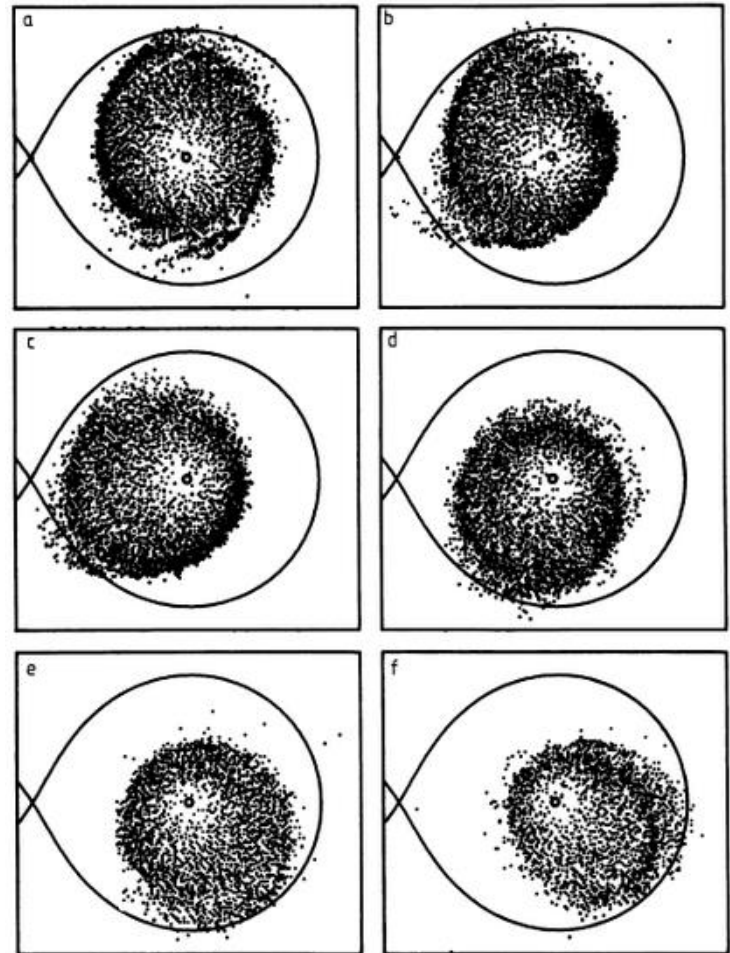
309

- The outburst does not leave the disk in exactly the same state as it was at the beginning of the outburst cycle:
not all the material stored in the disk has been lost to the white dwarf, so the disk is slightly more massive and **larger** at the beginning of the next cycle.
- The disk radius **grows** slowly from one cycle to the next, until the disk is large enough for tidal forces from the secondary to start distorting it.
- The disk becomes tidally unstable to a 3:1 resonance, in which the particle orbits have frequency $\Omega = 3\Omega_{\text{orb}}$
- **The relevance of the above idea about the growing disk is questionable! See Neustroev & Zharikov (2020) for a discussion.**

Superoutbursts and Superhumps (5)

310

- The resonant radius is within the disk if the mass ratio $q < 0.33$.
- The disk becomes elliptical, and its long axis precesses.
- Each snapshot is precisely 3 orbital period apart (Whitehurst 1988)



Superoutbursts and Superhumps (6)

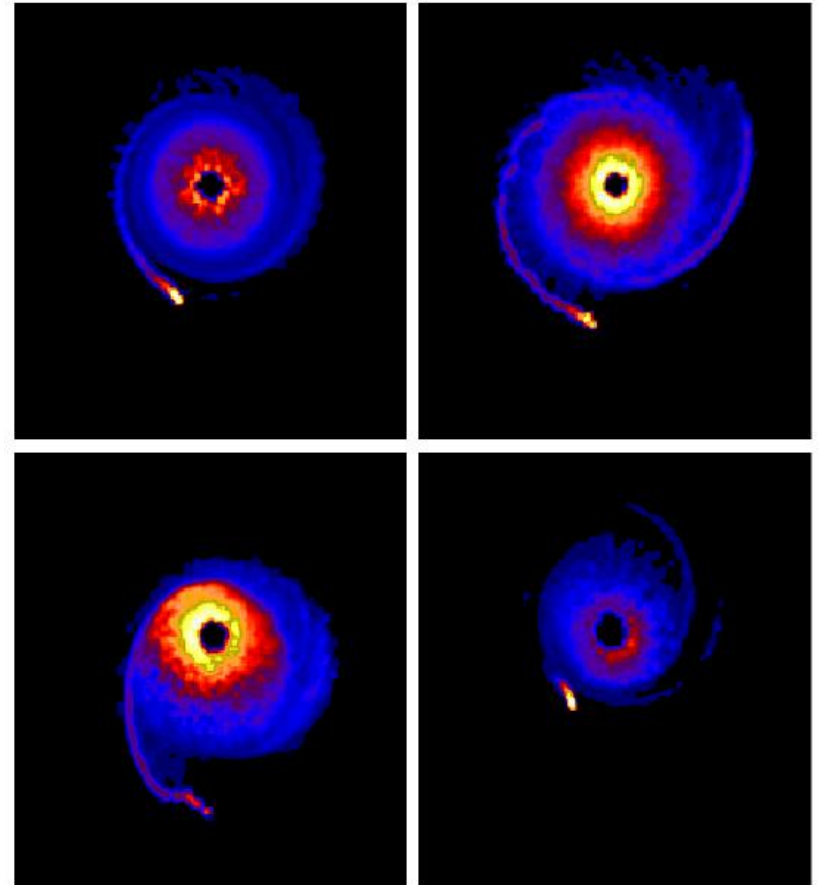
311

- Osaki (1989) proposed that the superoutburst phenomenon of SU UMa stars may be explained by the basic framework of the DI model in which the two intrinsic instabilities within accretion disks (i.e., the thermal and the tidal instabilities) are properly combined, and this DI model for SU UMa stars is called the "thermal-tidal instability" model.

Superoutbursts and Superhumps (7)

312

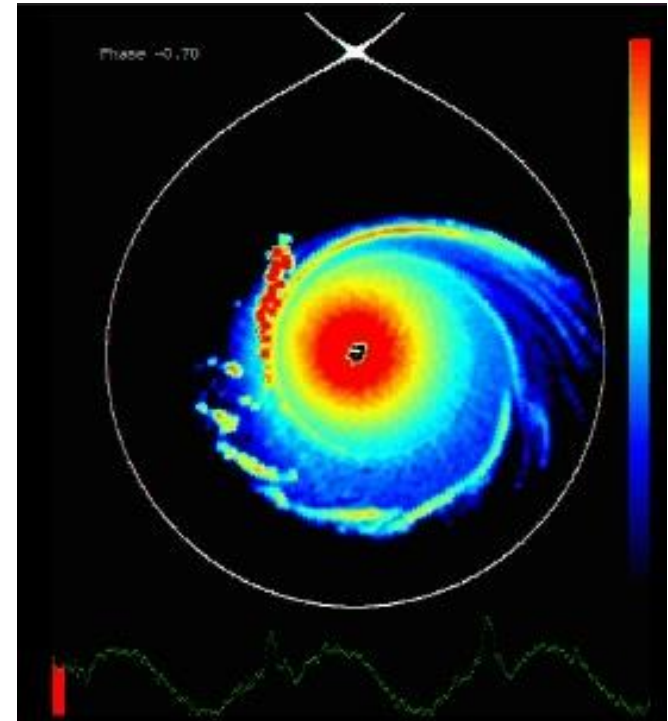
- Outburst starts in normal way;
- Disk expands past 3:1 radius;
- Eccentricity: superhumps appear;
- Enhanced tidal heating drives more gas in and prolongs the outburst.



Superhumps: Video (1)

313

- 2D accretion disk surface dissipation animation using a logarithmic colour scale. The secondary rotates anti-clockwise with respect to the inertial binary frame. The curve at the bottom of the movie shows the simulated dissipation light curve.

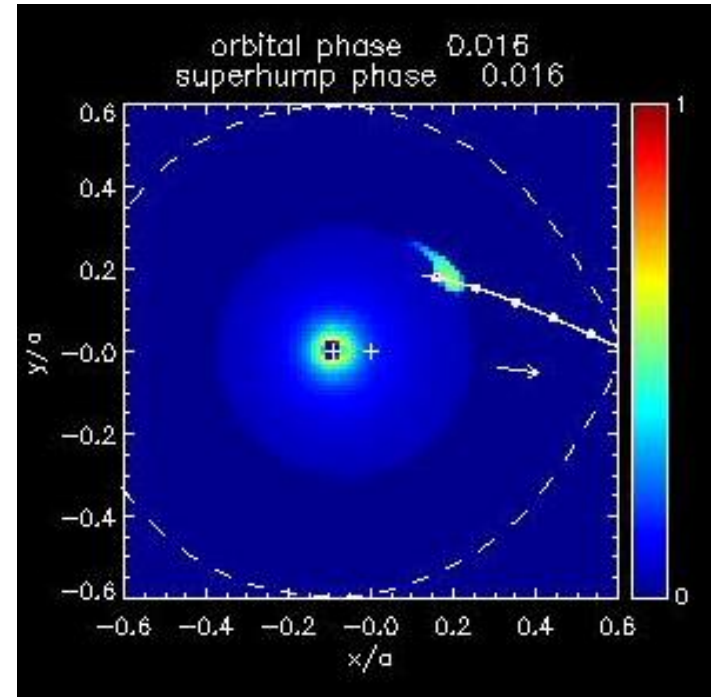


Simulation & visualisation by Steve Foulkes et al. The Open University.
<http://www.physics.open.ac.uk/FHMR/dudt.html> (dudt.avi)

Superhumps: Video (2)

314

- 3D analytical accretion disk surface dissipation animation using a linear colour scale. The secondary rotates anticlockwise with respect to the inertial binary frame. The arrow indicates a fixed direction to an observer.

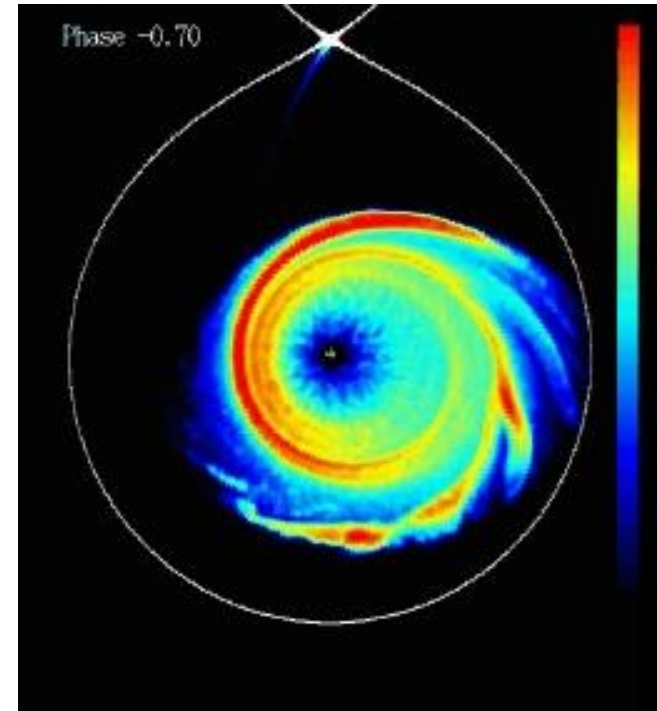


Simulation & visualisation by Steve Foulkes et al. The Open University.
<http://www.physics.open.ac.uk/FHMR/analytical.html> (dan7.avi)

Superhumps: Video (3)

315

- 2D accretion disk surface density animation using a logarithmic colour scale. The secondary rotates anticlockwise with respect to the inertial binary frame.

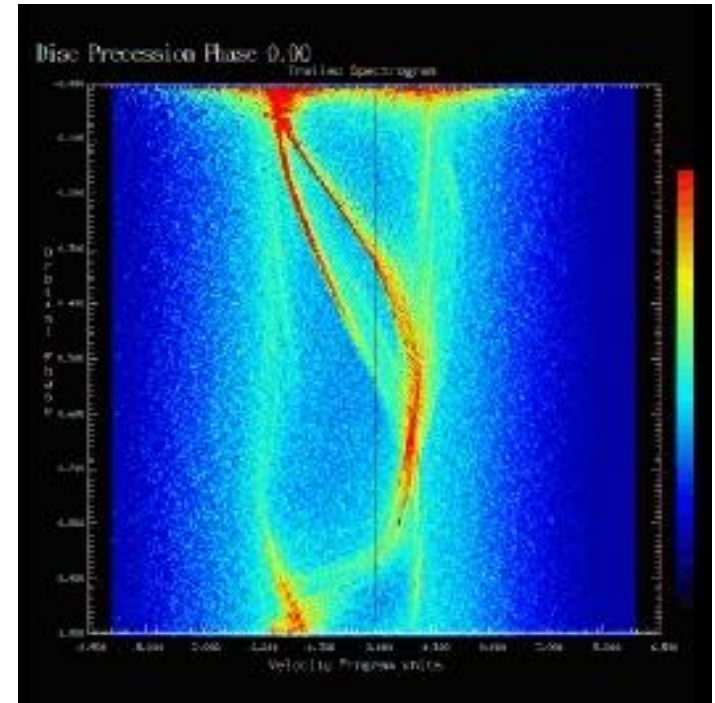


Simulation & visualisation by Steve Foulkes et al. The Open University.
<http://www.physics.open.ac.uk/FHMR/density.html> (dens1.avi)

Superhumps: Video (4)

316

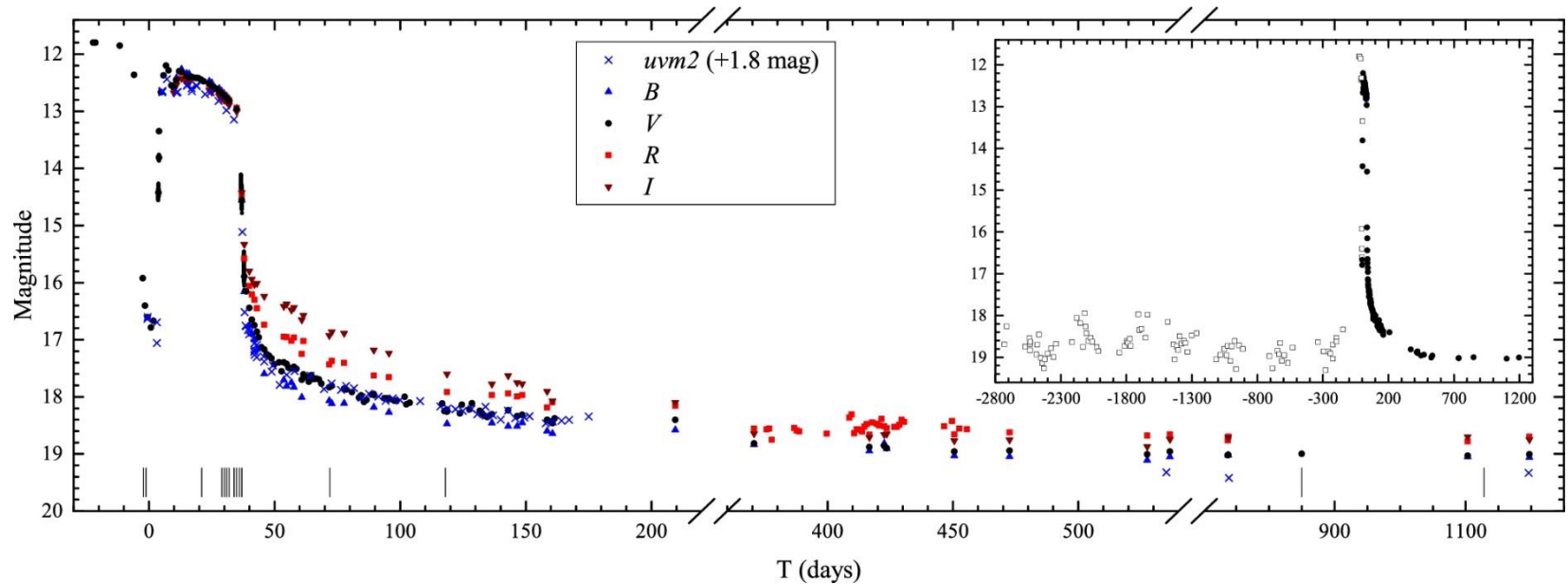
- Trailed spectrogram animation for two complete disk precessions from a SPH simulation. The spectrograms use a linear colour scale and the number in the upper left-hand corner indicates the disk precession phase.



Simulation & visualisation by Steve Foulkes et al. The Open University.
<http://www.physics.open.ac.uk/FHMR/spectra.html> (spectrogram.avi)

Superoutbursts of WZ Sge-type stars: unexplained features (1)

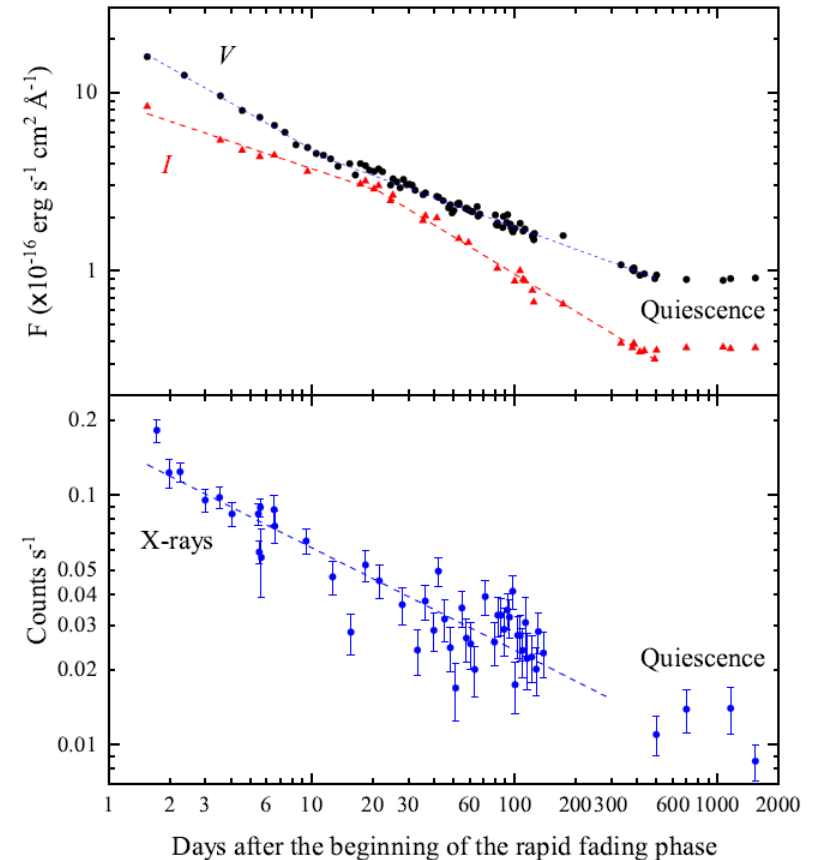
317



Superoutbursts of WZ Sge-type stars: unexplained features (2)

318

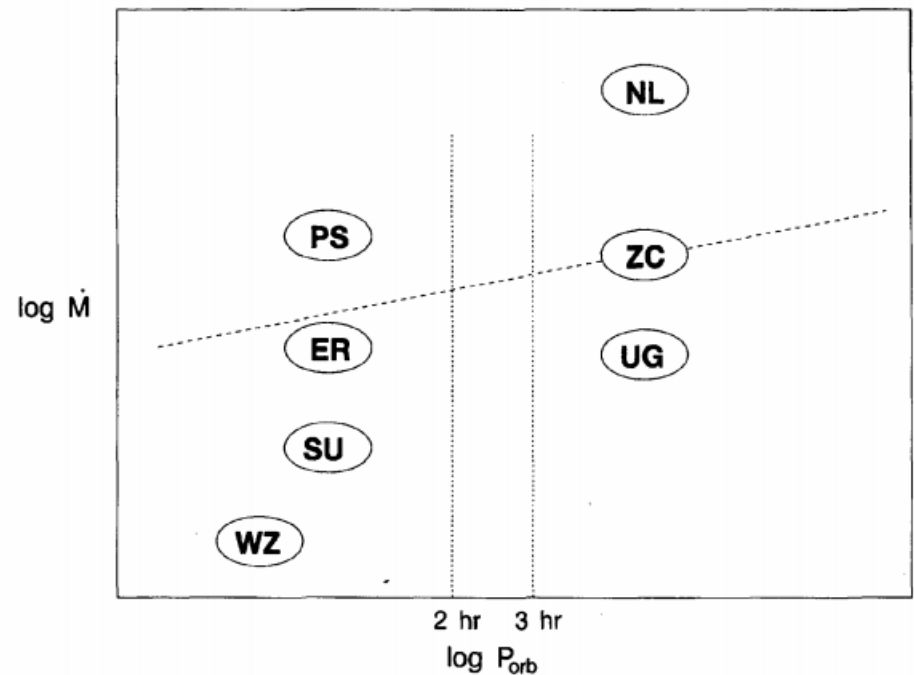
- A very extended optical and X-ray decline



Outbursts in CVs

319

- $P_{orb}-\dot{M}$ diagram showing different outburst behaviours of non-magnetic CVs.



320

The Evolution of CVs

Consequences of mass transfer (1)

321

- **Do the stars in a binary get closer or move further apart as a result of mass transfer?**
 - If separation declines - Roche lobes get smaller, so more mass transfer will occur. Normally this is unstable.
 - If separation increases - Roche lobes expand. This can allow stable mass transfer if there is some mechanism to allow the stars to slowly spiral together.

- **Binary angular momentum:** $J = (M_1 a_1^2 + M_2 a_2^2) \Omega$

$$a_1 = \frac{M_2}{M} a, \quad a_2 = \frac{M_1}{M} a, \quad \Omega = \sqrt{\frac{G(M_1 + M_2)}{a^3}}$$


Consequences of mass transfer (2)

322

- Substitute for a_1 , a_2 and Ω in the expression for the angular momentum of the binary system:

$$J = M_1 M_2 \sqrt{\frac{Ga}{M}}$$

- Differentiate this expression, assuming that **the total mass M of the binary remains constant** (all mass lost by one star is gained by the other):

$$\frac{dJ}{dt} = \dot{M}_1 M_2 \left(\frac{Ga}{M}\right)^{1/2} + \dot{M}_2 M_1 \left(\frac{Ga}{M}\right)^{1/2} + \frac{1}{2} M_1 M_2 \frac{G}{M} \left(\frac{Ga}{M}\right)^{-1/2} \frac{da}{dt}$$


$$\frac{dM_1}{dt}$$

...where the dots denote derivatives with respect to time

Consequences of mass transfer (3)

323

- Divide both sides through by J , and use $\dot{M}_1 + \dot{M}_2 = 0$:

$$\frac{\dot{a}}{a} = 2 \frac{\dot{J}}{J} - 2 \frac{\dot{M}_2}{M_2} \left(1 - \frac{M_2}{M_1} \right)$$

Conservative
mass transfer



- Finally, assume that

no angular momentum is lost from the system: $dJ/dt = 0$:

$$\frac{\dot{a}}{a} = -2 \frac{\dot{M}_2}{M_2} \left(1 - \frac{M_2}{M_1} \right)$$

Consequences of mass transfer (4)

324

$$\frac{\dot{a}}{a} = -2 \frac{\dot{M}_2}{M_2} \left(1 - \frac{M_2}{M_1} \right)$$

- Lets the secondary is losing mass, $\dot{M}_2 < 0$:
 - If $M_2 > M_1$: **Binary shrinks**, tends to lead to runaway mass flow from the more massive star onto the less massive
 - If $M_2 < M_1$: **Binary expands**, mass transfer from the less massive star onto the more massive is self-regulating, too much mass transfer itself slows the inspiral of the binary.
- **Long lived mass transfer binaries invariably have low mass secondaries losing mass, and higher mass primaries gaining mass.**

Consequences of mass transfer (5)

325

- The Roche lobe size is affected by the change in mass ratio as well as separation. Let's use Paczynski's approximation:

$$\frac{R_2}{a} = \frac{2}{3^{4/3}} \left(\frac{q}{1+q} \right)^{1/3} = 0.462 \left(\frac{M_2}{M_1 + M_2} \right)^{1/3}$$

- Its logarithmic differentiation gives

$$\frac{\dot{R}_2}{R_2} = \frac{\dot{a}}{a} + \frac{1}{3} \frac{\dot{M}_2}{M_2}$$

- Combining with $\frac{\dot{a}}{a} = 2\frac{\dot{J}}{J} - 2\frac{\dot{M}_2}{M_2} \left(1 - \frac{M_2}{M_1} \right)$ gives:

$$\frac{\dot{R}_2}{R_2} = 2\frac{\dot{J}}{J} - 2\frac{\dot{M}_2}{M_2} \left(\frac{5}{6} - \frac{M_2}{M_1} \right) = 2\frac{\dot{J}}{J} - 2\frac{\dot{M}_2}{M_2} \left(\frac{5}{6} - q \right)$$

Consequences of mass transfer (6)

326

$$\frac{\dot{R}_2}{R_2} = 2\frac{\dot{J}}{J} - 2\frac{\dot{M}_2}{M_2}\left(\frac{5}{6} - q\right)$$

$$\dot{M}_2 < 0$$

- For $q > 5/6$ conservative mass transfer shrinks the Roche lobe down on the mass-losing star, and any angular momentum loss ($\dot{J} < 0$) will accentuate this.
- Unless the star can contract rapidly enough to keep its radius smaller than $R < R_2$, the overflow process will become very violent.
- For $q < 5/6$ conservative mass transfer will expand the Roche lobe.
- Mass transfer therefore only continues if either
 1. the star expands, or
 2. the binary loses angular momentum.

In both cases the Roche lobe and the stellar radius will move in step.

Mass transfer in CVs

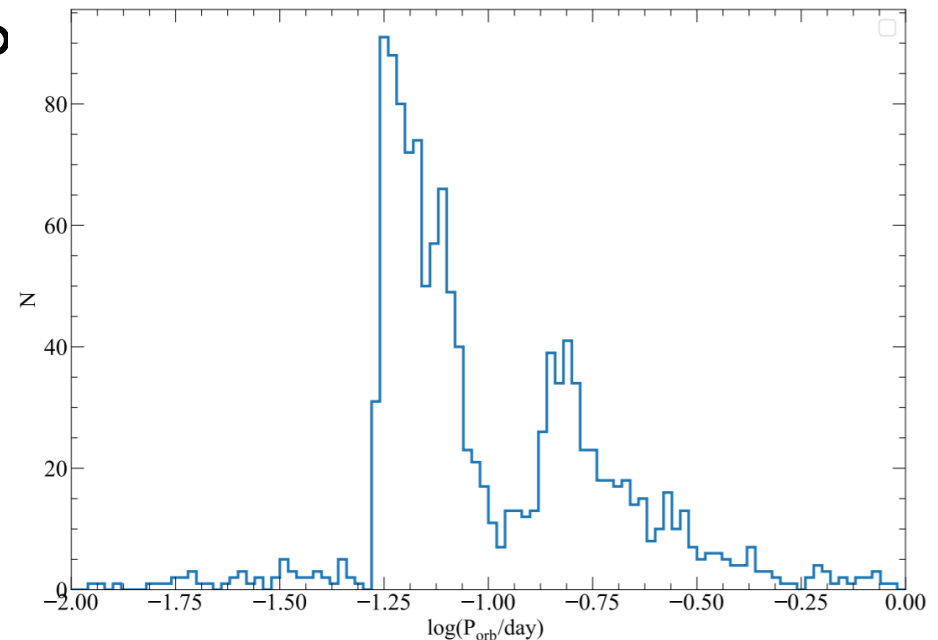
327

- The mass transfer process in CVs appears to be relatively **stable** on long time scales. This requires both that the mass ratio $q = M_2/M_1 < 1$ and also the existence of an **angular momentum loss** (AML) process that continually shrinks the system and thus keeps the Roche lobe in touch with the secondary star.
- The orbital period therefore initially **decreases** as a CV evolves, making the **period distribution a powerful tracer** of CV evolution.

CVs: Distribution of Orbital Periods

328

- Distinctive features in this distribution:
 - the 2-3 h **period gap**;
 - a sharp cut-off at ~ 80 min: the **minimum** period;
 - The existence of the gap and the minimum P_{orb} result from the way in which the secondary responds to mass loss.



Interacting Binary Stars

329

“Standard model” of CV evolution

Standard model of CV evolution (1)

330

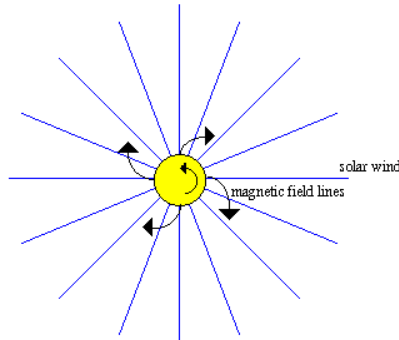
- Stable mass transfer in CVs **requires** *angular momentum loss* (**AML**) from the system.
- Mass transfer above the gap is driven primarily by **AML** mechanisms associated with a weak, magnetized stellar wind from the secondary (“magnetic braking” - **MB**).

Magnetic braking of the Sun

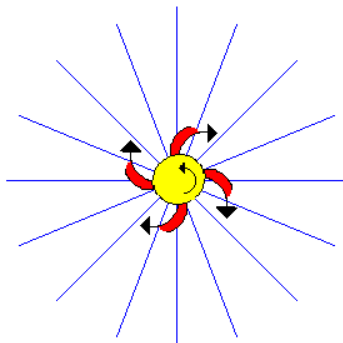
331

Magnetic Braking

The solar wind, a stream of charged particles, moves outward from the Sun in a radial direction. The magnetic field of the Sun also reaches outward, but is twisted due to the rapid rotation of the Sun.



Charged particles in the solar wind become trapped in the Sun's magnetic field and are 'dragged' along the field lines. The result is angular momentum is transferred from the Sun by the magnetic field to the charged particles.



- Solar wind co-rotates with the magnetic field for $r < r_A$ (Alfven radius). For the Sun, $r_A \sim 5-50 R_{\odot}$.
- The charged particles at some point escape the magnetic field lines and thus take away the Sun's angular momentum.
- Given an initial mass, rotation rate, and radius, we can thus calculate the rate of AML.
- This theory also explains why more massive stars rotate faster: they do not have proper winds like the Sun, and therefore are not as good at losing angular momentum.

Standard model of CV evolution (2)

332

- The period gap is interpreted as signaling a switch in the dominant **AML** mechanism. The period gap arises as a consequence of the cessation of MB at $P_{\text{orb}} \simeq 3$ hr.
- The donor mass at the **upper edge of the period gap** corresponds roughly to the mass where the donor is expected to transit from a star with **a radiative core to a fully convective object** ($M_2 \simeq 0.2 - 0.3 M_{\odot}$).
- This transition effectively shuts down the magnetic field on the secondary and hence also disrupts MB.
- Mass transfer below the gap is driven solely by gravitational radiation (GR).

Standard model of CV evolution (3)

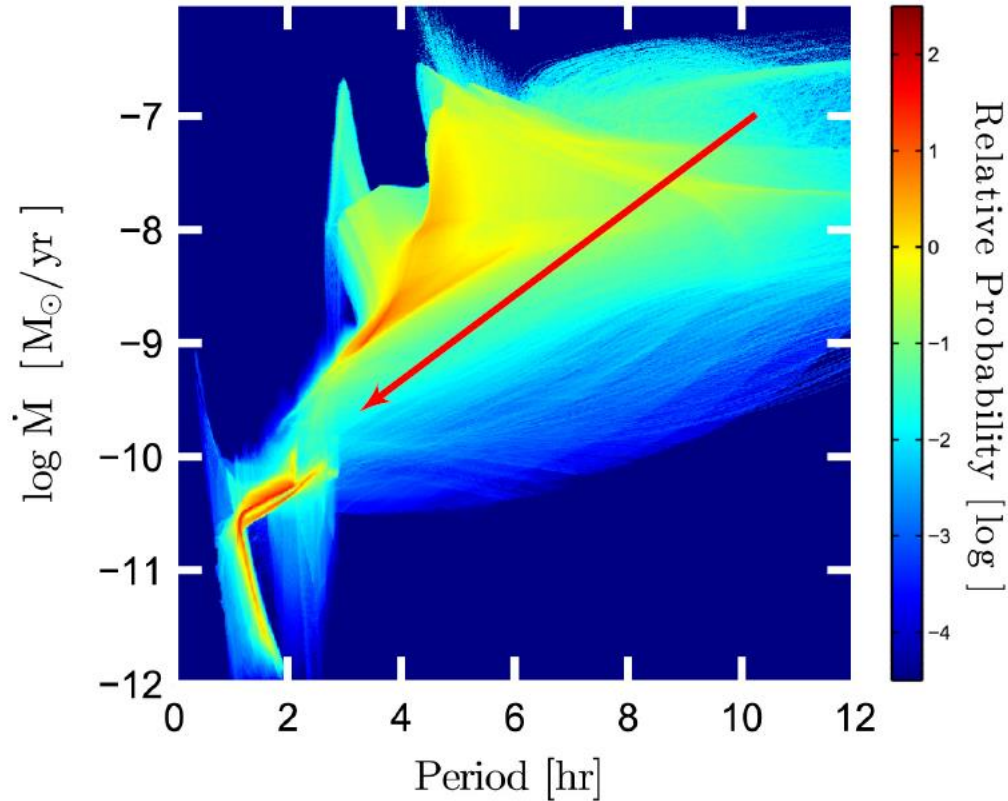
333

- The period minimum is also associated with a change in the structure of the donor:
 - P_{\min} marks the transition of the donor from a star to a sub-stellar object.

- Since the radius of a brown dwarf increases in response to mass loss, this transition must also lead to a change in the direction of orbital period evolution. Systems that have already evolved beyond P_{\min} are often referred to as “period bouncers”.

CV evolution: theory

334



Goliasch & Nelson, 2015, ApJ, 809, 80

Binary star evolution (1)

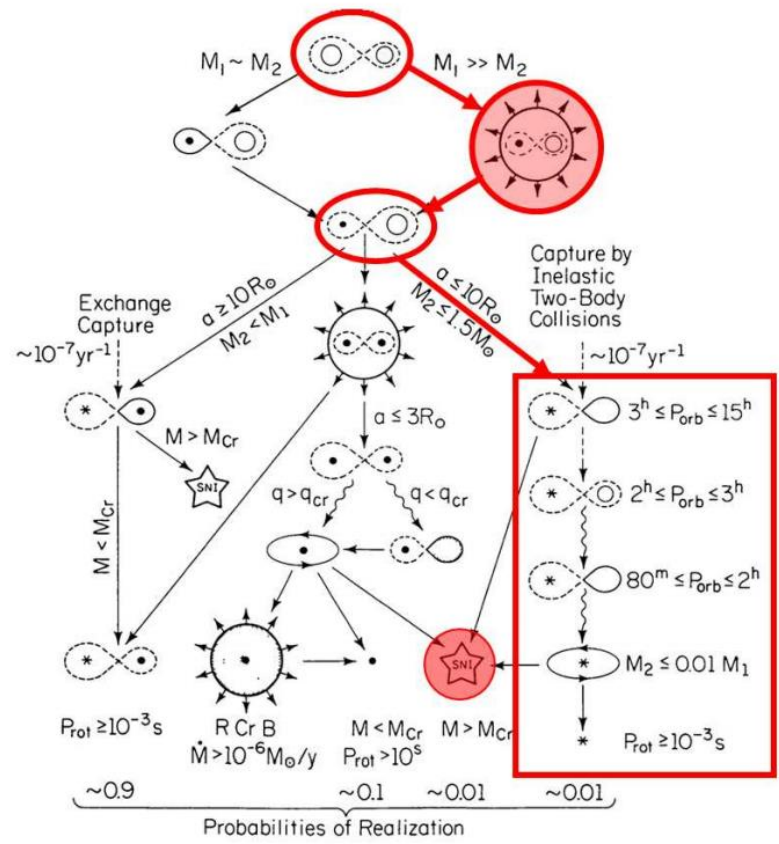
335

- Understanding the evolution of CVs – in the first instance by testing this standard model – is astrophysically important:
 - Even though many binary stars interact with each other at some stage of their lives, CVs provide a rare opportunity to observe long-lived stable mass transfer in action;
 - The physical processes that are relevant to CV evolution – not just MB and GR, but also the infamous “common envelope” (CE) phase that brings these systems into (or close to) contact – are also key to many other types of binary systems;
 - Some CVs are expected to be Type Ia supernova progenitors;
 - Most aspects of the accretion process in neutron star and black hole binary systems (including variability, accretion disk winds and jets) have direct counterparts in CVs.
- CVs are relatively numerous, nearby, bright and characterized by observationally “convenient” orbital time-scales, this makes them extremely useful as laboratories for the study of accretion onto compact objects more generally.

Binary star evolution (2)

□ **Basic scenarios for binary star evolution.**

- Rings are unevolved stars; filled circles are electron-degenerate helium, carbon-oxygen, or oxygen-neon cores in giants; six-pointed stars are white dwarfs or neutron stars.
- Wavy lines mark transitions driven by the radiation of gravitational waves; counter-clockwise rotating ellipses are heavy disks.
- Open stars represent Type Ia supernova explosions.
- Roche lobes are shown by dashed loops (when not filled) or by solid loops (when filled).
- The evolutionary channel marked in red is that expected to produce most CVs. The CV phase itself is marked by the red box.



From Iben (1991, ApJS, 76, 55)

The Physics of CV Secondaries

337

- The evolution of CVs is closely connected to – and in some sense controlled by – the properties of their secondary stars.
- **In order to understand CV evolution, we must therefore understand the properties of their donor stars.**

338

Secondary stars in CVs

The Physics of CV Secondaries (1)

339

- The Roche-lobe radius is:
$$\frac{R_L}{a} = \frac{2}{3^{4/3}} \left[\frac{q}{1+q} \right]^{1/3}$$
- Kepler's third law:
$$P_{orb}^2 = \frac{4\pi^2 a^3}{G(M_1 + M_2)}$$
- Combining them together yields the well-known *period-density relation* for Roche-lobe-filling stars with $R_2 = R_L$:

$$\bar{\rho} = \frac{M_2}{\frac{4}{3}\pi R_2^3} \cong 110 P_{hr}^{-2} g cm^{-3}$$

The Physics of CV Secondaries (2)

340

- Assume that CV donors are low-mass, near-MS stars. Then their mass-radius relationship will be roughly:

$$R_2/R_\odot = f(M_2/M_\odot)^\alpha \quad \text{with } f \simeq \alpha \simeq 1.$$

- Combining with the period-density relation immediately gives approximate mass-period and radius-period relations for CV donors:

$$M_2/M_\odot = R_2/R_\odot \cong P_{orb,hr}$$

- **The period gap between 2 hr and 3 hr corresponds to $M_2 \simeq 0.2 - 0.3M_\odot$, which is where the secondary is expected to change structure from partly radiative to fully convective.**

Are CV Donors on the Main Sequence?

341

- Compare the mass-loss time scale:

$$\tau_{\dot{M}_2} \simeq \frac{M_2}{\dot{M}_2}$$

- and the thermal time scale on which the donor can correct deviations from thermal equilibrium:

$$\tau_{th} \simeq \frac{GM_2^2}{L_2 R_2} \simeq 10^8 (M_2/M_\odot)^{-3/2} \text{yrs.}$$

- The thermal and mass-loss time scales are expected to be comparable for CV donors, both above and below the period gap.

Are CV Donors on the Main Sequence?

342

- This means that the donor cannot shrink fast enough to keep up with the rate at which mass is removed from its surface.
- It is therefore driven slightly out of thermal equilibrium and becomes somewhat **oversized** for its mass.
- This slight deviation from thermal equilibrium ultimately explains both the period gap and the period minimum.

The Origin of the Period Gap (1)

343

- If the period gap is “somehow” associated with a sudden cessation of MB at $P_{\text{orb}} \simeq 3$ hrs then
Why should this produce a period gap in the CV population?
 - Mass transfer in CVs is driven entirely by AML.
 - A sudden reduction in AML will also result in a sudden reduction in the mass-loss rate the donor experiences.
 - The donor responds to the lower mass-loss rate by shrinking closer to its thermal equilibrium radius.
 - This results in **a loss of contact with the Roche lobe.**

The Origin of the Period Gap (2)

344

- CVs evolve through the period gap as detached systems.
- During this detached phase, the binary orbit and Roche lobe continue to shrink, since AML due to GR continues.
- However, since the thermal relaxation of the donor in this phase is faster than the shrinkage of the Roche lobe, the donor manages to relax all the way back to its TE radius.
- The bottom edge of the period gap thus corresponds to the location where the Roche lobe radius catches up once again to the TE radius of the donor.
- At this point, mass transfer restarts, and the system emerges from the gap as an active CV once again.

The Origin of the Period Gap (3)

345

- **How bloated must CV donors be to account for the observed size of the period gap?**
- No mass transfer in the gap \rightarrow the donor mass just above and below the gap must be the same, $M_2(P_{\text{gap},+}) = M_2(P_{\text{gap},-})$.
- From the period-density relation, we then get

$$\bar{\rho} \sim \frac{M_2}{R_2^3} \sim P^{-2} \quad \longrightarrow \quad \frac{R_2(P_{\text{gap},+})}{R_2(P_{\text{gap},-})} = \left[\frac{P_{\text{gap},+}}{P_{\text{gap},-}} \right]^{2/3} \simeq \left[\frac{3}{2} \right]^{2/3} \simeq 1.3$$

- The donor at the bottom edge is in or near equilibrium, so that donors at the upper edge of the period gap must be oversized by $\simeq 30\%$ relative to equal-mass, isolated MS stars.

The Origin of the Period Minimum (1)

346

- The period minimum is also closely connected to the properties of the donor stars:
The donor transition from a **Hydrogen-burning star** to a **substellar object**.
- The point here is that stars generally have a **positive** mass-radius index, whereas sub-stellar objects with masses below the hydrogen-burning limit ($M_{\text{H}} \simeq 0.07M_{\odot}$) have a **negative** one.
- We can therefore expect the condition $M_2 \simeq M_{\text{H}}$ to set the minimum period a CV can reach.

The Origin of the Period Minimum (2)

347

- If we combine the period-density relation with the simple power-law approximation to the donor mass-radius relation, we find: $P_{orb}^{-2} \propto M_2^{1-3\alpha}$.
- Differentiating this logarithmically yields a simple expression for the orbital period derivative:
$$\frac{\dot{P}_{orb}}{P_{orb}} = \frac{3\alpha - 1}{2} \frac{\dot{M}_2}{M_2}$$
- The period minimum must correspond to $\dot{P}_{orb} = 0 \Rightarrow \alpha = 1/3$
- Sub-stellar objects are out of TE by definition and respond even to slow mass loss by increasing in radius, i.e. $\alpha \leq 0$
- P_{min} correspond roughly to $M_2 \simeq M_H$

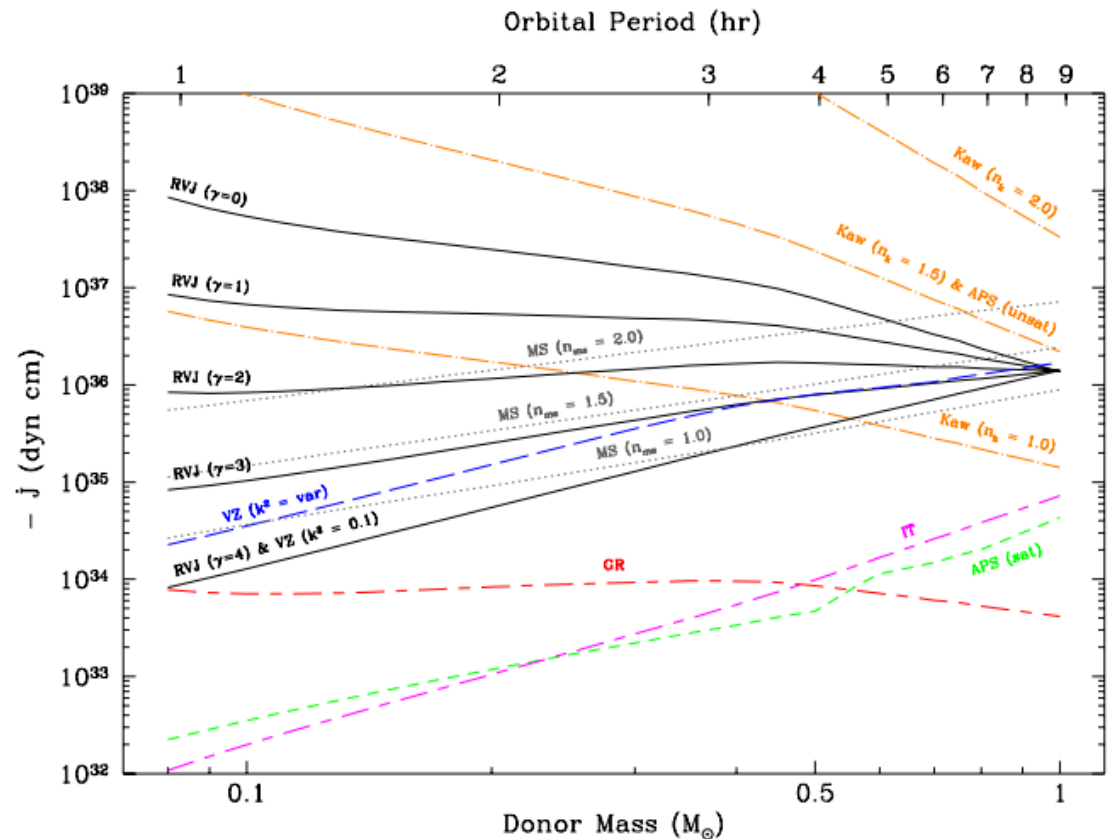
Magnetic Braking (1)

348

A comparison of the AML rates predicted for CV donors.

The red long-dash-short-dash line corresponds to GR-driven AML.

From Knigge et al. (2011)



How well do we understand MB? Not really good.
There are huge differences between different AML recipes.

Interacting Binary Stars

Magnetic Braking (2)

349

- The standard “disrupted magnetic braking” model provides reasonable explanations for the existence of the period gap and the period minimum.
- However, this is what it was designed to do.
- **But how to test it?**
- Direct observational tests of other fundamental predictions of the model have only become possible over the last few years.

CV evolution: observational tests (1)

350

□ Predictions:

1. Donors just above and below the gap should have identical masses, but different radii.
2. The Period Spike: the Reversal of the Direction of Period Evolution at P_{\min} .
3. The Existence of CVs with Brown Dwarf Secondaries.

CV evolution: observational tests (2)

351

1. Donors just above and below the gap should have identical masses, but different radii:

- The donors above the gap have been significantly inflated by mass loss, while CVs below the gap have just emerged from a detached phase with their donors in thermal equilibrium.

CV evolution: observational tests (3)

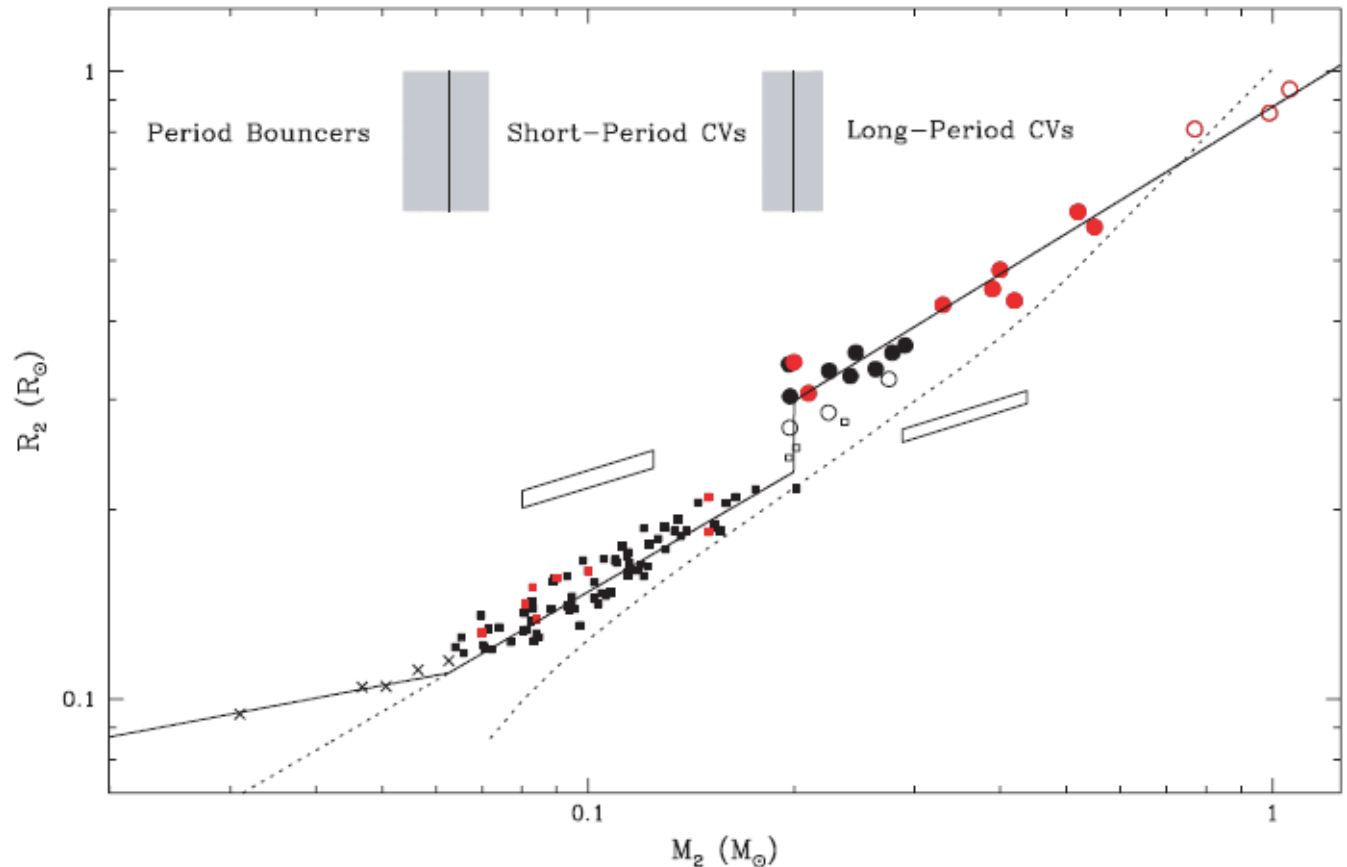
352

The dotted line is a theoretical mass-radius relation for MS stars.

There is a clear discontinuity in donor radii at $M_2 \approx 0.2M_{\odot}$.

From Knigge (2006)

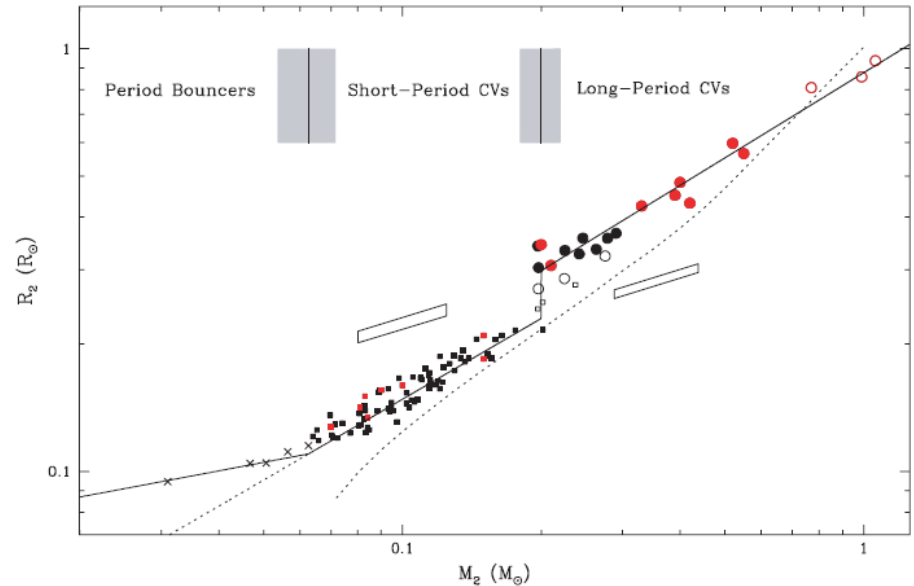
The mass-radius relation of CV donor stars.



CV evolution: observational tests (4)

353

- However, this Figure alone cannot tell us the **exact nature** of the disruption in AML responsible for the period gap.
- Any significant reduction of AML at $P \simeq 3$ hrs will produce a period gap and a discontinuity in the donor mass-radius relationship.



Interacting Binary Stars

CV evolution: observational tests (5)

354

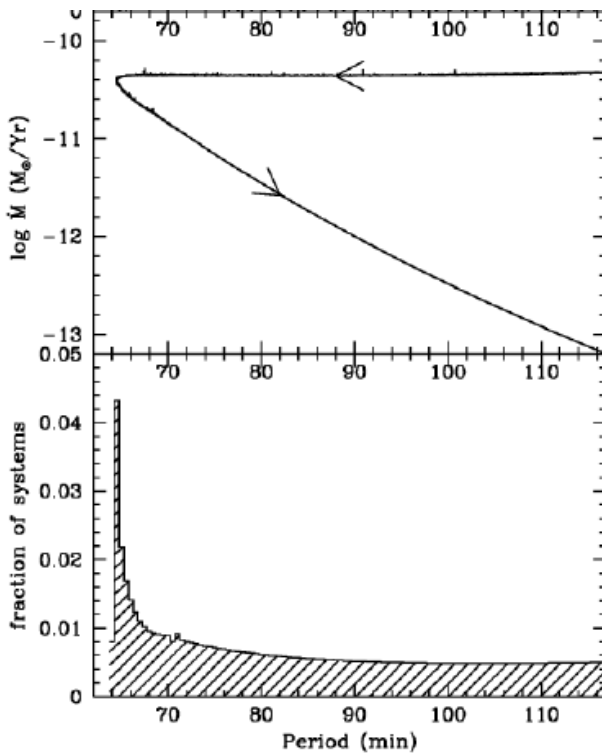
2. The Period Spike: the Reversal of the Direction of Period Evolution at P_{\min} :

Population synthesis models show that there should be a significant accumulation of systems near the period minimum, and that 99% of CVs should have orbital periods below the period gap, whilst the period distribution plot shows **similar numbers** of CVs above and below the period gap.

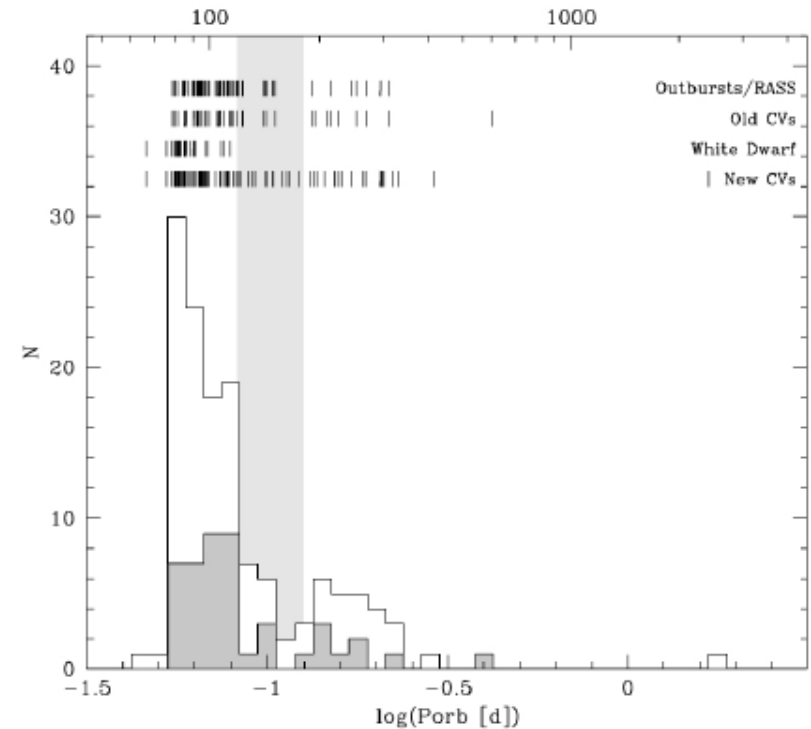
CV evolution: observational tests (6)

355

The Period Spike: Prediction



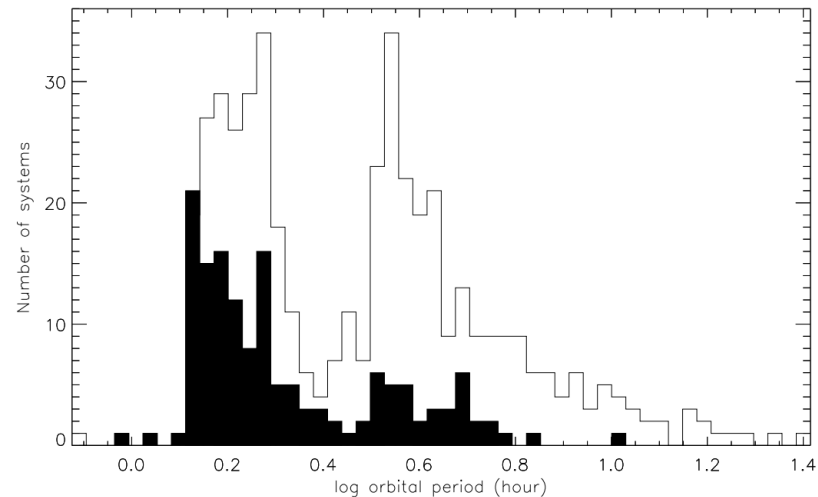
Old and Newly identified CVs



CV evolution: observational tests (7)

356

- However, the existence of the period spike does not necessarily imply that the standard model is **quantitatively** correct.
- The theory predicts a minimum period for hydrogen-rich CVs at $P_{\text{orb}} \simeq 65\text{min}$, while the observed period distribution shows a sharp cut-off at $\sim 75\text{--}80\text{ min}$.

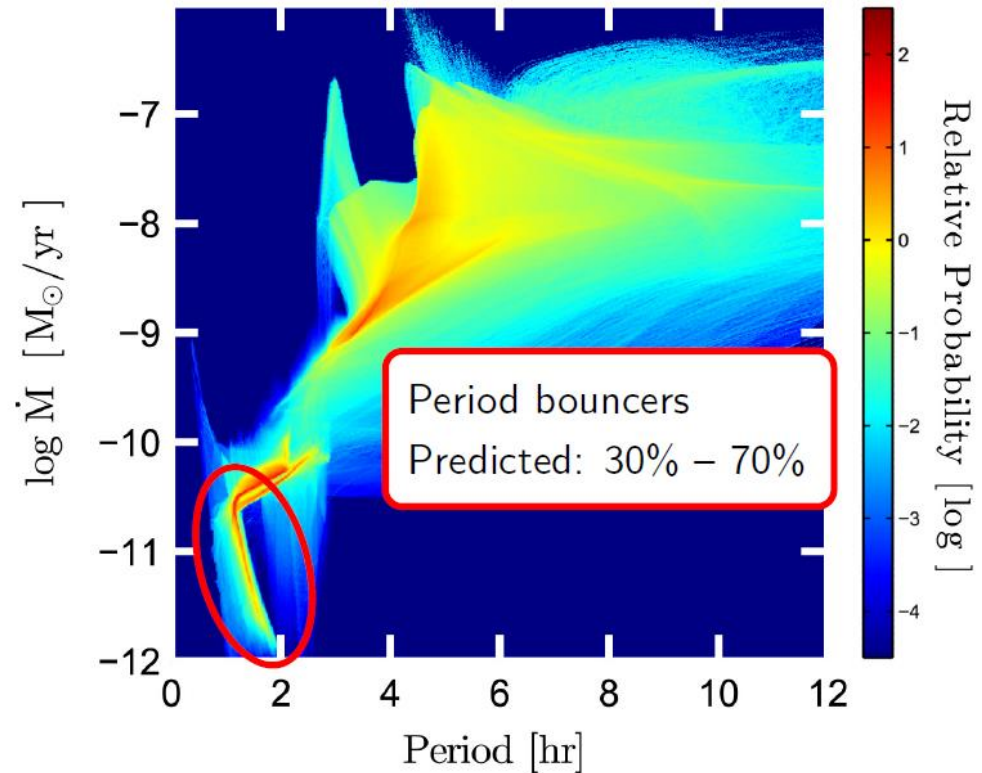


Interacting Binary Stars

CV evolution: observational tests (8)

357

The standard model predicts that about 70% of present day CVs should be period bouncers, with all of these possessing sub-stellar donor stars.



Goliasch & Nelson, 2015, ApJ, 809, 80

Interacting Binary Stars

CV evolution: observational tests (9)

358

The Existence of CVs with Brown Dwarf Secondaries:

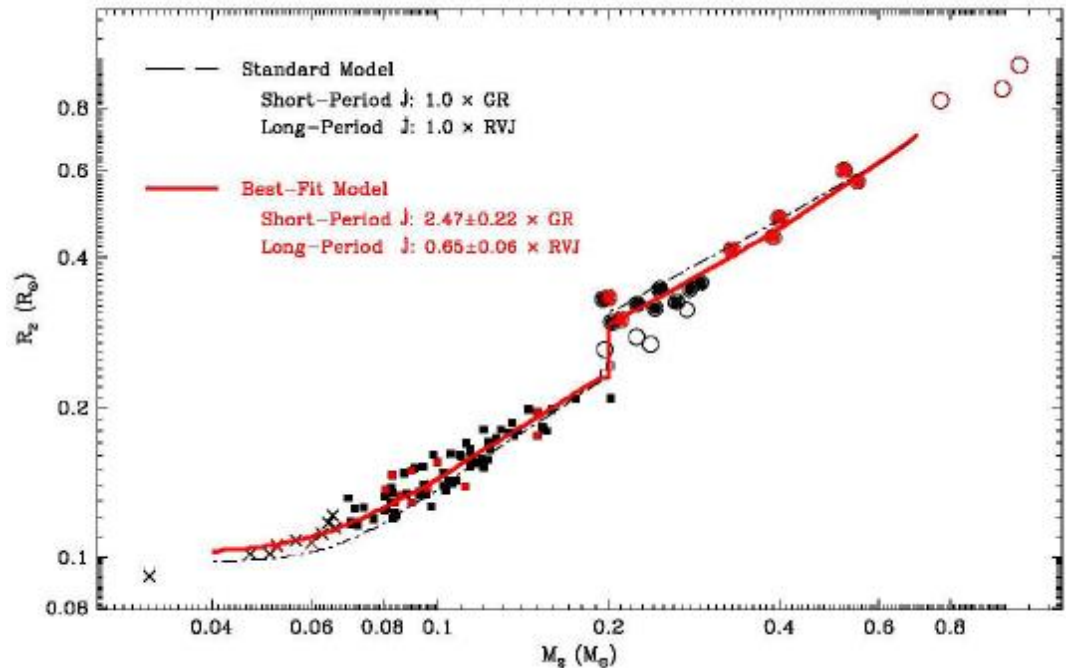
- The standard model predicts that about 70% of present day CVs should be period bouncers, with all of these possessing sub-stellar donor stars.
- Until recently, only a few of candidate period bouncers were known.
- There was not even one CV with a well-determined donor mass below the Hydrogen-burning limit.

This situation has also now changed for the better.

CV evolution: Conclusion

359

The observational tests provide strong evidence that our basic ideas about CV evolution are at least **qualitatively** correct.



360

Non-magnetic Nova-like Variables

Nonmagnetic Nova-like Variables

361

- Non-magnetic Nova-like variables (NL) resemble novae between eruptions;
- NLs include all of the “non-eruptive” CVs.
 - ▣ However, many of them may have “low states”
 - ▣ However, some may also exhibit “stunted” outbursts

Nova-like Variables (1)

362

The NL class is a very heterogeneous group of stars, and the definition of the subclasses within NLs is mostly based on **observational features** of objects.

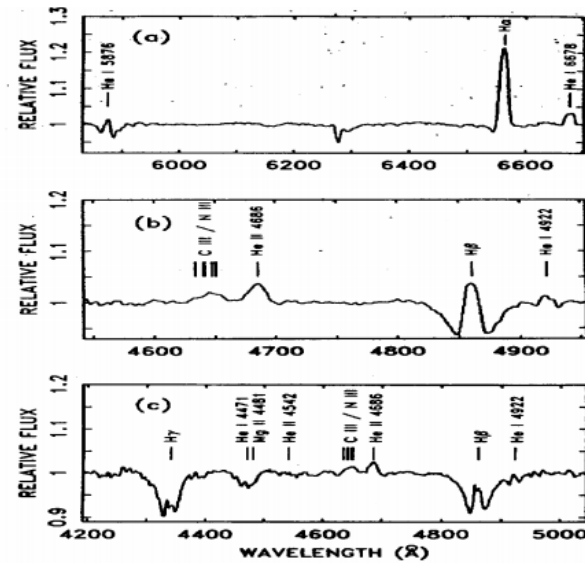
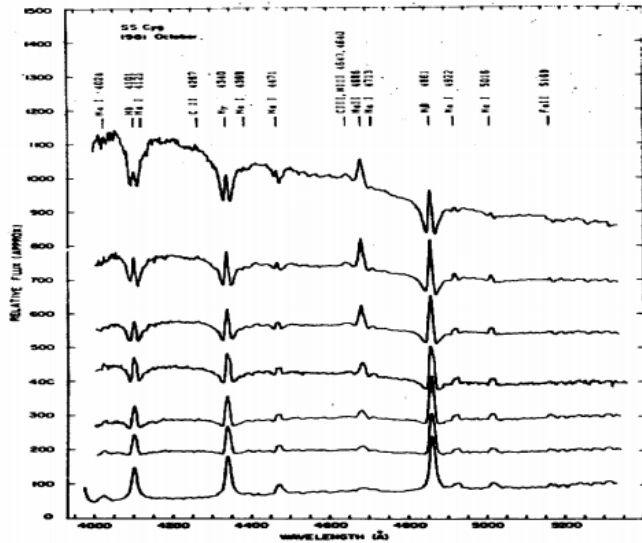
□ **Classification:**

- The UX Ursae Majoris stars (UX UMa) show persistent broad Balmer absorption lines.
- The RW Triangulum stars (RW Tri), per contra, have pure emission-line spectra.
- SW Sextantis stars (SW Sex) show many unusual yet consistent properties (will discuss later).
- VY Sculptoris stars (VY Scl) show states of low luminosity (drops) exceeding 1 mag.

The absence of DN outbursts in NLs is believed to be due to their high mass transfer rates, producing ionised accretion disks in which the disk instability mechanism is suppressed.

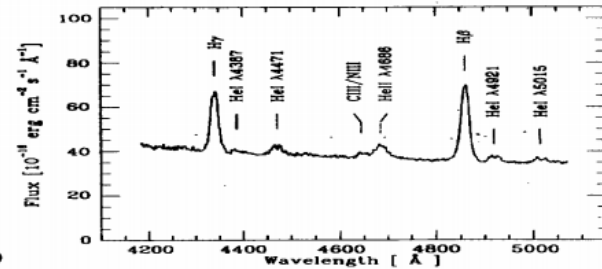
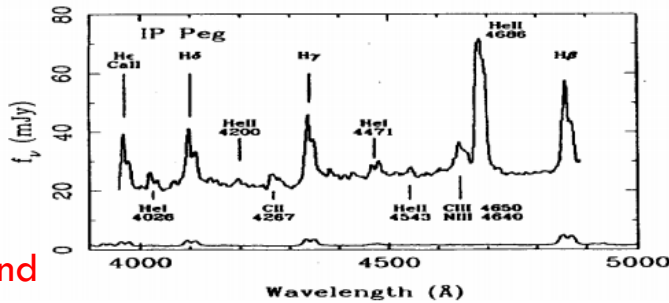
Nova-like Variables (2)

The DN
SS Cyg in
outburst and
quiescence



The UX UMa-star
IX Vel

The DN
IP Peg in
outburst and
quiescence



The SW Sex-star
WX Ari

SW Sextantis stars (1)

364

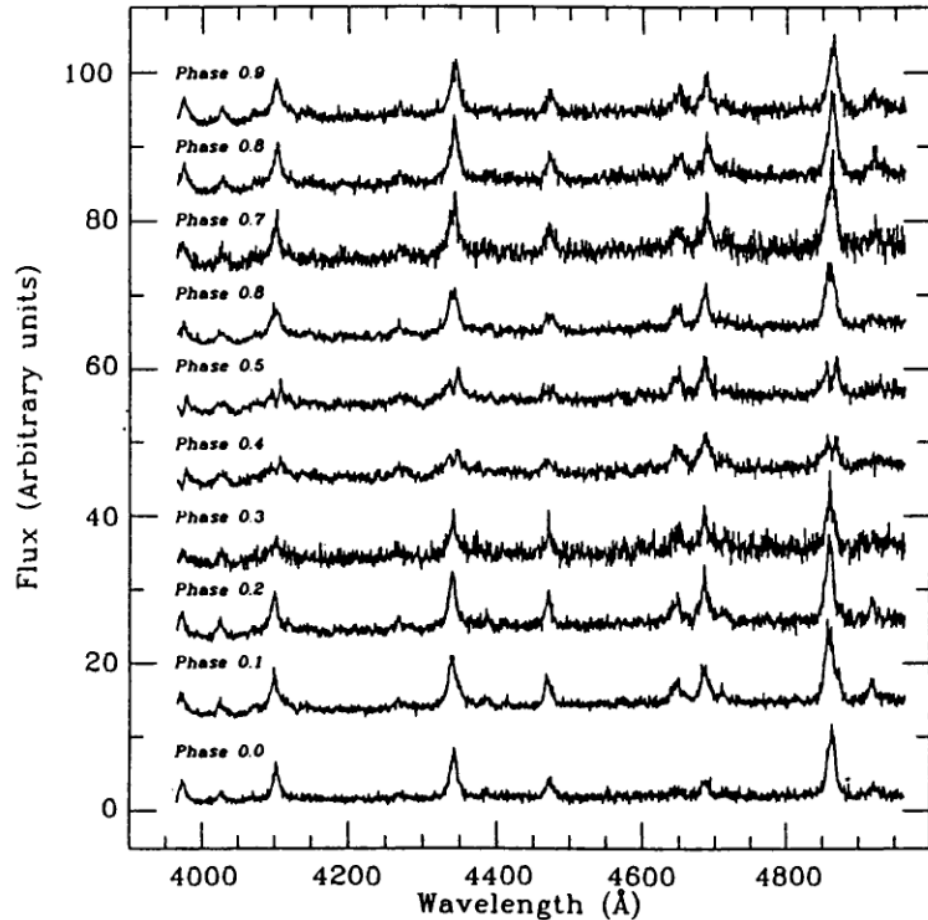
- Relatively large group of NLs, which was initially populated by eclipsing systems only (**high inclination!**);
- Largely occupy the narrow orbital period stripe between 3 and 4.5 hours;
- Single-peaked emission lines despite the high inclination;
- Strong high excitation spectral features (He II, C III/N III);
- Central absorption dips in the emission lines around phase 0.4 – 0.7;
- High-velocity emission S-waves with maximum blueshift near phase ~ 0.5 .

SW Sextantis stars (2)

365

Time-resolved spectra of
V1315 Aql.

From
Dhillon, Marsh & Jones
(1991).



SW Sextantis stars (3)

366

- The unusual spectroscopic behaviour of the SW Sex systems has led to their intensive studies.
- Many NLs above the 3 – 4.5 hr period interval have been found to show distinctive SW Sex behaviour;
- Even some LMXBs!
- Even the proto-typical NL UX UMa!

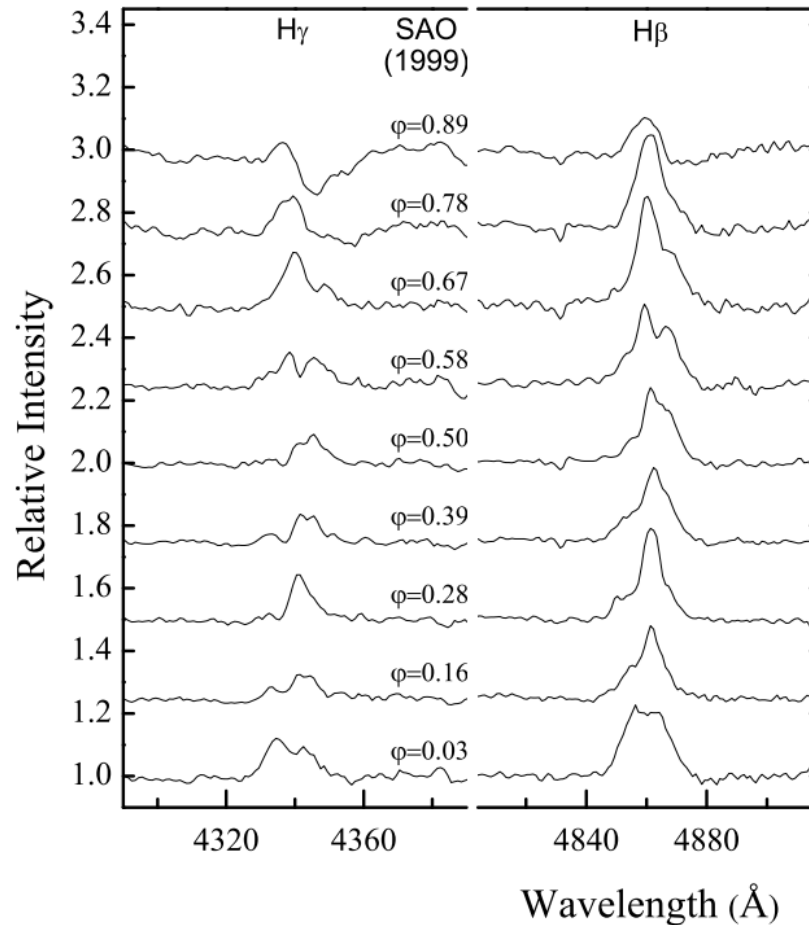
SW Sextantis stars (4)

367

Even the proto-typical NL UX UMa has now been shown to exhibit SW Sex-like behaviour.

Time-resolved spectra of UX UMa.

From Neustroev et al. (2011).



Nova-like Variables

368

□ Classification:

- The UX Ursae Majoris stars (UX UMa) show persistent broad Balmer absorption lines.
- The RW Triangulum stars (RW Tri), per contra, have pure emission-line spectra.
- SW Sextantis stars (SW Sex) show many unusual yet consistent properties (will discuss later).
- VY Sculptoris stars (VY Scl) show states of low luminosity (drops) exceeding 1 mag.

We now suspect that all NLs could be classified as SW Sex stars if one looks long and hard enough.

369

Magnetically-Controlled Accretion

Polars

Intermediate Polars

Magnetically-Controlled Accretion (1)

370

- In some CVs we observe interesting features:
 - ▣ Strongly polarized emission (up to 60 % circular polarisation in the optical);
 - ▣ Strong X-ray emission;
 - ▣ Unexpectedly long soft X-Ray component;
 - ▣ Highly variable light curves in optical and X-Ray;
 - ▣ In some objects: short-period coherent variability.

⇒ Strong Influence from a magnetic field on the binary system

Magnetically-Controlled Accretion (2)

371

- Magnetic Field of the WD in First Approximation:
 - Both stars have a magnetic field;
 - The magnetic flux is roughly conserved during star evolution: $B \cdot R^2 \approx \text{const}$
- ⇒ **High field strengths up to 20MG near the WD;**
- Magnetic field is usually approximated as a Dipole.

Magnetically-Controlled Accretion (3)

372

- Important parameter:

The magnetospheric radius, R_M - the distance from the WD where the magnetic pressure is equal to the ram pressure:

$$\frac{B^2}{8\pi} = \rho(r)v_{in}^2(r)$$

- For polars, $B_{wd} \sim 10^7$ G, $R_M \sim 10^{11}$ cm $\sim a$

NO DISK!

- For intermediate polars, $B_{wd} \sim 10^6$ G, $R_M \sim 10^{10}$ cm

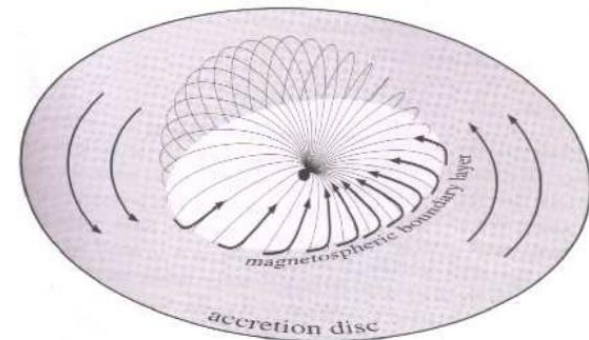
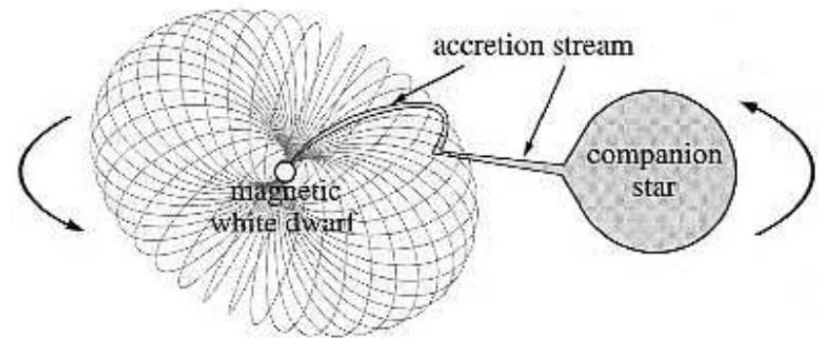
TRUNCATED DISK

Magnetically-Controlled Accretion (4)

373

- Pressure balance defines the inner edge of the accretion disk:
 - ▣ For strong magnetic fields of the WD no disk is formed, instead the accretion stream follows the field lines directly;
 - ▣ For weaker magnetic fields a truncated accretion disk will form.

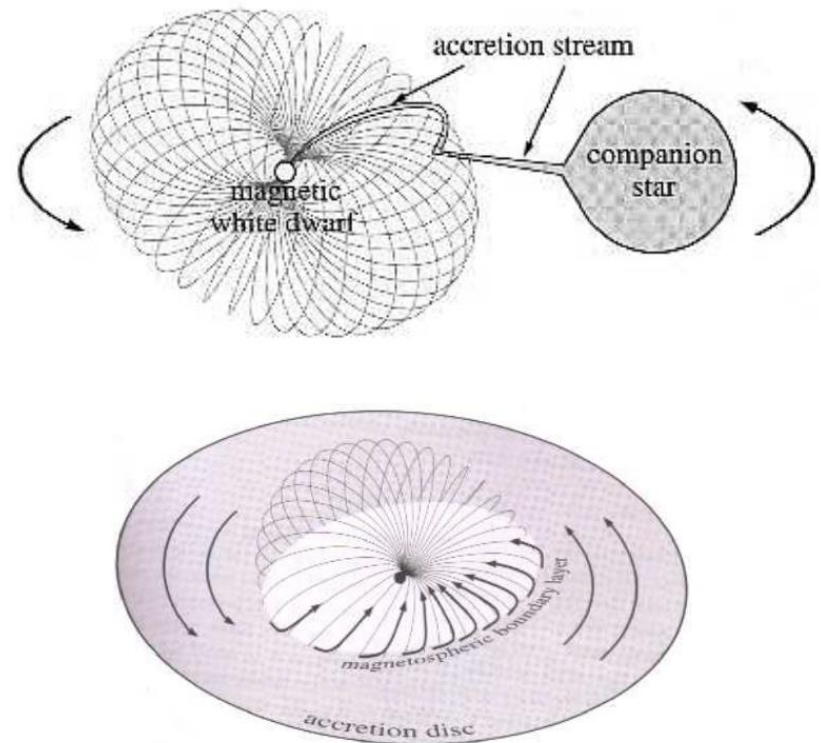
- These two scenarios are called an accretion column and an accretion curtain, respectively.



Magnetically-Controlled Accretion (5)

374

- The corotation radius is the radius at which the disk corotates with the magnetic field. This is usually near the inner edge of the disk, which is the magnetospheric radius.



Magnetically-Controlled Accretion (6)

375

- Spin Periods and Angular Momentum:
 - System has an orbital period P_{orb} ;
 - the WD has a spin period P_{spin} ;
 - Therefore modulations should be observed;
 - Accretion stream transfers angular momentum to WD
 - ⇒ **Spin-up ?**
 - Consider interaction of magnetic moments of the two stars!
 - Magnetic moments can **balance** transfer of angular momentum, if interaction is strong enough

Polars (1)

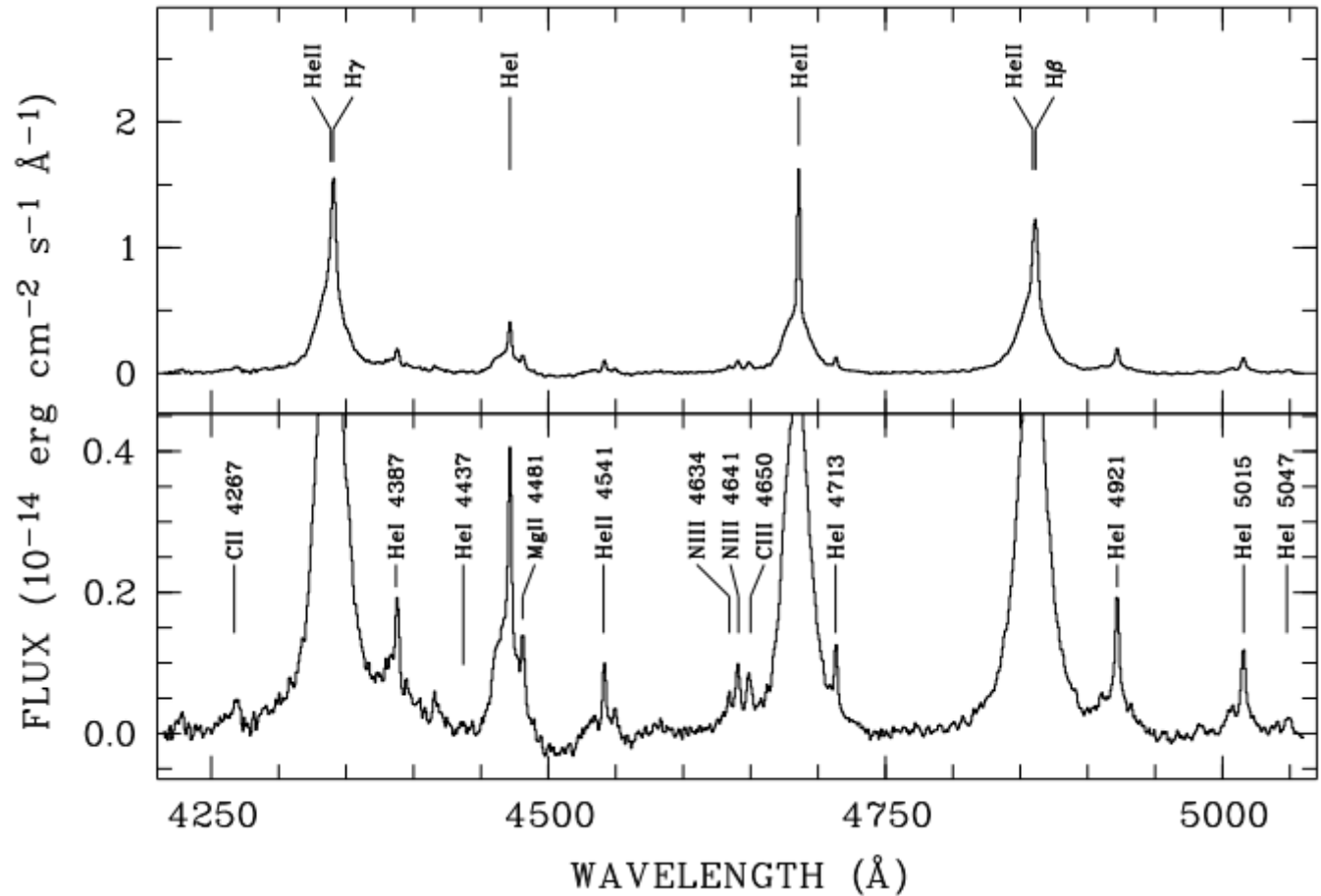
376

- **Polars or AM Her Stars:**
Systems with Strong Magnetic Field and Strong Magnetic Interaction:
 - ▣ Synchronise orbital period and spin period of the WD, due to magnetic interaction;
 - ▣ Don't have accretion disks;
 - ▣ Can be identified through strong polarisation in optical wavelength.

Polars (2)

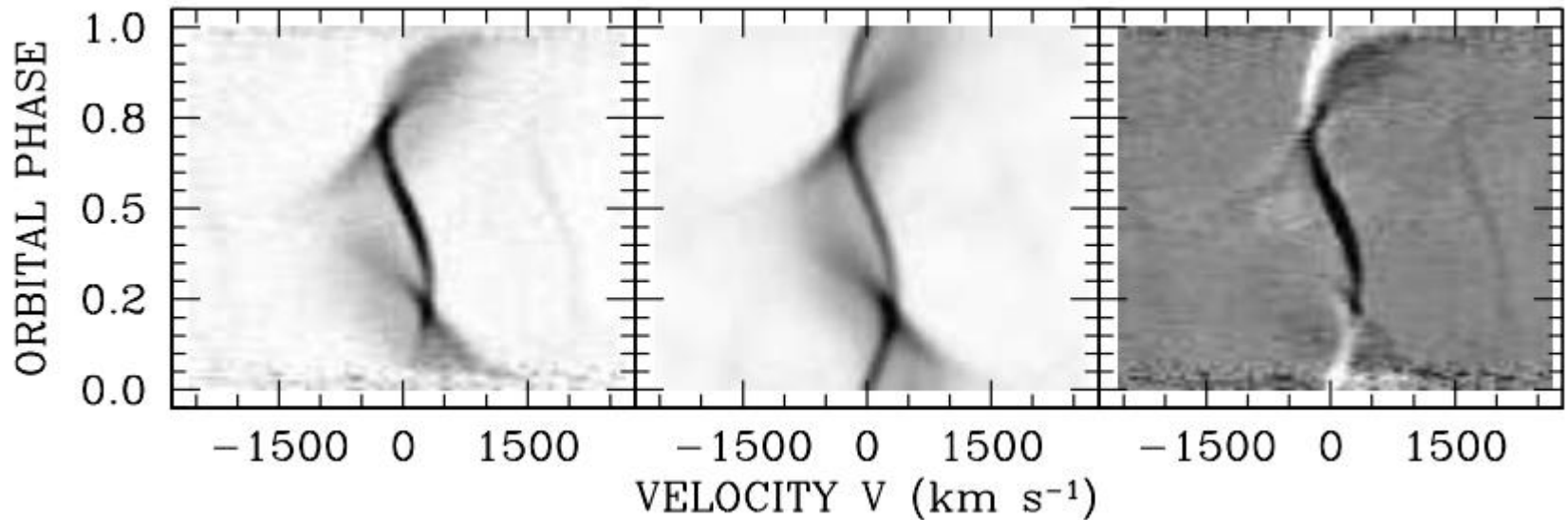
377

Mean-orbital
high-resolution
spectrum of
the polar
HU Aqr



Polars (3)

378

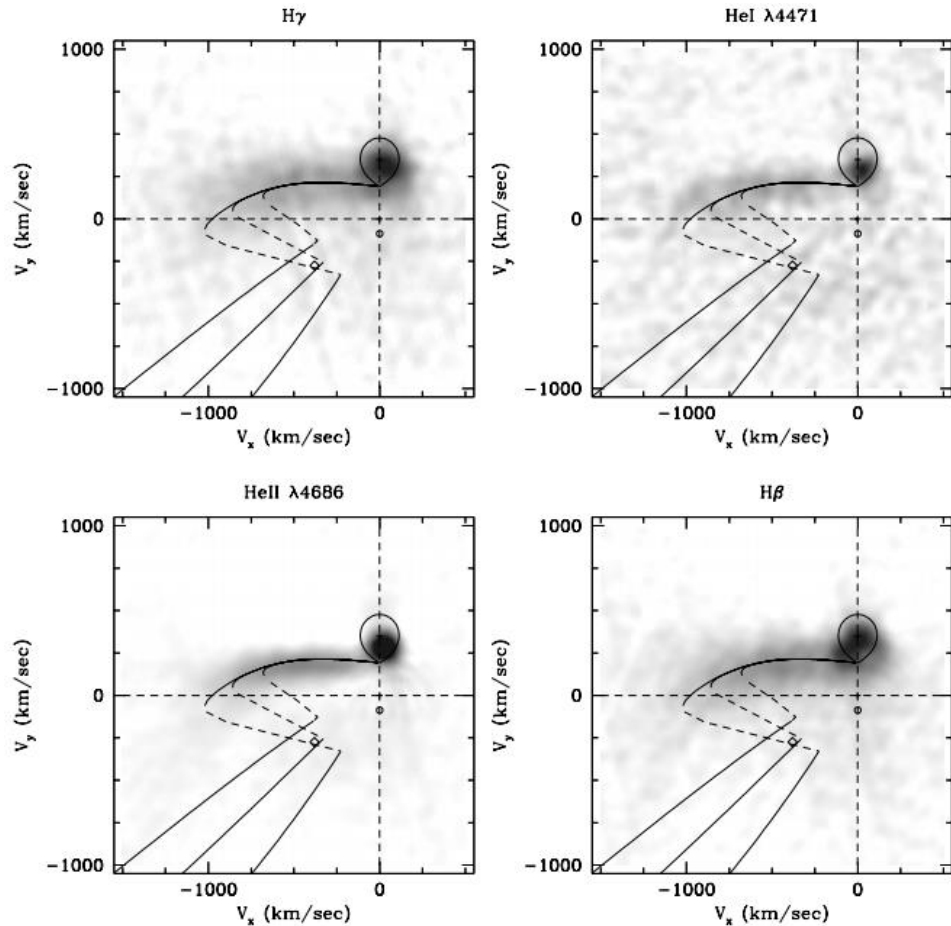


Trailed spectrogram of the He II emission line of the polar HU Aqr

Polars (4)

379

Doppler maps of the four main emission lines of the polar HU Aqr



Intermediate Polars (1)

380

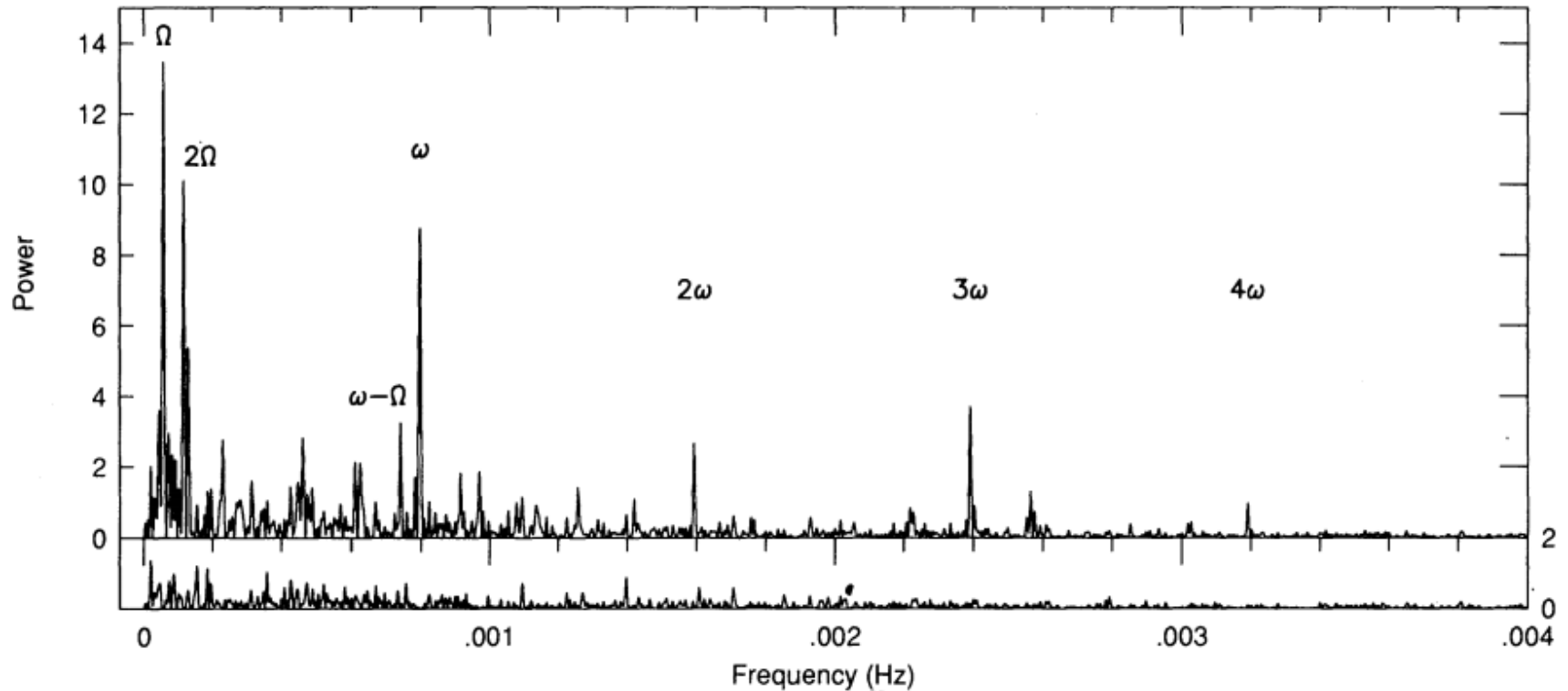
- **Intermediate Polars or DQ Her Stars:**
Systems with Weaker Magnetic Field:
 - ▣ Low Interaction between magnetic moments;
 - ▣ Spin Up, due to transfer of angular momentum;
 - ▣ No synchronised state of the rotation periods, but rotation at high velocities;
 - ▣ A truncated accretion disk, as magnetic pressure can't control the plasma far enough.

Not always the case!

Video

Intermediate Polars (2)

381



The power spectrum of the X-ray light curve of FO Aqr: **multiple periodicities**

382

AM CVn Binaries

Close Binary Systems

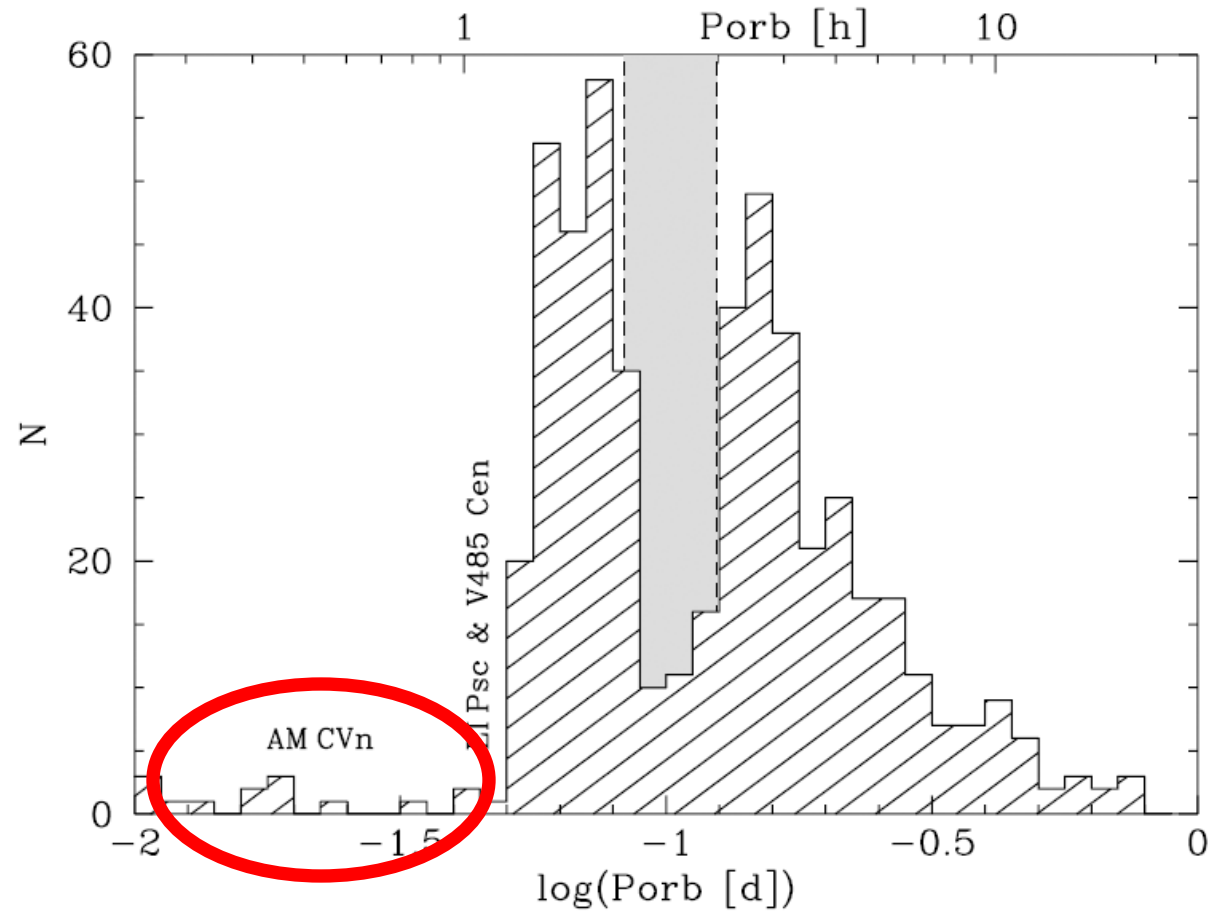
secondary \ primary	main-sequence star ^{*)}	evolved star ^{**)}	white dwarf	neutron star or black hole
main-sequence star ^{*)}	[binary T Tauri stars] [RS CVn stars] Algols (AD) (TAD) {W UMa stars = contact systems}	symbiotic stars Type I as e.g. CI Cyg, Z And, AR Pav (AD) Algols (AD), (TAD)	^{*)} main-sequence star or slightly evolved ^{**)} evolved star, but not yet a compact star [] detached systems	
evolved star ^{**)}	[Wolf-Rayet binaries] [binary planetary nebulae]		(AD) evidence for an accretion disk (TAD) evidence for a detached accretion disk	
white dwarf	[pre-cataclysmic binaries] non-magnetic CVs: UX UMa stars (AD) dwarf novae (AD) DQ Her stars (AD) AM Her stars	long period CVs as GK Per (AD) recurrent nova (AD) symbiotic stars (AD) symbiotic novae (AD)	[double white dwarfs] AM CVn stars (AD)	
neutron star or black hole	massive X-ray binaries (AD) (wind accretion) low mass X-ray binaries (AD) HZ Her/Her X-1 (AD) SS 433 (AD)	long period low mass X-ray binaries (AD)	[binary pulsars] 4U1820-30 (AD)	[binary pulsars]

Comments: in semi-detached systems the mass gaining star is listed as the primary
in detached systems the more evolved star is listed as the primary

CVs: Distribution of Orbital Periods

384

The orbital period distribution of 531 CVs from Ritter & Kolb (2003, V7.3).



The AM Canum Venaticorum binaries

385

- Key properties:
 - ▣ No hydrogen
 - ▣ Very short periods (5 – 10 to 65 minutes)
 - ▣ Spectra characteristic of accretion disks
 - ▣ Weak X-ray emission

- AM CVn binaries are a class of ultracompact systems in which the donor stars are hydrogen deficient. The accretors are white dwarfs.

AM CVn stars

386

- To fit within their Roche lobes, the donor stars must be dense ($\bar{\rho}_2 = 100 - 4000 \text{ g cm}^{-3}$), suggesting they may be degenerate too:
“double degenerate” (Faulkner et al 1972).

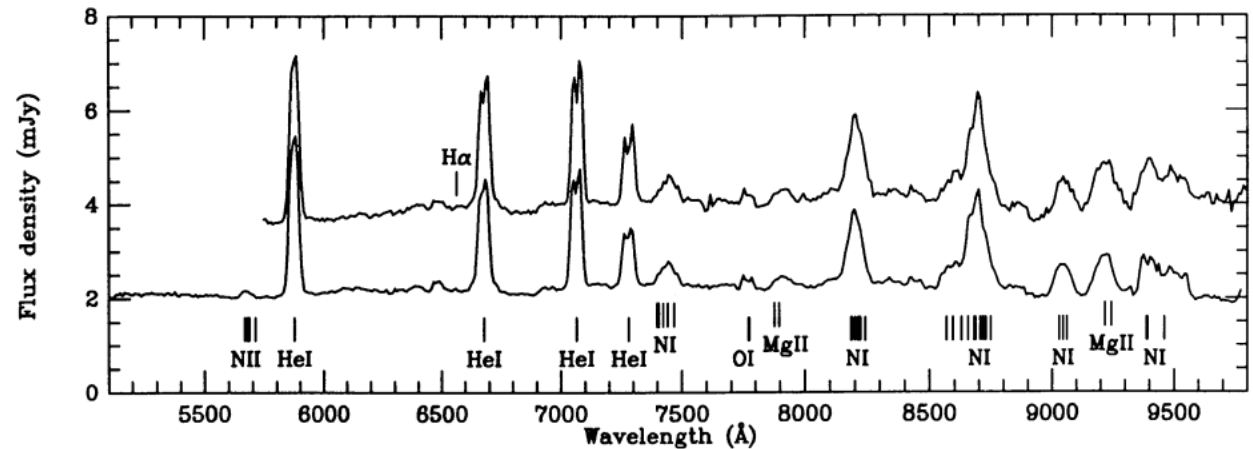
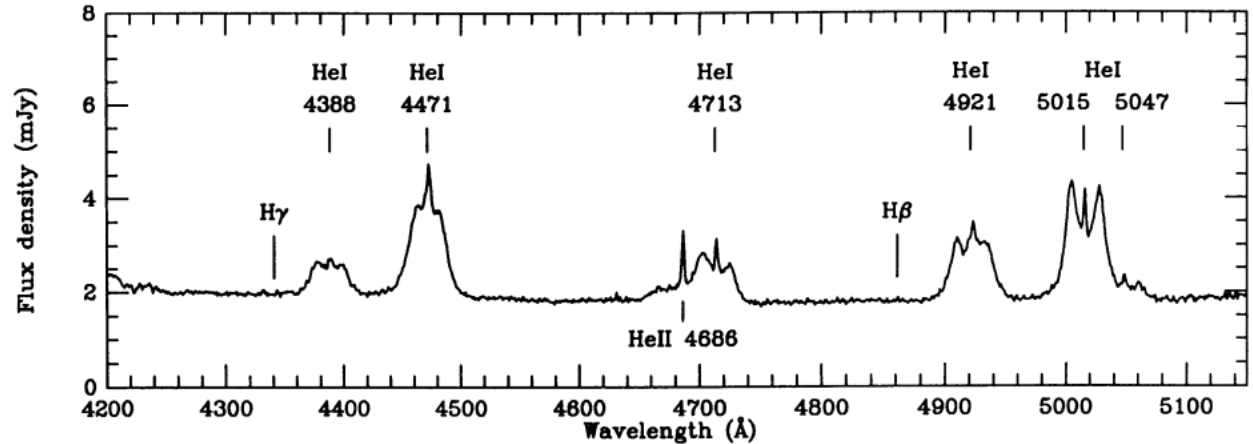
- Currently 56 known AM CVn systems.
(Ramsay et al., 2018, A&A, 620, A141)

Spectra of AM CVn's (1)

387

The most obvious observational signature is their optical spectrum - lack of hydrogen lines.

GP Com, P=46 min
(Marsh et al. 1991)

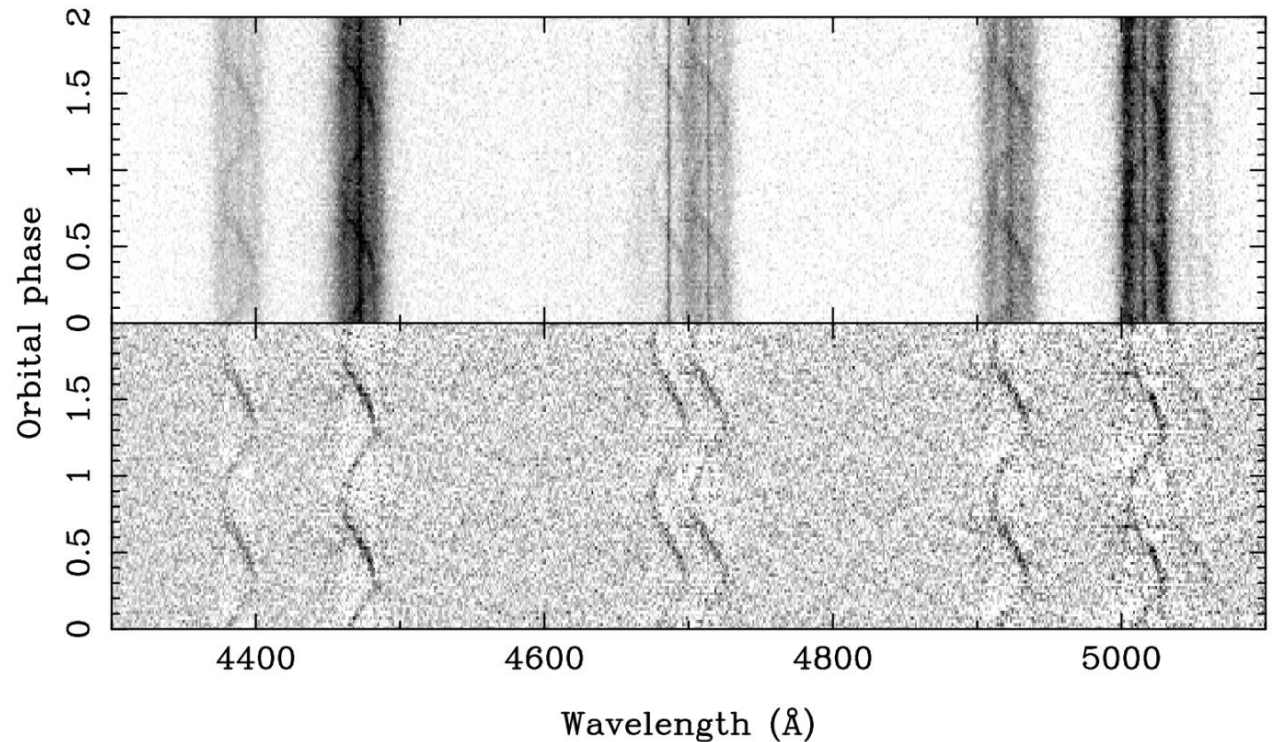


Spectra of AM CVn's (2)

388

The most obvious observational signature is their optical spectrum - lack of hydrogen lines.

GP Com, $P=46$ min
(Marsh et al. 1991)



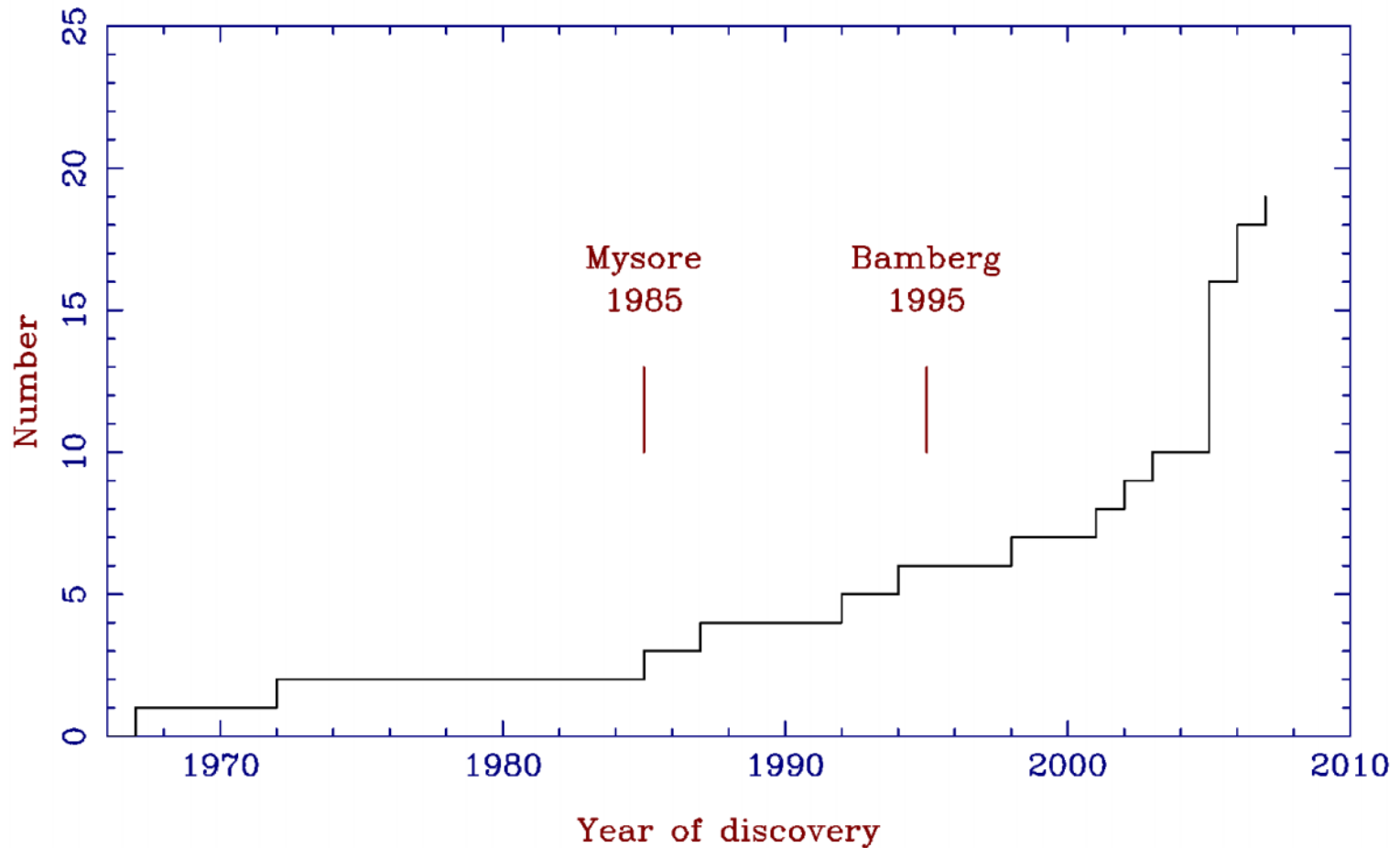
AM CVn stars

389

- Total number in Galaxy: $3 \times 10^5 - 3 \times 10^6$
(Roelofs et al 2007)
- Accreting white dwarfs: $M_1 \sim 0.6M_{\odot}$
- Mass donors: $M_2 = 0.015 - 0.15M_{\odot}$
- Orbital separations: $a = 0.1 - 0.4 R_{\odot}$
- Disk size: $R_d \sim 0.35a$
- Mass transfer rates: $\dot{M} = 10^{-12} - 10^{-8} M_{\odot} / \text{yr}$
- Absolute magnitudes: $M_V = 5 - 13$

AM CVn stars: Discovery history

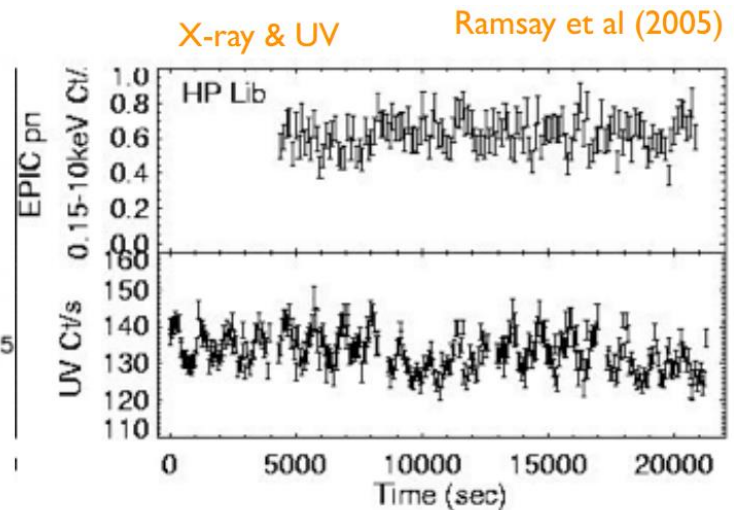
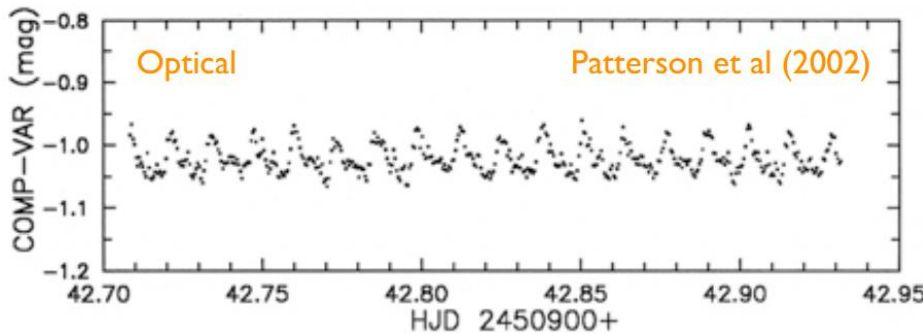
390



Light curves of AM CVn's

391

- Can be split into systems in low state, high state and those which undergo outbursts. Systems in outburst and in a high state show characteristic modulations in their optical light curve.



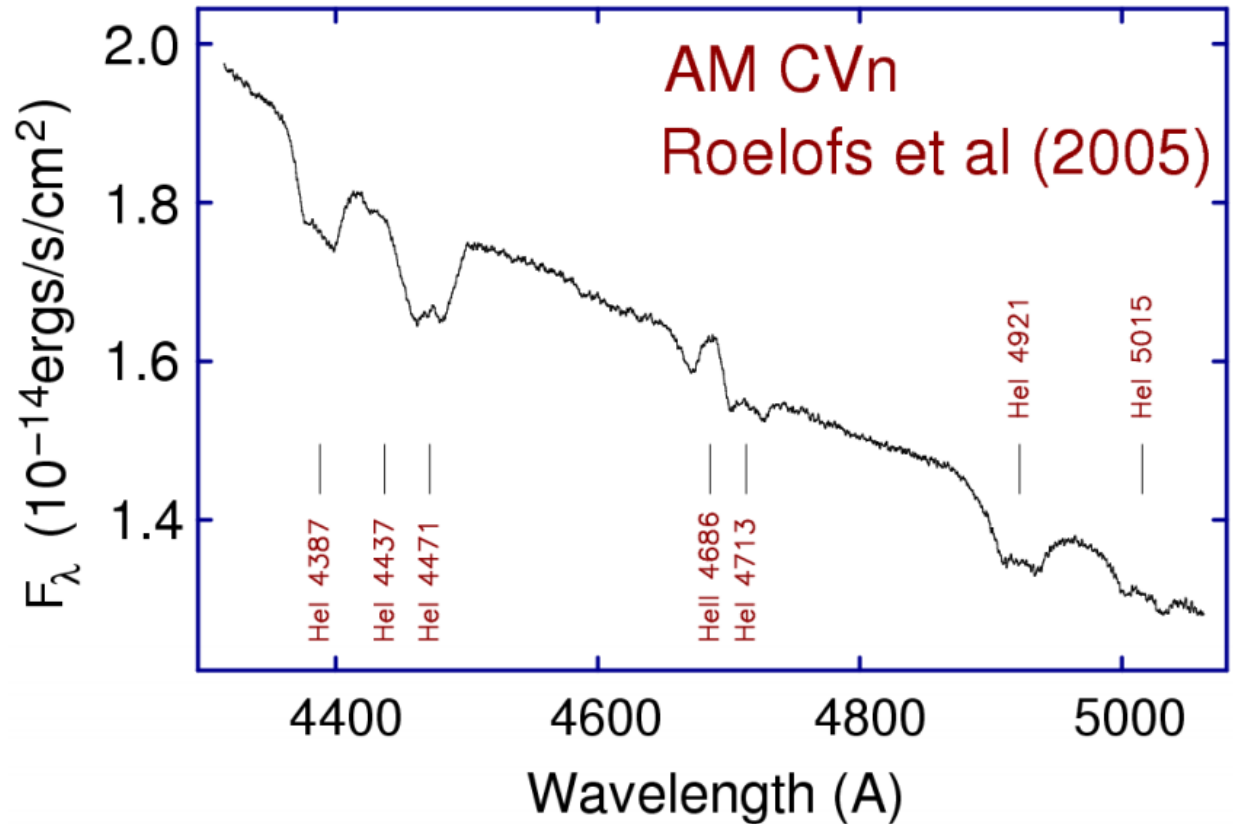
HP Lib ($P_{orb}=18.4\text{min}$) Optical and UV light curves show modulation due to precession period of the accretion disc.

Three groups of AM CVn's (1)

392

AM CVn stars split into three groups:

1) High \dot{M} , permanently bright, dominated by the accretion disk, $P < 20$ mins

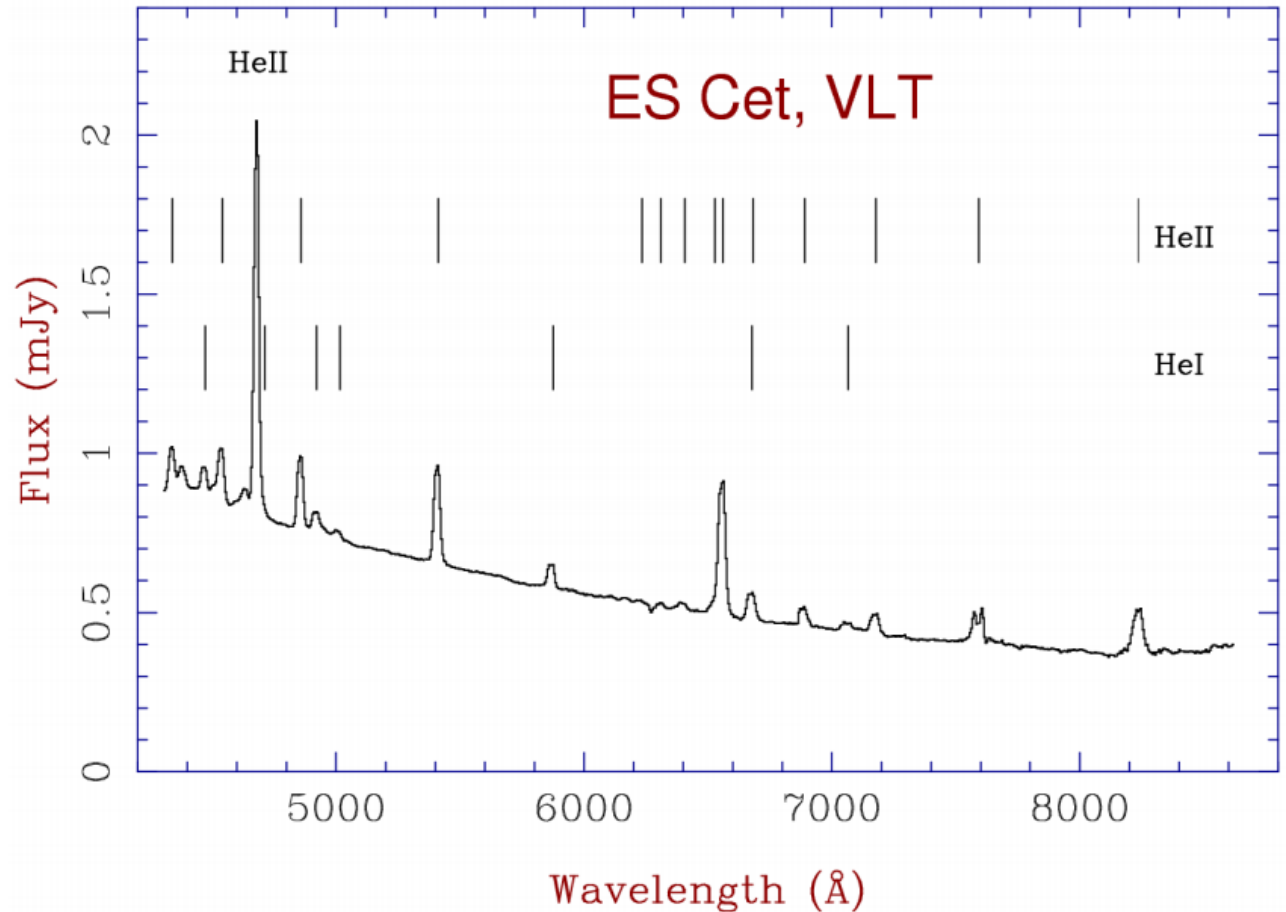


Three groups of AM CVn's (2)

393

AM CVn stars split into three groups:

1) High \dot{M} , permanently bright, dominated by the accretion disk, $P < 20$ mins

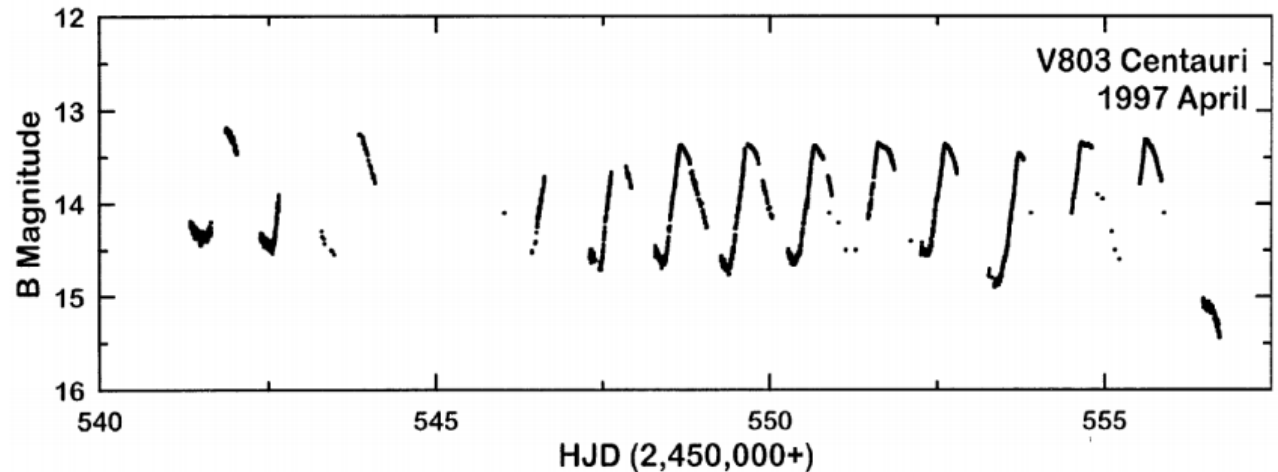


Three groups of AM CVn's (3)

394

AM CVn stars split
into three groups:

2) Medium \dot{M} ,
“dwarf novae”,
 $20 < P < 40$ mins



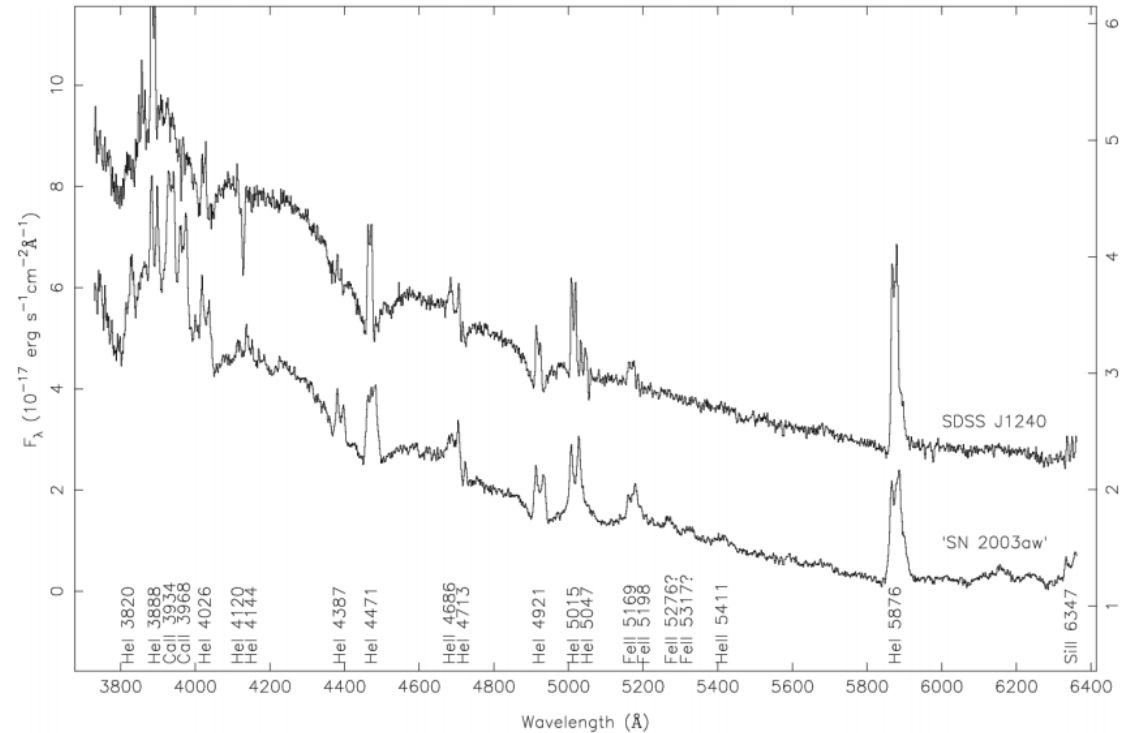
V803 Cen, Patterson et al. (2002)

Three groups of AM CVn's (4)

395

AM CVn stars split into three groups:

3) Low \dot{M} , permanently faint. Continuum from the accreting white dwarf, emission lines from the disk, $P > 40$ mins



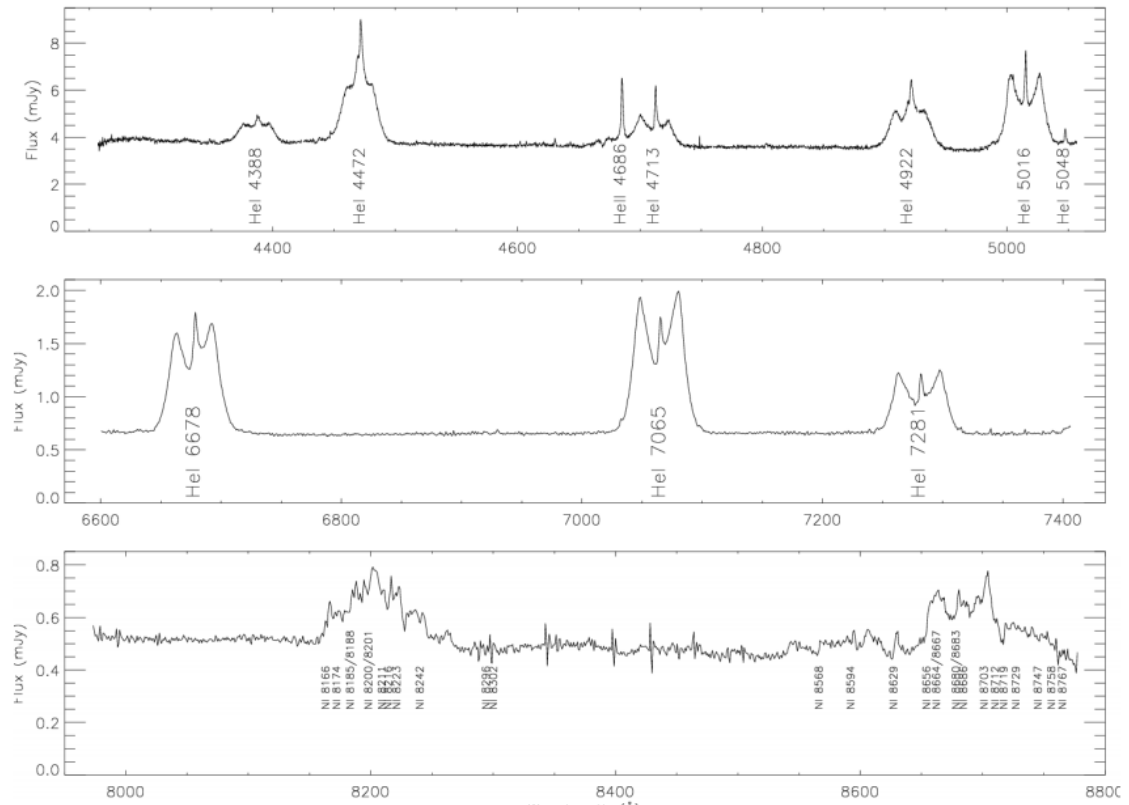
SN 2003aw, SDSS1240, Roelofs et al
(2005)

Three groups of AM CVn's (5)

396

AM CVn stars split into three groups:

3) Low \dot{M} ,
permanently faint.
Continuum from the
accreting white
dwarf, emission
lines from the disk,
 $P > 40$ mins



GP Com, Morales-Rueda et al (2003)

Orbital period/accretion rate relation

397

If

- (a) the donors in AM CVn stars are degenerate,
- (b) mass transfer is driven by gravitational radiation, and
- (c) $M_2 \ll M_1$:

□ Can eliminate a , R_2 and M_2 to show:

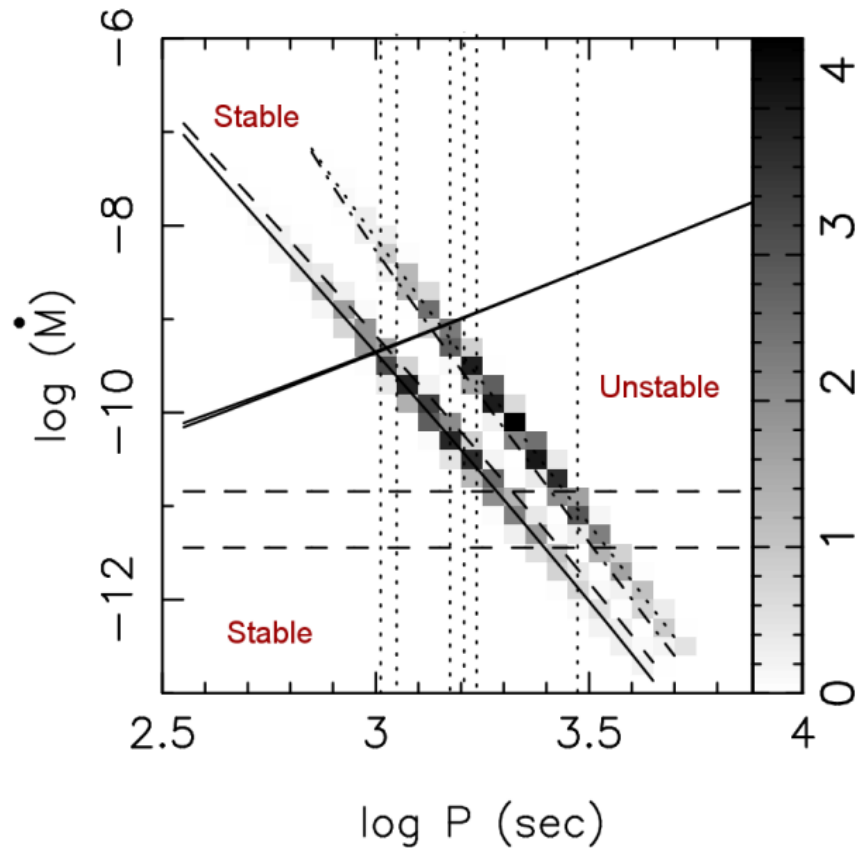
$$\dot{M}_{accr} \propto P^{-14/3}$$

□ **\Rightarrow AM CVn stars vary much more strongly with orbital period than their hydrogen-rich counterparts.**

The evolution of AM CVn stars (1)

398

The steep drop of \dot{M} with period combined with a thermal instability caused by the ionisation of helium (Tsugawa & Osaki 1997) can explain the 3 types of systems.

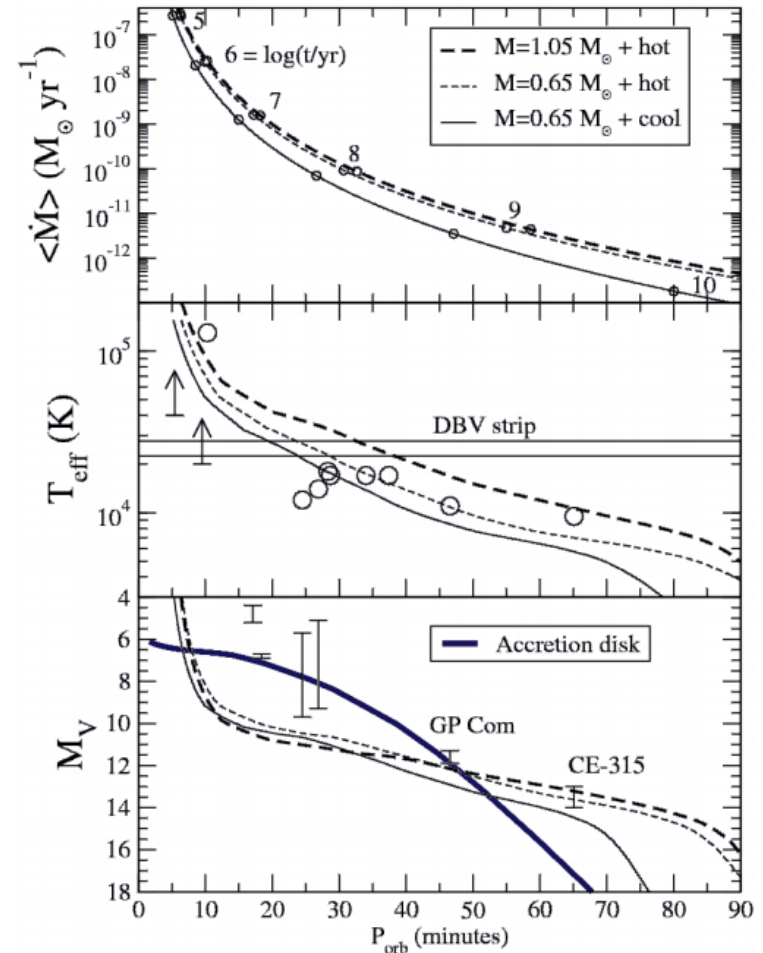


Nelemans et al (2001)

The evolution of AM CVn stars (2)

399

- The accreting white dwarf's temperature is a combination of normal evolutionary cooling and compressional heating (Bildsten et al 2006).
- It may dominate over the accretion luminosity at both short (< 10 min) and long (> 40 min) orbital periods.



The first eclipsing AM CVn star

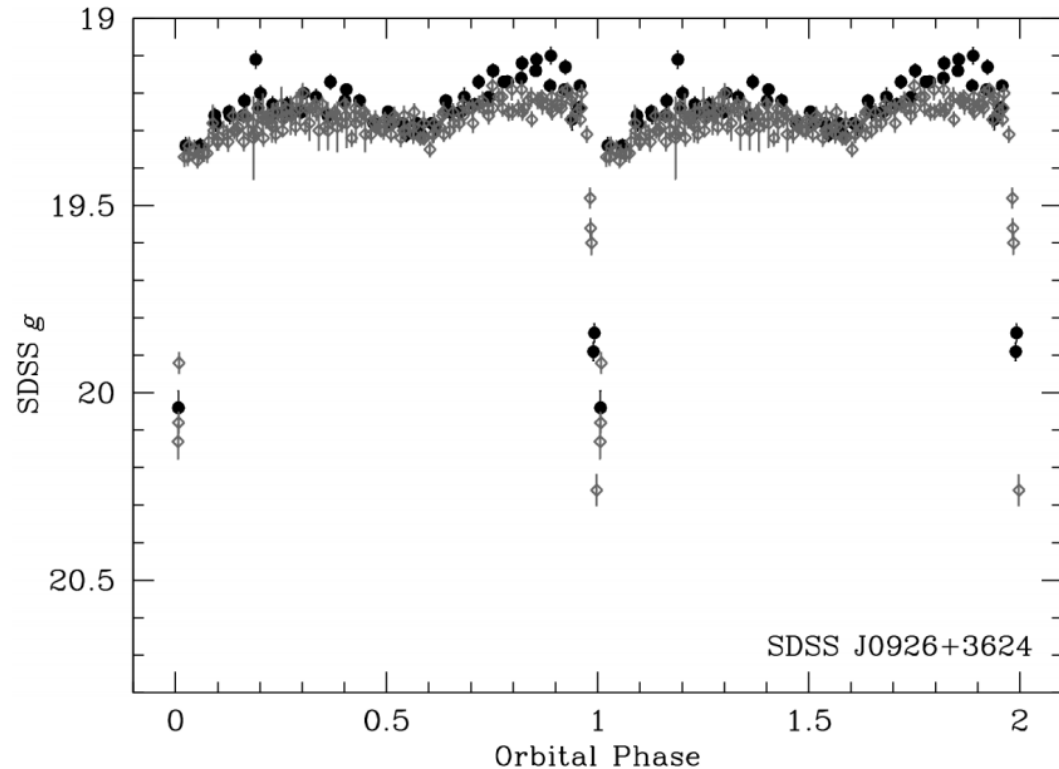
400

SDSS0926+3624

$P = 28$ minutes,
the only eclipsing
AM CVn known

$g' = 19.3$ with
eclipses that last 1
minute.

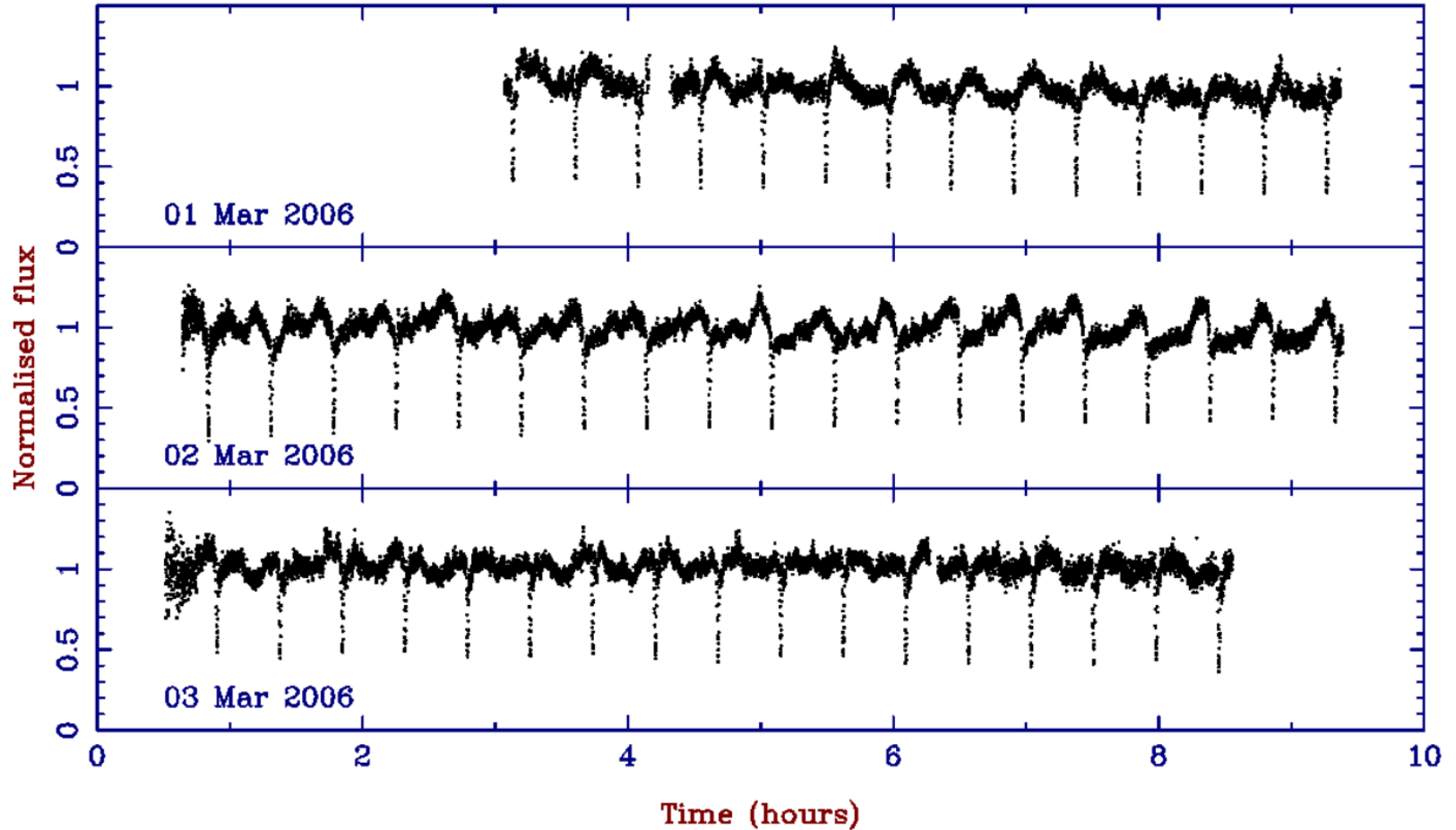
Our first chance to
measure
component masses
directly.



Anderson et al (2005)

SDSS0926+3624 with WHT+Ultracam

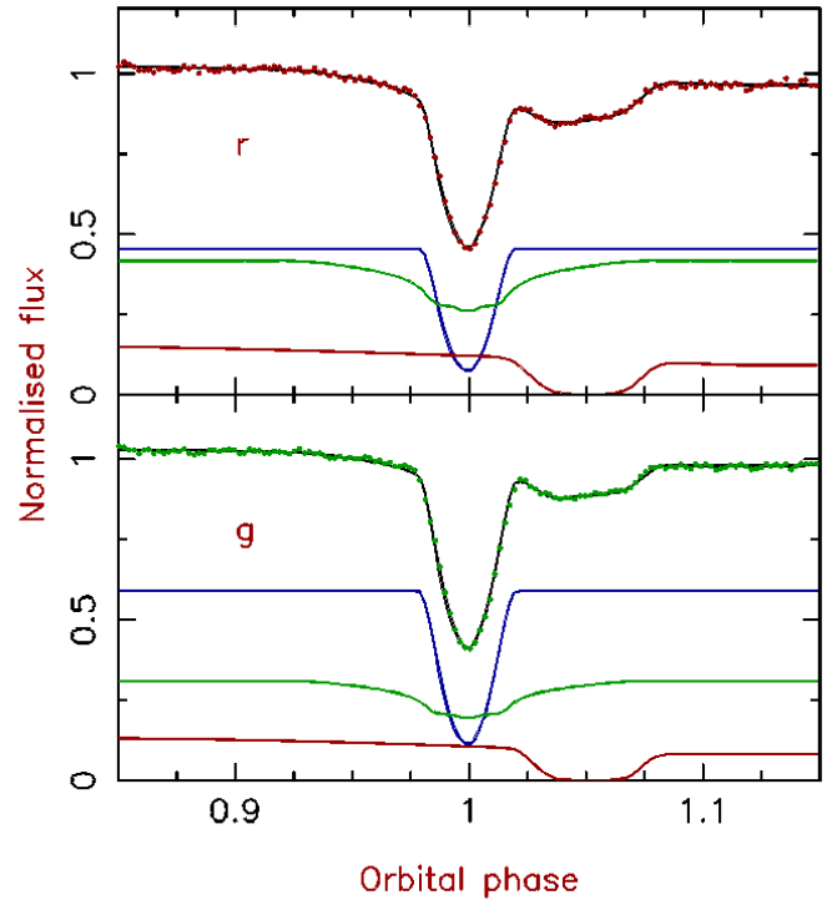
401



SDSS0926+3624 with WHT+Ultracam

402

- Light curve fit \Rightarrow
 $M_2 = 0.029 \pm 0.002 M_{\odot}$,
higher than expected for
complete degeneracy
($0.019 M_{\odot}$).
- Indicates significant thermal
energy in the donor,
nevertheless it is consistent
with a double white dwarf
progenitor
(Deloye et al 2007).

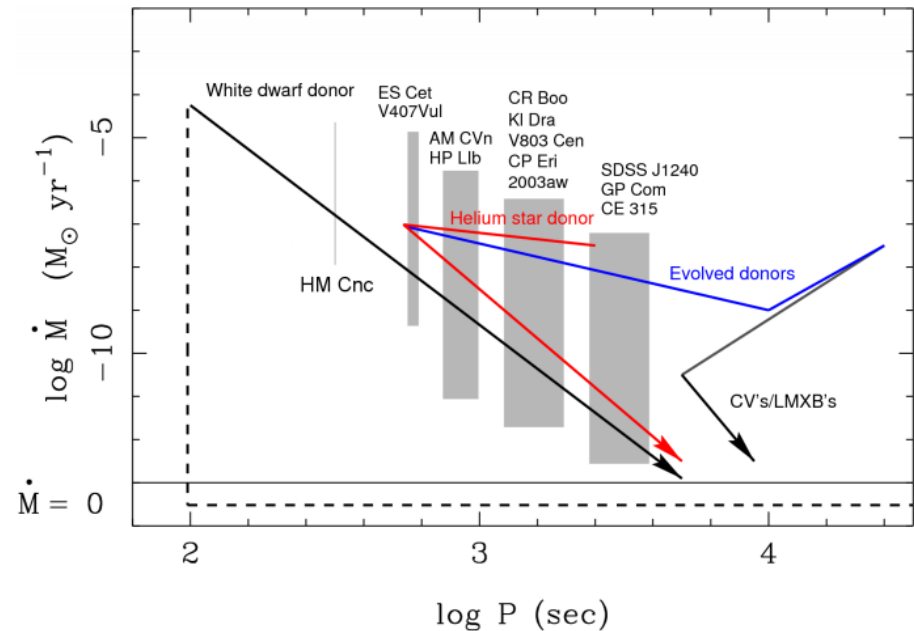


AM CVn puzzles I. – their origin

403

- Three possibilities:
 - 1. Double white dwarfs (Paczynski 1967; Nelemans et al 2001).
 - 2. White dwarf/helium star binaries (Iben & Tutukov 1991).
 - 3. CVs with evolved donors (Posiadlowski et al 2003).

- Other than the possible-but-disputed 5 minute binary HM Cnc, all models can explain the orbital periods.



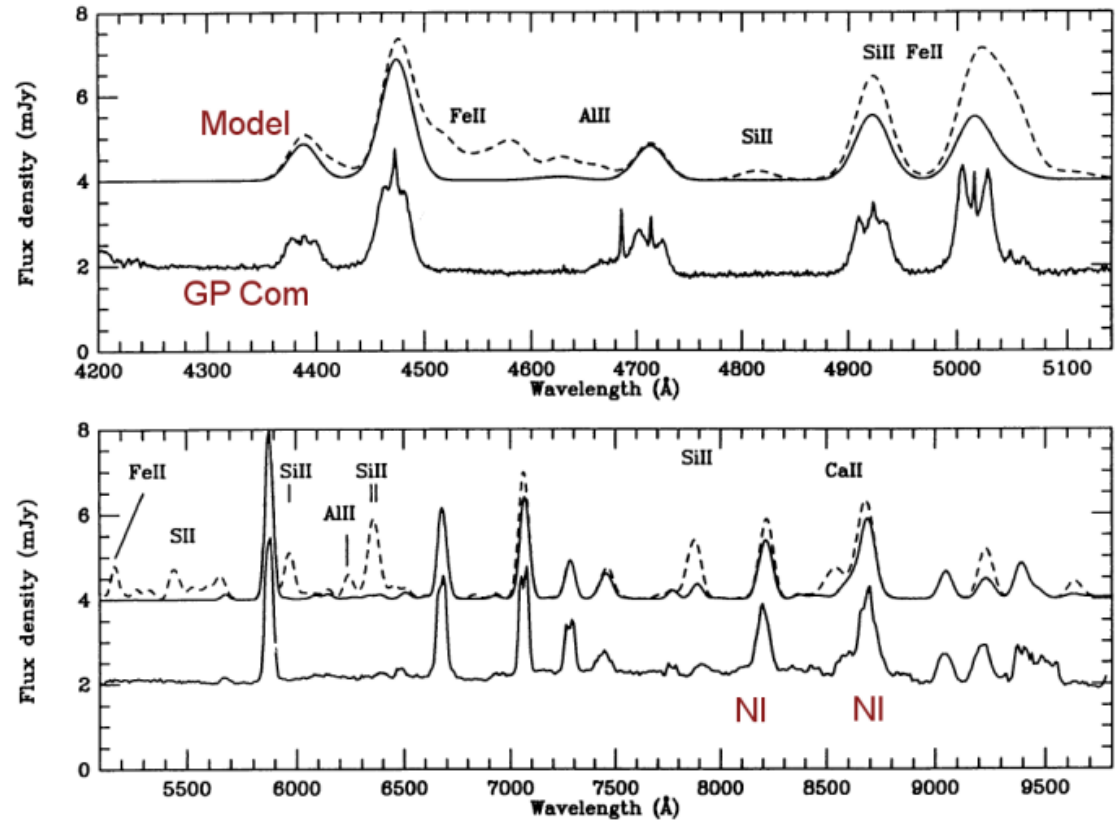
Nelemans et al (2001)

AM CVn puzzles II. – abundances

404

GP Com appears to have \sim solar CNO/He (mostly N), but lacks Ca, Si and Fe.

However, the model (single-temperature LTE slab) is crude.

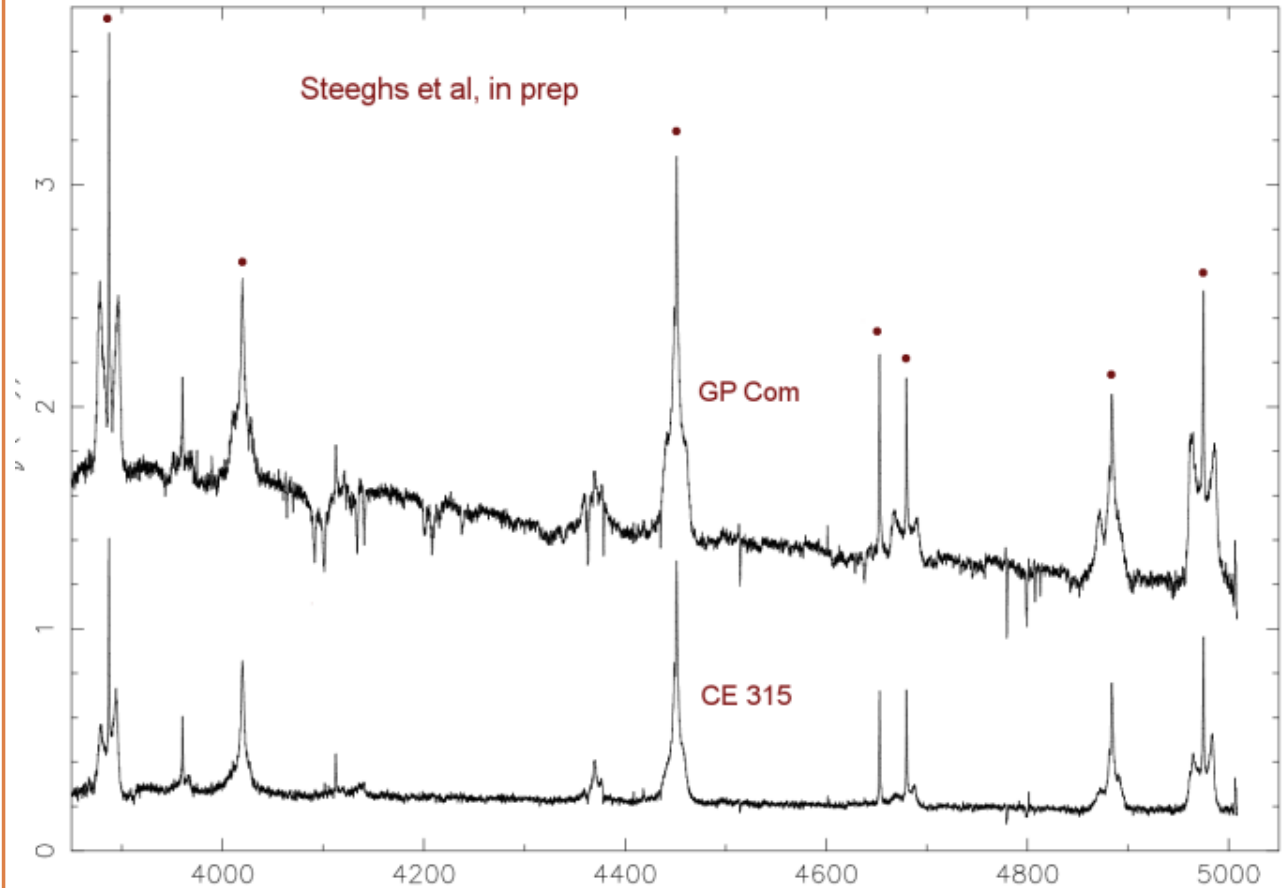


Marsh et al (1991)

AM CVn puzzles III. – spikes (1)

405

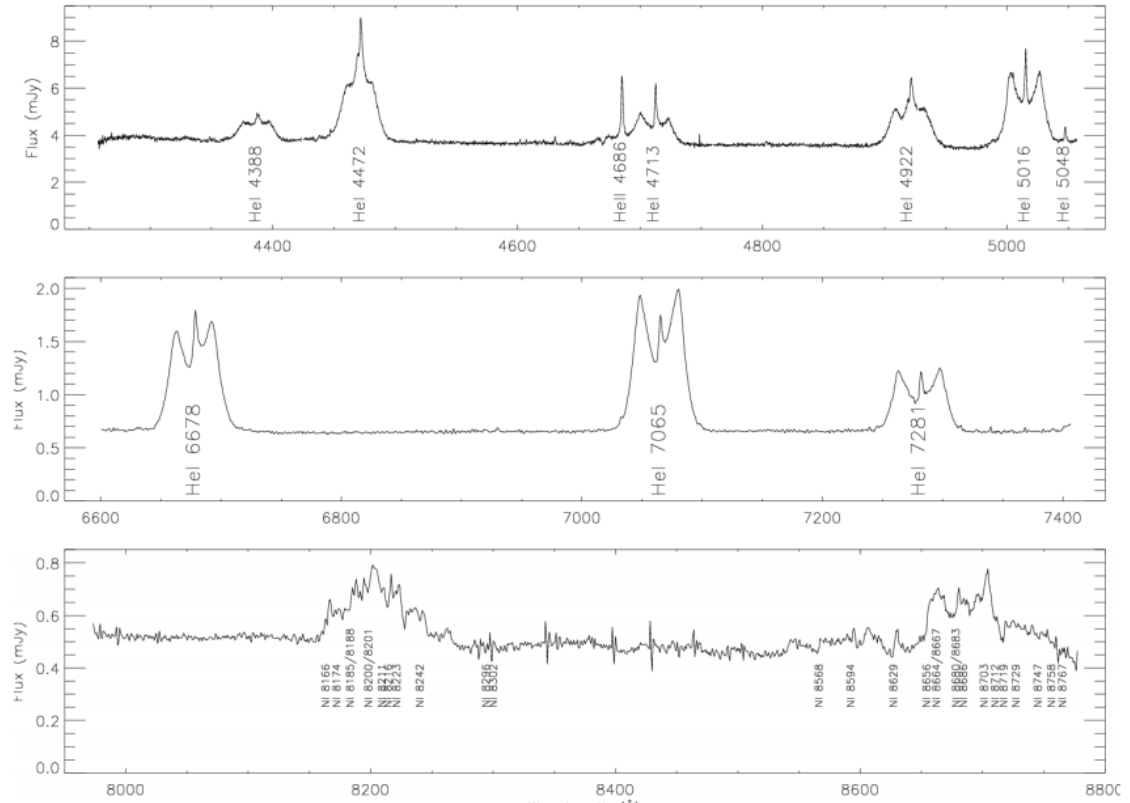
Several systems show sharp components at the centres of the double-peaked lines from the disks.



AM CVn puzzles III. – spikes (2)

406

Several systems show sharp components at the centres of the double-peaked lines from the disks.

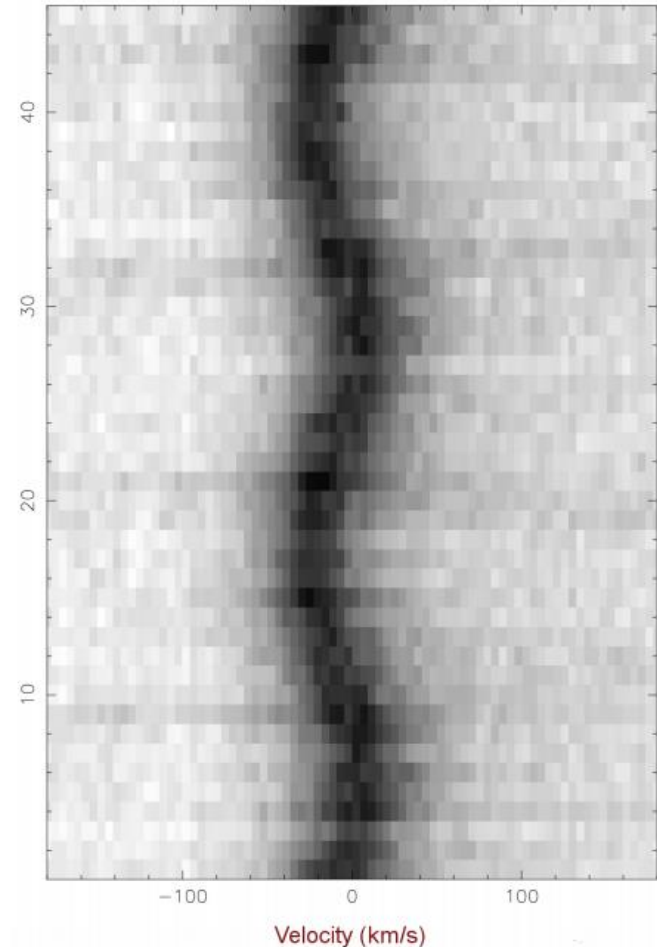


GP Com, Morales-Rueda et al (2003)

AM CVn puzzles III. – spikes (3)

407

- Kinematic constraints show that they come from the accreting white dwarfs, (Marsh 1999)
⇒ slow rotation,
 $v \sin i < 50 \text{ km/s}$,
cf breakup $\sim 5000 \text{ km/s}$.

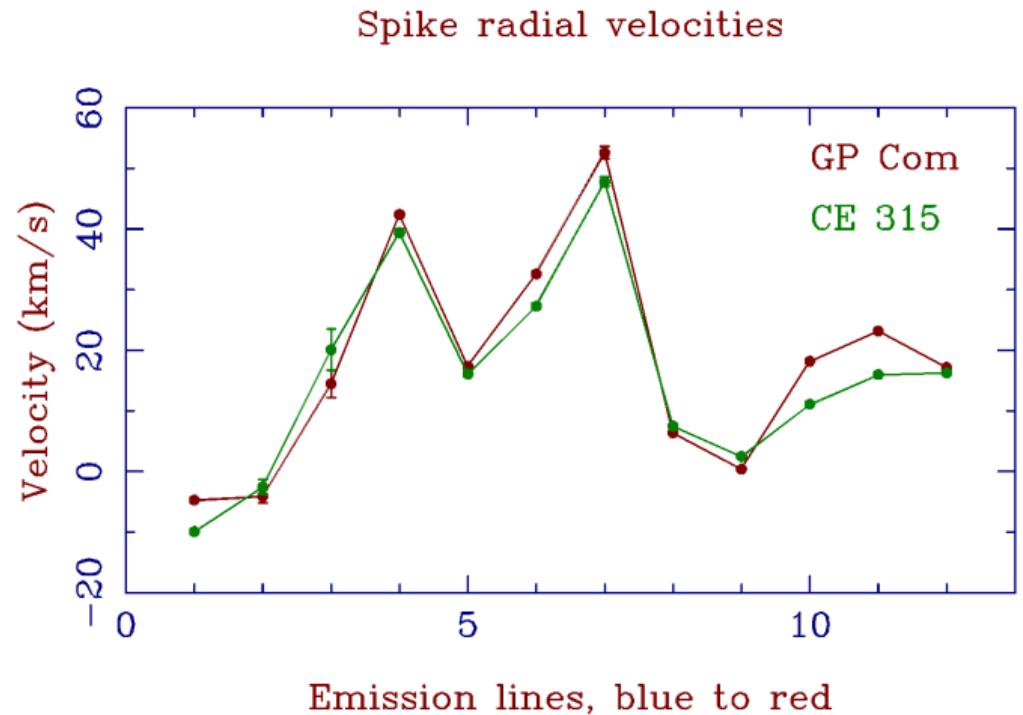


Interacting Binary Stars

AM CVn puzzles III. – spikes (4)

408

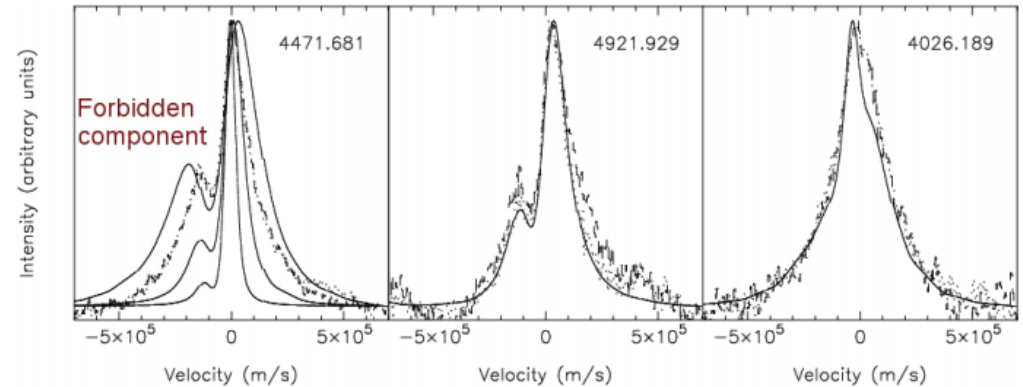
- Spikes should show a gravitational redshift, but the mean spike velocity is observed to vary from line-to-line.



AM CVn puzzles III. – spikes (5)

409

- Spike shifts & profiles probably the result of Stark broadening (Morales-Rueda et al 2003)
- $n_e \sim 10^{15} - 10^{16} \text{ cm}^{-3}$

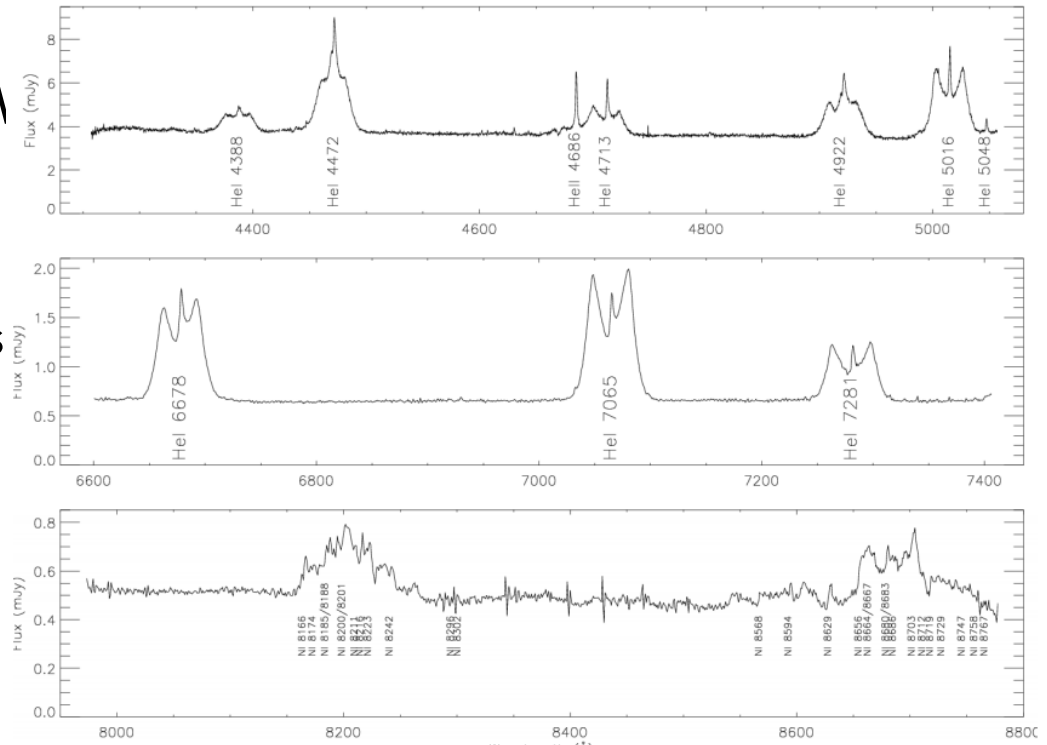


Steeghs, Roelofs et al, based on models of
Beauchamp et al (1997)

AM CVn puzzles III. – spikes (6)

410

- How do the spikes form?
- Why are they seen in AM CVn stars but not in hydrogen-rich CVs?
- Why are they not always seen in AM CVn stars?
- How can the accretors rotate so slowly?

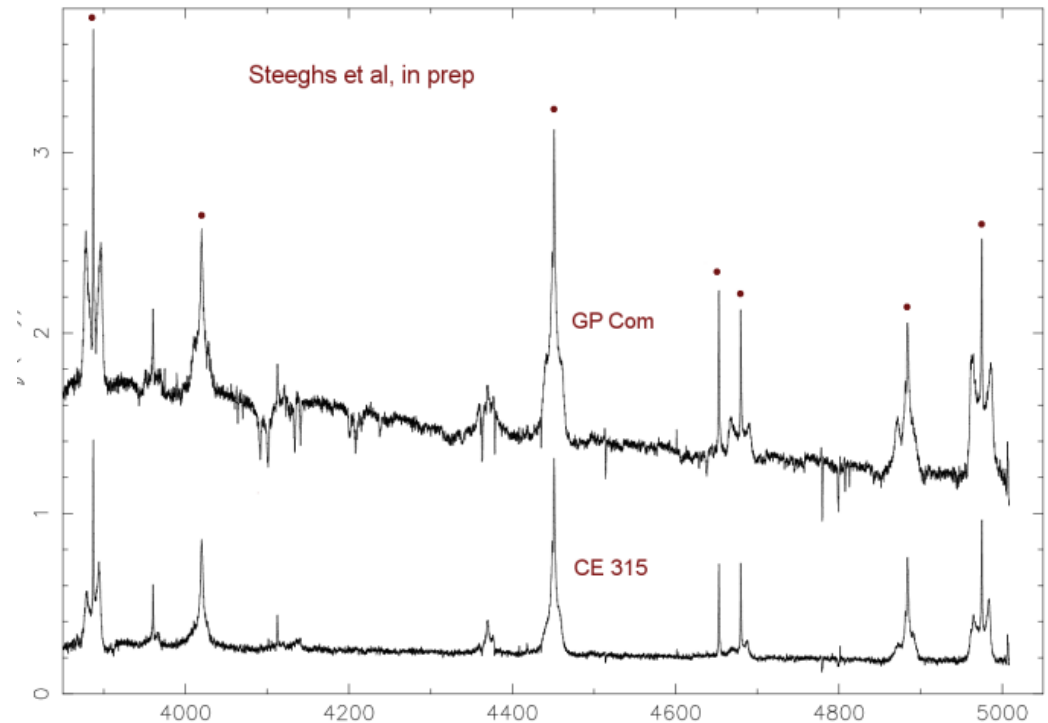


GP Com, Morales-Rueda et al (2003)

AM CVn puzzles IV. – dips

411

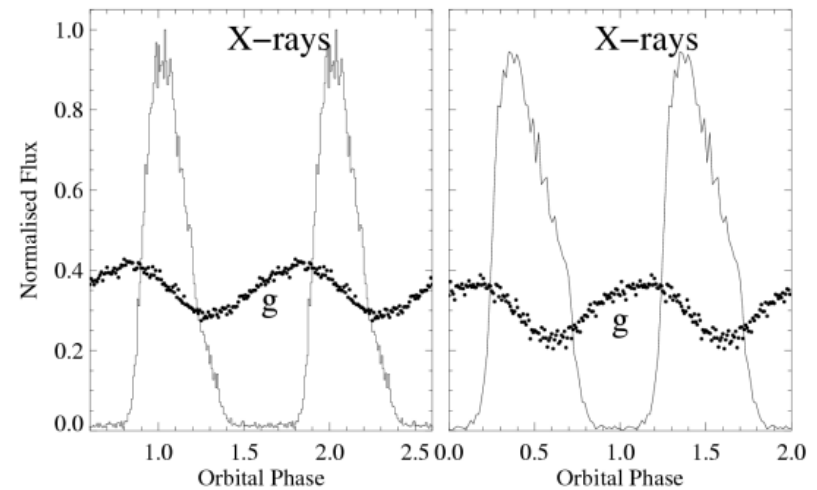
- Photosphere? If so, what element(s)?
- Time-variable? Accretion vs sedimentation. Critical $\dot{M} \sim 10^{-12} M_{\odot} \text{ yr}^{-1}$ (Bildsten et al 2006).
- Request: cool white dwarf model atmospheres for 98% helium, 2% nitrogen plus heavier elements.



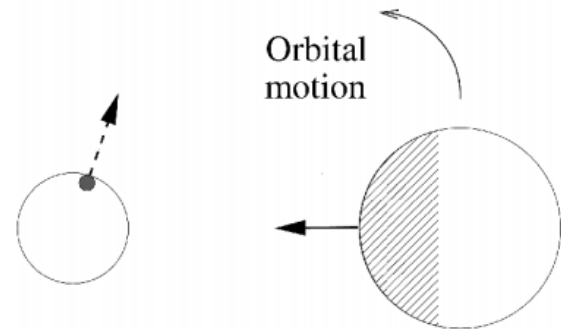
The shortest period binaries?

412

- Two stars, V407 Vul and RX J0806+1527, have very similar light-curves and periods of 569 and 321 seconds.
- These are thought to be orbital periods \Rightarrow strong emitters of gravitational waves.
- If accreting, double white dwarf avoidance of mergers will be established.



Barros et al



Interacting Binary Stars

AM CVn stars

413

1. The advent of large scale surveys has lead to the discovery of many new AM CVn stars.
2. The basic semi-detached, gravitational-wave driven model has held up well under the onslaught.
3. There have been significant advances in our understanding of the stellar components.
4. These stars pose a number of fascinating evolutionary and spectroscopic problems that we have yet to solve; the accretion disks remain an area of considerable uncertainty.
5. We need more good parameter estimates. These may only come from finding a few more of the million-odd systems in our Galaxy.

414

X-ray Binaries

LMXBs

HMXBs

X-ray Binaries

415

- X-ray binaries are a class of binary stars that are luminous in X-rays.
- They were among the first X-ray sources to be discovered (apart from the Sun and other Solar System sources).
 - ▣ Sco X-1 and Cyg X-1 were the first X-ray sources to be discovered in the constellations of Scorpius and Cygnus respectively and they are both X-ray binaries.

Black Body Radiation (1)

416

- Light can be produced in many ways. The most fundamental source of radiation is a so-called “black body”.
- A black body is an idealized physical body that absorbs all incident electromagnetic radiation. Because of this perfect absorptivity at all wavelengths, a black body is also the best possible emitter of thermal radiation.
- Black body radiation is thus radiation which is in thermal equilibrium and which continuous spectrum depends only on the body's temperature.

Black Body Radiation (2)

417

Depending on its temperature T , a black body emits radiation according to Planck's law:

$$L_{\lambda}(T) = \frac{2 h c_0^2}{\lambda^5} \left[\exp \left(\frac{h c_0}{\lambda k_B T} \right) - 1 \right]^{-1}$$

where $k_B = 1.38 \times 10^{-16}$ erg/K is the Boltzmann constant and $L_{\lambda}(T)$ is the spectral radiance at the wavelength λ .

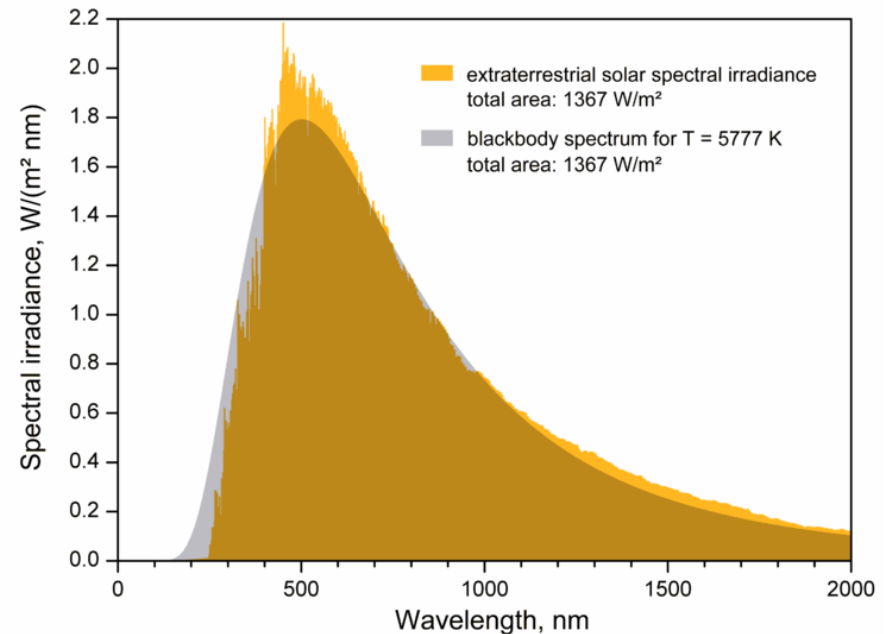
The corresponding formula for $L_{\nu}(T)$ is

$$L_{\nu}(T) = \frac{2 h \nu^3}{c_0^2} \left[\exp \left(\frac{h \nu}{k_B T} \right) - 1 \right]^{-1}$$

Black Body Radiation (3)

418

- A black body is the extreme case of an optically thick medium. In the Universe, many plasma systems emit radiation approximately according to Planck's law, at least, in certain wavelength ranges.

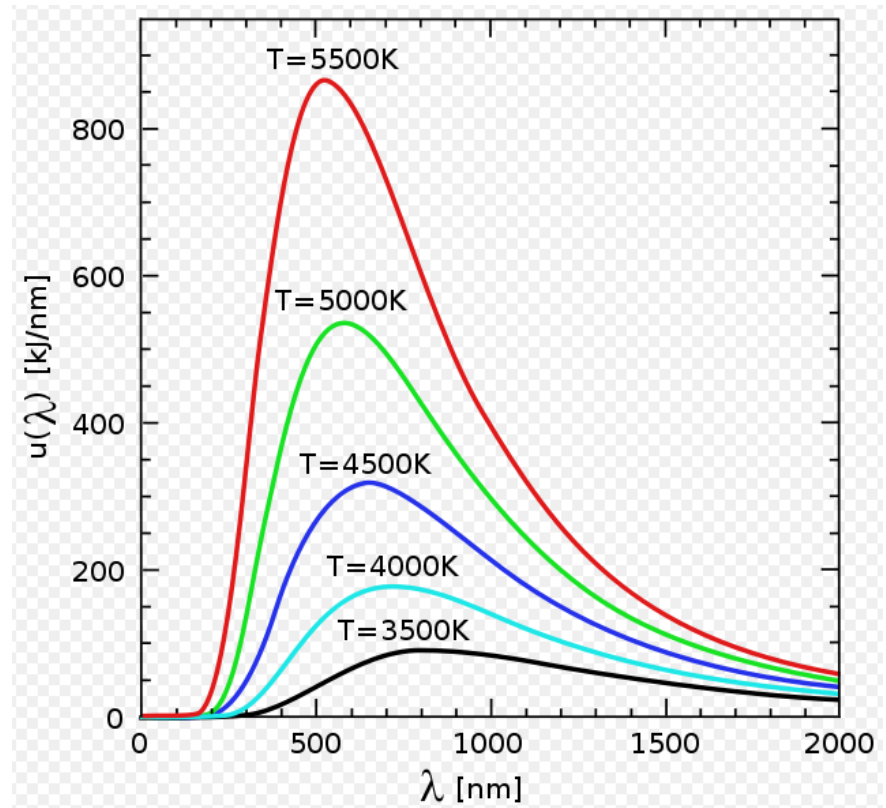


Properties of the blackbody spectrum

419

- As the temperature increases, the peak of the blackbody radiation curve moves to higher intensities and shorter wavelengths.
- Wien's displacement law:
 $\lambda_{\max} \approx 0.29(\text{cm})/T$
 λ_{\max} is a function only of the temperature

For $T=10^7$ K we have $\lambda_{\max} \approx 2.9 \text{ \AA}$
This is a typical X-ray wavelength range



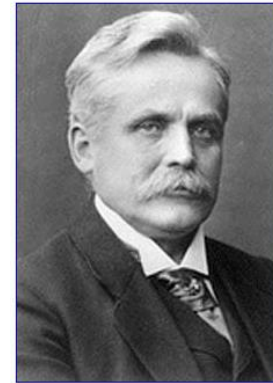
$L(T+\Delta T) > L(T)$ at all λ for positive ΔT

X-ray Photons

420

- **Wien's Displacement Law (1893):**

$$T = 5 \times 10^7 \text{ }^\circ\text{K} / \lambda_{\text{max}} \text{ (Angstroms)}$$



→ 10 Angstroms
is very hot !

Wilhelm Carl Werner Otto Fritz Franz Wien

- **X-rays: Photons 0.6-12 Angstroms → Energies 20-1 keV**
 - Thermal Equivalent $kT = 4$ to 80 million $^\circ\text{K}$
 - Heating mechanisms → non-thermal processes
 - synchrotron radiation (high energy e^- in B field)
 - inverse Compton (photon upscattered by high energy e^-)

Energetics of accretion (1)

421

- The accretion of gas onto a compact object can be a very efficient way of converting gravitational potential energy into radiation.
- The amount of energy released by accreted gas is

$$E_{acc} = \frac{GM_*\dot{M}}{R_*}$$

M_* and R_* are the mass and radius of the accreting star.

- By comparison, the conversion of the hydrogen into helium would yield an energy

$$E_{H \rightarrow He} \approx 0.007 \dot{M} c^2$$

Energetics of accretion (2)

422

- Efficiency of the accretion process (fraction of the nuclear fusion [hydrogen to helium] energy that is radiated) is

$$\frac{E_{acc}}{E_{H \rightarrow He}} \approx \frac{GM_* \dot{M}}{0.007 \dot{M} R_* c^2} \approx \frac{70 R_{Sch}}{R_*}$$

$$R_{Sch} = \frac{2GM_*}{c^2} \approx 3km \frac{M_*}{M_{\odot}} \rightarrow \text{The Schwarzschild radius}$$

- Thus, accretion on to a compact object with $R_* \leq 70 R_{Sch}$ is a more efficient mechanism than nuclear fusion of hydrogen to helium.

Energetics of accretion (3)

423

- **A white dwarf:** typical mass $2 \cdot 10^{30} \text{g}$ ($1 M_{\odot}$)
 $R = 7000 \text{ km} \gg 70 R_{Sch}$
- **A neutron star:** typical mass $3 \cdot 10^{33} \text{g}$ ($1.5 M_{\odot}$)
 $R = 10 \text{ km} \ll 70 R_{Sch}$
- **A black hole**

Accreting neutron stars and black holes are luminous sources, normally in X-ray radiation.

Where does accreted matter come from? ISM?

No – captured mass is too small. Companion? Yes.

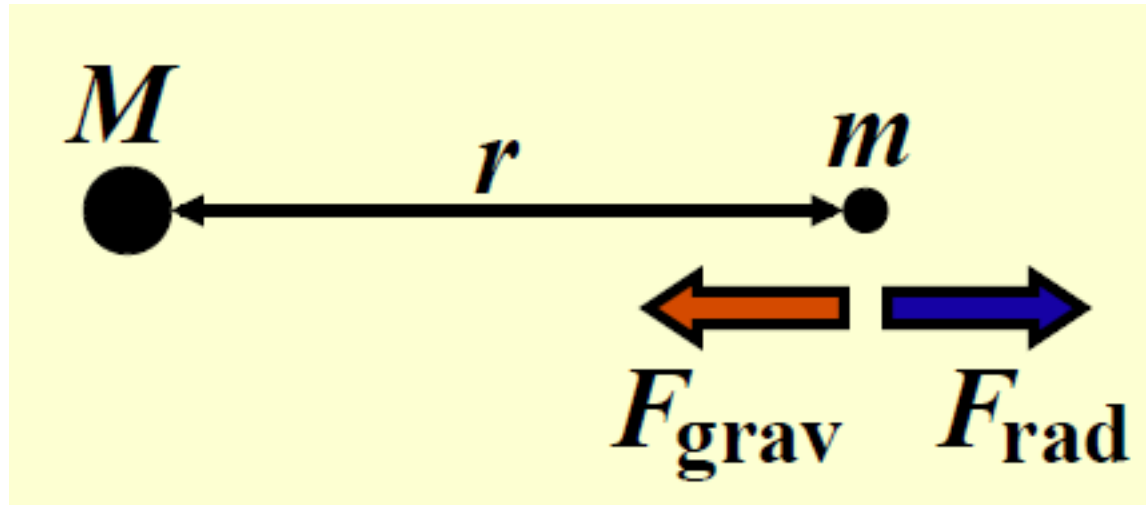
The Eddington Luminosity (1)

424

- There is a (not strict) limit to the rate \dot{M} at which a compact object can accrete matter.
- Accordingly, there is a limit to the luminosity that can be produced by a steadily accreting object, known as the **Eddington luminosity**.
- Effectively it is reached when the inward gravitational force on matter is **balanced** by the outward transfer of momentum by radiation.

The Eddington Limit (1)

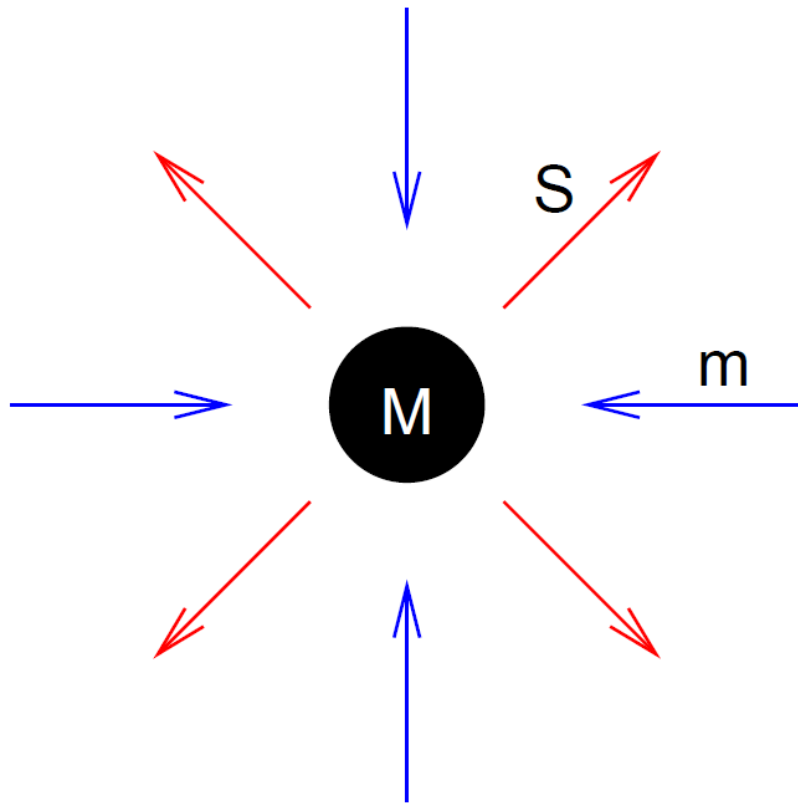
425



Accretion rate controlled by momentum transferred
from radiation to mass

The Eddington Limit (2)

426



- Assume mass M spherically symmetrically accreting **ionized hydrogen gas**.
 - Inward force: **gravitation**:
- $$F_{grav} = \frac{GM_* m_p}{r^2}$$
- At radius r , accretion produces **energy flux S** :

$$S = \frac{L}{4\pi r^2}$$

- The luminosity L of the central compact object exerts a radiation force on the free electrons by **Thomson scattering**:

$$F_{rad} = \frac{\sigma_T S}{c}$$

- **Note:** the Thomson cross-section of protons is $\sim 10^6$ times smaller than that of electrons. But: electrostatic forces between electrons and protons bind them so they act as a pair: **F_{rad} also has effect on protons!**

The Eddington Limit (3)

427

- Accretion is only possible if gravitation dominates:

$$\frac{GM_* m_p}{r^2} > \frac{\sigma_T S}{c} = \frac{\sigma_T}{c} \frac{L}{4\pi r^2}$$

- and therefore

$$L < L_{Edd} = \frac{4\pi GM_* m_p c}{\sigma_T}$$

where L_{Edd} is called **the Eddington luminosity**.

- or, in astronomically meaningful units

$$L < 1.3 \times 10^{38} \text{ erg s}^{-1} \frac{M}{M_\odot}$$

- When the luminosity of the central compact object is greater than this value, the surrounding hydrogen gas will be blown away by the radiation pressure.

The Eddington Luminosity (2)

428

- If the Eddington luminosity is emitted as black-body radiation, the temperature will be

$$T_{bb} = \left(\frac{L_{\text{Edd}}}{4\pi R_*^2 \sigma_{SB}} \right)^{1/4} = \left(\frac{GM_* m_p c}{R_*^2 \sigma_{SB}} \right)^{1/4}$$

where σ_{SB} is the Stefan-Boltzmann constant, and R_* is the radius of the surface from which the radiation is emitted (for a black hole, of course, this surface will be outside the Schwarzschild radius).

- For a black hole accreting at the Eddington limit, the temperature of the radiation will be $T_{bb} \sim 4 \times 10^7 \text{ K } (M_*/M_\odot)^{-1/4}$, if the radiation comes from immediately outside the Schwarzschild radius.
- The spectrum of the emitted photons will then peak at a photon energy $E \sim 20 \text{ keV } (M_*/M_\odot)^{-1/4}$.

Maximum Accretion Rate

429

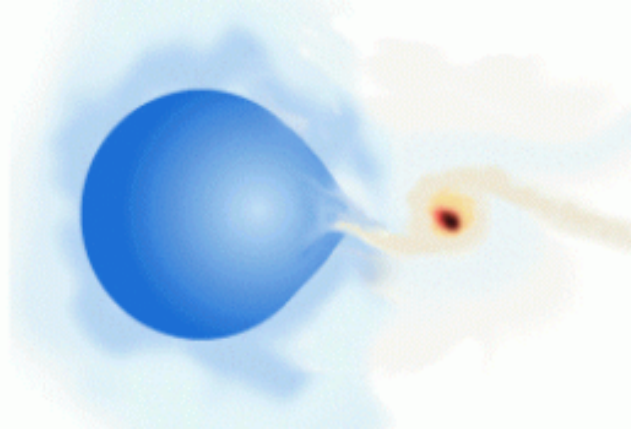
- The existence of the Eddington luminosity implies the existence of a maximum accretion rate, \dot{M}_{Edd} , for an accreting compact object. If the accretion energy E_{acc} is converted entirely into radiation, then the luminosity is $L_{acc} = GM_*\dot{M}/R_*$, and the maximum possible accretion rate is

$$\dot{M}_{Edd} = \frac{4\pi m_p c R_*}{\sigma_T} = 9 \times 10^{16} \text{ g sec}^{-1} \left(\frac{R_*}{1 \text{ km}} \right) = 1 \times 10^{-3} M_\odot \text{ yr}^{-1} \left(\frac{R_*}{R_\odot} \right)$$

- In reality, the conversion is not 100% efficient, the accretion is not perfectly spherically symmetrical, and the radiation is not perfectly spherically symmetrical; thus, matter can be accreted at rates somewhat greater than \dot{M}_{Edd} .

X-ray Binaries

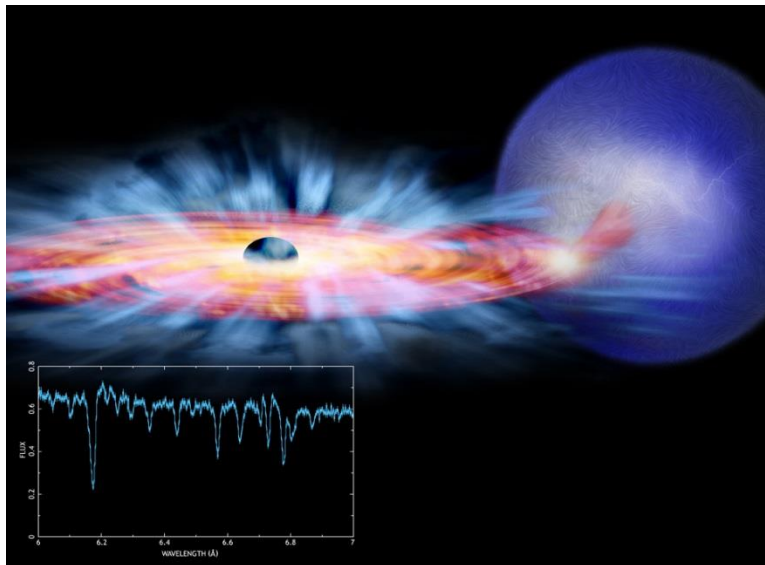
430



Scenario 1: Stellar Wind Accretion

- More massive star dies first
- Stellar wind captured
(with possible inner accretion disk)

Common for High-Mass (Companion)
X-ray Binaries (**HMXB**)



Scenario 2: Roche Lobe overflow

- More massive star dies first
- Binary separation can shrink
(magnetic braking and/or grav. radiation)
- Companion may evolve and grow

Common for Low-Mass (Companion)
X-ray Binaries (**LMXB**)

High-mass X-ray Binaries (1)

431

- **HMXBs** are binary systems, in which the normal stellar component is a massive star: usually an O or B star, a Be star, or a blue supergiant. The compact, X-ray emitting, component is generally a neutron star or black hole.
- A fraction of the stellar wind of the massive normal star is captured by the compact object, and produces X-rays as it falls onto the compact object.
- In a HMXB, the massive star dominates the emission of optical light, while the compact object is the dominant source of X-rays. The massive stars are very luminous and therefore easily detected.

High-mass X-ray Binaries (2)

432

- Because of the large mass ratio, mass transfer generally becomes unstable, leading to a common-envelope and spiral-in phase
- Mass transfer is either due to atmospheric Roche-lobe overflow (short-lived) or wind accretion (relatively low luminosity)
- Massive stars have very strong radiation-driven stellar winds - the steady loss of mass from the surface of a star into interstellar space
- Stellar wind from OB stars: $\dot{M}_w = 10^{-5} - 10^{-8} M_{\odot}/\text{year}$
Compare with the Sun: $\dot{M}_{\odot} = 3 \times 10^{-14} M_{\odot}/\text{year}$

Low-mass X-ray Binaries

433

- **LMXB** is a binary star where one of the components is either a black hole or neutron star. The other, donor, component usually fills its Roche lobe and therefore transfers mass to the compact star.
- The donor is less massive than the compact object, and can be on the main sequence, a degenerate dwarf (white dwarf), or an evolved star (red giant).
- A typical LMXB emits almost all of its radiation in X-rays, and typically less than one percent in visible light, so they are among the brightest objects in the X-ray sky, but relatively faint in visible light. The brightest part of the system is the accretion disk around the compact object. The orbital periods of LMXBs range from ten minutes to hundreds of days.
- A couple of hundred LMXBs have been detected in the Milky Way.

Properties of X-ray Binaries

435

Properties	HMXBs	LMXBs
Donor star	O-B ($M > 5 M_{\odot}$)	K-M ($M < 1 M_{\odot}$)
Population	I (10^7 yr)	II ($5-15 \times 10^9$ yr)
L_X/L_{opt}	0.001-10	100-1000
Optical spectrum	stellar like	reprocessing
Orbital Period	1-100 d	10 min-10 d
Accretion disc	yes, small	yes
X-ray Eclipses	common	rare

Bondi-Hoyle wind accretion (1)

436

- Massive stars have very strong radiation-driven stellar winds.

$$V_w \sim V_{esc} = \sqrt{\frac{2GM_d}{R_d}}$$

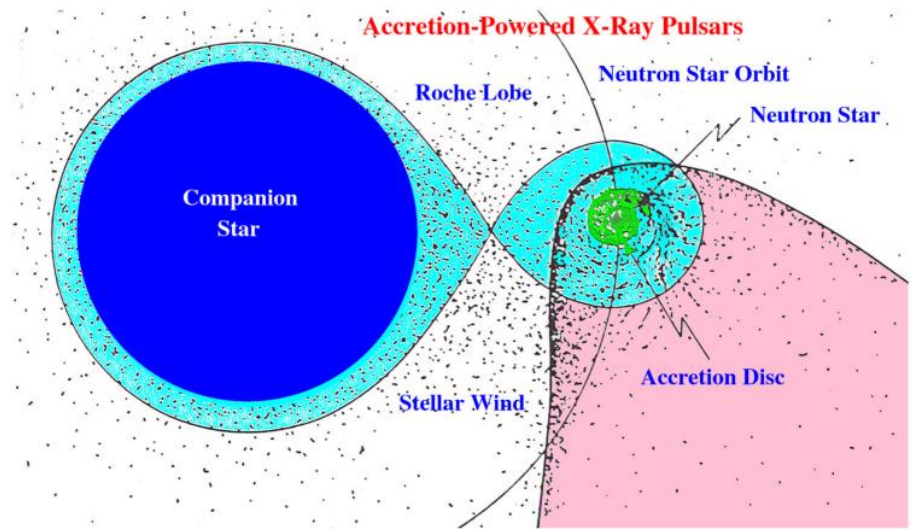
where M_d and R_d are the mass and radius of the primary star and V_{esc} is the escape velocity at its surface.

For typical parameters V_{esc} is generally a few thousand km/s which greatly exceeds the sound speed c_s . As a consequence the accreting gas is far to be in hydrostatic equilibrium.

Bondi-Hoyle wind accretion (2)

437

A compact object with mass M_x moving with velocity V_{rel} through a medium will gravitationally capture matter from a roughly cylindrical region with axis along the relative wind direction which represents the volume where wind particle kinetic energy is less than the gravitational potential one.



Bondi-Hoyle wind accretion (3)

438

- The material in the wind is captured once

$$\frac{mV_{rel}^2}{2} \cong \frac{GmM_x}{R_{acc}}$$

- V_{rel} -relative velocity of a compact object and a stellar wind

$$V_{rel}^2 = V_{orb}^2 + V_w^2$$

- V_{orb} -orbital velocity of a compact object around a companion

$$V_{orb}^2 = \frac{G(M_d + M_x)}{a}$$

- a – binary separation

- The radius of the cylinder, called the accretion radius or gravitational capture radius, is given by:

$$R_{acc} = \frac{2GM_x}{V_{rel}^2}$$

Bondi-Hoyle wind accretion (4)

439

- The mass loss rate is

$$\dot{M}_w = 4\pi a^2 \rho_w(a) V_w(a)$$

- The mass accretion rate is

$$\dot{M}_{acc} = \pi R_{acc}^2 \rho_w(a) V_{rel}$$

- Therefore, the fraction of the stellar wind captured by the compact star is

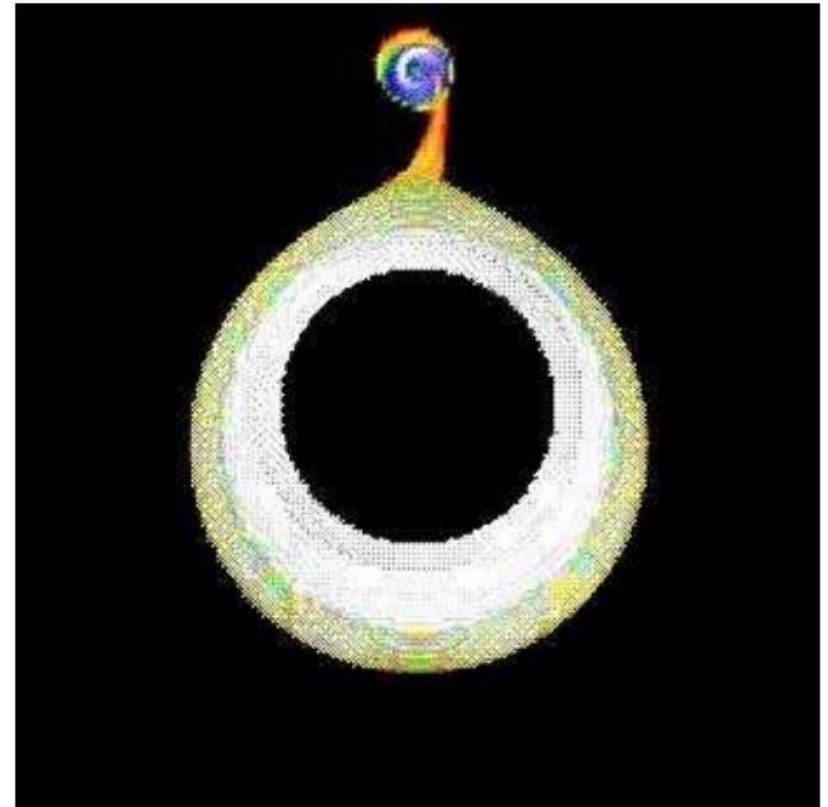
$$\frac{\dot{M}_{acc}}{\dot{M}_w} = \frac{1}{(1 + M_w/M_x)^2} \left(\frac{V_{orb}}{V_w} \right)^4 \frac{1}{(1 + (V_{orb}/V_w)^2)^{3/2}}$$

which is of order 10^{-5} - 10^{-3} for typical parameters of HMXBs. The accretion luminosity can be as high as 10^{36} - 10^{38} erg/s depending on the orbital periods.

Bondi-Hoyle wind accretion (5)

440

- In realistic HMXB, because the accreted material still has some angular momentum, a small accretion disk still forms.

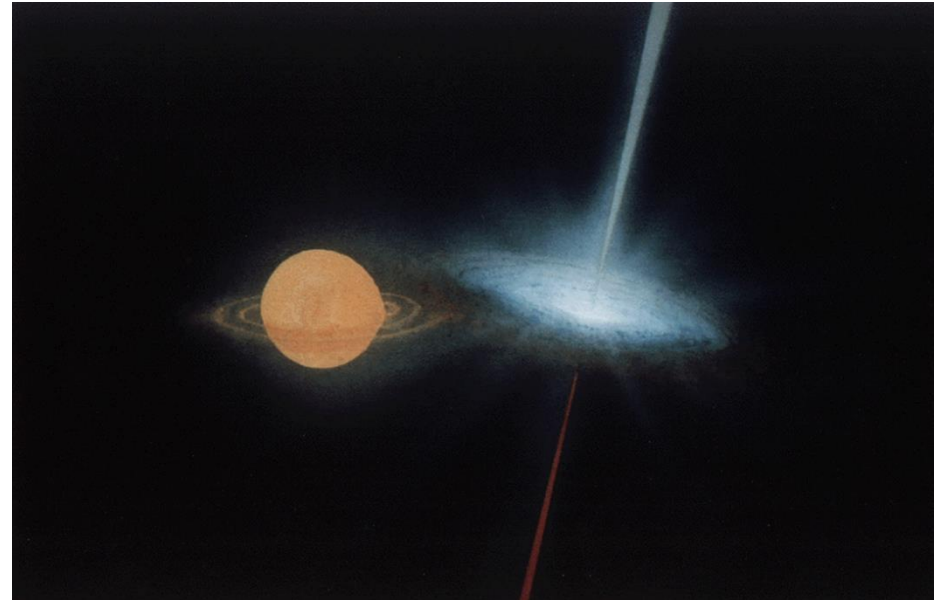


courtesy J. Blondin

SS 433 (1)

441

- An eclipsing X-ray binary system, with the primary most likely a black hole, or possibly a neutron star. The spectrum of the secondary companion star suggests that it is a late A-type star.



SS 433 (2)

442

- The jets from the primary are emitted perpendicular to its accretion disk.
- The jets and disk precess around an axis inclined about 79° to a line between us and SS 433.
- The angle between the jets and the axis is around 20° , and the precessional period is around 162.5 days
- The spectrum of SS 433 is affected not just by Doppler shifts but also by relativity: when the effects of the Doppler shift are subtracted, there is a residual redshift which corresponds to a velocity of about 12000 km/s.
- Material of jets moves with the velocity of ~ 80000 km/s ($0.27 c$).

